Enhancing Oncolytic Virotherapy of Glioblastoma by Targeting Innate Immune Ligands With a Bispecific T Cell Engager

Richard Baugh

Department of Oncology

Exeter College, University of Oxford



A thesis submitted for the degree of Doctor of Philosophy to the Department of Oncology, University of Oxford, Hilary Term 2022

Supervisors: Professor Len Seymour, Dr Hena Khalique

A statement addressing the impact of the COVID-19 pandemic upon this thesis

I was unable to access any laboratories from March 2020 until August 2020, owing to the SARS-CoV-2 outbreak and the nationwide restrictions imposed as a result. All students have been advised to attach documentation of the effects that these restrictions had upon their research.

During the 6 months out of the lab due to the pandemic, I wrote the review article “Convergent Evolution by Cancer and Viruses in Evading the NKG2D Immune Response”, which forms a basis of the literature review section of this thesis.

Upon returning to onsite working, access to the laboratories was restricted and on a limited basis, impacting the amount of work being able to be achieved. I very was fortunate to have been granted a 6-month funding extension by Brain Research UK, who have funded my DPhil studentship.

Nevertheless, impacts of the pandemic have made acquiring primary GBM tissue challenging. So far, I have only received primary GBM tissue from a single patient but look to expand this in the time between thesis submission and viva examination.

Before the pandemic, alongside the NKG2D BiTE work presented in this thesis, my research project was investigating developing novel ways to encourage phagocytosis of GBM cells by tumour associated macrophages using bispecific macrophage engagers. However, due to the disruption of the pandemic, this phagocytosis project was deprioritised to focus on the NKG2D project described in this thesis. The phagocytosis project will not be discussed in this thesis.

Declaration of Authentication

The material presented in this thesis was performed under the supervision of Professor Leonard Seymour, Department of Oncology, Medical Sciences Division, University of Oxford. This work is entirely my own and any contribution made by others has been acknowledged. The work submitted does not form part of another thesis in this or any other university.

Richard Baugh

April 2022

Publication note

Material from the following review article in MDPI Cancers is used in the Introduction (Chapter 1) and discussion throughout:

Baugh, R., Khalique, H., Seymour, L.W., 2020. Convergent Evolution by Cancer and Viruses in Evading the NKG2D Immune Response. https://doi.org/10.3390/cancers12123827

Contributions to published work made over the course of this DPhil:

Baugh, R., Khalique, H., Seymour, L.W., 2020. Convergent Evolution by Cancer and Viruses in Evading the NKG2D Immune Response. https://doi.org/10.3390/cancers12123827

Khalique, H., **Baugh, R**., Dyer, A., Scott, E.M., Frost, S., Larkin, S., Lei-Rossmann, J., Seymour, L.W., 2021. Oncolytic herpesvirus expressing PD-L1 BiTE for cancer therapy: exploiting tumor immune suppression as an opportunity for targeted immunotherapy. J. Immunother. Cancer 9, e001292. https://doi.org/10.1136/jitc-2020-001292

Pokrovska, T.D., Jacobus, E.J., Puliyadi, R., Prevo, R., Frost, S., Dyer, A., **Baugh, R**., Rodriguez-Berriguete, G., Fisher, K., Granata, G., Herbert, K., Taverner, W.K., Champion, B.R., Higgins, G.S., Seymour, L.W., Lei-Rossmann, J., 2020. External beam radiation therapy and enadenotucirev: Inhibition of the DDR and mechanisms of radiation-mediated virus increase. Cancers (Basel). 12, 1–22. https://doi.org/10.3390/cancers12040798

Dyer, A.; **Baugh, R**.; Chia, S.L.; Frost, S.; Iris, Jacobus, E.J.; Khalique, H.; Pokrovska, T.D.; Scott, E.M.; Taverner, W.K.; Seymour, L.W.; Lei-Rossman, J. “Turning cold tumours hot: oncolytic virotherapy gets up close and personal with other therapeutics at the 11th Oncolytic Virus Conference.” Cancer Gene Therapy 2018, Sep 4.

Abstract

Glioblastoma (GBM) is a highly aggressive brain tumour in adults, often becoming resistant towards conventional therapy of radiotherapy and temozolomide (TMZ) chemotherapy. The oncolytic herpes simplex virus-1 (oHSV-1) G207 is a promising approach for GBM immunotherapy, capable of selective infection, replication and causing cell lysis within GBM but not healthy cells. However, G207 has demonstrated only limited efficacy in GBM clinical trials.

The Natural Killer Group 2 Member D (NKG2D) receptor plays a key role in the innate immune control of cancers. The ligands for this receptor (NKG2DLs) are minimally expressed or absent on healthy cells, while stressed or malignant cells upregulate NKG2DLs, resulting in innate immune activation. We have developed a strategy targeting upregulated NKG2DLs on GBM cells with a bispecific T cell engager (BiTE) consisting of a recombinant NKG2D receptor linked to an anti-CD3 domain. Simultaneous binding of the NKG2D BiTE to NKG2DLs on GBM cells and CD3 on T cells causes antigen-independent T cell activation, pro-inflammatory cytokine release, and tumour cell death.

Here, we engineer G207 to express the NKG2D BiTE from infected GBM cells, allowing the G207-NKG2DBiTE virus to combine direct viral oncolysis and BiTE-mediated cytotoxicity via activation of local T cells. NKG2DL expression was elevated on GBM cells following pre-treatment with sublethal doses of TMZ and radiation, sensitising them to NKG2D BiTE activity and achieving synergistic cytotoxicity with G207-NKG2DBiTE virus.

We also demonstrate a novel strategy for targeting glioma stem-like cells (GSCs), which are a source of resistance to conventional therapies. In contrast to differentiated GBM cells, GSCs are non-permissive to G207 infection, but they

remain sensitive to NKG2D BiTE. Therefore, we propose a potential model for targeting GSCs in heterogeneous tumours, whereby differentiated GBM cells infected with G207-NKG2DBiTE virus produce NKG2D BiTE locally, directing T cell cytotoxicity towards the GSC sub-populations in the tumour microenvironment.

Acknowledgements

Looking back at my last four (and a half – thanks, COVID…) years, I can honestly say I have loved every minute. So much of this is down to the people I shared my lab space with, thanks to their continued support and friendship throughout this DPhil. I am truly fortunate to be able to say I have worked with the brightest, most talented, most caring, and funniest bunch of Oncolleagues that I could have ever asked for. With people like them working in the field of oncology, cancer doesn't stand a chance.

Firstly, I'd like to acknowledge Professor Len Seymour for his guidance, wisdom, humour, approachability, and mentorship. I wouldn't be the scientist I am today without his support. Also, acknowledgement must also be given to Len for cultivating such a lively, lovely, intelligent, driven, and diverse lab group, that I am honoured to be a part of.

I could not have done much of this work, were it not for Dr Hena Khalique. She has been with me every step of the way throughout my DPhil journey and has gone far, far above and beyond what was asked of her. Her valuable insight, feedback, proof-reading, ideas, and mentorship have steered me through my DPhil, especially in this final year. I will never be able to put into words the scale of my appreciation towards her.

I must also thank Brain Research UK, and all their donors, for funding my studies. It has given me a tremendous sense of drive and motivation to know I am being sponsored by such a brilliant charity. Following the pandemic, their 6-month extension funding made a significant impact, enabling me to continue generating data for this thesis.

It is not often you find a lab group that have their own nickname and logo. Len's Angels are truly unique. I've had the absolute pleasure of working alongside some remarkable people. Every single member, past and present, has had a profound impact on me, and have made my experience in the lab such a joy. I could always be sure of a laugh, a few donuts, and even scientific discussion whenever I entered the office. Thank you especially to Dr Arthur Dyer for welcoming me into the group, showing me the ropes and being a constant source of strength, wisdom, and warmth. Also, special thanks to Dr Janet Lei-Rossmann, who laid the groundwork for this project and was a helping hand when things didn't go to plan.

I have been fortunate enough to think of my colleagues as friends. To Dr Sally Frost, Dr Ellie Scott, Dr Tzveta Pokrovska and Dr William Taverner, thank you for your continued friendship and guidance to this day, despite moving on from the lab. I am extremely lucky to have worked with you all and learnt a great deal from each of you. It was a privilege to be your Quiz Master every Tuesday. To Flurin Caviezel, thank you for bringing so much life and joy to the lab each and every day. To my current Oncolleagues, Dr Ahmet Hazini, Alex Stephens, Mahnoor Nadeem, Peter

Wan, Kate Friesen, Emma Page, Yuqian Ou, Sichen Liu, Anna Zavalani, Jamie D'Costa, and Constantinos Demetriou, thank you all for making each day an adventure. I have cherished working with each of you, and am grateful for all the support and friendship, especially in the past few months. Thank you also to the other post-Docs and students, Dr Kerry Fisher, Dr Brian Lyons, Dr Margaret Duffy, Dr Egon Jacobus, Dr Phil Jakeman, Dr Sarah Larkin and Dr Weiheng Su, who have all imparted invaluable advice.

To my dear friends across the pond, Dr Sidney May, and Dr Matt Holmes, you both have been a tremendous source of comedy and friendship. To my BGS mates, Alfred Chapman, Pete Gouldesbrough, Will Garforth, and Will Paget, I have treasured our friendship over the many years. I am so grateful for all your support, especially in these recent months. To the Pembroke Crew, Matt, and Britt, thank you for your friendship in Oxford.

Beth, you have been my rock since day one in Oxford, and I couldn't have gotten this far without you. I am so proud of us going through this PhD journey together. Thank you for the endless love and support, and for helping me get across the finish line. We have both come so far since we first met on our first day in Oxford, and who knows where we will go next!

And finally, thank you to my family, Mum, Dad, Grandpa and Will, all of whom I dedicate this thesis to. Mum, Dad, and Grandpa, thank you for all that you did bringing me up, all the sacrifices made, and for all the unwavering love and support. Will, thanks for being the best Big Bro and role model I could ask for. I hope I have made you all proud. Also thank you to most recent members of my family, Laura, and Freya, who have been a source of strength and optimism.

Murphy's Law *– "Anything that can go wrong, will go wrong…"*

Cole's Law *– "Diced cabbage and mayonnaise*"

Table of Contents

A statement addressing the impact of the COVID-19 pandemic upon this thesis..... i
Declaration of Authentication ii
Publication note iii
Abstract iv
Acknowledgements vi
Table of Contents viii
List of Figures xii
List of Tables xiv
List of Abbreviations xv

1 Introduction 1

1.1 Introduction to cancer 1
1.1.1 Cancer Biology 1
1.1.2 Conventional cancer therapies 1
1.2 Cancer and the immune system 3
1.2.1 Introduction to cancer and the immune system 3
1.2.2 Cancer immune evasion 5
1.2.2.1 Immune evasion in the tumour microenvironment 5
1.2.2.2 Immune checkpoints 8
1.2.2.3 Deficiencies in antigen presentation 9
1.3 Cancer immunotherapy 10
1.3.1 Introduction to cancer immunotherapy 10
1.3.2 Cancer vaccines 10
1.3.3 Monoclonal antibodies 11
1.3.4 Immune checkpoint blockade 12
1.3.5 Adoptive cell therapies 13
1.3.6 Bispecific T cell Engagers 14
1.4 Glioblastoma 17
1.4.1 Overview 17
1.4.2 Challenges to treating GBM 18
1.4.2.1 Resistance to conventional therapy 18
1.4.2.2 Glioma stem-like cells 19
1.4.2.3 Heterogeneity 20
1.4.2.4 Blood brain barrier 20
1.4.2.5 Tumour microenvironment 21
1.4.3 GBM immunotherapy 23
1.4.3.1 ACT for GBM 23
1.4.3.2 BiTEs as GBM therapy 23
1.5 Oncolytic viruses 24
1.5.1 Introduction to oncolytic viruses 24
1.5.2 'Arming' oncolytic viruses 26
1.5.3 Delivery of oncolytic viruses 29
1.6 Oncolytic Herpes Simplex Viruses 31
1.6.1 Herpes Simplex Virus-1 31
1.6.2 Achieving cancer-selectivity with oHSV-1 mutants 34
1.6.3 'Armed' oHSV-1 39
1.6.4 oHSV-1 in GBM 41
1.7 Effects of oncolytic viruses on the GBM tumour microenvironment 47
1.8 NKG2D receptor and its ligands 49
1.8.1 NKG2D receptor and its ligands 49
1.8.1.1 NKG2D receptor 49
1.8.1.2 NKG2D ligands 50
1.8.2 NKG2DL expression in healthy cells and autoimmunity 52
1.8.2.1 Cell stress induces NKG2DL mRNA and protein expression 53
1.8.2.2 DNA damage induces NKG2DL expression 53

1.8.2.3 Post-transcriptional regulation of NKG2DL expression during cell stress 54
1.8.3 NKG2DLs in virally infected cells 56
1.8.3.1 NKG2DL expression is induced in virally infected cells 56
1.8.3.2 Viral evasion of the NKG2D immune response 57
1.8.4 NKG2DL expression in transformed cells 59
1.8.4.1 Transformed cells have upregulated NKG2DL expression 59
1.8.4.2 Cancer strategies to evade NKG2D immune response 62
1.8.5 Strategies employed by the immune system to counter viral and tumour immune evasion 63
1.9 Thesis overview and aims 65
1.9.1 Thesis overview 65
1.9.2 Thesis aims and hypotheses 67

2 Materials and methods 68

2.1 Cell lines and tissue culture 68
2.1.1 Cell lines and passage 68
2.1.2 Storage of cell lines 69
2.1.3 Cell seeding 70
2.2 Flow cytometry 70
2.2.1 Cell dissociation for flow cytometry 70
2.2.2 Cell surface staining 70
2.2.3 Intracellular staining 71
2.2.4 Antibodies 72
2.2.5 Data acquisition and analysis 73
2.3 rhNKG2D 74
2.3.1 Conjugation of NKG2D-Biotin 74
2.3.2 Optimisation of rhNKG2D-Fc-Bio staining 75
2.4 Immune cell isolation, culture, and assays 75
2.4.1 General statement 75
2.4.2 Isolation of human PBMC-derived monocytes and lymphocytes 76
2.4.3 Differentiation and polarisation of macrophages 77
2.4.4 T cell isolation 78
2.4.5 T cell co-culture and BiTE assays 78
2.4.6 Characterisation of T cell activation and target cell viability 79
2.4.7 T cell co-culture and virus assays 80
2.4.8 Lactate dehydrogenase release cytotoxicity assays 80
2.4.9 MTS viability assays 81
2.4.10 BiTE conditioned media on ascites polarised macrophages 82
2.5 Pre-treatment assays 83
2.5.1 BiTE with G207 infection 83
2.5.2 TMZ and radiation pre-treatment 83
2.6 Molecular cloning 84
2.6.1 Agarose gel electrophoresis 84
2.6.2 DNA purification from agarose gels 85
2.6.3 DNA restriction digests 85
2.6.4 Cloning of NKG2D BiTE into pTransfer plasmid by Gibson Assembly 85
2.6.5 Bacterial transformation 87
2.6.6 DNA plasmid preparation and purification 87
2.6.7 DNA quantification 88
2.6.8 DNA sequencing 88
2.7 NKG2D BiTE 88
2.7.1 NKG2D BiTE sequence and structure 88
2.7.2 Production of NKG2D BiTEs 89
2.7.3 SDS-PAGE gel electrophoresis 90
2.7.4 Immunoblotting 90
2.7.5 Enzyme-linked immunosorbent assay (ELISA) to assess BiTE concentration 91
2.8 G207-NKG2DBiTE and G207-ControlBiTE virus cloning 92
2.8.1 Production of DH10β competent cells with fHSVQuik-1 BAC 94
2.8.2 Generation of fHSVQuik-1-BiTE BAC plasmids 95

2.8.3 Transfection of HSVQuik-1-BiTEs and excision of the BAC to produce viral particles 96
2.8.4 Isolation of G207-NKG2DBiTE and G207-ControlBiTE viral clones 98
2.8.5 Assessment of BiTE production by G207-NKG2DBiTE and G207-ControlBiTE viruses 99
2.9 Production and characterisation of G207-NKG2DBiTE and G207-ControlBiTE viruses 100
2.9.1 Amplification of armed G207 viruses 100
2.9.2 Purification of armed G207 viruses 101
2.9.3 PicoGreen assay 104
2.9.4 G207 titration by plaque-forming agar assay 105
2.9.5 G207 infection assays 105
2.9.6 Quantification of NKG2D BiTE production from G207-NKG2DBiTE virus-infected cell lines 106
2.9.7 U87 GSC infection conditions 107
2.9.8 Quantification of soluble NKG2DLs 107
2.10 Patient-derived GBM samples 107
2.10.1 General statement 107
2.10.2 Primary GBM sample preparation 108
2.10.3 Primary GBM staining 108
2.10.4 Primary GBM BiTE and virus assays 109
2.11 Statistical tests 109
2.11.1 Tests of significance 109
2.11.2 Bliss independence score 110

3 Targeting NKG2DLs with BiTEs 111

3.1 Introduction 111
3.2 Chapter hypothesis and aims 113
3.2.1 Hypothesis 113
3.2.2 Chapter aims 114
3.3 Results 115
3.3.1 Expression of surface NKG2DLs on cancer cell lines 115
3.3.2 Comparison of different orientations for NKG2D BiTEs 118
3.3.3 Investigating the dose-dependent response to NKG2D BiTE 121
3.3.4 Evaluating NKG2D BiTE activity and T cell activation profile against GBM cell lines 123
3.3.5 Assessing the specificity of the NKG2D BiTE compared to a BiTE targeting PD-L1 128
3.3.6 Activated T cells express NKG2DLs 132
3.3.7 Determining surface expression of NKG2DLs in primary ex vivo GBM samples 134
3.3.8 Immunophenotyping primary GBM tissue 135
3.4 Discussion 137
3.5 Conclusions 144

4 Combining NKG2D BiTE with oHSV-1 and conventional GBM therapy 146

4.1 Introduction 146
4.2 Chapter hypothesis and aims 149
4.2.1 Hypothesis 149
4.2.2 Chapter aims 149
4.3 Results 150
4.3.1 Effects of oHSV infection on expression of NKG2DLs in infected cells 150
4.3.2 Combining G207 oHSV-1 and NKG2D BiTE immunotherapies 153
4.3.3 TMZ chemotherapy increases surface NKG2DL expression on GBM cells 158
4.3.4 Radiation increases surface NKG2DL expression on GBM cells 160
4.3.5 Pre-treatment of U87 cells with TMZ and radiation enhances NKG2D BiTE-mediated T cell activation 164
4.3.6 Pre-treatment synergises with NKG2D BiTE-mediated cytotoxicity of U87 cells 169
4.3.7 Pre-treatment does not sensitise macrophages to NKG2D BiTE immunotherapy .. 173
4.3.8 NKG2D BiTE activity triggers macrophage polarisation via soluble mediators 178
4.4 Discussion 184

4.5 Conclusions 189

5 Arming oHSV-1 with NKG2D BiTE for use alongside conventional GBM therapy 190

5.1 Introduction 190
5.2 Chapter hypothesis and aims 193
5.2.1 Hypothesis 193
5.2.2 Aims 193
5.3 Results 194
5.3.1 Design and engineering of oHSV expressing NKG2D BiTE 194
5.3.2 Characterisation of G207-NKG2DBiTE and G207-ControlBiTE clones 195
5.3.3 Functional testing of G207-NKG2DBiTE and G207-ControlBiTE viruses 200
5.3.4 Quantification of NKG2D BiTE production from G207-NKG2DBiTE-infected cell lines 205
5.3.5 Pre-treatment of TMZ and radiation enhances G207-NKG2DBiTE virus activity 210
5.3.6 Comparing TMZ and radiation pre-treatment versus concomitant treatment alongside G207-NKG2DBiTE virotherapy 221
5.3.7 GSCs are non-permissive to G207 virus but are sensitive to NKG2D BiTE 227
5.3.8 Primary GBM cells are permissive to G207-NKG2DBiTE virus and targeted by NKG2D BiTE 232
5.4 Discussion 236
5.5 Conclusions 242

6 Thesis overview, final discussion, and conclusions 243

6.1 Thesis summary 243
6.2 Final discussion 247
6.3 Concluding remarks 258
References 260

7 Appendices 283

7.1.1 Representative flow cytometry histograms for MICA/B and NKG2DL staining 283
7.1.2 Optimisation of TMZ and radiation pre-treatment dosages 284
7.1.3 Viral quality control assessment, titration, and replicative ability 291
7.1.4 Assessment of shedding of NKG2DLs from GBM cells 293
7.1.5 Pre-treatment of TMZ and radiation enhances G207-NKG2DBiTE virus activity 295
7.2 Supplementary information and tables 297
7.2.1 Recipe table 297
7.2.2 DNA and protein sequences 298
7.2.3 Plasmid maps 300
7.2.4 Oligonucleotides used for PCR and Sanger sequencing 302

List of Figures

Figure 1.1 Schematic of Bispecific T cell Engager (BiTE) structure and function 16
Figure 1.2 Overview of oncolytic virotherapy mechanism of action 25
Figure 1.3 'Arming' oncolytic viruses 29
Figure 1.4 Overview of HSV-1 genome structure 32
Figure 1.5 Overview of HSV-1 lytic infection cycle 33
Figure 1.6 Basis of cancer-selectivity of oHSV-1 39
Figure 1.7 NKG2D receptor and ligands 52
Figure 2.1 Representative flow cytometry gating strategy 74
Figure 2.2 Overview of NKG2D and Control BiTE sequences 89
Figure 2.3 Schematic overview of G207-NKG2DBiTE cloning 93
Figure 2.4 Assessment of successfully recombined viral clones 97
Figure 2.5 Interphase layer of oHSV-1 following density gradient ultracentrifugation 104
Figure 3.1 Expression of surface MICA/B and total NKG2DLs on cancer cell lines. 117
Figure 3.2 Schematic of NKG2D BiTE and mutant Control BiTE orientations 118
Figure 3.3 Assessment of T cell activation in response to both orientations of NKG2D BiTEs and Control BiTEs 121
Figure 3.4 NKG2D BiTE activity dose curve 122
Figure 3.5 Characterisation of T cell activation in response to NKG2D BiTE 127
Figure 3.6 Assessing the specificity of NKG2D BiTE against macrophages 131
Figure 3.7 Surface NKG2DL expression on activated and resting T cells 133
Figure 3.8 Surface NKG2DL expression on primary human GBM cells. 135
Figure 3.9 Immune profile of human GBM tissue 136
Figure 4.1 Effects of infection with G207 oHSV-1 on surface NKG2DL expression 152
Figure 4.2 Combination of G207 oHSV-1 with NKG2D BiTE and T cells in GBM cell lines 157
Figure 4.3 Effect of TMZ on surface MICA/B expression on GBM cell lines 160
Figure 4.4 Effects of radiation on NKG2DL expression on GBM cell lines. 163
Figure 4.5 Surface expression of NKG2DLs on U87 cells pre-treated with conventional GBM therapies 165
Figure 4.6 Conventional GBM therapy pre-treatment enhances NKG2D BiTE-mediated T cell activation 168
Figure 4.7 Conventional GBM therapy pre-treatment synergises with NKG2D BiTE to mediate decrease in U87 viability 172
Figure 4.8 NKG2DL expression on PBMC-derived macrophages after conventional GBM pre-treatment 175
Figure 4.9 Autologous T cell activation in co-culture with autologous PBMC-derived macrophages after conventional GBM pre-treatment 177
Figure 4.10 Effects of NKG2D BiTE-conditioned media on macrophage polarisation 182
Figure 5.1 Selection of G207-NKG2DBiTE and G207-ControlBiTE viral clones 198
Figure 5.2 Time course and dose response of G207-NKG2DBiTE and G207-ControlBiTE viruses 204
Figure 5.3 Quantification of functional NKG2D BiTE production from cell lines infected with G207-NKG2DBiTE 209
Figure 5.4 Assessment of the effects of combination of TMZ and radiation pre-treatment on G207-NKG2DBiTE virus infectivity and T cell activation 213
Figure 5.5 Conventional GBM therapy pre-treatment synergises with G207-NKG2DBiTE virus to decrease U87 viability 217
Figure 5.6 Conventional GBM therapy pre-treatment synergises with G207-NKG2DBiTE virus to increase U87 cytotoxicity. 220
Figure 5.7 Overview of experimental set up for concomitant TMZ and radiation with G207-NKG2DBiTE immunotherapy 222

Figure 5.8 Investigating the effects of concomitant TMZ and radiation on G207-NKG2DBiTE immunotherapy. 226
Figure 5.9 Activity of G207-NKG2DBiTE and free NKG2D BiTE against differentiated versus GSC-like U87 cells 231
Figure 5.10 G207-NKG2DBiTE virus infects human primary GBM cells and triggers NKG2D BiTE-mediated T cell activation 235
Figure 7.1 Representative flow cytometry histograms of cell lines stained for MICA/B and total NKG2DLs 283
Figure 7.2 Effects of TMZ and radiation combinations on NKG2DL expression on GBM cell lines 285
Figure 7.3 Initial investigation into the effects of pre-treatment with 100 μM TMZ and 2 Gy on NKG2D BiTE activity 289
Figure 7.4 G207 and BiTE-armed G207 viral titres and replicative ability. 293
Figure 7.5 Measurement of sNKG2DLs produced from U87 cells infected with G207 viruses 294
Figure 7.6 Conventional GBM therapy pre-treatment synergises with G207-NKG2DBiTE virus to kill U87 cells 296

List of Tables

Table 1.1. Key characteristics of adult glioma subtypes 18
Table 1.2 Overview of Oncolytic viruses in GBM 44
Table 1.3. Clinical trials using oHSV-1 in GBM 46
Table 1.4. Summary of viral NKG2D evasion mechanisms 57
Table 1.5 Summary of cancer immune evasion of the NKG2D response 62
Table 2.1. Culture conditions for cell lines and primary cells 68
Table 2.2 List of antibodies, constructs and dyes used for flow cytometry 72
Table 2.3 Density gradient centrifugation and wash steps to isolate lymphocytes from human peripheral blood 77
Table 2.4 PCR protocol 86
Table 7.1 Recipes for buffers, solutions and media used for multiple applications 297
Table 7.2 Oligonucleotides used for PCR and Sanger sequences 302

List of Abbreviations

β_2-MG	β_2-microglobulin
96F	Flat bottom 96 well plate
96V	V bottom 96 well plate
A3G	Apolipoprotein B-editing complex 3 G
ACT	Adoptive cell therapy
Ad5	Adenovirus serotype 5
ADAM	A disintegrin and metalloprotease
ADCC	Antibody-dependent cellular cytotoxicity
ADCP	Antibody-dependent cellular phagocytosis
ALL	Acute lymphoblastic leukaemia
ANOVA	Analysis of Variance
APC	Antigen presenting cell
ARE	AU-rich element
ATCC	American type culture collection
ATM	Ataxia telangiectasia mutated
ATM	Ataxia telangiectasia, mutated
ATP	Adenosine triphosphate
ATR	ATM- and Rad3-related
ATRX	α-thalassemia/mental-retardation-syndrome-X-linked
AUF1	AU-rich element/poly(U)-binding/degradation factor 1
BAC	Bacterial artificial chromosome
BBB	Blood-brain barrier
BiTE	Bispecific T cell engager
bsAb	Bispecific antibody
CAF	Cancer-associated fibroblast
CAR-T cell	Chimeric antigen receptor T cell
CD	Cluster of differentiation
CDC	Complement-dependent cytotoxicity
cGAMP	Cyclic-GMP-AMP
cGAS	Cyclic-GMP-AMP synthase
Chk	Checkpoint kinase
CMV	Cytomegalovirus
CNS	Central nervous system
CPE	Cytopathic effect
CSC	Cancer stem cell
CSF	Colony stimulatory factor
CSF	Cerebrospinal fluid

CTLA-4	Cytotoxic T lymphocyte-associated antigen
CXCL	C-X-C motif ligand
DAMP	Danger associated molecular pattern
DAP	DNAX activating protein
DC	Dendritic cell
DDR	DNA damage response
DMEM	Dulbecco's Modified Eagle's Medium
DMSO	Dimethyl sulfoxide
dNTP	Deoxynucleotide triphosphate
DPBS	Dulbecco's phosphate-buffered saline
dsDNA	Double stranded DNA
dsRNA	Double stranded RNA
E: T	Effector: Target cell ratio
EBV	Epstein-Barr virus
ECM	Extracellular matrix
EDTA	Ethylenediaminetetraacetic acid
EGF	Epidermal growth factor
EGFR	Epidermal growth factor receptor
EGFRvIII	Epidermal growth factor receptor variant III
eIF	Eukaryotic translation initiation factor
ELISA	Enzyme-linked immunosorbent assay
EnAd	Enadenotucirev
EpCAM	Epithelial cell adhesion molecule
EphA2	Erythropoietin-producing human hepatocellular carcinoma A2 receptor
ER	Endoplasmic reticulum
FAP	Fibroblast activation protein
FasL	Fas ligand
Fc	Fragment crystallisable
FcR	Fragment crystallisable receptor
FCS	Foetal calf serum
FcγR	Fragment crystallisable gamma receptor
FDA	Food and Drug Administration
FGF	Fibroblast growth factor
FLP	Flippase
FRβ	Folate receptor β
GA	Gibson assembly
GADD34	Growth arrest and DNA damage protein 34
GALV	Gibbon ape leukaemia virus
GBM	Glioblastoma
GDNF	Glial cell-derived neurotrophic factor

GFP	Green fluorescent protein
GM-CSF	Granulocyte-macrophage colony stimulating factor
GPI	Glycophosphatidylinositol
GRB2	growth factor receptor-bound protein 2
GSC	Glioma stem-like cell
Gy	Gray
HBV	Hepatitis B virus
HCMV	Human cytomegalovirus
HCV	Hepatitis C virus
HDAC	Histone Deacetylase
HEPES	N-2-Hydroxyethylpiperazine-N'-2-Ethanesulfonic Acid
HGF	Hepatocyte growth factor
HHV	Human herpes virus
HIV-1	Human immunodeficiency virus - 1
HLA	Human leukocyte antigen
HRP	Horseradish peroxidase
HSE	Heat shock element
HSV	Herpes simplex virus
HVEM	Herpesvirus entry mediator
ICB	Immune Checkpoint blockade
ICP	Infected cell protein
IDH	Isocitrate dehydrogenase
IDO	indoleamine-2,3-dioxygenase
IEC	Intestinal epithelial cells
IFN	Interferon
IHC	Immunohistochemistry
IL	Interleukin
IRES	Internal ribosomal entry site
IRF	Interferon regulatory factor
ISG	Interferon stimulated gene
IT	Intratumoural
IV	Intravenous
Klf-4	Krüppel-like factor 4
KSHV	Kaposi’s sarcoma-associated virus
LAG-3	Lymphocyte activation gene - 3
LB	Lysogeny broth
LDH	Lactate dehydrogenase
LOH	Loss of heterozygosity
LoxP	Locus of X-over P1
LPS	Lipopolysaccharide

MAPK	Mitogen-activated protein kinase
MARCH	Membrane-associated RING-CH
MCMV	Murine cytomegalovirus
MCP-1	Monocyte chemoattractant protein 1
MEK	MAPK kinase
MFI	Mean fluorescence intensity
MGMT	methylguanine–DNA methyltransferase
MHC	Major Histocompatibility Complex
MHV	Murine hepatitis virus
MICA	MHC-class-I-polypeptide-related sequence A
MICB	MHC-class-I-polypeptide-related sequence B
miRNA	Micro RNA
miRNA	MicroRNA
MMP	Matrix metalloproteinase
MOI	Multiplicity of infection
mRNA	Messenger RNA
MSC	Mesenchymal stem cell
mTOR	Mammalian target of rapamycin
MTS	[3-(4, 5-dimethylthiazol-2-yl)-5-(3-carboxymethoxyphenyl)-2-(4-sulfophenyl)-2H-tetrazolium, inner salt]
MULT	Murine UL16 binding protein-like transcript
NBM	Neurobasal medium
NDV	Newcastle disease virus
NHL	Non-Hodgkin’s lymphoma
NK	Natural Killer
NKG2A	Natural killer group 2 member A
NKG2D	Natural Killer Group 2 Member D
NKG2DL	Natural Killer Group 2 Member D Ligand
NKT	Natural Killer T cell
O.D	Optical density
OMCP	Orthopox MHC class I-like protein
ORF	Open reading frame
OV	Oncolytic virus
PAMP	Pathogen associated molecular patter
PBMC	Peripheral blood mononuclear cells
PBST	PBS-Tween
PCR	Polymerase chain reaction
PD-1	Programmed cell death protein-1
PD-L1	Programmed death-ligand 1
PE	Phycoerythrin

PI3K	Phosphatidylinositol 3-kinase
PKR	Protein kinase R
PP1α	Protein phosphatase 1 α
pRb	Retinoblastoma protein
PRR	Pattern recognition receptor
PV	Poliovirus
PyV	Polyoma virus
RAE	Retinoic acid early inducible
RFP	Red fluorescent protein
RMFI	Relative mean fluorescence intensity
RPMI	Roswell Park Memorial Institute
RR	Ribonucleotide reductase
RT	Room temperature
scFv	Single chain variable fragment
SDF	Stromal-derived factor
SDS	Sodium dodecyl sulphate
SDS-PAGE	Sodium dodecyl sulphate-polyacrylamide gel electrophoresis
siRNA	Short interfering RNA
sNKG2DL	Soluble NKG2DL
SOC	Catabolite repression medium
STI-1	Stress-inducible protein-1
STING	Stimulator of interferon genes
Strep	Streptavidin
T-VEC	Talimogene Laherparevac
TAE	Tris-Acetate-EDTA buffer
TAM	Tumour associated macrophage
TAN	Tumour associated neutrophil
TAP1	Transporter associated with antigen processing -1
TBK	TANK-binding protein kinase
TCR	T cell receptor
TGF-β	Transforming growth factor β
T_h	T helper
TIGIT	T cell immunoglobulin, ITIM domain
TIL	Tumour infiltrating lymphocyte
TIM-3	T cell immunoglobulin and mucin-domain containing-3
TIMP	Tissue inhibitor of metalloproteinases
TL	True late
TME	Tumour microenvironment
TMZ	Temozolomide
TNF-α	Tumour necrosis factor α

TRAIL	Tumour necrosis factor-related apoptosis-inducing ligand
T_{reg}	Regulatory T cells
ULBP	UL16 binding protein
U_S11	Unique short 11
UTR	Untranslated region
VISTA	V-domain Ig suppressor of T cell activation
vp	Viral particles
VSV	Vesicular stomatitis virus
VV	Vaccinia virus
VZV	Varicella-zoster virus
WHO	World Health Organisation
YT	Yeast extract typtome
ZIKV-LAV	Live attenuated Zika virus
ZPXV	Zoonotic orthopox virus

1 Introduction

1.1 Introduction to cancer

1.1.1 Cancer Biology

Cancer is a neoplastic disease that arises spontaneously because of genetic mutations, driven by genetic and epigenetic factors as well as external carcinogens and factors. These result in aberrantly proliferating cells that can lead to progressive disease and metastasis to distal sites, disrupting the physiology of various organs and tissues. Generally, cancer is characterised by a set of hallmarks including sustained proliferative signalling, evading growth suppressors, immune evasion, replicative immortality, tumour-promoting inflammation, metastasis, angiogenesis, genomic instability, resistance to cell death and deregulated metabolism, as well as more recently defined hallmarks including epigenetic reprogramming, polymorphic microbiomes, senescence and phenotypic plasticity (Hanahan, 2022; Hanahan & Weinberg, 2011).

1.1.2 Conventional cancer therapies

Surgery, chemotherapy, and radiotherapy are traditionally the most common treatments for cancer and are often used in combination to increase efficacy. In theory, the simplest cancer therapy is its physical removal by surgery. However, while surgery can be effective at removing the primary lesion in some cancers, it is often unsuitable for secondary lesions, and even primary lesions may not be

accessible by surgery, or too diffused through the tissue for resection (Arruebo et al., 2011).

Conventional chemotherapy agents, in contrast, aim to kill aberrantly proliferating cancer cells by targeting cellular pathways used for cell growth and cell division, including DNA replication and DNA damage repair (Chabner & Roberts, 2005). However, as these processes are not specific to cancer cells only, this often results in adverse side effects, which affect the quality of life of patients (Carelle et al., 2002). Furthermore, many cancers acquire resistance to chemotherapy, rendering it ineffective (Chabner & Roberts, 2005).

Radiotherapy is a key treatment strategy for many cancers, with approximately half of all cancer patients receiving radiotherapy (Baskar, Lee, Yeo, & Yeoh, 2012). Radiotherapy exposes cancer cells to high energy radiation to induce DNA damage and cell death. This allows the targeting of sites that may not be reachable by surgery, and limits systemic toxicities. However, normal cells in the path of the radiation beam are still damaged by radiation (Baskar et al., 2012), and various factors in the tumour such as hypoxia can limit the sensitivity of cancer cells to radiotherapy (Sørensen & Horsman, 2020).

Together, surgery, chemotherapy and radiotherapy have shown some success, but in many cases are insufficient to achieve a cancer-free survival and often result in relapse. This has led to advances in cancer therapy, such as targeted chemotherapy, advanced radiotherapy techniques and more recently, immunotherapy (discussed in section 1.3).

1.2 Cancer and the immune system

1.2.1 Introduction to cancer and the immune system

The relationship between cancer and the immune system has been investigated for over a century, with early observations that tumours treated with bacterial toxins and bacteria led to tumour regression, and that the induction of fever was essential (Coley, 1895; Hoption Cann, Van Netten, & Van Netten, 2003). Evidence in the latter half of the 20th century has grown in support of the importance of the immune system in cancer, such as the discovery of tumour-specific T cells (Van Der Bruggen et al., 1991), the correlation between tumour infiltrating lymphocytes (TILs) and patient survival (Clemente et al., 1996; Galon et al., 2006), and increased incidence of cancer in immunodeficient mice and humans (G. P. Dunn, Bruce, Ikeda, Old, & Schreiber, 2002).

Despite evidence for a protective role of the immune system, cancers still develop which indicates a means of immune evasion. This process is referred to by Dunn et al. as cancer immunoediting, and consists of three main phases: elimination, equilibrium and escape (G. P. Dunn et al., 2002).

Cancer immunoediting - Elimination

Elimination is the first stage of cancer immunoediting, and likely occurs multiple times during the human lifespan (G. P. Dunn et al., 2002). Elimination involves the recognition and destruction of transformed cells by the innate immune system, such as natural killer (NK), γδ cells and natural killer T (NKT) cells. These cells recognise and kill transformed cells based on their expression of germline-encoded receptors, such as natural killer group 2 member D (NKG2D) (discussed later in section 1.8). These innate immune cells produce inflammatory factors, like interferon gamma (IFN-γ), which activate antigen presenting cells (APCs) such as

dendritic cells (DCs) to take up tumour associated antigens (TAAs) released from lysed cancer cells. The activated APCs migrate to lymph nodes and present TAAs in the context of major histocompatibility complex (MHC) class I and II molecules. In the lymph nodes, T cells are selected and primed through interaction with cognate T cell receptors (TCR) and MHC-peptide on the APC, resulting in T cell activation and proliferation. T cells then egress from the lymph nodes and infiltrate the tumour and kill cancer cells expressing the TAA via TCR-peptide-MHC recognition (G. P. Dunn et al., 2002; Shankaran et al., 2001).

Cancer immunoediting – Equilibrium

The next stage of cancer immunoediting is an equilibrium, which arises when cancer cells survive the elimination stage and can occur over many years. This stage involves a gradual selective pressure applied to the cancer cells by the immune system, leading to the emergence of sub-populations of cancer cells that are less immunogenic and more immunosuppressive over multiple generations (G. P. Dunn et al., 2002; Teng, Swann, Koebel, Schreiber, & Smyth, 2008).

Cancer Immunoediting – Escape

The final stage of cancer immunoediting is escape, whereby cancer cells that have been selected under immune pressure are able to progress and emerge from the dormancy of the equilibrium stage, resulting in tumour growth and possibly metastasis. The selected cancer cells may have escaped immune pressure either by intrinsic mechanisms, such as genetic or epigenetic changes resulting in low immunogenicity, or by extrinsic mechanisms, such as co-opting an immunosuppressive tumour microenvironment (TME) (Bhatia & Kumar, 2014; G. P. Dunn et al., 2002). Mechanisms of cancer immune evasion are discussed below.

1.2.2 Cancer immune evasion

1.2.2.1 Immune evasion in the tumour microenvironment

Extrinsic factors that contribute towards cancer cell escape from immunoediting are often generalised as the TME. The TME is highly complex, consisting of many different cells, cytokines and physical characteristics that establish and maintain an immunosuppressive niche enabling the immune escape of cancer cells.

Cellular components

The cellular components of the TME comprise of both malignant and non-malignant stromal cells. Tumours that advance out of the equilibrium phase and into escape phase of immunoediting often co-opt these stromal cells to aid in evasion of anti-tumour immune responses. Stromal cells in the TME that contribute towards immunosuppression include immune cells, such as tumour associated macrophages (TAMs), myeloid-derived suppressor cells (MDSCs), tumour associated neutrophils (TANs), and regulatory T cells (T_{regs}); and non-immune cells like cancer-associated fibroblasts (CAFs) vascular endothelial cells and pericytes (Labani-Motlagh, Ashja-Mahdavi, & Loskog, 2020).

Macrophages: Macrophages are highly plastic, and can occupy a range of phenotypes, from classically activated, pro-inflammatory M1 macrophages, to alternately activated, anti-inflammatory M2 macrophages (Mantovani, Sozzani, Locati, Allavena, & Sica, 2002). Circulating monocytes migrate into the TME in response to growth factors and cytokines produced by cells in the TME such as vascular endothelial growth factor (VEGF), colony stimulating factor (CSF), granulocyte macrophage-CSF (GM-CSF), Interleukin (IL)-6, IL-10 and transforming growth factor (TGF)-β (Mantovani et al., 2002). Once in the TME, monocytes

differentiate into immunosuppressive M2-like TAMs (Labani-Motlagh et al., 2020; Mantovani et al., 2004). M2-like TAMs then contribute towards tumour progression and immune evasion in several ways, including expression of immunosuppressive ligands (discussed in section 1.2.2.2), like programmed death-ligand 1 (PD-L1) or cytokines like TGF-β or IL-10, and contributing towards angiogenesis (Labani-Motlagh et al., 2020; Mantovani et al., 2004, 2002).

MDSCs: MDSCs are bone marrow-derived immature myeloid cells that comprise a heterogenous population. They migrate towards the TME and contribute towards tumour escape by the secretion of immunosuppressive TGF-β, IL-10, arginase and PD-L1 (Ben-Meir, Twaik, & Baniyash, 2018).

T_{regs}: T_{regs} are cluster of differentiation (CD) 4^+ T cells that differentiate into immunosuppressive phenotypes in response to immunosuppressive cytokines like TGF-β and IL-10. T_{regs} contribute greatly towards immunosuppression in the TME, for instance by producing immunosuppressive cytokines TGF-β and IL-10, contributing to the general immunosuppression milieu (Tanaka & Sakaguchi, 2017). Furthermore, T_{regs} constitutively express the checkpoint receptor cytotoxic T lymphocyte-associated protein 4 (CTLA-4), which binds to CD80/CD86 with high affinity on APCs, out-competing CD28 on conventional T cells and thus reducing T cell co-stimulation (Tanaka & Sakaguchi, 2017). Furthermore, T_{regs} constitutively express the IL-2 receptor (CD25), thus acting as a sink of IL-2 in the TME and limiting TIL proliferation (Tanaka & Sakaguchi, 2017).

CAFs: CAFs can make up a significant proportion of the cells in solid tumours. For instance, in pancreatic and breast cancer, up to 80% of the tumour mass in can consist of CAFs (Gascard & Tlsty, 2016). CAFs contribute towards tumour progression in a range of ways, such as deposition of extracellular matrix (ECM),

secretion of immunosuppressive TGF-β and IL-10, and M-CSF, and promotion of metastasis by expression of matrix metalloproteases (MMPs) (Labani-Motlagh et al., 2020).

Physical characteristics

Acidic pH: Cancer cells shift their metabolism away from aerobic respiration and oxidative phosphorylation and towards glycolysis in a process known as the Warburg effect (Warburg, Wind, & Negelein, 1924). Increased glycolysis results in an extracellular accumulation of lactate and protons, subsequently reducing the pH. In several cancers, the pH in the TME is considerably lower (5.7-7) than in normal tissues (7.4) (Erra Díaz, Dantas, & Geffner, 2018). Acidic pH has been shown to inhibit T cell proliferation, cytokine production and cytotoxicity (Fischer et al., 2007).

Hypoxia: Alongside low pH, tumours are often characterised by hypoxia due to restricted blood supply at the tumour core. Hypoxia not only contributes towards therapeutic resistance and tumour progression, but it also contributes towards immunosuppression in the TME. Hypoxia has been shown to limit T cell proliferation (Caldwell et al., 2001; Lukashev et al., 2006) as well as induce increased expression of immunosuppressive ligands on cancer cells including PD-L1 and human leukocyte antigen (HLA)-G (Y. Li, Patel, Roszik, & Qin, 2018).

Metabolites: The balance of metabolites released into the TME also contribute towards immunosuppression. L-arginine is an essential amino acid for T cells, and is required for expression of CD3ζ, and so TCR functioning is reduced without it (Geiger et al., 2016; Rodriguez, Zea, Culotta, Zabaleta, & Ochoa Augusto C Ochoa, 2002). However, the enzyme arginase is expressed by TAMs, TANs and MDSCs, and converts L-arginine to urea and L-ornithine, reducing TIL TCR function (Szefel, Danielak, & Kruszewski, 2019). Additionally, adenosine triphosphate (ATP),

released into the TME during cellular stress, is broken down into adenosine, which inhibits TIL and NK function (Vigano et al., 2019). Finally, tryptophan is converted to the immunosuppressive metabolite kynurenine by indoleamine-2,3-dioxygenase (IDO), which is released into the TME by tumour cells. Kynurenine in the TME has several effects, including inhibiting NK and $CD8^+$ T cell cytotoxicity, and inducing T_{reg} differentiation and MDSC infiltration (Holmgaard et al., 2015; Hornyák et al., 2018).

ECM: Finally, the physical scaffold of the tumour itself contributes towards immunosuppression. The extracellular matrix (ECM) is a complex network of proteins and proteoglycans but is dysregulated and more abundant in many cancers, comprising up to 60% of the tumour mass in some cases (Henke et al., 2020). ECM in the TME is deposited mostly by CAFs, but also some cancer cells (Henke et al., 2020). The dysregulated and increased deposition of ECM in cancers can physically encapsulate cancer cells, generating a high interstitial pressure and shielding them from exterior threats, as well as contributing towards hypoxia and immune exclusion (Hallmann et al., 2015; Henke, Nandigama, & Ergün, 2020). Finally, TGF-β is deposited on the ECM in a latent form, and so tumour ECM can act as a significant source of TME-derived TGF-β (Henke et al., 2020; Horiguchi, Ota, & Rifkin, 2012).

1.2.2.2 Immune checkpoints

Many cancer cells also control immune anti-cancer immune responses directly with the expression of immunosuppressive ligands on their surface. As mentioned in section 1.2.2.1, stromal cells in the TME frequently express immune checkpoint inhibitors, such as PD-L1 and CTLA-4. Increased expression of immune checkpoint ligands, such as PD-L1, are also observed on many cancer, and triggers T cell

inhibition upon binding to the checkpoint receptor programmed cell death protein-1 (PD-1) on TILs (Wei, Duffy, & Allison, 2018).

As the field advances, more immune checkpoints have been discovered and investigated, such as lymphocyte activation gene-3 (LAG-3), T cell immunoglobulin and mucin-domain containing-3 (TIM-3), T cell immunoglobulin, ITIM domain (TIGIT) and V-domain Ig suppressor of T cell activation (VISTA) (Qin et al., 2019).

1.2.2.3 Deficiencies in antigen presentation

One of the most direct ways for a cancer cell to avoid immune destruction by adaptive immune cells is to prevent their expression of TAAs on MHC-I, also known as HLA-I molecules (Dhatchinamoorthy, Colbert, & Rock, 2021). Many cancers exhibit HLA loss by loss of heterozygosity (LOH) in the HLA locus (Garrido et al., 2017), meaning the cells lose expression of one of their two HLA alleles, thus reducing the range of TAAs that can be presented (Fisher, Hazini, & Seymour, 2021).

Another immune escape mechanism often observed in cancer cells is the loss of expression of β_2-microglobulin (β_2-MG). β_2-MG is essential for HLA-I surface expression, and so loss of β_2-MG expression results in a downregulation of all HLA-I molecules. Cancers with high immune pressure, such as microsatellite unstable colorectal cancer, exhibit greater mutations in β_2-MG and HLA-I alleles, demonstrating the importance of HLA-I expression in cancer immunoediting (Fisher et al., 2021; Ozcan, Janikovits, von Knebel Doeberitz, & Kloor, 2018). Other components of the antigen processing machinery can also be dysregulated in cancers, such as transporter associated with antigen processing-1 (TAP1) (Dhatchinamoorthy et al., 2021).

LOH and loss-of-function mutations in antigen presenting are considered irreversible. However, cancers can also have reversible defects in HLA expression, such as epigenetic hypermethylation of HLA regulatory elements or deficiencies in IFN signalling (Fisher et al., 2021; Garrido et al., 2017).

1.3 Cancer immunotherapy

1.3.1 Introduction to cancer immunotherapy

Cancer immunotherapy is a rapidly expanding field which relies on either using the patient's own immune system or implanted immune cells to eradicate the tumour. The goal of many cancer immunotherapies is to not only eradicate the tumour at primary and secondary sites, but to also develop immunological memory to allow rapid tumour-specific responses should it arise again, such as with the use of cancer vaccines.

1.3.2 Cancer vaccines

The discovery of T cells specific to TAAs (Van Der Bruggen et al., 1991) led to much attention being focussed on developing anti-cancer vaccines. The principle of cancer vaccines is like that of prophylactic vaccination against pathogens, i.e., introducing the immune system to antigens of the target, in this case, TAAs. Challenges of this approach include prediction of TAAs and heterogeneity of TAAs between sub-clonal populations. For a cancer vaccine to be successful, the TAA used would need to be common to all cells, arising from a truncal mutation. Upon identification of a suitable TAA, issues of tumour immune evasion, particularly HLA-loss (as described in section 1.2.2) may affect efficacy.

1.3.3 Monoclonal antibodies

Antibody engineering technology has enabled the large-scale production of monoclonal antibodies (mAbs) with high affinities against specific proteins of interest (Hammers & Stanley, 2014; Köhler & Milstein, 1975; Lu et al., 2020). The first mAb to gain Food and Drug Administration (FDA) approval was Rituximab (Rituxan), an anti-CD20 mAb approved for use for non-Hodgkin lymphoma (NHL) in 1997. Since then, over 30 more mAbs have been approved for use in the USA (Si et al., 2021).

Most therapeutic mAbs are human immunoglobulin G (IgG) and can be one of four different isotypes (IgG1-4), based on their fragment crystallisable (Fc) region, which imparts them with different activities and affinities for Fc-gamma receptors (FcγR) on immune effector cells. For instance, Cetuximab, an anti-epidermal growth factor receptor (EGFR) mAb has an IgG1 structure, which enables the antibody-dependent cellular cytotoxicity (ADCC), antibody-dependent cellular phagocytosis (ADCP) and complement-dependent cytotoxicity (CDC) by engaging FcγRs on immune effector NK cells and macrophages (A. Y. Liu et al., 1987). Meanwhile, Nivolumab (Opdivo), an anti-PD-1 mAb is IgG4, which does not bind to FcγRs with high affinity and so is a poor inducer of ADCC, ADCP or CDC, but neutralises PD-1 on T cells and prevents interaction with PD-L1 (Sundar, Cho, Brahmer, & Soo, 2015).

The therapeutic antibody field is rapidly advancing, however, mAbs still have some limitations, such as antigen loss, heterogeneity of target cells and poor penetration into solid tumours (Friedberg, 2005; Thurber, Zajic, & Wittrup, 2007).

1.3.4 Immune checkpoint blockade

Immune checkpoints refer to a range of inhibitory pathways that are critical for maintaining self-tolerance. However, they can also be usurped by cancer and stromal cells in the TME, which express surface ligands that engage inhibitory checkpoint receptors on immune cells (section 1.2.2.2). Targeting these immune checkpoints has become an enormous focus of the cancer immunotherapy field in recent years, even leading to a Nobel prize for Physiology and Medicine being awarded in 2018.

Immune checkpoint blockade (ICB) involves the use of mAbs against these immune checkpoint molecules, with the aim of inhibiting binding to their partner proteins and thus releasing the 'brakes' on effector immune cells. Ipilimumab (Yervoy) is an anti-CTLA-4 IgG1 mAb that targets CTLA-4 on T_{regs} and activated T cells, preventing its binding to CD80/CD86 on APCs and allowing conventional T cells to receive co-stimulatory signals (Sondak, Smalley, Kudchadkar, Grippon, & Kirkpatrick, 2011; Wei et al., 2018). Ipilimumab received FDA approval in 2011 for treatment of metastatic melanoma (Sondak et al., 2011).

Nivolumab (Opdivo) and pembrolizumuab (Keytruda) are anti-PD-1 IgG4 mAbs approved for the treatment of several tumour types. These mAbs both bind to PD-1 on T cells, preventing it from binding to its ligands PD-L1/PD-L2 on tumour cells and immunosuppressive cells, and releasing T cell inhibition (Wei et al., 2018). The use of ipilimumab, nivolumab and pembrolizumab is being explored extensively in combination with other therapies also, such as cancer vaccines (Saxena, van der Burg, Melief, & Bhardwaj, 2021).

However, clinical success of ICB therapies have been somewhat limited due to adverse effects, such as with Ipilimumab; but also due to the limitations of tumour

immune evasion as discussed in section 1.2.2, such as HLA loss (Schoenfeld & Hellmann, 2020)

1.3.5 Adoptive cell therapies

Adoptive cell therapy (ACT) is based on the expansion or generation of anti-tumour T cells *ex vivo,* before being re-administered to the patient (June, Riddell, & Schumacher, 2015). ACT is typically divided into three main categories: expansion of TILs taken from the tumour itself, transducing peripheral blood mononuclear cell (PBMC)-derived T cells with specifically engineered TCRs against TAAs, and transducing PBMC-derived T cells with a chimeric antigen receptor (CAR) specific to a TAA (June et al., 2015).

The most advanced strategy of ACT is the use of CAR-T cells. CAR-T cells use CD3ζ intracellular signalling domains linked to an extracellular domain with a single chain variable fragment (scFv) specific to a TAA, enabling CAR-T cell activation in a TCR- and MHC-independent manner (June et al., 2015). Later generations of CAR-T cells have also included co-stimulatory domains in the CAR construct to further boost T cell activation (Rohaan, Wilgenhof, & Haanen, 2019).

CAR-T cells have been granted FDA approval for the treatment of haematological malignancies, targeting $CD19^+$ cancer cells in acute lymphoblastic leukaemia (ALL) and NHL (Rohaan et al., 2019).

Although CAR-T cells and other T cell-based ACT strategies have shown some success, they are limited by the cost and time required to expand autologous cells from each patient individually. Therefore, other approaches have been taken to generate allogeneic cell therapies using effector cells with broader cancer-selectivity that can be used as universal ‘off-the-shelf’ therapies, such as γδ T cells,

or CAR-T cells without their endogenous TCR specificities (Perez, Gruber, & Arber, 2020). Additionally CAR-T cells can also trigger some on-target, off-tumour adverse effects, as demonstrated in the case of a patient who died after treatment with CAR-T cells against human epidermal growth factor receptor 2 (HER2), which reacted with HER2-expressing tissue in the lung (Morgan et al., 2010). Furthermore, CAR-T cells can still be limited by general immunosuppression and obstacles posed by the TME.

1.3.6 Bispecific T cell Engagers

Antibody engineering has led to the development of bispecific molecules, capable of binding to two independent epitopes, either on the same cell or crosslinking two cells together. This technology enables directing immune cells towards target cells or achieving greater tumour selectivity.

Bispecific antibodies (BsAbs) can take the conventional IgG structure, complete with an Fc domain, but more recent advances have led to the development of bispecific T cell engagers (BiTEs), consisting of two scFvs that target CD3 on T cells and tumour antigens, joined by a flexible linker. These BiTEs mediate CD3 clustering and T cell activation specifically towards tumour cells expressing the desired surface antigen (Figure 1.1). Crucially, BiTEs can activate T cell independent of TCR specificity, CD28 co-stimulation, HLA expression on target cells, and whether the T cell is $CD4^+$ or $CD8^+$ (Wolf, Hofmeister, Kufer, Schlereth, & Baeuerle, 2005). This makes BiTEs attractive candidates for cancers exhibiting HLA loss (section 1.2.2.3).

BiTEs have several advantages over full-length bsAbs. Firstly, they are considerably smaller (55 kDa), and their single chain nature and no need for

glycosylation means they are easier for cells to produce (Wolf et al., 2005). Additionally, their smaller size endows greater penetration into solid tissues than full chain IgG mAbs (Wolf et al., 2005). The short flexible linker endows BiTEs with enough flexibility to engage two cells independently, but is short enough to encourage the formation of a tight immunological synapse that excludes the inhibitory phosphatase CD45 (Offner, Hofmeister, Romaniuk, Kufer, & Baeuerle, 2006). Together, these characteristics have shown that BiTEs targeting CD3 on T cells to have between 100 – 10000 higher fold activity compared to other CD3 bsAbs (Wolf et al., 2005). BiTE-induced CD3 clustering results in strong intracellular signalling that activates T cells without the requirement for co-stimulation (Wolf et al., 2005). Finally, BiTE-mediated activation of T cells leads to the release of cytotoxic granules containing effector molecules like perforin and granzyme B, which induce caspase 3 and 7 activation in target cells, resulting in target cell death (Wolf et al., 2005).

BiTEs have demonstrated clinical success, with blinatumomab (Blincyto), an anti-CD3-anti-CD19 BiTE gaining FDA approval in 2014 for the treatment of B cell malignancies (Przepiorka et al., 2015). BiTEs targeting other TAAs are also being investigated, such as epithelial cell adhesion molecule (EpCAM), EGFR, HER2, erythropoietin-producing human hepatocellular carcinoma A2 receptor (EphA2) and more (Baeuerle & Reinhardt, 2009).

One major advantage of BiTEs is that they have the potential to activate T cells to a greater level than conventional TCR-mediated activation. Typical tumour cell expression of HLA is estimated to be around 100,000 molecules per cell, with each presenting a single peptide to which a cognate TCR may or may not recognise (Schellens et al., 2015). However, BiTEs target surface molecules that tend to be

upregulated on cancer cells, for example EpCAM has been estimated to be expressed at 1,000,000 molecules per cell (Yao et al., 2013), meaning more binding interactions with BiTEs compared to TCR and peptide: MHC (Freedman et al., 2017).

However, BiTEs are not without their limitations. Due to their small size, BiTEs have a short serum half-life when administered systemically compared to IgG, mostly due to renal clearance (Stork, Campigna, Robert, Müller, & Kontermann, 2009). For example, blinatinomab is administered continuously via intravenous (IV) infusion over the entire course of treatment (Klinger et al., 2012). Although, this can also be considered an advantage, as it enables fine control of drug dosage in real time (Baeuerle & Reinhardt, 2009). Additionally, IV administration of BiTEs may trigger adverse effects such as cytokine release syndrome (Teachey et al., 2013).

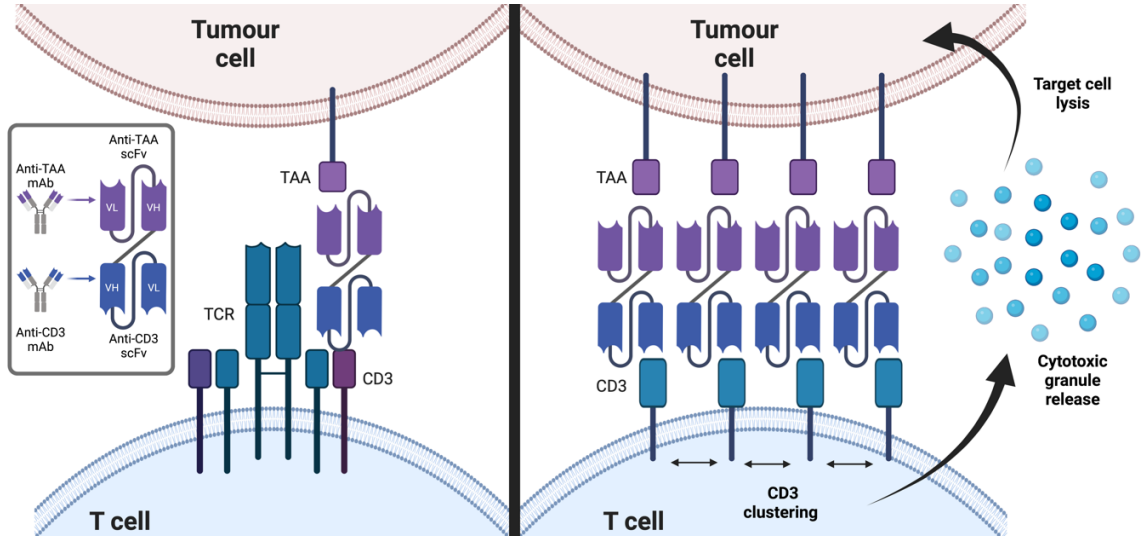

Figure 1.1 Schematic of Bispecific T cell Engager (BiTE) structure and function

(Left) Bispecific T cell engagers (BiTEs) typically comprise of two single chain variable fragments (scFv) taken from a monoclonal antibody (mAb), each consisting of a variable light (VL) and variable heavy (VH) domain. One scFv is specific to CD3 on a T cell, while the other is specific to a tumour-associated antigen (TAA), expressed on the surface of a target tumour cell. (Right) Multiple BiTEs binding to TAAs and CD3 on a nearby T cell forms an immune synapse, triggers CD3 clustering, T cell activation and cytotoxic granule release. The cytotoxic granules released into the immune synapse cause target cell lysis.

1.4 Glioblastoma

1.4.1 Overview

Diffuse gliomas are the most common primary central nervous system (CNS) malignancies in adults, and can be split into subtypes; astrocytomas (World Health Organisation (WHO) grade II-IV), oligodendrogliomas (WHO Grade II-III) and glioblastoma (GBM) (WHO grade IV) (Louis et al., 2021). These different adult diffuse gliomas are differentiated by certain mutations and molecular or genetic profiles, such as mutations in isocitrate dehydrogenase (IDH) (listed in Table 1.1).

GBM is the most common of these adult primary brain malignancies, contributing 15% of total primary brain tumours and 46% of malignant brain tumours with an incidence of 3.2 per 100,000 population (Ostrom et al., 2015). Whilst treatments for other cancers have improved survival, GBM prognosis remains bleak, with a median survival of 14.6 months (McFaline-Figueroa & Lee, 2018). The current strategy to manage GBM includes tumour resection, radiotherapy and temozolomide (TMZ) chemotherapy (Stupp et al., 2005). GBMs are one of the most infiltrative, heterogeneous and immunosuppressive adult tumours (C. Jackson, Ruzevick, Phallen, Belcaid, & Lim, 2011). As a result, nearly all tumours recur and are lethal.

GBMs are highly infiltrative throughout the brain itself but are contained within the brain and don't metastasise to other organs; however, GBMs can become 'multi-focal' with multiple lesions within the brain. (Silbergeld, Rostomily, & Alvord, 1991). The causes of death for GBM patients are multifactorial, but the most common cause of death is severe cerebral oedema and increased intra-cranial pressure, resulting in brain herniation (Silbergeld et al., 1991).

Table 1.1. Key characteristics of adult glioma subtypes

Adult-type diffuse glioma subtypes	Glioblastoma (GBM)	Astrocytoma	Oligodendroglioma
Genes/molecular profiles characteristically altered	*IDH*-WT *TERT* promoter-mut *EGFR* amplification *PTEN*-mut Chromosomes 7/10 copy number	*IDH*-mut *ATRX*-mut *TP53*-mut *CDKN2A/B* deletion	*IDH*-mut 1p/19q co-deletion *CIC*-mut *FUBP1*-mut *NOTCH1*-mut
WHO grade	IV	II, III, IV	II, III
Precursor lesions	No	Yes	Yes

Abbreviations: Isocitrate dehydrogenase (IDH), Wild-type (WT), mutant (mut), Glioblastoma (GBM), Telomerase reverse transcriptase (TERT), Epidermal growth factor receptor (EGFR), Phosphatase and tensin homolog (PTEN), Cyclin-dependent kinase inhibitor (CDKN), α-thalassemia/mental-retardation-syndrome-X-linked (ATRX), Far upstream element binding protein (FUBP1). Table adapted from Louis et al., 2021.

1.4.2 Challenges to treating GBM

1.4.2.1 Resistance to conventional therapy

The initial obstacle posed by GBM therapy is the infiltrative nature of the tumour itself. GBMs lack clear margins, and when combined with the delicate nature of the brain tissue and neural connections, surgical resection of the tumour is a significant challenge. Despite recent advances in surgical techniques, such as using fluorescence to label cancer cells for real-time visualisation of tumour margins during surgery (Maragkos et al., 2021; Neira et al., 2017), malignant cells almost invariably remain infiltrated in the margins, leading to tumour recurrence.

Following resection, most GBM patients undergo a course of concomitant radiation and TMZ chemotherapy. TMZ is a DNA alkylating agent that adds methyl groups at N^7 and O^6 sites on guanines and O^3 site on adenines (S. Y. Lee, 2016). This methylation of guanines leads to mispairing and insertion of thymine in the opposite strand during DNA replication, which can trigger cell cycle arrest and apoptosis (S. Y. Lee, 2016). Meanwhile, radiation also induces DNA damage by introducing double stranded and single stranded breaks (Baskar, Dai, Wenlong,

Yeo, & Yeoh, 2014). GBM patients receive 2 Gray (Gy) radiation administered daily for five days a week for six weeks (60 Gy total), with 75 mg/m^2 TMZ per day for seven days a week. This is then followed up with six cycles of adjuvant TMZ at 150 – 200 mg/m^2 for five days out of every monthly cycle (Stupp et al., 2005).

Despite the combination of TMZ and radiation, median overall survival is only slightly improved (14.6 months) compared to treatment with radiation alone (12.1 months) (Stupp et al., 2005). Patient responsiveness to TMZ has been found to relate to the methylation status of the O^6-methylguanine–DNA methyltransferase (*MGMT*) gene promoter, a DNA repair enzyme that removes the DNA methylation caused by TMZ (Hegi et al., 2005). High levels of MGMT expression in GBM correlates with resistance to TMZ therapy (S. Y. Lee, 2016). Patients with methylated *MGMT* promoters had lower expression due to gene silencing, and so responded to TMZ; whereas *MGMT*-unmethylated promoters were resistant to TMZ (Hegi et al., 2005).

1.4.2.2 Glioma stem-like cells

Cancer stem cells (CSCs) are sub-populations of tumour cells capable of self-renewal and differentiation. CSCs have been identified in several different tumours, including GBM (Singh et al., 2004). Glioma stem-like cells (GSCs) are a key factor in resistance of GBM towards radiotherapy and TMZ (Bao et al., 2006; Qiu et al., 2014), enabling re-population of the tumour with resistant cells (M. Jackson, Hassiotou, & Nowak, 2014). Furthermore, GSCs have demonstrated immune evasion mechanisms such as downregulation of MHC-I (Di Tomaso et al., 2010; W. Yang, Li, Gao, Xiu, & Sun, 2020).

1.4.2.3 Heterogeneity

GBMs are highly heterogeneous, with sub-populations of differentiated tumour cells and undifferentiated GSCs. This heterogeneity is observed not only between patients, but also within the same tumour, making GBM therapy highly challenging (reviewed in (DeCordova et al., 2020)). Sources of this heterogeneity originate from a variety of sources including: histone methylation, DNA methylation, copy number alterations, extrachromosomal DNA, expression changes, genetic mutations, and receptor tyrosine kinase expression (Lauko, Lo, Ahluwalia, & Lathia, 2021). Intratumoural heterogeneity can further arise temporally, such as the primary tumour compared to recurrent, and also spatially (Lauko et al., 2021).

1.4.2.4 Blood brain barrier

The blood-brain barrier (BBB) is a physical barrier that separates the brain vasculature from the brain parenchyma in order to conserve the microenvironment for the correct function of the CNS, and is maintained by prominent tight junctions between endothelial cells, pericytes, smooth muscle cells and astrocyte end-feet processes (Deli, Ábrahám, Kataoka, & Niwa, 2005; S. W. Lee et al., 2006; Liebner et al., 2018). GBM is among the most vascularised human tumours (Takano, Yamashita, & Ohneda, 2010), and the BBB also protects GBM from drugs in the circulation, posing an obstacle to therapy (Dubois et al., 2014). However, in advanced GBM, the new vasculature is often dysregulated and disorganised (Dvorak, 2003), owing to high expression of VEGF (Bergers & Benjamin, 2003). This leaky tumour vasculature then leads to oedema, one of the major morbidities associated with GBM (Silbergeld et al., 1991). However, it also allows increased access for chemotherapeutic molecules and immune effector cells to reach the tumour (Lorger, 2012).

1.4.2.5 Tumour microenvironment

Among the most abundant non-cancerous cells in GBMs are TAMs, which comprise up to 30-70% of the total cells in the tumour (Morantz, Wood, Foster, Clark, & Gollahon, 1979). TAMs may be recruited either from brain-specific tissue-resident macrophages called microglia, or from circulating bone marrow-derived macrophages. In the GBM TME, TAMs tend to be shifted towards an anti-inflammatory, pro-tumour M2-like polarisation state (Ding, Wang, Wang, Yang, & Xue, 2014), and the proportion of M2-like TAMs in gliomas correlates with tumour grade (Komohara, Ohnishi, Kuratsu, & Takeya, 2008). GBM cells trigger microglia/macrophage recruitment with the production of chemokines and factors like monocyte chemoattractant protein-1 (MCP-1) and 3, colony stimulatory factor (CSF), C-X-C motif ligand 1 (CXCL1), glial cell-derived neurotrophic factor (GDNF), ATP, stroma-derived factor-1 (SDF-1), GM-CSF and hepatocyte growth factor (HGF) (Hambardzumyan, Gutmann, & Kettenmann, 2016).

TAMs actively contribute towards tumour growth in several ways. TAMs produce various molecules which increase proliferation and migration of GBM cells *in vitro* and *in vivo*, such as stress-inducible protein-1 (STI-1) (da Fonseca et al., 2014), epidermal growth factor (EGF) (Coniglio et al., 2012), IL-6 and TGF-β (Wick, Platten, & Weller, 2001). Furthermore, TAMs play a significant role in generating and maintaining a highly immunosuppressive TME in GBM with the production of immunosuppressive cytokines, like prostaglandin, TGF-β, IL-6 and IL-10 (DeCordova et al., 2020; Lorger, 2012), poor antigen presentation (Flügel, Labeur, Grasbon-Frodl, Kreutzberg, & Graeber, 1999), expression of PD-L1 (Bloch et al., 2013) and by triggering of Fas- Fas ligand (FasL)-mediated T cell apoptosis (Badie, Schartner, Prabakaran, Paul, & Vorpahl, 2001). MDSCs also are recruited to the

GBM TME and are significant producers of TGF-β and PD-L1 expression (Dubinski et al., 2016; Umemura et al., 2008).

The GBM TME has been shown to have relatively poor infiltration of TILs. Orrego et al. demonstrated using immunohistochemistry (IHC) of a range of GBM samples that $CD3^+$ TILs amounted to an average of 1.6% of total cells, with a majority being $CD8^+$ (Orrego et al., 2018). However, the concept that the brain was immunologically isolated compared to other organs is being challenged, with evidence of functional lymphatics within the brain and trafficking of lymphocytes to the CNS (das Neves, Delivanoglou, & Da Mesquita, 2021). Furthermore, the dysregulated vasculature in GBM can lead to increased patency and allows greater influx of effector immune cells, including TILs (Cribaro et al., 2021).

Furthermore, those T cells that do make it into the TME are often exhausted or dysregulated (Woroniecka, Rhodin, Chongsathidkiet, Keith, & Fecci, 2018). T_{regs} are often also present in the GBM TME (Tumangelova-Yuzeir et al., 2019), with evidence that GBM cells drive the expansion of T_{regs} (H. Wang et al., 2021). T_{regs} contribute further towards GBM immunosuppression with the expression of checkpoint inhibitor molecules and cytokines (Woroniecka et al., 2018).

NK cells are one of the most under-represented immune cells in the GBM TME (around 2% of the total immune cells) (Kmiecik et al., 2013). Despite this, NK cells have been shown to play a role in prolonging survival *in vivo* (Gras Navarro et al., 2014) as well as preferentially killing GSCs *in vitro* (Haspels, Rahman, Joseph, Navarro, & Chekenya, 2018). However, GBM cells also begin to evade NK cell responses, for instance, TGF-β expressed by GBM cells causes downregulation of the activatory NKG2D receptor on NK cells (Crane et al., 2010) and increases NK cell inhibitory receptor expression (Friese et al., 2004). Additionally GBM cells have

been shown to evade NK cell responses by upregulation of HLA-E resulting in NK cell inhibition (Wischhusen, Friese, Mittelbronn, Meyermann, & Weller, 2005).

1.4.3 GBM immunotherapy

As described above, conventional GBM therapies are in desperate need of improvement. Immunotherapy is a highly innovative approach for cancer therapy (section 1.3) and may have a bright future for GBM treatments. Below are a few key examples of GBM immunotherapeutic approaches that highlight some of the approaches under investigation. Oncolytic virotherapy for GBM will be discussed later in a separate section (section 1.6.4).

1.4.3.1 ACT for GBM

ACT therapy (section 1.3.5) has been investigated extensively in GBM (J. Wang et al., 2020). For instance, CAR-T cells targeting HER2, which is upregulated in some GBM patients, is being evaluated in phase I clinical trials. Additionally, a splice variant mutation that is often upregulated in some GBM patients, EGFR variant 3 (EGFRvIII), has been targeted with CAR-T cells; although this has shown limited success and even failed the pilot trial, likely due to loss of EGFRvIII expression in recurrent tumours (O'Rourke et al., 2017; J. Wang et al., 2020). In another example, Weiss and colleagues constructed an NKG2D-CAR-T cell and demonstrated efficacy in a fully immunocompetent orthotopic murine GBM model, which synergised when in combination with radiotherapy (Weiss, Weller, Guckenberger, Sentman, & Roth, 2018).

1.4.3.2 BiTEs as GBM therapy

BiTE therapy (section 1.3.6) for GBM is limited by the BBB, and so most BiTEs used involve a delivery system. For instance, Gardell et al. engineered

macrophages to secrete an anti-EGFRvIII BiTE, which trafficked to the tumour in orthotopic murine models and reduced tumour burden (Gardell et al., 2020), Meanwhile, Choi and colleagues encoded an anti-EGFR BiTE into an EGFRvIII CAR-T cell, which achieved cytotoxicity towards both GBM cells expressing mutated EGFRvIII (via the CAR) and GBM cells that overexpressed non-mutated EGFR (via the BiTE) (Choi et al., 2019). This strategy helped to overcome the limitations described earlier with the EGFRvIII CAR-T cell of antigen loss-mediated escape (O'Rourke et al., 2017).

1.5 Oncolytic viruses

1.5.1 Introduction to oncolytic viruses

There is a considerable overlap in the phenotypes of cancer cells and virally infected cells, including immune evasion, deregulated cellular energetics, prevention of apoptosis and sustained synthesis of genetic information (Seymour & Fisher, 2016). These overlapping phenotypes of virally infected cells and cancerous cells give some viruses an inherent preference towards replicating within cancer cells. Indeed, observations were made as early as the 19th century that cancer patients sometimes went into remission following viral infection (Dock, 1904). In the mid-20th century, WT viruses such as West Nile virus, Adenovirus (Ad) and Mumps, were trialled for the treatment of various cancers, with some promising results. However, as WT viruses were used in these instances, adverse side effects were common (Kelly & Russell, 2007). Interest in the use of viruses for cancer therapy gained momentum again with the advent of genetic engineering in the late 20th century. Efforts were made to engineer new generations of oncolytic viruses (OVs)

that were attenuated to reduce pathogenicity and increase their cancer cell selectivity (Kelly & Russell, 2007).

OVs act on the basic principle of infecting, replicating within, and killing cancer cells but not normal healthy cells (Figure 1.2). Viral replication, production of viral progeny and release of these progeny virions after infected cell lysis then enables subsequent rounds of infection of other cancer cells in the vicinity. Alongside the direct method of action of cancer cell lysis (Dyer et al., 2017), OVs also indirectly contribute towards the anti-cancer response through the release of danger-associated molecular patterns (DAMPs) from the host cell and pathogen-associated molecular patterns (PAMPs) from the viruses themselves (J. Ma et al., 2020). These DAMPs and PAMPs help to trigger pro-inflammatory immune responses within the TME, directed towards the virus itself but also the cancer cells. Release of PAMPs and DAMPs triggers the innate immune system, as well as promoting APC maturation leading to adaptive T cell anti-tumour immune responses (Di Paolo et al., 2009; Ylösmäki & Cerullo, 2020).

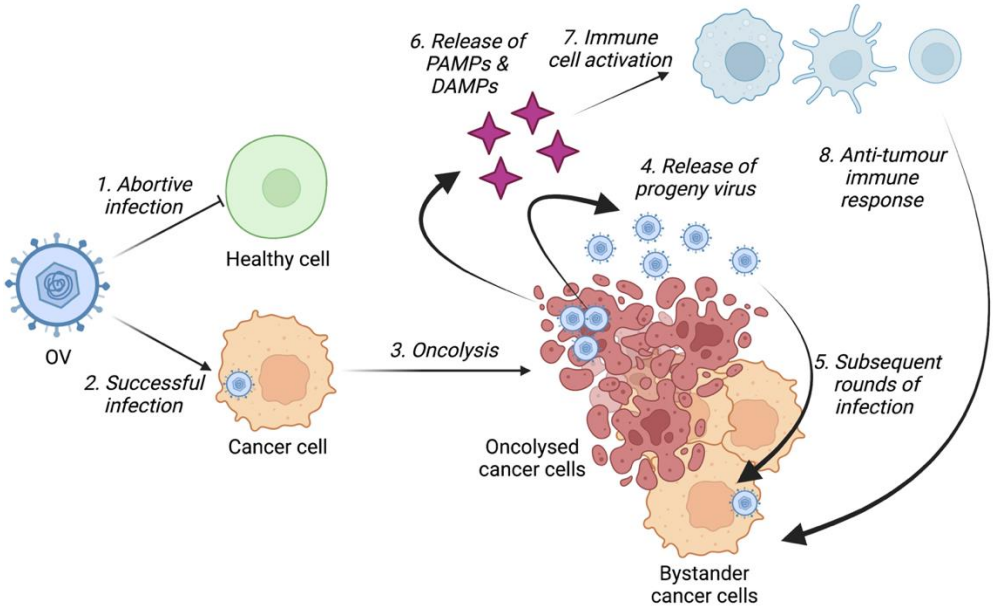

Figure 1.2 Overview of oncolytic virotherapy mechanism of action

(**1**) Oncolytic viruses (OV) are unable to infect and replicate within healthy cells, resulting in abortive infection. (**2**) OV can selectively infect and replicate within cancer cells, resulting in (**3**) cancer cell death (oncolysis). (**4**) Oncolysis releases progeny viral particles into the tumour microenvironment to (**5**) undergo subsequent rounds of infection of nearby cancer cells. (**6**) Release of pathogen-associated molecular patterns (PAMPs) and damage-associated molecular patterns (DAMPs) from viral oncolysis leads to (**7**) immune cell activation and (**8**) anti-tumour immune response. Diagram created with BioRender.com

Cancer selectivity of OVs has been approached in different ways, including: changing the viral entry receptors to target surface proteins upregulated in certain cancers (Pesonen et al., 2012); placing key viral genes under the control of tumour-specific promoters (Chung, Saeki, & Chiocca, 1999); directed evolution of OVs for candidates with enhanced cancer selectivity (Kuhn et al., 2008); or generating OVs by rationally designed, genetically engineered attenuated viruses that rely on dysregulated cancer cell phenotypes for productive infection (Mineta, Rabkin, Yazaki, Hunter, & Martuza, 1995) (reviewed in Russell & Peng, 2007).

The exploration of OVs for cancer therapy has increased dramatically in recent years, with a broad range of viruses being investigated, including measles viruses, reoviruses, coxsackieviruses, vaccinia viruses, herpes simplex viruses, picornaviruses and adenoviruses. Two OVs are currently approved for clinical use: H101 (Oncorine), an engineered serotype 5 Ad which was approved for treatment of head and neck cancer in China in 2005 (Liang, 2018), and Talimogene Laherparevac (T-VEC); Imlygic), an engineered oncolytic herpes simplex virus -1 (oHSV-1), approved by the FDA in 2015 for use against metastatic melanoma (Conry, Westbrook, McKee, & Norwood, 2018; Kaufman et al., 2010).

1.5.2 'Arming' oncolytic viruses

Alongside direct killing of infected cancer cells (oncolysis), and indirect anti-tumour response triggered by the release of DAMPs and PAMPs, OVs may be

'armed' with effector molecules. This strategy involves the engineering of OVs to express therapeutic transgenes as they replicate within the TME, enabling the OVs to also behave as gene therapy vectors (reviewed in Hermiston & Kuhn, 2002; Wan et al., 2021). By localising expression of OV-encoded transgenes to the TME, an added degree of selectivity is gained for the transgenes, thus allowing for the use of biologics that would otherwise not be suitable for systemic administration (Figure 1.3).

OVs have been armed to express a range of different molecules, including cytokines, (Conry et al., 2018; Saha, Martuza, & Rabkin, 2017), full-length antibodies (B. Xu et al., 2021), pro-drug activating enzymes (Cloughesy et al., 2018), fusogenic proteins (S. Thomas et al., 2019), proteins from a different virus (Ghonime et al., 2018), and BiTEs (Arnone et al., 2021; Freedman et al., 2018, 2017; Khalique et al., 2021; Scott et al., 2019). Many of these examples will be discussed in greater detail later in this chapter, although given the subject of this thesis, the use of BiTEs with OVs will be the area of focus for this section.

As described in Section 1.3.6, BiTEs are capable of activating T cells in a TCR-independent manner by crosslinking CD3 on a T cell with an antigen on the surface of a target cell. The first BiTE to be encoded in an OV was a BiTE targeting EphA2 from an oncolytic vaccinia virus (VV), which significantly enhanced tumour cell killing *in vitro* and *in vivo* (Yu et al., 2014). In light of the success from this strategy, other BiTEs targeting TAAs have been encoded into OVs, such as EGFR and EpCAM (Fajardo et al., 2017; Freedman et al., 2017)

By expressing BiTEs from an OV, it enables the targeting of tumour antigens which may be expressed on other tissues in the body without fear of the BiTE reaching those sites at active concentrations. In the example of the EpCAM BiTE,

although EpCAM is upregulated on many epithelial cancers, it is also expressed by most epithelial cells and so would be an unsuitable BiTE target for systemic administration. A phase I clinical trial using systemic administration of MT110, an EpCAM BiTE, the majority of patients experienced significant target-related adverse effects (Kebenko et al., 2018). However, Freedman et al. engineered an oncolytic adenovirus, Enadenotucirev (EnAd), to locally express an EpCAM BiTE, and demonstrated BiTE-mediated destruction of $EpCAM^+$ tumour cells when infected with EnAd-EpCAM BiTE virus (Freedman et al., 2017).

OVs can also be armed to express BiTEs targeting other stromal cells within the TME that contribute towards tumour progression and immunosuppression but are otherwise insensitive to OV oncolysis. For example, Scott et al. armed EnAd with BiTEs and tri-valent T cell engagers (TriTEs) targeting CD206 or folate receptor β (FRβ) to direct T cell cytotoxicity towards immunosuppressive TAMs (Scott et al., 2019). OVs such as EnAd and VV also have been engineered to express a BiTE targeting fibroblast activation protein (FAP), to kill immunosuppressive CAFs (Freedman et al., 2018; Yu, Hong, & Song, 2017). Furthermore, Khalique et al. engineered an oHSV-1 with a BiTE targeting PD-L1, which targeted both $PD\text{-}L1^+$ tumour cells and TAMs (Khalique et al., 2021)

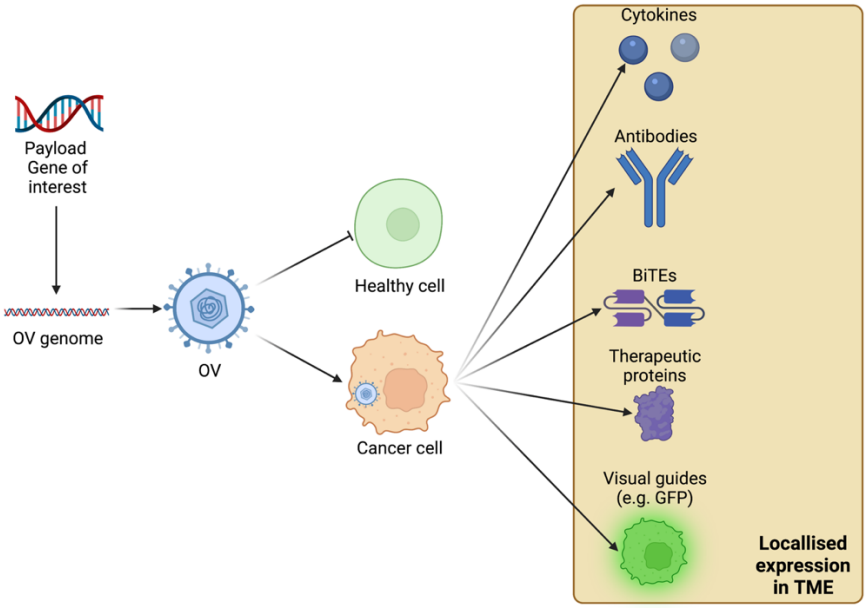

Figure 1.3 'Arming' oncolytic viruses
Armed oncolytic viruses (OVs) involve inserting the gene of interest of the 'Payload' into the OV genome. The OV then selectively infects and replicates within cancer cells but not healthy cells. Selective infection of cancer cells leads to localised expression of the desired payload within the tumour microenvironment (TME). Localised expression restricted to the TME allows for the use of therapeutic proteins that would otherwise not be suitable for systemic use, such as cytokines, antibodies, bispecific T cell engagers (BiTEs) or other therapeutic proteins. Cancer-selective infection also allows for visualisation of infected cancer cells, for example with the use of green fluorescent protein (GFP). Diagram created with BioRender.com.

1.5.3 Delivery of oncolytic viruses

The cancer-selective nature of OVs allows some of them to potentially be administered systemically via IV injection in relative confidence that the virus will circulate in the body without successfully infecting non-cancerous cells. This also means in theory, the virus could reach distal metastatic sites or difficult-to-reach primary sites via systemic administration, that would otherwise not be possible by direct intratumoural (IT) administration. The major limitation of systemic OV delivery, however, is ensuring the virus reaches the tumour cells at a therapeutically effective concentration, and that the OV is not cleared and neutralised by the patient's immune system before it reaches the tumour (Ferguson, Lemoine, & Wang, 2012). Antibodies, complement, antiviral cytokines and viral sequestration by the liver and

spleen all contribute towards the challenge of IV delivery for OVs (Ferguson et al., 2012). Furthermore, physical barriers such as the ECM, overcoming the high interstitial pressure of tumours for extravasation, and in the case of GBM, getting through the BBB (Ferguson et al., 2012).

For example, it is estimated that around 67% of the population in the United States is seropositive for herpes simplex virus-1 (HSV-1) (F. Xu et al., 2006), and so systemic oHSV-1 administration would be unsuitable oHSV-1. Likewise, pre-existing immunity towards reovirus, VV and some Ad serotypes limit the use of these viruses systemically (Ferguson et al., 2012).

Nevertheless, some OVs have demonstrated success via IV administration. Samson et al. demonstrated evidence of viral infection and replication in GBM tumours using IV delivery of an oncolytic reovirus, indicating the virus had not only remained stable in the blood, but also crossed the BBB (Samson et al., 2018).

Efforts have also been made to use OVs that are less seroprevalent to evade viral neutralisation. EnAd is a chimeric adenovirus (Ad) generated via directed evolution by serial passage of various Ad serotypes in cancer cells under conditions that encourage viral recombination, resulting in an Ad3/Ad11p chimera (Kuhn et al., 2008). The viral capsid is derived from Ad11p, a serotype with low seroprevalence in western populations, giving EnAd enhanced stability in whole human blood compared to other widely used serotypes (Di, Seymour, & Fisher, 2014)

Most OVs, however, are currently administered via IT injection directly into the lesion(s). In the example of T-VEC, the FDA-approved oHSV-1 therapy for metastatic melanoma, virus is administered IT to the dermal or superficial lesions guided by sight or palpation; or guided by ultrasound for deeper nodules (Conry et al., 2018).

However, IT injection is also not without its limitations. Tumours may possess multiple nodules, or may be spread out over a wide area of tissue, or be inaccessible for injection altogether (Aldrak et al., 2021). In the context of GBM OV therapy, virus is typically administered following debulking surgery to the surgical cavity, However, the cavity can quickly fill up with blood and cerebrospinal fluid (CSF), washing out the virus (Kaur, Antonio Chiocca, & P. Cripe, 2012).

1.6 Oncolytic Herpes Simplex Viruses

1.6.1 Herpes Simplex Virus-1

HSV-1 is an enveloped, large double stranded DNA (dsDNA) virus, with a genome of around 150 kb. HSV-1 is highly prevalent in humans, with an estimated 67% of the population being seropositive (F. Xu et al., 2006). HSV-1 is neurotropic, and can establish life-long latency in sensory neurones, to then re-establish a lytic lifecycle periodically, where it emerges to infect epithelial cells, resulting in cold sores (Nicoll, Proença, & Efstathiou, 2012).

A diagram of the HSV-1 viral structure and genome is displayed in Figure 1.4, while an overview of the HSV-1 lytic lifecycle is outlined in Figure 1.5.

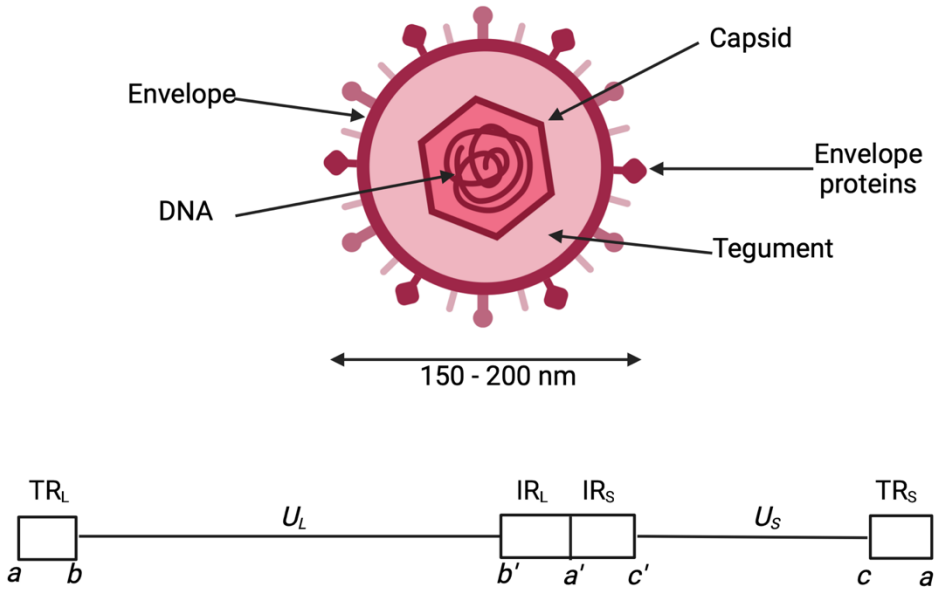

Figure 1.4 Overview of HSV-1 genome structure
(**Top**) HSV-1 viral particle consists of a capsid containing a double stranded DNA (dsDNA) genome. Surrounding the capsid are a host of tegument proteins, followed by an outer lipid envelope. The envelope is studded with envelop glycoproteins used for viral attachment and cellular entry. The overall size of the HSV-1 particle is 150 – 200 mm. (**Bottom**) Linear overview of the viral genome structure, consisting of unique long (U_L) and unique short (U_S) sequences, flanked by terminal inverted repeats: terminal repeat long (TR_L; *ab*), terminal repeat short (TR_S; *ca*), internal repeat long (IR_L; *b'a'*) and internal repeat short (IR_L; *a'c'*). Diagram created with BioRender.com.

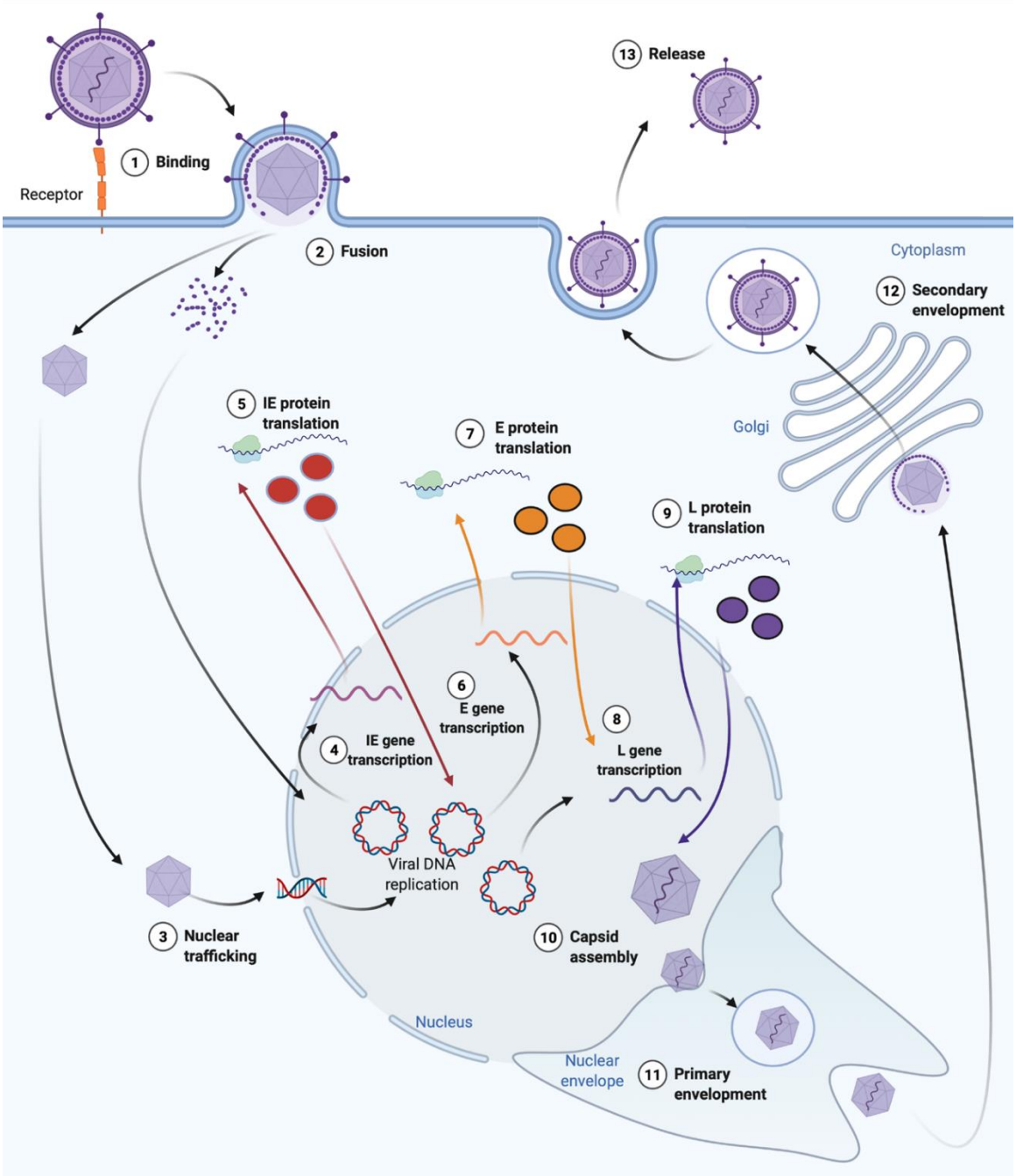

Figure 1.5 Overview of HSV-1 lytic infection cycle

(**1**) Herpes simplex virus-1 (HSV-1) binds to cell surface receptors herpesvirus entry mediator (HVEM), nectin-2 and 3-O-sulphated heparin sulphate, which enables (**2**) membrane fusion followed by viral capsid and tegument protein entry into the cytoplasm. (**3**) Viral capsid is trafficked towards the nucleus and dsDNA genome is delivered into the nucleus. Double-stranded DNA (dsDNA) genome circularises and (**4**) transcription of immediate early (IE) genes begins, leading to the (**5**) translation of IE proteins. IE proteins mediate (**6**) transcription of Early (E) genes and DNA replication. (**7**) E genes are translated and mediate further DNA replication and (**8**) late (L) gene transcription. (**9**) L proteins are translated, including structural capsid proteins. (**10**) Viral capsid assembly and genome packaging in the nucleus. (**11**) Capsid undergoes primary envelopment through the nuclear membrane and subsequent de-envelopment before being released into cytoplasm. (**12**) Viral capsid is trafficked towards the endosomal compartments, where it is equipped with tegument proteins and undergoes secondary envelopment in the Golgi apparatus. (**13**) Fully mature HSV-1 particle is trafficked

towards the cell surface membrane for release by exocytosis. Diagram created with BioRender.com.

1.6.2 Achieving cancer-selectivity with oHSV-1 mutants

Within the 150kb HSV-1 genome, 30kb are nonessential. This allows a great deal of flexibility for modification and attenuation of the virus without making it incapable of infection and replication. In addition, its large genome size allows the insertion of several genes of interest without hampering the viral replicative ability. These characteristics have led to oHSV-1 being among the most studied OVs, as well as the first genetically modified OV (Martuza, Malick, Markert, Ruffner, & Coen, 1991).

One of the most critical genes in generating cancer-selective oHSV-1 is *γ34.5* gene, of which HSV-1 has two copies. To ensure biological safety and tumour selectivity, all oHSV-1 candidates thus far have had deletions in both copies of the *γ34.5* gene, encoding the viral infected cell protein 34.5 (ICP34.5). ICP34.5, also known as the neurovirulence gene, has a number of roles, including antagonism of the protein kinase R (PKR) (Bin He, Gross, & Roizman, 1997). PKR is a double stranded RNA (dsRNA)-dependent kinase and plays a vital role in the anti-viral defence for cells. PKR senses the dsRNA produced during viral replication and becomes activated, but can also become activated in response to cell stress, lipopolysaccharide (LPS) and IFN (Williams, 1999). Once activated, PKR phosphorylates the α subunit of eukaryotic translation initiation factor 2 (eIF-2α), inducing a global inhibition of translation in the cell (Williams, 1999). When infected with WT HSV-1, ICP34.5 then recruits protein phosphatase 1 α (PP1α) to dephosphorylate eIF-2α, thus counteracting the PKR response and enabling translation of viral polypeptides (Bin He et al., 1997).

Cancer cells often have a suppressed PKR response as a consequence of hyperactive Ras signalling (Farassati, Yang, & Lee, 2001) or mitogen-activated protein kinase (MAPK) kinase (MEK) (Smith et al., 2006). As a result, the dysregulated PKR phenotype in cancer cells complements *γ34.5*-deleted oHSV-1, allowing selective infection and viral protein translation. However, infection of normal cells with a functioning PKR response results in abortive infection.

The type I IFN response is also involved in the selectivity of *γ34.5*-deleted oHSV-1. WT HSV ICP34.5 not only inhibits the PKR response, but also prevents TANK-binding kinase-1 (TBK1) from interacting with and phosphorylating interferon regulatory factor-3 (IRF3) (Y. Ma et al., 2012; Verpooten, Ma, Hou, Yan, & He, 2009). Therefore, by preventing IRF3 activation, ICP34.5 inhibits the expression of IFN-α and β. The type I IFN response is critical in normal cells in preventing viral infection, resulting in the expression of interferon-stimulated genes (ISGs) which encode for proteins which affect viral replication, induce more IFN signalling, and activation of the PKR response. However, cancer cells often have a disrupted type I IFN response, and so are permissive to ICP34.5-deleted oHSV-1 (Pansky et al., 2000; K. X. Zhang et al., 2010).

ICP34.5 also plays a role in inhibiting the signalling induced by the sensing of cytoplasmic dsDNA by cyclic-GMP-AMP synthase (cGAS). Upon binding to cytoplasmic dsDNA, cGAS synthesises the soluble secondary messenger cyclic-GMP-AMP (cGAMP). cGAMP molecules then potently activate stimulator of interferon genes (STING), leading to phosphorylation of IRF3. Activated pIRF3 then causes transcriptional upregulation of type I IFN genes and triggers innate immune responses (Corrales, McWhirter, Dubensky, & Gajewski, 2016) ICP34.5 prevents STING translocation from the ER to the Golgi, thus preventing it from interacting

with TBK1 to continue the signalling pathway which culminates in IRF3 phosphorylation and type I IFN expression (Pan, Liu, Ma, Cao, & He, 2018). ICP34.5-deleted oHSV-1 therefore is unable to inhibit this STING-mediated responses in healthy cells.

Autophagy is also involved in the antiviral response and involves the digestion of intracellular components. ICP34.5 has been demonstrated to play an essential role in inhibiting Beclin-1-mediated autophagy, and is essential for HSV-1 neurovirulence (Orvedahl et al., 2007). Therefore, ICP34.5-deleted oHSV-1 is unable to inhibit the antiviral autophagic digestion of intracellular viruses.

Another genetic modification commonly used in oHSV-1 is the deletion of ICP6. ICP6 is a viral ribonucleotide reductase (RR), responsible for catalysing the reduction of ribonucleotides into deoxynucleotides (dNTPs) for DNA synthesis (Preston, Palfreyman, & Dutia, 1984). Deletion of viral ICP6 renders the HSV-1 dependent on host cell's pool of deoxynucleotides, which is typically low in senescent non-dividing cells, but high in dividing cells. Hence, deletion of oHSV-1 ICP6 gives added selectivity towards actively dividing cells with high dNTP pools (Goldstein & Weller, 1988; Mineta, Rabkin, & Martuza, 1994). One of the most studied oHSV-1s to feature this genetic modification and used for oHSV-1 experiments in this thesis, is G207. G207 contains a *LacZ* insertion in the ICP6 locus (i.e. deleting ICP6), as well as the double deletions of *γ34.5* (Mineta et al., 1995).

T-VEC, the most advanced OV to gain FDA approval, has deletions in both copies of *γ34.5*, but also *α47* (encoding ICP47). ICP47 is normally involved in inhibiting the antigen presentation machinery by MHC class I molecules (Goldsmith, Chen, Johnson, & Hendricks, 1998). The deletion of ICP47 in T-VEC allows the

presentation of viral peptides on the surface of infected cells, allowing immune destruction of infected cells and preventing viral replication. Another consequence of ICP47 deletion is that the expression of the gene *unique short 11* (*US11*), encoding the protein U_S11, is brought under the control of the *α47* promoter (normally controlling ICP47 expression), resulting in earlier expression of U_S11 during the viral infection. U_S11 also inhibits the PKR response (Poppers, Mulvey, Khoo, & Mohr, 2000). Therefore, earlier expression of U_S11 endows T-VEC with greater ability to inhibit the dysfunctional PKR response in cancer cells, but is still unable to overcome normal PKR signalling in healthy cells (Cassady, Gross, & Roizman, 1998; B He et al., 1997). Other oHSV-1s also have made use of the deletion of ICP47 and subsequent early expression of U_S11, such as G47Δ, an oHSV-1 with double deletions in ICP34.5, an insertion of LacZ into ICP6 (deleting ICP6), and the deletion of ICP47 (Chambers et al., 1995).

Together, these deletions of ICP34.5 and other non-essential genes give oHSV-1 a dependency on cells with faulty PKR and type I IFN responses, as well as actively dividing cells, which are typically cancer cells. By introducing multiple mutations, it is highly unlikely the oHSV-1 can revert to its WT phenotype and regain its virulence, therefore making oHSV-1 safe for use in patients. See Figure 1.6 for overview of oHSV-1 selectivity. It is important to also note that HSV-1 (and oHSV-1) also express a host of other proteins involved in augmenting cellular processes to enable successful infection. The HSV-1 genes mentioned here are the key ones in generating oHSV-1 cancer selectivity.

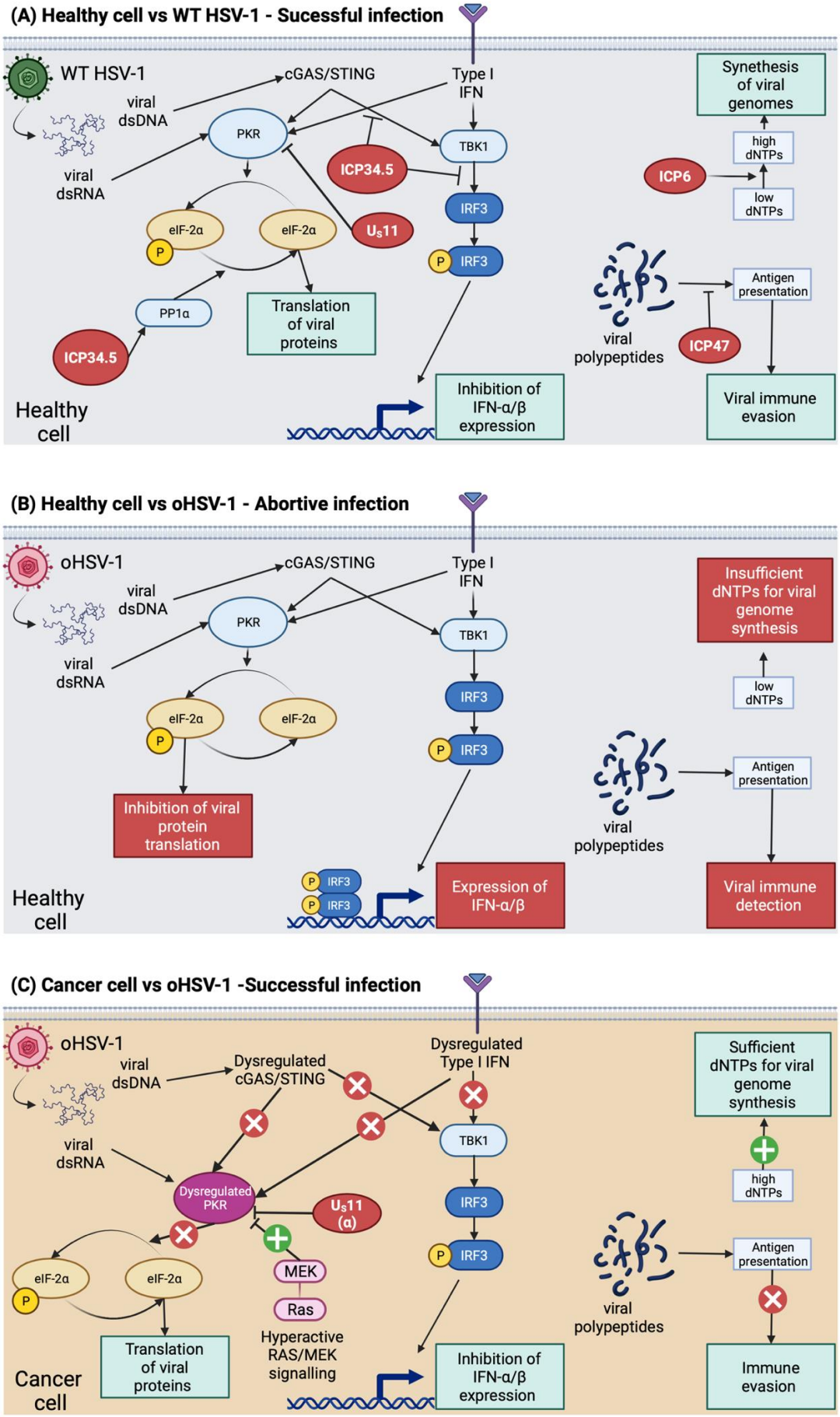
(A) Healthy cell vs WT HSV-1 - Sucessful infection
WT HSV-1
viral dsDNA
viral dsRNA
cGAS/STING
Type I IFN
PKR
TBK1
ICP34.5
IRF3
eIF-2α
eIF-2α
P
U_S11
P IRF3
PP1α
ICP34.5
Translation of viral proteins
Synethesis of viral genomes
high dNTPs
low dNTPs
ICP6
viral polypeptides
Antigen presentation
ICP47
Inhibition of IFN-α/β expression
Viral immune evasion
Healthy cell
(B) Healthy cell vs oHSV-1 - Abortive infection
oHSV-1
viral dsDNA
viral dsRNA
cGAS/STING
Type I IFN
PKR
TBK1
IRF3
eIF-2α
eIF-2α
P
P IRF3
Inhibition of viral protein translation
Insufficient dNTPs for viral genome synthesis
low dNTPs
viral polypeptides
Antigen presentation
P IRF3
P IRF3
Expression of IFN-α/β
Viral immune detection
Healthy cell
(C) Cancer cell vs oHSV-1 -Successful infection
oHSV-1
viral dsDNA
viral dsRNA
Dysregulated cGAS/STING
Dysregulated Type I IFN
TBK1
IRF3
Dysregulated PKR
U_S11 (α)
P IRF3
eIF-2α
eIF-2α
P
MEK
Ras
Hyperactive RAS/MEK signalling
Translation of viral proteins
Sufficient dNTPs for viral genome synthesis
high dNTPs
viral polypeptides
Antigen presentation
Immune evasion
Inhibition of IFN-α/β expression
Cancer cell

Figure 1.6 Basis of cancer-selectivity of oHSV-1
(**A**) Some of the HSV-1 proteins involved in achieving successful infection of healthy cells. Wild type (WT) herpes simplex virus-1 (HSV-1) infection in healthy cells triggers protein kinase R (PKR) activation due to detection of viral double stranded RNA (dsRNA). HSV-1 double stranded DNA (dsDNA) activates cyclic GMP-AMP synthase (cGAS) and stimulator of interferon genes (STING), which also activates PKR. Activated PKR phosphorylates eukaryotic translation initiation factor-2 α (eIF-2α) but is counteracted by late viral expression of U_S11, and by protein phosphatase 1 α (PP1α) recruited to eIF-2α by HSV-1 infected cell protein 34.5 (ICP34.5). Unphosphorylated eIF-2α allows translation of viral proteins. ICP34.5 also inhibits TANK-binding kinase-1 (TBK1)-mediated phosphorylation of interferon response factor-3 (IRF3) after type I interferon (IFN) and cGAS/STING signalling, and also prevents translocation of STING to the Golgi, thus preventing the expression of type I IFN. HSV-1 ICP6 is a ribonucleotide reductase and increases the pool of deoxynucleotide triphosphates (dNTPs), enabling viral genome synthesis. HSV-1 ICP47 inhibits presentation of viral polypeptides, enabling viral immune evasion. Overall results in successful viral infection. (**B**) Healthy cell infected with oncolytic herpes simplex virus-1 (oHSV-1). Viral dsRNA and dsDNA-mediated cGAS-STING activation results in activated PKR response, triggering phosphorylation of eIF-2α and inhibition of oHSV-1 protein translation. Type I IFN also leads to PKR signalling and TBK1-mediated phosphorylation of IRF3. Phosphorylated IRF3 translocates to the nucleus to induce expression of more type I IFN (IFN-α/β) for autocrine and paracrine signalling. Low dNTP pool in non-dividing healthy cells results in insufficient dNTPs for oHSV-1 genome synthesis. oHSV-1 polypeptides can be presented as viral antigens, evoking an anti-viral immune response and immune detection. Overall results in abortive infection. (**C**) Cancer cell infected with oHSV-1. PKR response in cancer cells is dysregulated by hyperactive RAS and mitogen activated protein kinase (MAPK) kinase (MEK), dysregulated cGAS-STING and dysregulated IFN signalling. PKR dysregulation means eIF-2α is not phosphorylated in response to oHSV-1 infection, thus enabling translation of oHSV-1 proteins. Deletion of ICP47 in some oHSV-1 viruses leads to early (α) expression of U_S11, enabling further inhibition of PKR. Dysregulated type I IFN response in cancer cells leads to a lack of IFN production in response to oHSV-1 infection. High dNTP pools in dividing cancer cells leads to sufficient resources for oHSV-1 genome synthesis. Antigen presentation is dysregulated in many cancer cells, enables viral immune evasion. Results in successful infection. Red crosses denote deficiencies commonly seen in cancer cells which lead to dysregulation. Green pluses denote hyperactive signalling commonly seen in cancer cells. Image created with BioRender.com.

1.6.3 'Armed' oHSV-1

'Arming' oHSV is a key step for the next generation of oHSV-1 candidates, as it appears the anti-cancer efficacy of the oHSV-1 alone may not be sufficient to eradicate tumours. Therefore, exploiting the genome capacity and tumour-restricted expression of their encoded payloads enables the augmentation of oHSV-1 cancer immunotherapy.

T-VEC, the FDA-approved oHSV-1 for the treatment of metastatic melanoma, has been 'armed' to express the cytokine GM-CSF, which is released by infected tumour cells into the TME (Kaufman et al., 2010). GM-CSF then helps to stimulate the anti-tumour immune response in a number of ways, including DC differentiation

and maturation, and macrophage activation (Kaufman, Ruby, Hughes, & Slingluff, 2014). In phase II and III trials for unresectable stage IIIb, IIIc or IV melanoma, intratumoural delivery of T-VEC achieved superior overall survival compared to the GM-CSF control arm, with a 17% complete response rate and only mild side effects (Andtbacka et al., 2019).

oHSV-1s have been engineered to express other pro-inflammatory cytokines including: IL-12, to boost anti-tumour T cell and NK cell responses and disrupt angiogenesis in brain tumours (Cheema et al., 2013; Patel et al., 2016); and IL-15, to stimulate $CD8^+$ T cell and NK cell proliferation in murine GBM (R. Ma et al., 2021).

OVs can also be armed to express agents which have direct effects on the cells within the tumour environment. For example, an oHSV-1 deleted in ICP34.5 and ICP47 was also encoded to express a constitutively active fusogenic glycoprotein from gibbon ape leukaemia virus (GALV) (S. Thomas et al., 2019). Expression of GALV glycoprotein (GALV-GP-R^-) from infected rat and murine cancer cells *in vivo* resulted in highly immunogenic cell death, and increased the spread of oncolysis of cancer cells (S. Thomas et al., 2019).

oHSV-1 has also been used to express therapeutics to target cells in the TME. Khalique et al. encoded a BiTE targeting PD-L1 into the G207 oHSV-1, which resulted in T cell-mediated destruction of PD-$L1^+$ tumour cells and immunosuppressive macrophages (Khalique et al., 2021). When using patient-derived ascites fluid and cells as a model system (Scott et al., 2020), the PD-L1 expression on patient ascites-derived cancer cells increased, further increasing the activity of the PD-L1 BiTE despite the immunosuppressive fluid (Khalique et al., 2021).

Likewise, tumour necrosis factor-related apoptosis-inducing ligand (TRAIL), a tumour-selective inducer of apoptosis, has been explored for use as an anti-cancer agent for systemic delivery, but demonstrated off-target toxicity (Rozanov et al., 2009). However, when encoded into an oHSV-1 (oHSV-TRAIL), restricted tumour expression of TRAIL resulted in increased survival in murine GSC models with limited off-target toxicities (Tamura et al., 2013)

These are just a few examples of the many 'armed' oHSV-1 candidates for cancer therapy (reviewed in more detail in (Jahan, Ghouse, Martuza, & Rabkin, 2021)).

1.6.4 oHSV-1 in GBM

GBM is one of the most challenging tumours to treat; with no significant progress being made in terms of patient survival statistics (14.6 months (McFaline-Figueroa & Lee, 2018)) in recent years using conventional cancer therapies, much focus has been put on immunotherapies, including OVs, as novel therapeutic options for GBM therapy.

oHSV-1 is one of the most studied and successful OVs in the treatment of other solid tumours and has been the centre of attention for OV-based GBM therapies. The first generation of oHSV-1s to be generated, HSV1716 and R3616 (Chou, Kern, Whitley, & Roizman, 1990; MacLean, Ul-Fareed, Robertson, Harland, & Brown, 1991), had double-deletions of ICP34.5 to give the viruses cancer selectivity, and demonstrated efficacy and safety in murine GBM models (S. J. Advani et al., 1998; Kesari et al., 1995).

The following generation of oHSV-1 sought to improve cancer cell selectivity. One of the key candidates in the second generation of oHSV-1 was G207, described

in the section above. G207 had the same deletions in ICP34.5, but also an inactivation of ICP6 by the insertion of *LacZ*, thus giving the oHSV-1 a dependence on actively dividing cells (Mineta et al., 1994). G207 demonstrated promise preclinically in human cancer cell lines and murine xenograft models (Mineta et al., 1994, 1995).

Early clinical trials using HSV1716 in high grade glioma patients demonstrated a good safety profile with some evidence of viral replication (Papanastassiou et al., 2002), and long-term survival in some cases (Harrow et al., 2004). Meanwhile, phase I/Ib clinical evaluation of G207 in patients with malignant glioma or recurrent GBM also demonstrated a good safety profile using multiple-dose stereotactic IT delivery and some evidence of viral replication within the tumour (J. M. Markert et al., 2009). Furthermore, one patient had an extended disease-free interval of six years, and survival time of over seven years following G207 treatment and some adjuvant chemotherapy (Whisenhunt, Rajneesh, Hackney, & Markert, 2015).

However, as these early generations of oHSV-1 made pre-clinical progress and clinical proof of principle, it began to emerge that the deletion of ICP34.5 to ensure safety severely resulted in attenuation in GBM. While ICP34.5-deleted viruses such as HSV1716 and G207 were able to infect and lyse differentiated GBM cells, viral replication was severely inhibited in GSCs (Kanai et al., 2012). This was found to involve a global inhibition of translation late after infection with ICP34.5-deleted oHSV-1 (G207) in GSCs which restricted expression of HSV-1 true late (TL) proteins but not early or leaky late viral proteins (Peters et al., 2018).

Since GSCs pose a major obstacle in the treatment of GBM, subsequent generations of oHSV-1 have sought to enhance efficacy against GSCs. G47Δ was developed from the G207 virus, and involves a further deletion of ICP47, which not

only enhances infected cell antigen presentation, but also enables PKR antagonism by earlier expression of U_S11 (Chambers et al., 1995). G47Δ was shown to inhibit tumour growth more than G207 in murine xenograft and syngeneic GBM models, as well as increased antigen-dependent TIL stimulation with human melanoma cells (Todo, Martuza, Rabkin, & Johnson, 2001). In a human GBM model using patient-derived GSCs, G47Δ killed GSCs as effectively as WT HSV-1 and inhibited the self-renewal of the GSCs, but G207 did not, due to its inability to replicate in the GSCs (Wakimoto et al., 2009). The mechanism underlying this enhanced potency in GSCs by G47Δ compared to G207 was found to be due to earlier expression of U_s11 (because of ICP47 deletion), which rescued the expression of TL viral proteins via earlier PKR inhibition (Figure 1.6) (Peters et al., 2018). G47Δ recently demonstrated success in clinical trials in Japan, using multiple stereotactic injections into the tumour for patients with residual or recurrent GBM, and was made eligible for fast-track approval by the Pharmaceuticals and Medical Devices Agency of Japan (PMDA) in 2019 (Taguchi, Fukuhara, & Todo, 2019). On the basis of these trials, G47Δ (DELYTACT) received approval for treatment of GBM in Japan in 2021 (Daiichi Sankyo, 2021).

Another example of an oHSV-1 further engineered to boost potency for GBM OV therapy is M032. M032 is also based on the G207 genome, but armed to express human IL-12 to induce NK and T cell cytotoxicity and promote anti-angiogenesis effects (Patel et al., 2016). M032 is also currently undergoing a phase I clinical trial for GBM.

New generations of oHSV-1 have sought to overcome the severe attenuation by ICP34.5. One key example is to reintroduce conditional expression of ICP34.5. rQNestin34.5 is an oHSV-1 deleted in both copies of ICP34.5 and ICP6, but has

been re-engineered to express one copy of ICP34.5 under control of a synthetic nestin promoter (Kambara, Okano, Chiocca, & Saeki, 2005). Nestin is expressed during neuronal embryonic development but not in normal healthy adult brains; however, expression is upregulated in malignant glioma (Dahlstrand, Collins, & Lendahl, 1992). Therefore, by placing ICP34.5 under control of a synthetic nestin promoter, rQNestin34.5 is able to regain tumour-selective ICP34.5 expression only in cancer cells which are expressing nestin (Kambara et al., 2005). rQNestin34.5 has demonstrated good pre-clinical efficacy, low toxicology and is undergoing phase I clinical trials (Chiocca, Nakashima, Kasai, Fernandez, & Oglesbee, 2020).

Other examples of oHSV-1 engineered to overcome the PKR response are C130 and C134. C130 and C134 are engineered to express human cytomegalovirus (HCMV) gene products TRS1 and IRS1, respectively (Cassady, 2005). TRS1 and IRS1 are HCMV proteins involved in PKR inhibition, and are essential for successful HCMV infection (Marshall, Bierle, Brune, & Geballe, 2009). By engineering the ICP34.5-deleted oHSV-1 to express HCMV proteins IRS1 and TRS1 which can help to inhibit the PKR translation shut-off response, it allows greater translation of oHSV-1 proteins, boosting infection (Cassady, 2005). C134 is currently being evaluated clinically for recurrent GBM. A summary of the modifications of oHSV-1 candidates, and other key OVs also investigated for GBM is listed in Table 1.2., and a summary of clinically evaluated oHSV-1 candidates in clinical trials can be seen in Table 1.3.

Table 1.2 Overview of Oncolytic viruses in GBM

Family	Virus	Modification	Tumour specificity	Comments	Reference
Herpesvirus	HSV1716	ICP34.5 deletion	Dysregulated PKR, Rb, p16 and IFN	1st gen oHSV-1	(Kesari et al., 1995; Papanastassiou et al., 2002)

	R3616	ICP34.5 deletion	Dysregulated PKR, Rb, p16 and IFN	1st gen oHSV-1	(Chou et al., 1990)
	G207	ICP34.5 deletion Insertion of *LacZ* into ICP6	Dysregulated PKR, Rb, p16 and IFN High dNTPs	2nd gen oHSV-1 ***Used in this thesis***	(Mineta et al., 1995)
	M032	ICP34.5 deletion Insertion of *LacZ* into ICP6 IL-12 expression	Dysregulated PKR, Rb, p16 and IFN	G207 armed with IL-12	(Patel et al., 2016)
	C130	ICP34.5 deletion HCMV TRS1 expression to inhibit PKR	Dysregulated PKR, Rb, p16 and IFN	Armed with HCMV protein to inhibit PKR	(Cassady, 2005)
	C134	ICP34.5 deletion HCMV IRS1 expression to inhibit PKR	Dysregulated PKR, Rb, p16 and IFN	Armed with HCMV protein to inhibit PKR	(Cassady, 2005)
	G47Δ	ICP34.5 deletion ICP6 deletion *α47* deletion (Early U_s11)	Dysregulated PKR, Rb, p16 and IFN High dNTPs	Enhanced potency in GSCs vs G207 Approved for GBM in Japan (DELYTACT)	(Chambers et al., 1995) (Daiichi Sankyo, 2021)
	rQnestin-HSV-1	ICP34.5 deletion γ34.5 expression under control of nestin promoter	Dysregulated PKR, Rb, p16 and IFN GBM nestin expression	GBM-specific ICP34.5 expression	(Kambara et al., 2005)
Adenovirus	Onyx-015	E1B-55k and E3B deletions	Dysregulated p53, cell cycle, late viral RNA export		(Cheng, Wechman, McMasters, & Zhou, 2015; Heise et al., 1997)
	Delta24-RGD	24-bp deletion in *E1a* region Integrin-binding tripeptide of Arg-Gly-Asp (RGD) into adenoviral fibre protein	Dysregulated Rb GBM expressing αvβ3 and αvβ5 integrins		(Fueyo et al., 2000; Staba, Wickham, Kovesdi, & Hallahan, 2000)

Paramyxovirus	NDV	Natural tropism	Dysregulated IFN		(García-Romero et al., 2020)
Reovirus	R124 Dearing type 3	Natural tropism	Dysregulated Ras	Systemic delivery for GBM	(Gong & Mita, 2014; Samson et al., 2018)
Picornavirus	PVSRIPO	Poliovirus type 1 (Sabin) vaccine with IRES substituted with human rhinovirus type 2 IRES	Entry receptor CD155 overexpression		(Gromeier, Alexander, & Wimmer, 1996)
Flavivirus	ZIKV-LAV	Live attenuated vaccine candidate with 10-nucleotide deletion in 3' UTR	Natural tropism for NPCs	Selectively infects GSCs in adult GBM	(Q. Chen et al., 2018)

Abbreviations: Infected cell protein (ICP), protein kinase R (PKR), retinoblastoma (Rb), interferon (FN), oncolytic herpes simplex virus-1 (oHSV-1), deoxynucleotide triphosphate (dNTP), interleukin (IL), human cytomegalovirus (HCMV), Unique short 11 (*U_S11*) Newcastle disease virus (NDV), glioma stem-like cell (GSC), glioblastoma (GBM), internal ribosomal entry site (IRES), live attenuated vaccine zika virus (ZIKV-LAV), untranslated region (UTR), neuronal progenitor cell (NPC). Table adapted from Stavrakaki *et al., 2021*.

Table 1.3. Clinical trials using oHSV-1 in GBM

oHSV-1	Combination	Condition	Clinical trial	Reference
HSV1716	-	Recurrent malignant glioma	N/A	(Rampling et al., 2000)
	-	High-grade glioma	N/A	(Harrow et al., 2004; Papanastassiou et al., 2002)
	Dexamethasone	Refractory or recurrent high-grade glioma	I	NCT02031965
G207	-	Recurrent malignant glioma	I	(J. Markert et al., 2000)
	-	Recurrent brain cancer	Ib/2	NCT00028158
	-	Recurrent GBM	Ib	(J. M. Markert et al., 2009)
	Radiation	Recurrent malignant glioma	I	(J. M. Markert et al., 2014)
	Radiation	Progressive or recurrent supratentorial brain tumours (paediatric)	I	NCT02457845 (Waters et al., 2017)
	Radiation	Recurrent or refractory cerebellar brain tumours (paediatric)	I	NCT03911388 (Bernstock et al., 2020)
	Radiation	Recurrent high-grade glioma	II	NCT04482933

G47Δ	-	Progressive GBM	I/II	UMIN000002661 (Taguchi et al., 2019)
	-	Residual or recurrent GBM	II (Approved for use in Japan – DELYTACT)	UMIN000015995 (Taguchi et al., 2019)
M032	-	Recurrent/progressive GBM	I	NCT02062827
rQNestin34.5v.2	Cyclophosphamide	Recurrent malignant glioma	I	NCT03152318
C134	-	Recurrent GBM	I	NCT03657576

Table adapted from Nguyen & Saha, 2021.

1.7 Effects of oncolytic viruses on the GBM tumour microenvironment

The TME in GBM is considered immunologically 'cold', consisting of immunosuppressive cytokines and myeloid cells, and relatively poor infiltration of TILs. OV therapy has the potential to turn the 'cold' GBM TME 'hot', influenced by the presence of the OV and its associated PAMPs, and the subsequent release of DAMPs following oncolysis (Figure 1.2).

Converting TAM immunophenotypes towards being more pro-inflammatory may be an important step in improving GBM outcomes. There are multiple reports that the presence and activity of OVs can induce pro-inflammatory macrophage and TAM phenotypes. Co-culture of human PBMC-derived immunosuppressive macrophages with human GSCs infected with the oncolytic adenovirus, Delta24-RGD (Table 1.2), lead to a shift towards pro-inflammatory signatures due to secreted soluble factors from infected cells and the presence of the virus itself (Van Den Bossche et al., 2018). CSF collected from Delta24-RGD-treated patients had elevated pro-inflammatory cytokines (Van Den Bossche et al., 2018) and TAMs

obtained from an infected patient displayed a significantly more pro-inflammatory signature compared to control GBM tissue (Van Den Bossche et al., 2018).

Similarly, OVs have been shown to shift TAM phenotypes in murine GBM. G47Δ armed to express murine IL-12 (G47Δ-mIL-12) was shown to cause an influx of macrophages and induce an M1-like TAM polarisation when used in triple combination with anti-CTLA-4 and anti-PD-1 blockade in murine glioma models (Saha et al., 2017). Also, Brown et al. demonstrated that sublethal infection of DCs and macrophages with PVSRIPO (due to monocytic expression of CD155) resulted in a potent induction of type I IFN-dependent activation, which subsequently led to tumour-specific adaptive immune responses *in vivo* (Brown et al., 2017).

Although GBM is relatively sparse for TILs compared to other solid tumours, there is growing evidence that OVs can boost the number and activity of TILs in GBM both in humans and mouse models For example, post-treatment specimens obtained from patients after clinical trial using Delta24-RGD demonstrated increased TILs, NK cells and T helper (T_h) 1 and T_h2-associated cytokines (van Putten et al., 2022). Additionally, in paediatric GBM, immunofluorescence multiplexing of pre- and post-administration of G207 oHSV-1 revealed a significant influx of $CD4^+$ and $CD8^+$ TILs, and an increased expression of checkpoint inhibitors, paving the rational for ICB combination therapy (Bernstock et al., 2019). Meanwhile, in a murine orthotopic GSC model infected with G47Δ-mIL-12 significantly decreased T_{regs}, inhibited angiogenesis, whilst increasing IFN-γ and TILs (Cheema et al., 2013). When the same virus was used in triple combination with anti-CTLA4 and anti-PD-1 blockade in a murine orthotopic , a significant anti-tumour effect was observed which was dependent on $CD4^+$ and $CD8^+$ T cells, as well as macrophages, indicating the influx of TILs (Saha et al., 2017).

Therefore, OVs have the immunostimulatory capacity to generate a more pro-inflammatory TME in GBM (Figure 1.2), contributing to direct viral oncolysis and indirectly acting as a cancer vaccine adjuvant. These effects can be further enhanced with the local expression of virally encoded transgenes, such as cytokines and BiTEs.

1.8 NKG2D receptor and its ligands

The following sections on NKG2D ligands is based on a self-written published review article, titled “Convergent Evolution by Cancer and Viruses in Evading the NKG2D Immune Response” (Baugh, Khalique, & Seymour, 2020).

1.8.1 NKG2D receptor and its ligands

1.8.1.1 NKG2D receptor

NK cells play a critical role in the innate immune system’s immunosurveillance of both virally infected cells and tumours. They possess an extensive repertoire of both activatory and inhibitory receptors that recognise a range of ligands on target cells. These receptors process an array of signals from target cells, either resulting in NK cell stimulation or inhibition (Barrow, Martin, & Colonna, 2019). The overall balance of these signals determines the fate of either NK cell activation or inhibition. One of the most well-documented activatory receptors is NKG2D. NKG2D receptor and NKG2D ligands (NKG2DLs) are part of the early warning signals for the innate immune system; flagging up cells that may represent danger to the host organism. NKG2D receptor is an activatory receptor expressed on the surface of NK cells, $CD8^+$ T cells, NKT cells, γδ T cells and some $CD4^+$ T cell subsets (Allez et al., 2007; Bauer, 1999; Raulet, 2003). NKG2D is an invariant homodimeric receptor, with each

monomer consisting of a type-II transmembrane domain and a C-type lectin-like extracellular domain, and is associated with DNAX activating protein 10 (DAP10) or DAP12 in mice and DAP10 only in humans (Raulet, 2003) (Figure 1.7A).

NKG2D binding to NKG2DLs can directly activate NK cells that have already been stimulated with IL-2 or IL-15 (Horng, Bezbradica, & Medzhitov, 2007; Mukherjee et al., 2017), whereas additional co-stimulatory signals are required to activate T cells and freshly isolated NK cells (Bryceson, Ljunggren, & Long, 2009; Groh et al., 2001). Binding of NKG2D to NKG2DLs recruits phosphatidylinositol 3-kinase (PI3K) and growth factor receptor-bound protein 2 (GRB2), triggering a subsequent phosphorylation cascade. The fine balance of inhibitory and activatory signals presented to NK cells via various receptors and cytokines ultimately determine the outcome for NK cell activation. If balance of the overall signalling favours NK cell activation, it can stimulate effector functions including cytokine release and perforin/granzyme-mediated cytotoxicity (Lanier, 2005).

1.8.1.2 NKG2D ligands

Although the NKG2D receptor is germline-encoded, it can recognise a diverse range of MHC-class-I-related ligands. In humans, these NKG2DLs include MHC-class-I-polypeptide-related sequence A (MIC) A and MICB, and UL16 binding protein (ULBP) 1-6, also known as retinoic acid early inducible transcript 1 (RAET1) proteins (Bacon et al., 2004; Bauer, 1999; Cao et al., 2008; Cosman et al., 2001; Eagle, Traherne, Hair, Jafferji, & Trowsdale, 2009; Groh et al., 1996; Jan Chalupny, Sutherland, Lawrence, Rein-Weston, & Cosman, 2003). In contrast, murine NKG2DLs include retinoic acid early inducible (RAE-1) α-ε, H60a-c, and murine UL16 binding protein-like transcript (MULT) 1 (Carayannopoulos, Naidenko, Fremont, & Yokoyama, 2002; Cerwenka et al., 2000). All NKG2DLs share homology

with MHC class I molecules, featuring α1 and α2 domains, while MICA and MICB also have an α3 domain (Figure 1.7B). However, unlike MHC class I molecules, they cannot bind and present antigenic peptides and are not associated with β_2-microglobulin. Despite their overall similarities, NKG2DLs vary from each other in sequence; binding affinity to NKG2D; and membrane anchorage, either transmembrane proteins or glycophosphatidylinositol (GPI)-linked (Raulet, Gasser, Gowen, Deng, & Jung, 2013) (Figure 1.7B). NKG2DLs also display a high degree of polymorphism in humans, with 104 and 37 distinct alleles currently assigned for MICA and MICB genes, respectively ("HLA Nomenclature @ hla.alleles.org," n.d.).

Expression of NKG2DLs on normal, healthy cells is low or absent; however, is dramatically increased during events of cellular stress, virus infection or malignant transformation. This expression pattern in stressed, virus-infected or cancer cells is often referred to as 'induced self'; whereby germline-encoded NKG2DLs are upregulated, enabling NK or T cell recognition, and often occurs in parallel with viral- or cancer-mediated downregulation of MHC class I expression (i.e. 'missing-self') (M. B. Lodoen & Lanier, 2005). Upregulation of NKG2DLs allows for rapid NK or T cell-mediated immunosurveillance and elimination of cells that may pose as a threat to the organism: cells that have undergone DNA damage after heat or oxidative shock, and may therefore have acquired oncogenic mutations; cells that have been infected by a viral pathogen, and may lead to a larger-scale infection if left unchecked; or rapidly proliferating cells that may progress to become cancer.

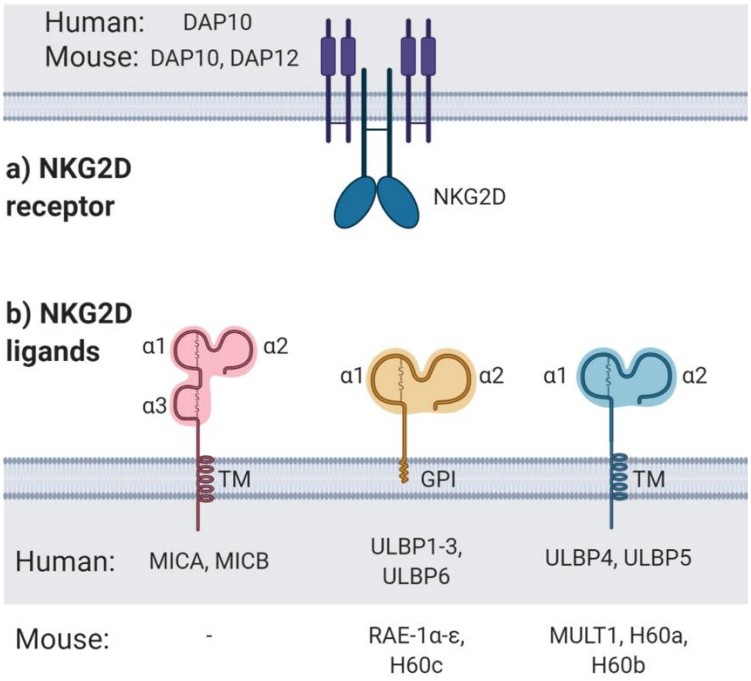

Figure 1.7 NKG2D receptor and ligands
(A) The natural killer group 2 member D (NKG2D) receptor is expressed by natural killer (NK) cells, γδ T cells, $CD8^+$ T cells, and some $CD4^+$ T cells. The NKG2D receptor is associated with DNAX activating protein (DAP) 10 in humans, but DAP10 and DAP12 in mice. (**B)** NKG2D ligands (NKG2DLs) include MHC-class-I-polypeptide-related sequence (MIC) A and MICB, and UL16 binding protein (ULBP) 1-6 in humans, and retinoic acid early inducible (RAE-1) α-ε, H60a-c, and Murine UL16 binding protein-like transcript (MULT) 1 in mice. All NKG2DLs feature MHC-class-I-like α1 and α2 domains, whilst MICA and MICB also have an α3-like domain but do not bind to β2-microglobulin. Some NKG2DLs are transmembrane proteins (TM), while others are linked to the membrane via glycophosphatidylinositol (GPI) anchors. Diagram created with BioRender.com. Figure adapted from Baugh et al., 2020.

1.8.2 NKG2DL expression in healthy cells and autoimmunity

NKG2DL expression can lead to NK and T cell-mediated cytotoxicity and inflammation. Therefore, surface expression of these ligands is minimal in healthy quiescent cells to prevent autoimmunity. For example, although MICA is expressed at a low level by healthy intestinal epithelial cells (IECs), MICA expression is increased in patients with Crohn's Disease, leading to activation and autoimmunity from a subset of $CD4^+NKG2D^+$ T cells (Allez et al., 2007). MICA and MICB mRNA transcripts have been found in healthy tissue as well as various tumours

(Schrambach, Ardizzone, Leymarie, Sibilia, & Bahram, 2007), suggesting regulation of surface NKG2DL expression is not solely controlled at a transcriptional level.

1.8.2.1 Cell stress induces NKG2DL mRNA and protein expression

NKG2DL expression in normal cells is increased following a variety of cellular insults. Human IECs exposed to heat shock demonstrated increased MICA and MICB expression, sensitising IECs to lysis by γδ T cells (Groh, 1998). A study using human colorectal carcinoma cell lines demonstrated that MICA and MICB mRNA and protein expression was low when cells were at high confluency and quiescent; however, mRNA and protein expression of both MICA and MICB was greatly increased in response to oxidative or heat stress, or when cells were proliferating (Venkataraman, Suciu, Groh, Boss, & Spies, 2007). This stress response is thought to be mediated, at least initially, at the level of transcription, since the promoter regions for MICA and MICB contained conserved heat shock elements (HSE), which bind to heat shock factor 1 (HSF1) in response to heat shock and oxidative stress (Groh et al., 1996; Venkataraman et al., 2007). Oxidative stress induced by H_2O_2 has also been shown to increase MICA and MICB mRNA expression, although surface protein levels were not measured (Yamamoto, 2001).

Other forms of cell stress have also been reported to induce NKG2DL expression; endoplasmic reticulum (ER) stress, induced with an inhibitor of the ER Ca^{2+} pump, increased NKG2DL expression in human cell lines and murine cells *in vivo* (Hosomi et al., 2017).

1.8.2.2 DNA damage induces NKG2DL expression

DNA damage is another form of cellular stress capable of upregulating surface NKG2DL expression. Gasser et al. demonstrated that activation of the DNA damage response (DDR) by chemotherapeutic agents, ionising radiation or stalling of DNA

replication cycles increased NKG2DL expression. This increased NKG2DL expression was found to occur in an ataxia telangiectasia, mutated- (ATM), ATM- and Rad3-related- (ATR) and checkpoint kinase (Chk) 1-dependent manner, sensitising cells to lysis by NK cells (Gasser, Orsulic, Brown, & Raulet, 2005). Further evidence towards the link between reactive oxygen species, DNA damage and NKG2DL upregulation was demonstrated by using sublethal doses of chemotherapeutic agents which cause oxidative stress, such as doxorubicin and melphalan, which triggered MICA upregulation in multiple myeloma cells. This transcriptional increase in MICA was attributed to DDR-dependent activity of the transcription factor E2F1 (Soriani et al., 2014). Additionally, the *ULBP1* and *ULBP2* genes have a response element for the tumour suppressor protein p53, which is stabilised during the DDR. Hence, p53 stabilisation during the DDR directly causes an increase in ULBP1 and ULBP2 transcription (H. Li et al., 2011; Textor et al., 2011).

1.8.2.3 Post-transcriptional regulation of NKG2DL expression during cell stress

NKG2DL expression is not only controlled at the level of transcription; mRNA stability, protein stability and intracellular localisation also play a significant role in regulating functional protein expression. MICA and MICB mRNA transcripts were found to be expressed in various healthy human tissues (Schrambach et al., 2007), which appears in contrast to the concept that NKG2DL proteins are not expressed by healthy cells, indicating that other regulatory mechanisms are involved beyond gene transcription.

Another mechanism has been described, in which ultraviolet B radiation upregulated NKG2DLs in human epithelial cells via stress-induced EGFR signalling,

rather than due to the DDR (Vantourout et al., 2014). Under normal conditions, AU-rich element/poly(U)-binding/degradation factor 1 (AUF1) protein targets AU-rich elements (AREs) in the 3' untranslated region (UTR) of human NKG2DL mRNAs. AUF1 binding to NKG2DL transcripts causes mRNA destabilisation and degradation. However, stress-induced EGFR signalling prevents AUF1 binding and NKG2DL mRNA destabilisation, thus allowing translation and NKG2DL protein expression (Vantourout et al., 2014).

MicroRNAs (miRNAs) have also been implicated in the regulation of many genes, including MICA and MICB. A particular set of miRNAs found to be expressed in normal human cells can bind to the 3' UTR of MICA and MICB mRNA transcripts, resulting in their destabilisation and degradation, hence preventing protein translation and restricting autoimmunity (Noam Stern-Ginossar et al., 2008). These miRNAs are expressed during normal conditions, establishing a threshold for MICA and MICB mRNA to reach for protein expression and NKG2D recognition. During transient cell stress such as heat shock, the MICA/B mRNA levels dramatically increase, while the miRNA expression remains unchanged, enabling a saturation of the miRNAs and for some MICA/B mRNA transcripts to escape miRNA-mediated degradation and thus allow protein translation. It has been speculated that this system endows several advantages, such as rapid increases in protein expression, while preventing unwanted autoimmunity towards otherwise healthy cells due to small fluctuations in MICA or MICB transcription (Noam Stern-Ginossar et al., 2008).

Additionally, healthy primary human bronchial epithelial cells constitutively expressed NKG2DL mRNA transcripts but lacked surface protein expression. Exposure to oxidative stress increased surface protein expression despite

unchanged mRNA and total protein levels, indicating a stress-mediated protein translocation mechanism (Borchers, Harris, Wesselkamper, Vitucci, & Cosman, 2006). This rapid method of protein translocation and increasing surface expression may allow quicker responses and immunological detection of oxidatively-stressed cells within the well-oxygenated pulmonary environment.

Protein stability has also been reported to play a role in regulating murine NKG2DL expression (Nice, Deng, Coscoy, & Raulet, 2010). Nice et al. report that during normal conditions, MULT1 is targeted by membrane-associated RING-CH (MARCH) 4 and MARCH9 E3 ubiquitin ligases and is subsequently degraded. Upon heat shock treatment, however, this degradation was inhibited, and surface MULT1 increased (Nice et al., 2010).

1.8.3 NKG2DLs in virally infected cells

1.8.3.1 NKG2DL expression is induced in virally infected cells

During viral infection, the changing of the cellular phenotype to enable viral genome replication, immune evasion and proliferation leads to a highly stressful environment for the host cell. Amplification of viral genetic material, production of viral proteins and progeny, altering cellular metabolism to support the infection and inhibiting normal cellular processes are all common traits shared by many viruses during infection, all of which induce some degree of stress to the host cell. Therefore, the process of viral infection is likely to trigger many of the cellular stresses mentioned in the previous section, which would induce the expression of NKG2DLs.

The DDR is heavily involved in NKG2DL upregulation during virus infection. Many viruses, especially dsDNA viruses, trigger the DDR during early stages of

infection, including HSV-1 (Shirata et al., 2005). Viral infection can also trigger NKG2DL expression via other means, including activation of PI3K signalling (Hsu, Wu, Chiang, Lai, & Hung, 2010; Johnson, Wang, Ma, Huong, & Huang, 2001; Kong, Kumar, Taruishi, & Javier, 2014). MCMV-induced PI3K activation has been demonstrated to increase NKG2DL expression in murine cells; although PI3K activation alone was not sufficient to induce expression without viral infection, suggesting other additional signals and virus-induced stresses were also required for NKG2DL expression (Tokuyama et al., 2011).

1.8.3.2 Viral evasion of the NKG2D immune response

It now is apparent that in the evolution of viruses from various distinct viral families, many have independently converged on interfering with the NKG2D immune response (Lanier, 2008). While the means employed by viruses to evade the NKG2D response are numerous, some of the key examples are outlined in Table 1.4, and reviewed in Baugh et al. 2020. Mechanisms of HSV-1 NKG2DL downregulation are discussed in section 4.4.

Table 1.4. Summary of viral NKG2D evasion mechanisms

Virus	Immunoevasin	Mechanism	Reference
MCMV	gp40	Downregulation of surface RAE-1α-γ expression	(M. Lodoen et al., 2003)
	m155	Targets H60 for degradation	(M. B. Lodoen et al., 2004)
	m145	Downregulation of MULT1 surface expression	(Krmpotic et al., 2005)
	Fcr-1	Downregulation of MULT1 and H60 surface expression	(Lenac et al., 2006)
HCMV	UL16	Retention of MICB, ULBP2 and ULBP3 in ER and cis-Golgi apparatus	(Cosman et al., 2001; C. Dunn et al., 2003; Valés-Gómez, Browne, & Reyburn, 2003; Welte et al., 2003; Wu et al., 2003)
	UL142	Retention of MICA in cis-Golgi apparatus	(Ashiru et al., 2009; Chalupny, Rein-Weston, Dosch, & Cosman, 2006; Zou,

			Bresnahan, Taylor, & Stastny, 2005)
	US9	Targets MICA *008 for degradation	(Seidel et al., 2015)
	US12, US13, US18, US20	Target MICA, MICB and ULBP2 for degradation	(Fielding et al., 2014, 2017)
	miR-UL112	Targets 3' UTR of MICA and MICB transcripts, causing mRNA destabilisation	(N. Stern-Ginossar et al., 2007; Noam Stern-Ginossar et al., 2008)
	miR-US25-2-3p	Downregulation of TIMP3, causing increasing shedding by ADAM17 and MMP14 shedding	(Esteso et al., 2014)
VZV	Unknown	Downregulation of ULBP2 and ULBP3 by unknown mechanism	(T. M. Campbell, McSharry, Steain, Slobedman, & Abendroth, 2015)
HSV-1	Late viral gene product(s)	Downregulation of MICA, ULBP1, ULBP2 and ULBP3 (cell-dependent) at a post-translational stage	(T. M. Campbell et al., 2015; Schepis et al., 2009)
	miR-H8	Disrupts expression of GPI-anchoring machinery, reducing ULBP2 and ULBP3 surface expression	(Enk et al., 2016)
HHV-7	U21	Targets ULBP1 for degradation and downregulates MICA and MICB by unknown mechanism	(Schneider & Hudson, 2011)
HHV-6	Early viral gene product(s)	Targets MICB, ULBP1 and ULBP3 for degradation	(Schmiedel, Tai, Levi-Schaffer, Dovrat, & Mandelboim, 2016)
KSHV	K5	Ubiquitinylates MICA, causing redistribution from surface	(M. Thomas et al., 2008)
	miR-K12-7	Targets 3' UTR of MICB transcripts, causing mRNA destabilisation	(Nachmani, Stern-Ginossar, Sarid, & Mandelboim, 2009)
EBV	miR-BART2-5p	Targets 3' UTR of MICB transcripts, causing mRNA destabilisation	(Nachmani et al., 2009)
HBV	HBx	Forms complex with GATA-2/3 to repress MICA and MICB transcription	(Guan et al., 2016)
	HBc	Binds to CpG islands in MICA/B promoters to repress transcription	(Guan et al., 2016)
HCV	NS3/4a	Decreases MICA and MICB by unknown mechanism	(Wen et al., 2008)
	NS5a	Stimulates immunosuppressive cytokine production and NKG2D receptor downregulation	(Sène et al., 2010)
Ad5	E3/19K	Retention of MICA and MICB in ER	(McSharry et al., 2008)
HIV-1	Nef	Downregulation of MICA, ULBP1 and ULBP2	(Cerboni et al., 2007)
	Vif	Degradation of A3G, preventing DDR-mediated NKG2DL expression	(Norman et al., 2011)

	Unknown	Shedding of MICA, MICB and ULBP2 by host MMP shedding	(Matusali et al., 2013)
VSV	Unknown	Unknown (post-transcriptional)	(Jensen, Andresen, Nielsen, Christensen, & Skov, 2011)
VV	EL3	Prevents detection of dsRNA viral genome from PRRs	(Esteso, Guerra, Valés-Gómez, & Reyburn, 2017)
PyVs (JCV and BK)	miR-J1-3p	Targets 3' UTR of ULBP3 mRNA and prevents translation	(Bauman et al., 2011)
ZPXV	OMCP	Antagonism of NKG2D receptor	(J. A. Campbell, Trossman, Yokoyama, & Carayannopoulos, 2007)

Abbreviations: Murine cytomegalovirus (MCMV), human cytomegalovirus (HCMV), varicella-zoster virus (VZV), herpes simplex virus-1 (HSV-1), human herpesvirus (HHV), Kaposi's sarcoma-associated herpesvirus (KSHV), Epstein-Barr virus (EBV), hepatitis B virus (HBV), hepatitis C virus (HCV), adenovirus serotype 5 (Ad5), human immunodeficiency virus-1 (HIV-1), vesicular stomatitis virus (VSV), vaccinia virus (VV), polyomavirus (PyV), zoonotic orthopoxvirus (ZPXV) Apolipoprotein B-editing complex 3 G (A3G), A disintegrin and metalloprotease (ADAM), matrix metalloprotease (MMP), tissue inhibitor of metalloproteinase (TIMP-3), untranslated region (UTR), DNA damage response (DDR), Orthopox MHC class I-like protein (OMCP). A Table adapted from Baugh et al., 2020.

1.8.4 NKG2DL expression in transformed cells

1.8.4.1 Transformed cells have upregulated NKG2DL expression

Early observations that tumour cell lines were killed by NK cells and T cells led to the discovery of the NKG2D receptor and its ligands (Bauer, 1999). Various studies revealed tumour cells induced to express RAE-1 and H60 proteins resulted in tumour rejection in mice in an NK cell-dependent manner (Cerwenka et al., 2000; Cerwenka, Baron, & Lanier, 2001; Diefenbach, Jamieson, Liu, Shastri, & Raulet, 2000; Diefenbach, Jensen, Jamieson, & Raulet, 2001). The importance of NKG2D immune surveillance has been made clear in NKG2D-deficient mouse models, which spontaneously developed cancer much more than wild type mice (Guerra et al., 2008). The expression of NKG2DLs in GBM will be discussed in Chapters 3 and 4.

Tumours upregulate NKG2DLs via chronic DDR

Increased NKG2DL expression has been reported in many human cancers including leukaemia (Salih et al., 2003), colorectal carcinoma (Watson et al., 2006), hepatocellular carcinoma (Jinushi et al., 2003), melanoma (Vetter et al., 2002), pancreatic carcinoma (Duan et al., 2011), breast carcinoma (de Kruijf et al., 2012) and glioma (Friese et al., 2003).

DDR has been identified in cells undergoing the early stages of tumourigenesis in precursor lesions, including phosphorylated histone H2AX, p53 and kinases ATM and Chk2 (Bartkova et al., 2005; Gorgoulis et al., 2005). These activated proteins are part of the DNA damage checkpoint, which can trigger cell cycle arrest or apoptosis of these cells undergoing the first stages of transformation to prevent tumourigenesis. Gasser et al. provided a mechanistic link between the DDR and immune surveillance of premalignant lesions by the upregulation of NKG2DLs. By using various genotoxic stressors on both mouse and human non-tumour cell lines to induce an ATM/ATR-mediated DNA damage checkpoint, they demonstrated increased NKG2DL expression. This upregulation could be abrogated by specific inhibition of this DNA damage checkpoint. Furthermore, they suggest that established tumour cells sustain their increased NKG2DL expression due to chronic activation of the DNA damage checkpoint (Gasser et al., 2005).

A further link between DNA damage in cancer cells and NKG2DL expression was later made with the observation that doxycycline-inducible p53 mediated ULBP1 and ULBP2 surface upregulation in p53-null human non-small cell lung cancer cells (Textor et al., 2011).

Detection of cytosolic dsDNA by PRRs is critical in triggering the innate immune response towards cytosolic DNA, either of viral origin, or because of DNA

damage associated with cancer cells. A study using mouse lymphoma cell lines demonstrated that the DDR in cancer cells resulted in cytosolic dsDNA, which activated the cGAS-STING pathway, triggering an IRF3-dependent induction of RAE-1 ligands (Lam et al., 2014).

NKG2DLs are upregulated in tumours through deregulation of the cell cycle and activated cell signalling

Excessive and dysregulated cell cycle entry is a feature of cancer cells. E2F transcription factors play a crucial role in regulating the transition from G1 phase to S phase and entering the cell cycle. Studies using proliferating mouse cells demonstrated that proliferative signals in these cells induced increased transcription of murine NKG2DLs (Jung, Hsiung, Pestal, Procyk, & Raulet, 2012). This proliferation-induced transcription was dependent on E2F transcription factors, which have binding sites in the promoter regions for NKG2DLs (Jung et al., 2012).

The PI3K pathway is a key regulator of cell survival and proliferation, and is commonly activated in the early stages of tumourigenesis (Cully, You, Levine, & Mak, 2006). PI3K activation is involved in maintaining sustained expression of RAE-1 and MULT1 in transformed mouse cell lines (Tokuyama et al., 2011). However activation of the PI3K pathway alone was not sufficient to induce expression in cells, suggesting other factors also influenced expression (Tokuyama et al., 2011). In line with this evidence, c-Myc activity (downstream of PI3K pathway) is involved in NKG2DL expression during early stages of tumourigenesis in a spontaneously developing murine lymphoma model (Unni, Bondar, & Medzhitov, 2008).

As mentioned earlier, ultraviolet B stress-induced EGFR signalling can cause MICA, MICB and ULBP2 upregulation in human epithelial cells (Vantourout et al., 2014). Given the EGFR signalling pathway is commonly hyperactivated in human

cancers, and the positive correlation between EGFR and NKG2DL expression in human carcinomas (Vantourout et al., 2014), this may highlight another mechanism in which cancer cell phenotypes induce NKG2DL expression.

1.8.4.2 Cancer strategies to evade NKG2D immune response

As observed with a variety of different viruses, achieving immune evasion is also a critical step in cancer progression, as discussed in section 1.2.1. Given this selective pressure applied to cancer cells, it is unsurprising that many cancers also acquire mechanisms to promote immune escape by modulating the NKG2D response. Many of the cancer NKG2D evasion mechanisms overlap with those observed by viruses (Table 1.4), suggesting a degree of convergent evolution between viruses and cancers (Baugh et al., 2020). For example, experimentally induced tumour cells were positive for RAE-1 protein expression in perforin-deficient mice, whereas expression was low or absent in WT mice, indicating a selection pressure exerted by the immune system for cancer cells to reduce or lose expression of NKG2DLs (Smyth et al., 2005). A wide variety of NKG2D immune evasion mechanisms have been documented in a range of cancers and are summarised in Table 1.5.

Table 1.5 Summary of cancer immune evasion of the NKG2D response

	Target	Mediated by	Mechanism	Cancer	Reference
Shedding	NKG2DLs	ADAM10, ADAM17, MMP14	Fewer surface ligands on cell surface	Various	(Boutet et al., 2009; Groh, Wu, Yee, & Spies, 2002; G. Liu, Atteridge, Wang, Lundgren, & Wu, 2010; Waldhauer et al., 2008)

	NKG2D receptor	ADAM10, ADAM17, MMP14	Shed NKG2DLs binding to NKG2D causes downregulation of NKG2D on TILs and PBMCs	Various	(Boutet et al., 2009; Groh et al., 2002; G. Liu et al., 2010; Waldhauer et al., 2008)
miRNA	MICA and MICB	Cancer associated miRNAs	Destabilisation of mRNA	Various	((Noam Stern-Ginossar et al., 2008).
Reduced transcription	NKG2DLs	2-Hydroxyglutarate	Epigenetic hypermethylation causing transcriptional silencing	IDH-mut gliomas	(X. Zhang et al., 2016)
	MICA, ULBP2, ULBP4	TGF-β	Reduced transcription	Glioma	(Eisele, 2006; Friese et al., 2004)
Intracellular retention and proteasomal degradation	MICA	?	Retained in ER and then trafficked for proteasomal degradation	Melanoma	(Fuertes et al., 2008)
Immune subversion	NKG2D receptor	TGF-β	Downregulation of NKG2D on TILs and PBMCs	Glioma	(Crane et al., 2010)
	Induced NKG2DL expression on monocytes	LDH-5	LDH-5 induces NKG2DL expression on monocytes which downregulates NKG2D on PBMCs and TILs	GBM	(Crane et al., 2014).

Abbreviations: Natural killer group 2 member D ligands (NKG2DLs), Natural killer group 2 member D (NKG2D), a disintegrin and metalloprotease (ADAM), matrix metalloprotease (MMP), tumour infiltrating lymphocyte (TIL), peripheral blood mononuclear cell (PBMC), microRNA (miRNA), MHC-class-I-polypeptide-related sequence (MIC), UL16 binding protein (ULBP), isocitrate dehydrogenase (IDH), transforming growth factor β (TGF-β), endoplasmic reticulum (ER), lactate dehydrogenase (LDH).

1.8.5 Strategies employed by the immune system to counter viral and tumour immune evasion

In parallel to the selection pressures exerted on viral and tumour evolution, they impart their own selection pressure on the immune system. While viruses and cancer cells develop ways to downregulate or subvert the NKG2D response, the immune system has developed various means to counteract.

For example, using a family of multiple different ligands that are all capable of binding to the NKG2D receptor endows certain advantages to the organism. It enables a degree of functional redundancy, in which various signals and pathways induce the expression of different ligands, all of which converge on binding to NKG2D and bringing about a similar immune response (Eagle & Trowsdale, 2007). However, evidence is emerging to suggest that NKG2DLs are non-redundant, and that induced expression of certain ligands reflects a specific danger signal and threat (Zingoni et al., 2018). For example, ULBP1 expression positively correlates with leukaemia sensitivity to NKG2D-mediated lysis by γδ T cells, and loss of ULBP1 conferred resistance to lysis, whereas MICA downregulation did not (Lança et al., 2010). Although specific pathways may induce expression of certain ligands, the pathways themselves tend to be shared by a general cellular phenotype that reflects danger: either stress, infection, or neoplastic transformation. Furthermore, ligand diversity makes total immune evasion as a result of viral gene products or a mutation during malignant transformation far more unlikely (Eagle & Trowsdale, 2007; Zingoni et al., 2018).

In addition to the range of different NKG2DLs, they are also some of the most polymorphic genes in humans. Different ligands, and even different alleles can change the extent of NKG2D receptor signalling. For example, the MICA-129Met variant has a far greater binding affinity to NKG2D compared to the MICA-129Val isoform, and results in stronger signalling and faster activation kinetics (Isernhagen, Malzahn, Bickeböller, & Dressel, 2016).

1.9 Thesis overview and aims

1.9.1 Thesis overview

GBM therapy is in desperate need of improvement, with patient survival statistics being left behind compared to the advancements seen in other cancers. Current GBM treatment strategies are limited by tumour heterogeneity, immunosuppressive TME and resistant GSCs (C. Jackson et al., 2011).

Oncolytic virotherapy is a promising strategy for GBM immunotherapy, offering the potential to selectively infect and replicate within cancer cells and cause direct cancer cell lysis, as well as promoting pro-inflammatory immune responses. oHSV-1 has been one of the most studied classes of OVs and have been explored extensively for GBM immunotherapy. G207 is an oHSV-1 that has been trialled clinically for GBM, with evidence of good safety profiles, viral replication within the tumour (J. M. Markert et al., 2009), and even increased survival times (Whisenhunt et al., 2015) when administered via stereotactic injection. However, despite pre-clinical efficacy (Mineta et al., 1994, 1995) and some clinical success (Whisenhunt et al., 2015), G207 lacks the potency required to eradicate tumours, owing, in part, to its inability to infect GSCs (Kanai et al., 2012; Peters et al., 2018). Therefore, this thesis aimed to develop means of enhancing this potency for GBM therapy.

BiTEs are a class of immunotherapeutic that direct T cell activation and cytotoxicity towards target cells expressing surface TAAs in a TCR- and HLA-independent manner and enable the activation of both $CD4^+$ and $CD8^+$ T cells. Although a powerful tool in the arsenal of cancer immunotherapy, BiTEs are limited by their poor half-life and on-target, off-tumour effects when given systemically (Klinger et al., 2012; Teachey et al., 2013). OVs offer an attractive means of BiTE delivery; by encoding within the OV genome, BiTE expression can be restricted to

the TME. The combination of OVs and BiTEs have been demonstrated in various instances previously, leading to improved cytotoxicity and immune responses (Freedman et al., 2017; Khalique et al., 2021; Yu et al., 2014). Compared to other tumour types, BiTE-armed OVs for GBM immunotherapy have not been explored as extensively. One of the few examples of OV-BiTE therapy for gliomas was performed by Arnone et al. engineered an oncolytic adenovirus armed with an anti-EphA2 BiTE for paediatric high-grade glioma, and showed enhanced cytotoxicity *in vitro* and *in vivo* (Arnone et al., 2021). Therefore, arming G207 with a BiTE provides a novel opportunity to boost its potency in GBM.

NKG2DLs have widely been reported to be upregulated on several cancer types, including gliomas (Chitadze et al., 2017; Friese et al., 2003), but expression is mostly absent on healthy tissues (Schrambach et al., 2007). Therefore, targeting NKG2DLs for GBM therapy have been explored, including relying on human γδ T cells *in vitro* (Chitadze et al., 2016), as well as ACT strategies with engineered γδ and NKG2D-CAR-T cells (Lamb et al., 2013; Weiss, Weller, et al., 2018). There is also growing evidence that following DNA damage induced by TMZ and radiation therapy, NKG2DLs are further upregulated on GBM cells and can increase sensitivity to NK cell lysis (Weiss, Schneider, et al., 2018). A BiTE targeting NKG2DLs in mice has previously been described, using the murine NKG2D receptor as the NKG2DL-binding domain (T. Zhang & Sentman, 2011). Therefore, a BiTE targeting human NKG2DLs may be an effective strategy for eradicating GBM cells and may complement the activity of the G207 virus. By using the NKG2D receptor as the NKG2DL-binding domain, as opposed to a mono-specific scFv used in conventional BiTE formats, the BiTE will be able to target all eight NKG2DLs effectively.

1.9.2 Thesis aims and hypotheses

1. **Overall hypothesis:** *NKG2DLs serve as a pan-cancer antigen associated with a malignant phenotype that can be targeted with BiTEs*
2. A BiTE targeting NKG2DLs on GBM cells will direct T cell activation and cytotoxicity (Chapter 3)
3. NKG2D BiTE activity will be enhanced by conventional GBM therapy of TMZ and radiation (Chapter 4)
4. G207 is a suitable platform with which to express NKG2D BiTE to achieve a dual mechanism of cytotoxicity towards GBM cells of viral oncolysis and BiTE-mediated killing (Chapter 5)

2 Materials and methods

2.1 Cell lines and tissue culture

2.1.1 Cell lines and passage

Adherent cell lines and the corresponding culture medium conditions used are summarised in Table 2.1. All cell lines were sourced from the American Type Culture Collection (ATCC). Cells were cultured in an incubator at 37 ˚C and 5% CO_2. Cells were routinely passaged once every 3-4 days by removing cell culture media, washing with Dulbecco's phosphate-buffered saline (1x DPBS; #14190250, Gibco™), then treating with an enzymatic solution consisting of 0.25% trypsin and 0.02% ethylenediaminetetraacetic acid (EDTA) (#T4049, Sigma-Aldrich®) until cells dissociated. Trypsin was neutralized with medium containing foetal calf serum (FCS; #10500064, Gibco) and cells were split at ratios denoted in Table 2.1. Cell lines were routinely tested for mycoplasma using the MycoAlert™ Mycoplasma Detection Kit (#LT07-318, Lonza).

Table 2.1. Culture conditions for cell lines and primary cells

Cell line/cell type	Medium and serum	Additional supplements	Subculture time	Notes
U87 – Human brain tumour cell line (likely of Glioma origin)	DMEM + 10% FCS		3-4 days	Normal culture
	NBM	B27 EGF FGF Glutamax P/S	3-4 days	GSC culture
A172 – Human GBM cell line	DMEM + 10% FCS		3-4 days	Normal culture
DLD-1 – human colorectal adenocarcinoma cell line	DMEM + 10% FCS		3-4 days	Normal culture

Vero – African Green Monkey kidney cells	DMEM + 10% FCS		3-4 days	Normal culture and G207 oHSV-1 production/titration
293Ad – Human embryonic kidney cells (with a stably integrated copy of adenovirus E1 gene)	DMEM + 10% FCS		3-4 days	Transfection and BiTE production
PBMC-derived macrophages	X-VIVO-10 + 2% HS			Monocyte to macrophage differentiation – 6 days
PBMC-derived T cells	RPMI + 10% FCS			Recovery after thawing
	RPMI + 2% FCS			Co-culture and treatment assays
Human patient- derived GBM cells	RPMI + 10% FCS			Normal culture
	NBM	B27 EGF FGF Glutamax P/S		GSC culture

Abbreviations and manufacturers: Dulbecco's Modified Eagle's Medium (DMEM; #D5796, Merck Life Science UK), Roswell Park Memorial Institute 1640 medium (RPMI; #R8758, Merck Life Science UK), X-VIVO-10 (#0000976232, Lonza), neurobasal media (NBM; #21103-049 Gibco), heat-inactivated foetal calf serum (FCS; #10500064, Life Technologies), heat-inactivated human serum (HS, #H3667, Merck), B27 Supplement (#17504044, ThermoFisher Scientific), epidermal growth factor (EGF; #1021AFC05, Peprotech), fibroblast growth factor (FGF; #052108, Peprotech), Glutamax (#3505-061, Gibco), penicillin/streptomycin (P/S; #1514-122, Gibco), glioblastoma (GBM).

GSCs were cultured in NBM, see Table 7.1 for list of ingredients.

2.1.2 Storage of cell lines

Cells were dissociated with trypsin, centrifuged at 400 x g for 5 minutes (mins) and resuspended in freezing medium consisting of FCS with 10% volume/volume (v/v) dimethyl sulfoxide (DMSO; #D2650, Sigma-Aldrich®), aliquoted into 1.8 mL cryogenic vials and frozen at 1 ˚C per minute in a freezing container (CoolCell®, Corning™) at -80 ˚C. To thaw cells, vials were incubated at 37 ˚C until thawed, then 30 mL of pre-warmed medium was added dropwise, and cells were pelleted by centrifugation (400 x g, 5 mins). Cells were resuspended in fresh, warmed medium

and left to adhere for 24 hours in an adherent flask before medium was aspirated and replaced.

2.1.3 Cell seeding

Cells were dissociated as described above and counted using a haemocytometer. Viability was assessed by trypan blue exclusion (#15250061, Gibco™). The cell number was adjusted to the required experimental seeding density, and the cells seeded into treated tissue culture plastic plates (Greiner Bio-One) in the relevant medium.

2.2 Flow cytometry

2.2.1 Cell dissociation for flow cytometry

For adherent cells, culture medium was removed and cells were washed twice with DPBS before adding enzyme-free dissociation buffer (#13151014, Gibco™) and allowing 5-10 min at 37 ˚C for cells to lift. Dissociated cells were removed and transferred into a 96-well V-bottom plate (Corning, #3894) (96V) for staining. Remaining cells in the original well were washed with further DPBS (or dissociation buffer if required) to ensure all adherent cells were collected.

Non-adherent T cells were harvested by collecting medium and subsequent DPBS washes and were transferred into 96V plates for staining.

2.2.2 Cell surface staining

All staining steps described below were performed in 96V plates. Following the collection of cells as described above, cells were centrifuged in the 96V plate

(400 x g, 5 mins), supernatant removed and washed with DPBS and centrifuged again. Any immune cells or patient-derived cells were blocked with 50 μL FcR blocking reagent (#130-059-901, Miltenyi Biotec) diluted 1/100 in MACS buffer (Table 7.1) for 10 mins at 4 ˚C. Cancer cell lines did not require FcR blocking. After the blocking step, wells were topped up to 200 μL total volume with DPBS. Control wells for each cell type used were included, including a Live/Dead positive control - 100 μL of the well was removed and heated at 95 ˚C for 5 min, followed by cooling at 37 ˚C for 5 min before adding back to the well, thus creating a 1:1 ratio of live and dead T cells. The whole 96V plate was then centrifuged again and the supernatant removed. Cells were resuspended in 50 μL/well MACS buffer containing a staining cocktail of antibodies and dyes for 10 mins at 4 ˚C (Table 2.2) and incubated for 30 mins at 4 ˚C whilst protected from light.

Following staining, cells were washed twice with DPBS, and fixed for 15 minutes at room temperature (RT) in 10% neutral buffered formalin (100 μL/well) (#MCFC00003274, Merck). Fixed cells were washed once with 1x DPBS and resuspended in 200 μL MACS buffer/well. Plates were stored protected from light at 4 ˚C until data acquisition as soon as possible (typically within 24 hours, but a maximum of 7 days).

2.2.3 Intracellular staining

For intracellular assessment of cytokines or secreted granules, cells were treated with GolgiStop (Monensin, #554724, BD Biosciences) and GolgiPlug (Brefeldin A, #555029, BD Biosciences), according to the manufacturer's instructions 5 hours before harvesting and staining. GolgiStop and GolgiPlug inhibit

intracellular trafficking and secretion, enabling intracellular detection of molecules such as IFN-γ and granzyme B.

Following on from the protocol described above, after surface staining and fixing, cells were centrifuged (400 x g, 5 mins). Cells were then resuspended in 150 µL/well of intracellular staining permeabilisation wash buffer (Perm/Wash; #421002, BioLegend) diluted 1/10 in dH_2O. Cells were then resuspended again in 150 µL Perm/Wash buffer per well and centrifuged (400 x g, 5 minutes). This step was repeated for a second time. Following permeabilisation, cells were stained for intracellular markers by incubating with fluorophore-conjugated antibodies (Table 2.2) diluted in MACS buffer (50µL/well) for 30 minutes at 4 ˚C whilst protected from light. Cells were then washed twice with 1x DPBS and resuspended in 200 µL MACs buffer/well. Plates were protected from light and stored at 4 ˚C until data acquisition.

2.2.4 Antibodies

Table 2.2 List of antibodies, constructs and dyes used for flow cytometry

Antigen	Clone	Isotype	Fluorophore(s)	Dilution	Manufacturer	Catalogue number(s)
CD3	UCHT1	Ms, IgG1, κ	Pacific blue	1: 200	Biolegend	#302606
CD4	OKT4	Ms, IgG2b, κ	APC, FITC, PE	1: 200	Biolegend	#317416, #317408, #317410
CD8a	HIT8a	Ms, IgG1, κ	APC	1: 200	Biolegend	#300912
CD11b	29E2A3	Ms, IgG2b, κ	BV421	1: 100	Biolegend	#329713
CD25	BC96	Ms, IgG1, κ	PE, PE-Cy7	1: 200	Biolegend	#302606, #302612
CD69	FN50	Ms, IgG1, κ	FITC, BV605	1: 200	Biolegend	#310904, #310938
CD80	2D10	Ms, IgG1, κ	PE	1: 100	Biolegend	#305208
CD107a	H4A3	Ms, IgG1, κ	PE-Cy7	1: 100 (Added during cell culture)	Biolegend	#394110

EGFR	9C4	Ms, IgG2b, κ	PE	1:100	Biolegend	#324206
Granzyme B	GB11	Ms, IgG1, κ	Pacific blue	1: 100	Biolegend	#515408
IFN- γ	4S.B3	Ms, IgG1, κ	FITC	1: 100	Biolegend	#502506
MICA/B	6D4	Ms, IgG2a, κ	APC	1: 100	Biolegend	#320908
PD-L1	29E2A3	Ms, IgG2b, κ	BV421	1: 100	Biolegend	#329713
Perforin	BD48	Ms, IgG1, κ	PE	1: 100	Biolegend	#353304
LIVE/DEAD ™ Fixable Near-IR dead cell stain			Near-IR	1: 5000	ThermoFisher Scientific™	#L10119
rhNKG2D-Fc		Hm, IgG1		1: 100	R&D Biosystems	#1299-NK-050
Streptavidin -PE			PE		ThermoFisher Scientific™	# SA10041
Species	Clone	Isotype	Fluorophore(s)	Dilution	Company	Catalogue number(s)
Mouse	MOPC-21	IgG1, κ	APC, FITC, Pacific blue, PE	As above	Biolegend	#400120, #400108, #400151, #981804
Mouse	MOPC-173	IgG2a, κ	APC	As above	Biolegend	#400219
Mouse	MPC-11	IgG2b, κ	APC, FITC, PE	As above	Biolegend	#400322, #400310, #400314
Human		IgG1		1: 100	R&D Biosystems	#110-HG

2.2.5 Data acquisition and analysis

Flow cytometric data acquisition was performed on an Attune™ NxT Flow Cytometer (ThermoFisher Scientific™). For each sample, either 155 μL (out of a total of 200 μL) was collected, or at least 10,000 events at a flow rate of no more than 500 μL/min. Data was analysed using with FlowJo™ v10.8.1 software (BD Biosciences). An example of a typical gating strategy for data processing is shown in Figure 2.1. For all experiments only single cell populations were considered using

a doublet discrimination strategy, followed by selection for live cells using viability stains.

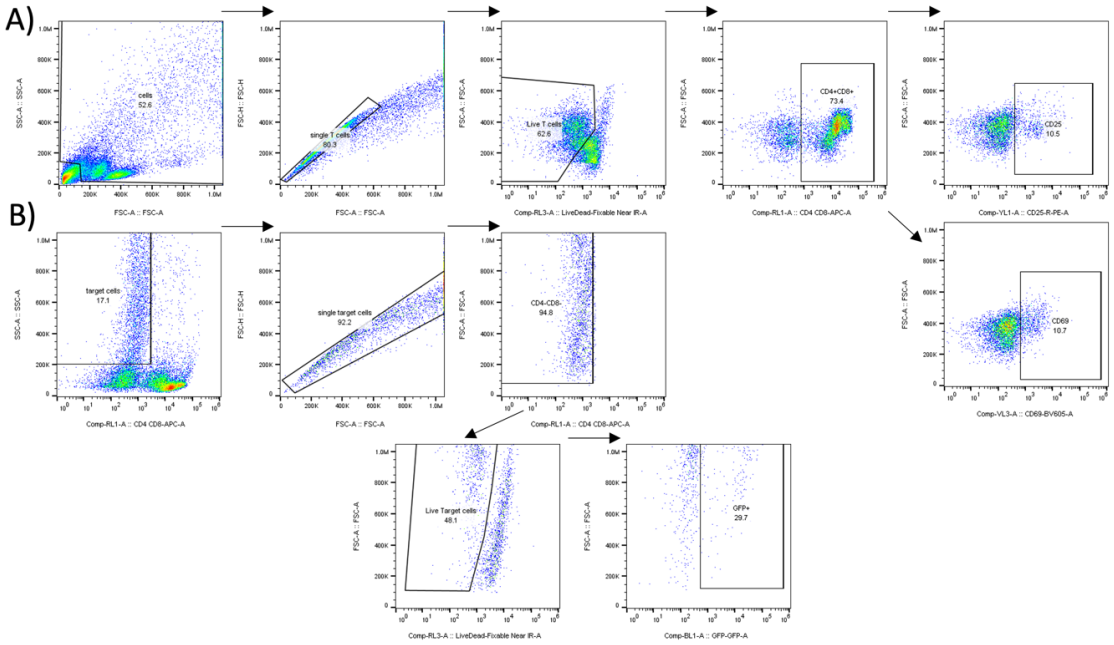

Figure 2.1 Representative flow cytometry gating strategy
The representative gating strategy is based on a typical flow cytometry analysis of U87 GBM cells co-cultured with T cells. The U87 cells are infected with G207-NKG2DBiTE virus, and so infected cells express GFP. After 96 hours of co-culture, T cells and U87 cells were harvested and stained for CD4-APC, CD8-APC, CD25-PE, CD69-BV605, and LIVE/DEAD Fixable Near-IR. Data was acquired using an Attune NxT flow cytometer and analysed with FlowJo software. (A) T cell gating. Firstly, all cell events were detected, and the debris from the bottom corner was excluded, followed by doublets. Live T cells were the identified by Live cells (LIVE/DEAD Fixable Near-IR-negative), then CD4+CD8+ T cells (CD4-APC and CD8-APC-postive). T cell activation was then measured by the percentage of cells positive for CD25-PE and CD69-BV605. (B) Tumour cell gating. From the same sample, the events derived from the initial gate were remove doublet cells gated to remove T cells (CD4-APC and CD8-APC negative), then the U87 cell viability was assessed (LIVE/DEAD Fixable Near-IR-negative), and the percentage of infected cells was measured by the percentage of GFP-positive live cells.

2.3 rhNKG2D

2.3.1 Conjugation of NKG2D-Biotin

To assess the expression of all NKG2DLs, a recombinant human NKG2D with human IgG Fc domain (rhNKG2D-Fc, R&D Biosystems, #1299-NK-050) fusion protein was used as a primary for staining. The rhNKG2D-Fc was biotinylated using a Biotin Conjugation Kit (Lightning-Link®, Abcam, #ab201795) according to the

manufacturer's instructions. As an isotype control, recombinant human IgG1 (rhIgG1-Fc; #110-HG-100, R&D Biosystems,) was also biotinylated. The biotinylated rhNKG2D-Fc (rhNKG2D-Fc-Bio) and IgG1-Fc (IgG1-Fc-Bio) were immediately ready to use, at a concentration of 80 μg/mL.

2.3.2 Optimisation of rhNKG2D-Fc-Bio staining

The rhNKG2D-Fc-Bio and rhIgG1-Fc-Bio were used like primary antibodies for staining, with Streptavidin conjugated to the fluorophore PE (Strep-PE, ThermoFisher Scientific, #SA10041) as the secondary stain. The primary staining protocol was as described in section 2.2.2. Cells were then washed with DPBS twice, before being resuspended with the Strep-PE secondary in MACS buffer. After secondary staining, the staining procedure in 2.2.2 was followed to completion, including fixation.

To determine the optimal concentration of primary and secondary stains, both were titrated on DLD-1 cells at 1: 50, 1: 100 and 1: 200 dilutions, and analysed by flow cytometry. For both rhNKG2D-Fc-Bio and Strep-PE, a dilution of 1: 100 gave the optimal signal to noise ratio.

2.4 Immune cell isolation, culture, and assays

2.4.1 General statement

Leukocyte cones used throughout this thesis were acquired from the NHS Blood and Transplant Service (NHSBT; Oxford, UK). Informed consent was obtained at the time of donation by the NHSBT. Ethical approval for the study was

obtained from the Health Research Authority (REC reference 19/LO/1848; IRAS ID 253836).

2.4.2 Isolation of human PBMC-derived monocytes and lymphocytes

Lymphocytes were obtained from whole blood leukocyte cones provided by the NHSBT, using double-density gradient centrifugation.

PBMCs were isolated by diluting the 10 mL of blood from the leukocyte cone in 130 mL 1x DPBS. Then, 35 mL of diluted blood was carefully overlaid onto 4 x 50mL falcon tubes each containing 15 mL Ficoll® Paque Plus (#GE17-1440-02, GE Healthcare) and centrifuged (Step 1 in Table 2.3). Four layers can be observed after centrifugation; from top to bottom, plasma, a PBMC interphase, Ficoll®, and a granulocyte and red blood cell (RBC) pellet. The PBMC layer was collected and washed 3x in DPBS (Steps 2-4 in Table 2.3).

Washed PBMCs were resuspended in 20 mL RPMI 1640 (#R8758, Merck Life Science UK) containing 10% FCS (10% RPMI), 5 mL of the suspension was overlaid onto 4 x 15 mL falcon tubes each containing 6 mL of a Percoll® PLUS solution (46%, 285 mOsm; #GE17-5445-01, GE Healthcare) and centrifuged (Step 1 in Table 2.3). Four layers can be observed after centrifugation; from top to bottom, 10% RPMI, a monocyte interphase, Percoll® and a lymphocyte pellet. Both the monocyte interphase and the lymphocyte fractions were collected separately and washed as before with 1x DPBS (Steps 2-4 in Table 2.3)

Table 2.3 Density gradient centrifugation and wash steps to isolate lymphocytes from human peripheral blood

Step	Speed (x g)	Time (minutes)	Acceleration	Deceleration
1	950	30	Half maximal	Off
2	950	10	Maximal	Half maximal
3	450	10	Maximal	Maximal
4	200	10	Maximal	Maximal

Lymphocytes were cryopreserved and stored at -80 ˚C until needed (20 x 10^6 cells/mL freezing medium). Monocytes were seeded in X-VIVO-10 medium (#0000976232, Lonza) (Table 2.1) supplemented with 2% heat inactivated human serum (HS; #H3667, Merck) at a density of 3-4 x 10^6 cells/mL in low adherence T175 flasks (#83.3912.500, Sarstedt)

2.4.3 Differentiation and polarisation of macrophages

PBMC-derived monocytes were polarised into macrophages using 2% HS in X-VIVO-10 media for 6 days in T175 low adherence flasks. On day 4, macrophages were either left untreated (unpolarised, M0), or treated with either 25 ng/mL IFN-γ (#130-096-873, Miltenyi Biotech) and 10 ng/mL LPS (#L2630, Merck) (classically activated, M1) or with 10 ng/mL IL-10 (#200-10-10UG, Peprotech) (alternatively activated, M2c) for the remaining 48 hours. For dissociation, macrophages were washed three times with DPBS before incubating with 5 mL 20 mM EDTA at 37 ˚C for 10 mins. If cells remained adhered after this time, they were manually dissociated using a cell scraper. Harvested macrophages were then seeded or stained depending on the experiment.

2.4.4 T cell isolation

Lymphocytes were thawed and incubated to rest in 10% RPMI for at least 12 hours at 37 ˚C, 5% CO_2 at a concentration of 5 x 10^6 cells/mL. $CD3^+$ cells were directly separated using the Pan T cell isolation kit (#130-096-535, Miltenyi Biotec) following manufacturer's instructions. In this process non-T cells are magnetically labelled with biotinylated antibodies and then bound by anti-biotin microbeads. Bound cells are retained in an LS column (#130-042-401, Miltenyi Biotech) when using a QuadroMACS® magnetic separator (Miltenyi Biotech) whilst T cells pass through and can be collected.

2.4.5 T cell co-culture and BiTE assays

All experiments requiring co-culture of T cells and target tumour cells were performed as described below unless otherwise stated. Target cells were seeded in flat bottom 96-well (96F) plates (#3595, Corning) in 100 µL of relevant cell culture medium (Table 2.1) at a density of 2 x 10^4 cells/well. Lymphocytes derived from a leukocyte cone were thawed and allowed to rest on the same day as target cells were seeded. The following day, $CD3^+$ T cells were isolated and resuspended in 2% RPMI. Target cell seeding medium was replaced with T cells seeded at an Effector: Target (E: T) cell ratio of 5: 1 (1 x 10^5 T cells/well) alongside the adherent target cells in 2% RPMI. Any treatments to be tested (such as BiTEs) were added at this stage alongside T cells at the relevant concentration to a final volume of 100 µL.

Human T-activator CD3/CD28 beads (Dynabeads™; #11131D, Gibco™) were added at 1 µL/well as a positive control for T cell activation. Plates were incubated

at 37 ˚C, 5% CO_2 before T cells and/or target cells were harvested for analysis at specified time points, depending on the experiment.

2.4.6 Characterisation of T cell activation and target cell viability

To assess T cell activation, surface marker expression was measured using flow cytometry. Staining for CD4 and CD8 instead of CD3 (a pan-T cell marker) was utilised, as BiTE or CD3/CD28 beads may interfere with anti-CD3 staining. CD25 and/or CD69 were used for surface markers of activation. T cells were stained with LIVE/DEAD™ Fixable Near-IR cell stain to exclude dead T cells during analysis.

To assess production of intracellular IFN-γ and granzyme B, co-cultures of T cells and target cells were treated with BiTE for 72 hours. All wells were then treated with GolgiStop and GolgiPlug (as described in section 2.2.3) for 5 hours before harvesting for staining of surface markers followed by intracellular staining for IFN-γ and granzyme B.

T cell degranulation was assessed by measuring CD107a surface expression. Co-cultures of T cells and target cells were treated with BiTE for 72 hours, wells were then treated with GolgiStop and GolgiPlug alongside a fluorescently conjugated anti-CD107a antibody in 2% RPMI for 5 hours before harvesting for staining of surface markers. GolgiStop and GolgiPlug prevent the re-internalisation of CD107a, allowing the anti-CD107a antibody in the media to bind receptors on the surface.

To assess T cell-mediated killing of target cells, all cells in the treated co-culture wells were collected and stained for T cell activation markers and LIVE/DEAD™ Fixable Near-IR dead cell stain. During flow cytometry data analysis,

target cell viability was assessed by calculating the percentage of live non-T cells ($CD4^-$ $CD8^-$).

2.4.7 T cell co-culture and virus assays

To assess the activation of T cells in response to infection with oHSV-1 and oHSV-1-produced BiTE, target cells were seeded as described above, and infected one day post-seeding (see section 2.9.5 for virus infection protocol) in 5% RPMI. Target cells were infected for 4 hours before T cells were added to the co-cultures. Cells were incubated at 37 ˚C, 5% CO_2 for specified time-points before harvesting. T cell activation and target cell viability were measured as described above. Use of virally-encoded green fluorescent protein (GFP) allowed quantification of infected cells.

2.4.8 Lactate dehydrogenase release cytotoxicity assays

Lactate dehydrogenase (LDH) is a cytosolic enzyme that is released into the supernatant upon cell lysis, hence its extracellular accumulation is proportional to cell lysis. To measure LDH in the supernatant, a CytoTox96® Non-Radioactive Cytotoxicity Assay kit (#G1780, Promega) was used according to the manufacturer's instructions. This kit includes a reagent containing tetrazolium salt which is converted into a red formazan product in an enzymatic reaction coupled with LDH, resulting in the conversion of lactate to pyruvate.

For each well, 50 μL of cell culture supernatants were collected from each were obtained after treatments at the desired time, transferred to 96V plates, centrifuged (400 x g, 5 mins) to pellet cellular debris, and the clarified 50 μL supernatant was transferred to a 96F plate. Supernatants were tested immediately

or stored at -20 ˚C for future use. In brief, 50 µL assay reagent was added to each well and plates incubated for 30 mins at RT protected from light. To stop the reaction, 50 µL Stop solution was added and the absorbance measured at 490 nm using a Varioskan LUX plate reader (Thermo).

Positive lysis controls were included in each experiment using the cell lysis reagent provided in the kit according to the manufacturer's instructions. Negative media blanks were also included.

The percentage cytotoxicity was calculated using the formula:

$$\%\ Cytotoxicity = \frac{Experimental - media\ blank}{Target\ maximum - media\ blank} \times 100$$

2.4.9 MTS viability assays

To measure cell viability of cells in culture, the CellTiter 96® AQ_{ueous} One Solution Cell Proliferation Assay (MTS) kit (#G3582, Promega) was used according to the manufacturer's instructions. The reagent contains [3-(4, 5-dimethylthiazol-2-yl)-5-(3-carboxymethoxyphenyl)-2-(4-sulfophenyl)-2H-tetrazolium, inner salt] (MTS) and an electron coupling agent (phenazine ethosulphate; PES). Metabolically active cells produce reducing equivalents that reduce MTS, resulting in a chromogenic reaction proportional to the number of live cells.

Target cells were seeded in 96F plates at a density of 2 x 10^4 cells/well and were infected the following day with increasing multiplicities of infection (MOIs) of oHSV-1 the following day (see section 2.9.5 for virus infection method). Three days after infection, media and dead cells were removed, the well was washed twice with

DPBS, and 100 µL of MTS reagent at working concentration (5-fold dilution in 1x DPBS) was added to each well. Plates were incubated at 37 ˚C in a humidified incubator for 1 – 4 hours and the absorbance was measured at 490 nm using a Varioskan LUX plate reader.

2.4.10 BiTE conditioned media on ascites polarised macrophages

Ascitic fluid used in section 4.3.8 of this thesis was acquired with informed consent from cancer patients at the Churchill Hospital, Oxford, UK, using a routine therapeutic paracentesis procedure. Ethical approval for the study was gained from the institutional review board and research ethics committee of the Oxford Centre for Histopathology Research (Reference 09/H0606/5+5) in accordance with the UK Human Tissue Act 2004 and Declaration of Helsinki.

Using aseptic technique, ascites fluids were collected into 50 mL falcon tubes and centrifuged (400 x g, 10 mins) at RT to separate the fluid components from the cellular fraction. The acellular supernatant was centrifuged again before being stored at -20℃ until required.

PBMC-derived monocytes were isolated and differentiated into macrophages as described in section 2.4.3. On day 4, the 2% HS X-VIVO medium was replaced with either fresh 2% HS X-VIVO or a 1: 1 mix of 2% HS X-VIVO and heterologous patient-derived ascites fluid (Sample ID #AS190823), previously determined by others to be immunosuppressive (data not shown), for a further 2 days. Macrophages were dissociated with 20 mM EDTA and seeded into 24 well plates at 1 x 10^5 cells/well in 250 µL 2% HS X-VIVO and 250 µL conditioned media. Conditioned media was pooled from U87 + T cell (autologous to the macrophages)

co-cultures treated with 1 nM NKG2D or Control BiTE for 96 hours or left untreated. As further controls, cytokines (IFN-γ, LPS and IL-10) were spiked into the macrophage wells. Macrophages were harvested with 20 mM EDTA 48 hours later and stained for flow cytometry analysis.

2.5 Pre-treatment assays

2.5.1 BiTE with G207 infection

For the experiment in section 4.3.2, cells infected with G207 oHSV-1 were also treated with NKG2D BiTE and T cells. A172 and U87 cells were seeded in 96F plates at 2 x 10^4 cells/well in 10% DMEM. The following day, seeding media was removed and cells were infected with G207 oHSV-1 across a range of MOIs (see section 2.9.5 for virus infection protocol). Following 4 hours of infection, 1 x 10^5 PBMC-derived T cells were added and treated with 1 nM NKG2D or left untreated. Cells were co-cultured for 96 hours before harvesting and staining for flow cytometric analysis.

2.5.2 TMZ and radiation pre-treatment

Target cells were seeded in T-25 (#83.3910.002, Sarstedt) flasks at 1 x 10^6 cells/flask in relevant culture media the day before TMZ or radiation treatment.

For TMZ treatment, seeding media was removed and replaced with fresh medium with the relevant concentration of TMZ (#466760010 ThermoFisher Scientific™) or equivalent volume of DMSO vehicle control.

For radiation treatment, all flasks were taken out of the incubator and taken to the radiation facility, where they were exposed to ionising radiation at the relevant

dose using a caesium-137 irradiator or left untreated (mock irradiated). Any potential stress induced by removing cells out of the incubator and during transit was therefore controlled for.

For TMZ and radiation viability and surface expression experiments, cells were incubated following pre-treatment and harvested at the relevant time-point (including any dead non-adherent cells in the media) using non-enzymatic cell dissociation buffer (as per section 2.2.2) Total cells were stained as described in section 2.3.2, and surface NKG2D, MICA/B or viability was assessed by flow cytometry.

For pre-treatment experiments involving BiTE or virus and T cell co-cultures, target cells were incubated for 48 hours following TMZ/radiation pre-treatment, before dissociating with non-enzymatic dissociation buffer. Cells were counted using trypan blue exclusion, and live cells were seeded in 96F plates at 2 x 10^4 cells/well in 10% DMEM containing fresh TMZ at the relevant concentration (or equivalent volume of DMSO). The following day, TMZ/DMSO media was removed and replaced with BiTE or virus treatment and T cell co-cultures as described in section 2.4.5 and 2.4.7. Treated co-cultures were incubated for the desired time before the relevant downstream application.

2.6 Molecular cloning

2.6.1 Agarose gel electrophoresis

Agarose gel electrophoresis was used to resolve DNA from purified plasmid preparations, restriction digest fragments and PCR reactions. 1% agarose (#A4718, Sigma Aldrich) gels were prepared using 1x Tris-Acetate-EDTA buffer (TAE; Table 7.1) containing GelRed nucleic acid gel stain (#BT41003, Biotium) for visualisation.

Samples were prepared with 6x loading dye (#B7025S, NEB) and run alongside a DNA ladder (#N0468S, NEB) for estimation of DNA molecule size. Gels were run in 1x TAE buffer at 120 volts (V) for 1 hour and were visualised and imaged using the ChemiDoc MP imaging system (BioRad).

2.6.2 DNA purification from agarose gels

For purification or visualisation of specific DNA bands after resolution on agarose gels, bands were visualised using the ChemiDoc MP imaging system (BioRad). These bands were then excised using a scalpel, and DNA extracted and purified using the Monarch® DNA gel extraction kit (#T1020L, NEB) according to manufacturer's instructions.

2.6.3 DNA restriction digests

Digests were performed according to the chosen restriction enzyme's manufacturer's instructions with the relevant enzyme buffer (NEB). Typically, 1 µg of DNA was digested in a 50 µL reaction using 0.4 units/µL restriction enzyme. Reactions were incubated at 37 ˚C for 2 hours. For vector backbones, 1-unit of alkaline phosphatase (#M0290S, NEB) was added to the mixture for the final hour to prevent re-ligation of the backbone.

2.6.4 Cloning of NKG2D BiTE into pTransfer plasmid by Gibson Assembly

The DNA sequences encoding the NKG2D BiTE and Control BiTE (currently in the pSF expression plasmid – BiTE sequences were designed and synthesised

by Dr Janet Lei-Rossmann and Emma Page, Seymour Group, Department of Oncology, University of Oxford) were cloned into the pTransfer shuttle plasmid using Gibson Assembly (GA) polymerase chain reaction (PCR). The BiTE transgenes were inserted into the pTransfer plasmid downstream of a CMV promoter (see appendices section 7.2.3 for plasmid map). The pTransfer plasmid also contains *FRT* and locus of X-over P1 (*loxP)* recombination sites, as well as an ampicillin resistance marker.

The empty pTransfer shuttle plasmid (a kind gift from Ennio A. Ciocca, Harvard Medical School) was linearised with EcoR1 (EcoR1-HF; R3101, NEB) and linear DNA was isolated with DNA gel electrophoresis and band excision. The NKG2D BiTE and Control BiTE were amplified out of the pSF plasmid by PCR using GA primers (Primer sequences in Table 7.2) and the PCR protocol below (Table 2.4)

Table 2.4 PCR protocol

Stage	Temperature	Time
1 - Initial denaturation	98 ˚C	30 seconds
2 - Denaturation	98 ˚C	10 seconds
3 - Annealing	65 ˚C	30 seconds
4 - Extension.	72 ˚C	90 seconds
Repeat cycles – to stage 2 – 27x		
Final extension	72 ˚C	10 minutes
Finish	4 ˚C	Forever

The GA reaction was then performed using the GA-amplified NKG2D and Control BiTE sequences, and the EcoR1-linearised pTransfer backbone at a 3: 1 molarity ratio respectively. The GA was performed with purified DNA fragments, using NEBuilder® HiFi DNA assembly master mix (#E2621L, NEB) following the manufacturer's instructions. Reactions were incubated in a thermocycler (MJ research) for 1 hour at 50 ˚C and immediately used to transform PIR1 bacteria.

2.6.5 Bacterial transformation

Bacterial transformation was performed using the heat-shock method. Aliquots of PIR1 cells were thawed on ice, mixed with 10-100 ng pTransfer plasmid DNA and incubated on ice for 20 mins. Cells were subsequently heated to 42 ˚C for 30 seconds (heat-shocked) and transferred back to ice for 5 mins. 1 mL of super optimal broth with catabolite repression medium (SOC; #15544034, Invitrogen™) was added before incubation at 37 ˚C in a shaker (SI-300R, Fisher Scientific) at 180 rpm for 90 mins. Transformation mixtures were spread on to pre-warmed lysogeny broth (LB) agar plates (#L2897, Sigma Aldrich) with 100 ng/mL ampicillin for selection, and incubated overnight at 37 ˚C.

2.6.6 DNA plasmid preparation and purification

Clonal populations of PIR1 bacteria transformed with the pTransfer-NKG2D or Control BiTE plasmid were picked, and the presence of the insert verified by colony PCR. The same primers and protocol (Table 2.4) initially used to amplify the NKG2D BiTE or Control BiTE insert were also used to screen colonies, alongside OneTaq® Quick-Load® DNA Polymerase (NEB, M0509). Colony PCR DNA was visualised using agarose gel electrophoresis. Successfully transformed colonies containing the insert were selected for Mini-prep cultures and incubated overnight in 3 mL LB broth (#L3022, Sigma Aldrich) supplemented with 100 μg/mL ampicillin. DNA from Mini-prep cultures was obtained using Monarch® Plasmid Miniprep Kit (NEB, #T1010) according to the manufacturer's instructions, and sent for DNA sequencing (Genewiz). A single clone containing the correct DNA sequence was then selected for further amplification and Maxi-prep.

For Maxi-prep cultures, a pick of the original bacterial colony was incubated in 3 mL LB broth with ampicillin for 2 hours at 37 ˚C to establish a pre-inoculum. This pre-inoculum was then added to 200 mL LB broth with 100 μg/mL ampicillin and incubated overnight in a shaker at 37 ˚C and 180 rpm. Maxi-prep DNA was obtained using Qiagen Plasmid Plus Maxi-prep kit (#12945, Qiagen) following the manufacturer's instructions, and sent for sequencing.

2.6.7 DNA quantification

DNA quantity was determined using a NanoDrop™ One spectrophotometer (ThermoFisher Scientific™), after blanking with H_2O.

2.6.8 DNA sequencing

Following cloning, DNA was sent for Sanger sequencing (Genewiz) (Primer sequences in Table 7.2) to ensure the fidelity of the sequence. Sequencing results were aligned to the predicted sequence *in silico* using SnapGene software.

2.7 NKG2D BiTE

2.7.1 NKG2D BiTE sequence and structure

The ectodomain of human NKG2D receptor (amino acids 78-216) was used for the NKG2D BiTE. For the Control BiTE, amino acid residues in the stirrup loop (B5-B5' loop) of NKG2D were mutated from IIEMQ to RGGKR, turning the hydrophobic NKG2DL-binding pocket hydrophilic, thus preventing recognition and binding to NKG2DLs. Both NKG2D and mutated NKG2D (NKG2Db5) were constructed into the BiTE scaffolds (Figure 2.2). The length of DNA was 1704 bp

and the protein size was 63 kDa. Full DNA and amino acid sequences are in Appendices section 7.2.2. Initial BiTE design, construction and characterisation was performed by Dr Janet Lei-Rossmann. Sequences were further optimised by Emma Page.

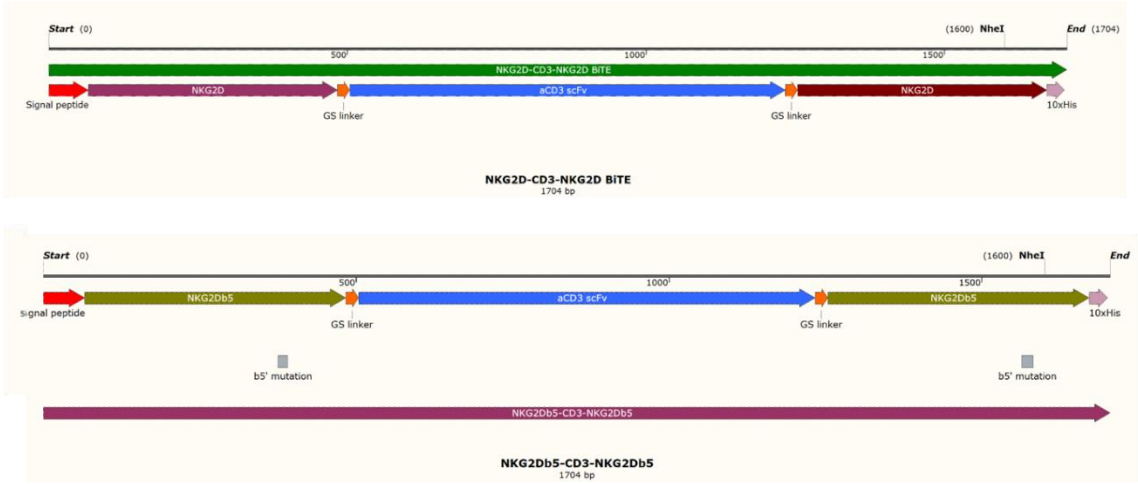

Figure 2.2 Overview of NKG2D and Control BiTE sequences
NKG2D-αCD3-NKG2D (NKG2D BiTE; top) consists of: Signal peptide for BiTE secretion, ectodomain from human NKG2D (amino acids 78-216), G_4S linker, anti-CD3 scFv, another NKG2D ectodomain and 10x His-Tag. NKG2Db5-αCD3-NKG2Db5 (Control BiTE; bottom) had the same sequence except for mutations in the stirrup loop (B5-B5' loop) of NKG2D, which turns the hydrophobic NKG2DL-binding pocket hydrophilic, and thus prevents recognition and binding to NKG2DLs. Total DNA size was 1704 bp, protein size was 63 kDa.

2.7.2 Production of NKG2D BiTEs

T-75 flasks (#658174, Greiner BioOne) were seeded with Ad-293 cells to 80% confluence 24 hours before DNA transfection with pTransfer-NKG2D or Control BiTE plasmid. Opti-MEM (#31985062, Gibco™) was used as the complete medium for the length of the transfection. For the transfection, 20 mg plasmid and 80 mL Lipofectamine™ 2000 (#11668019, Invitrogen™) were separately pre-mixed with 1.2 mL Opti-MEM (#31985062, Gibco™) for 5 mins at RT. The two solutions were then mixed at RT for a further 20 mins. Seeding medium was removed, Ad-293 cells washed with Opti-MEM, and the DNA: Lipofectamine: Opti-MEM mixture added for 4 hours. The mixture was then replaced with 10 mL fresh Opti-MEM.

Supernatant was collected from the Ad-293 cells 72 hours post-transfection, clarified by centrifugation (400 x g, 10 mins), concentrated 40-fold with Amicon® Ultra-15 10 kDa molecular weight cut-off centrifugal filter units (#UFC901024, Merck), aliquoted and stored at -80 ˚C. The NKG2D and Control BiTE were prepared as above. PD-L1 BiTEs were produced and kindly provided by Dr Hena Khalique (Seymour Lab, Department of Oncology, University of Oxford).

2.7.3 SDS-PAGE gel electrophoresis

Proteins were separated by molecular weight by sodium dodecyl sulphate-polyacrylamide gel electrophoresis (SDS-PAGE) using 4-20% gradient Mini-PROTEAN® TGX™ precast polyacrylamide gels (#4561096, BioRad) loaded with 15-50 µg protein per lane. Samples of concentrated BiTE were mixed with 6x Laemmli buffer (#J61337, Alfa Aesar) and dH_2O to the required concentration, aliquoted and stored at -20 ˚C until required. Samples were thawed on ice and denatured for 5 minutes at 95 ˚C before being loaded alongside PageRuler™ Plus pre-stained protein ladder (#26619, ThermoFisher Scientific™) and run initially at 80 V for 20 mins, then at 120 V for a further 1 hour, in sodium dodecyl sulfate (SDS) running buffer (Table 7.1) in a BioRad TGX system (BioRad).

2.7.4 Immunoblotting

For western blot analysis, resolved proteins were transferred to 0.2 µm nitrocellulose membranes using a transfer pack (#1704158, BioRad) and Trans-Blot® turbo transfer system (#1704150, BioRad) following the manufacturer's instructions. Membranes were stained with Ponceau S solution (#22001, Biotium)

to determine transfer efficiency before being washed with dH_2O to remove the stain, then PBS-Tween buffer (PBST; Table 7.1).

Membranes were blocked with blocking buffer (5% skim milk powder (#70166, Sigma Aldrich) diluted in PBST buffer) for 1 hour at RT before being incubated with mouse anti-C terminal 6x His antibody (1: 5000) (#40-0693, Invitrogen) overnight at 4 ˚C in blocking buffer on a roller. Membranes were washed 3x with PBST buffer and incubated with horse anti-mouse IgG horseradish peroxidase (HRP)-conjugated secondary antibody (1: 5000) (#7076, Cell Signalling Technology) for 1 hour at RT in blocking buffer. Membranes were washed again 3x with PBST buffer, and SuperSignal™ west dura extended duration substrate solution (#34075, ThermoFisher Scientific™) applied. Chemiluminescence was visualised with the ChemiDoc MP imaging system (BioRad).

2.7.5 Enzyme-linked immunosorbent assay (ELISA) to assess BiTE concentration

BiTE concentration was determined using a His-Tag enzyme-linked immunosorbent assay (ELISA) detection kit (#L00437, GenScript®) following the manufacturer's instructions. In duplicate, BiTE supernatants were diluted 1: 10 in the assay diluent provided and incubated alongside a serially diluted His Tag standard supplied with the kit. Concentration of BiTE was determined using linear regression analysis on GraphPad Prism 9.3.1, using the standard curve.

2.8 G207-NKG2DBiTE and G207-ControlBiTE virus cloning

The protocol for generating the G207-NKG2DBiTE and G207-ControlBiTE viruses was adapted from Terada et al (2006) (Terada, Wakimoto, Tyminski, Chiocca, & Saeki, 2006). An overview is shown in Figure 2.3.

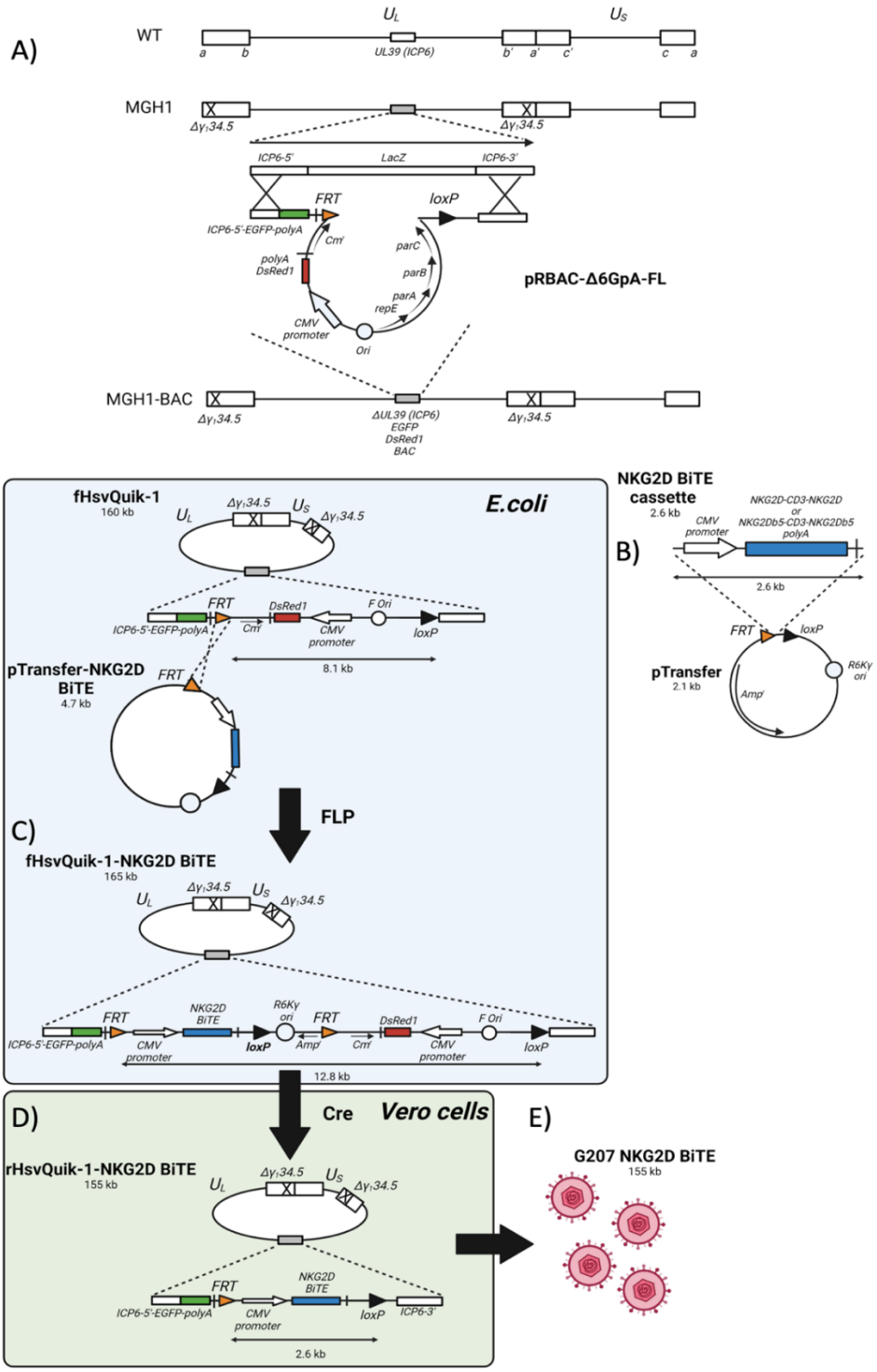

Figure 2.3 Schematic overview of G207-NKG2DBiTE cloning
(**A**) General schematic of the wild type (WT) HSV-1 genome (top) and the MGH1 mutant strain (bottom). The MGH1 genome contains deletions in both copies of *γ₁34.5* neurovirulence gene and the insertion of *LacZ* at the *U_L39* locus. A BAC plasmid (pRBAC-Δ6GpA-FL) was inserted into the *U_L39* locus via two homology arms (MGH1-BAC). Within the pRBAC-Δ6GpA-FL BAC sequence are: two recombination sequences (*FRT* and *loxP*) flanking the BAC, a green fluorescent protein (GFP) expression cassette in-frame of the *U_L39* coding sequence, and a red fluorescent protein (DsRed - RFP) expression cassette. (**B**) Schematic of the pTransfer shuttle plasmid with the NKG2D BiTE or Control BiTE expression cassette. Expression of BiTEs is driven by the CMV promoter. The BiTE sequence is flanked by *FRT* and *loxP*

recombination sites. (**C**) The pTransfer shuttle plasmid containing the BiTE sequences (pTransfer-NKG2D BiTE) is recombined into the MGH1-BAC (fHSVQuik-1) in *E. coli* via the FLP recombination site (fHSVQuik-1-NKG2D BiTE). (**D**) Transfection of the fHSVQuik-1-NKG2D BiTE into mammalian Vero cells alongside a Cre expression plasmid results in excision of the pRBAC-Δ6GpA-FL BAC sequence from the fHSVQuik-1-NKG2D BiTE sequence via the *loxP* sites. (**E**) Resulting oHSV-1 particles produced from co-transfected Vero cells (G207-NKG2DBiTE). Diagram created with BioRender.com. Figure and figure legend adapted from Terada et al., 2006.

2.8.1 Production of DH10β competent cells with fHSVQuik-1 BAC

Electrocompetent DH10β bacteria containing fHSVQuik-1 bacterial artificial chromosome (BAC) plasmid (a kind gift from Ennio A. Ciocca, Harvard Medical School) were electroporated to also express a plasmid (pFTP-T) (also a kind gift from Ennio A. Ciocca, Harvard Medical School) containing chlortetracycline-inducible Flippase (FLP). An overview of the fHSVQuik-1 BAC is shown in Figure 2.3A.

Firstly, the DH10β bacterial cells containing the fHSVQuik-1 BAC needed to be made electrocompetent to allow electroporation of the pFTP-T plasmid and eventually the pTransfer shuttle plasmids. The fHSV-Quik-1 glycerol stock was inoculated into LB broth containing 35 μg/mL chloramphenicol and incubated overnight. The following day, cultures were diluted 1:100 into 2x Yeast tryptome (YT) media (#Y2377, Merck) and incubated in a bacterial shaker at 37 ˚C. After 2 hours of incubation, the optical density $(O.D)_{600}$ of the bacterial suspension was determined by nanodrop every 10-20 mins (spectrophotometer blanked against 2xYT media) until the $O.D_{600}$ was between 0.4 and 0.6. The flask was then quickly put on ice to prevent further bacterial growth, before pelleting the bacteria by centrifugation at 5250 x g for 15 mins at 4 ˚C in 250 mL falcon tubes (#430775, Corning). The resulting bacterial pellet was washed with cold autoclaved H_2O, centrifuged again, washed twice in sterile cold 10% glycerol (#G7757, Sigma

Aldrich), then centrifuged and resuspended in sterile cold 10% glycerol. This was aliquoted, snap-frozen on dry ice, and stored at -80 °C.

The pFTP-T plasmid contains a tetracycline resistance marker and a temperature sensitive replication origin. All subsequent bacterial growth steps were therefore carried out at 30 °C. Electrocompetent fHSV-Quik-1 DH10β cells were electroporated with 1.5 μg of pFTP-T plasmid at 1800 V (untruncated time) in 1 mL electroporator cuvettes (#5510-11 Molecular BioProducts), using an electroporator (ECM 399, BTX Harvard Apparatus). Bacteria were then incubated at 30 ˚C in S.O.C. medium for 1 hour, plated onto LB agar plates containing 20 μg/mL tetracycline and 35 μg/mL chloramphenicol, and grown overnight at 30 ˚C.

The following day, colonies were selected and incubated overnight in LB broth containing 35 μg/mL chloramphenicol and 20 μg/mL tetracycline. The next day, the process of making electrocompetent cells was repeated as described above, generating electrocompetent fHSV-Quik-1-pFTP-T 10β cells.

2.8.2 Generation of fHSVQuik-1-BiTE BAC plasmids

Having generated NKG2D BiTE and Control BiTE pTransfer plasmids (Figure 2.3B) and fHSV-Quik-1-pFTP-T DH10β cells, the next stage was to insert the BiTE sequences into the BAC plasmid using FLP (Figure 2.3C).

The electrocompetent fHSV-Quik-1-pFTP-T DH10β cells (described above) were thawed on ice, mixed with 1 μg of pTransfer-NKG2D BiTE or pTransfer-Control BiTE and electroporated at 1800 V (untruncated time). The electroporated cells were then recovered in S.O.C medium containing 20 μg/mL heat-inactivated chlortetracycline to drive expression of FLP. The bacteria were incubated at 30 ˚C

with shaking or 4 hours before plating on LB agar plates containing 35 μg/mL chloramphenicol and 50 μg/mL ampicillin and incubating at 37 °C overnight.

The following day, colony PCR was used to screen colonies for the presence of the G207 genome and successful recombination of the NKG2D or Control BiTE. Primers for the HSV-1 gene UL42 and the NKG2D/Control BiTE sequences (Primer sequences in Table 7.2) were used. Five colonies each of NKG2D BiTE and Control BiTE were selected for colony PCR. Successful colonies were determined as containing both the HSV-1 UL42 PCR product (150 bp) and the NKG2D BiTE or Control BiTE PCR product (2.7 kbp).

One successful colony from each of fHSV-Quik-1-NKG2D and fHSV-Quik-1-Control BiTE were grown in 500 mL LB broth containing 20 μg/mL chloramphenicol and 50 μg/mL ampicillin overnight at 37 ˚C in a bacterial shaker. BAC plasmid DNA was isolated using the Large Construct Isolation Kit (#12362, Qiagen) primarily according to the manufacturer's instructions, but omitting digestion of contaminating cellular DNA using an ATP-dependent exonuclease, as this resulted in poor yield of BAC plasmid DNA. The fHSV-Quik-1-NKG2D and fHSV-Quik-1-Control BiTE BAC plasmids were then sent for sequencing.

2.8.3 Transfection of HSVQuik-1-BiTEs and excision of the BAC to produce viral particles

To obtain G207 viral particles expressing NKG2D or Control BiTE, the fHSV-Quik-1-BiTE BAC was transfected into mammalian Vero cells alongside a Cre recombinase expression vector (pc-nCre) (a kind gift from Ennio A. Ciocca, Harvard Medical School). This drives recombination of the *loxP* sites and excision of the superfluous BAC DNA sequences (Figure 2.3D), yielding G207 genomes containing

the NKG2D BiTE or Control BiTE sequence (rHSVQuik-1-NKG2D BiTE or rHSVQuik-1-Control BiTE, respectively). Resulting viral particles are termed either G207-NKG2DBiTE or G207-ControlBiTE (Figure 2.3E).

Vero cells were seeded at 0.6 x 10^6 cells/well in a 6-well plate (#3516, Corning) the day before transfection, to ensure near confluence on the day of transfection. For transfection, 2 μg of fHSV-Quik-1-NKG2D or fHSV-Quik-1-Control BiTE BAC plasmids were mixed with 1 μg pc-nCre plasmid in Opti-MEM, then with 9 μL lipofectamine 2000 at a 3: 1 DNA: lipofectamine ratio. This mixture was carefully added to Vero cells, incubated for 6 hours, removed, and Vero cells overlayed with 1x DMEM containing 0.7% agarose, 2% FCS, and 1% pen/strep, pH 7.2. (Table 7.1). The Vero cells were monitored daily for the expression of GFP (indicating the presence of G207 genome) but the absence of red fluorescent protein (RFP) (indicating the excision of the BAC) using a Zeiss Axiovert 25 fluorescent microscope (Figure 2.4). This transfection and recombination achieved relatively high efficiency, with several viral plaques being formed, all of which expressed GFP but not RFP.

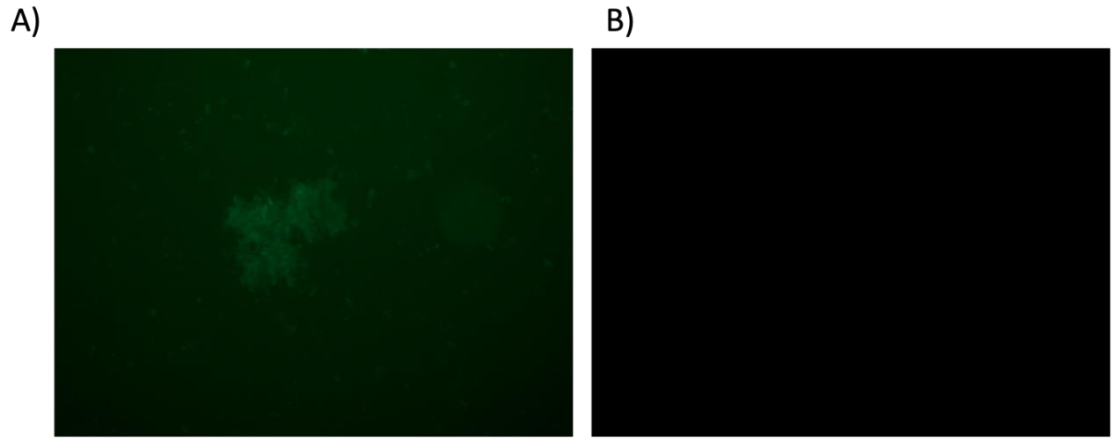

Figure 2.4 Assessment of successfully recombined viral clones
(**A**) Vero cells co-transfected with fHSV-Quik-1-NKG2D or fHSV-Quik-1-Control BiTE bacterial artificial chromosome (BAC) plasmids and pc-nCre to induce Cre-mediated recombination and excision of the BAC from the G207 genome, resulting in infectious viral particles of G207 oHSV-1. Viral plaques were assessed for presence of green fluorescent protein (GFP), indicating the presence of G207 viral genome but the (**B**) absence of RFP (encoded in the

BAC). The absence of RFP but presence of GFP indicates successful excision of the BAC. Images taken using a Zeiss Axiovert 25 fluorescent microscope.

Viral plaque growth was monitored over 3-5 days, and each successful plaque was allowed to grow until it became large enough to verify the replicative ability and cytotoxic activity of the viruses. Plaque growth was halted before any plaques could merge and contaminate viral clones.

2.8.4 Isolation of G207-NKG2DBiTE and G207-ControlBiTE viral clones

Viral clones resulting from the co-transfection of fHSV-Quik-1-NKG2D or fHSV-Quik-1-Control BiTE BAC plasmids with pc-nCre plasmid were selected based on plaque size, plaque growth, presence of GFP, and absence of RFP

Vero cells were seeded at 1 x 10^4 cells/well in a 96F plate the day before infection. Successful plaques on the original transfection plate were highlighted using a marker pen. They were carefully picked using a sterile 20 μL pipette tip and transferred to an Eppendorf tube containing 100 μL 5% FCS DMEM with 10 mM N-2-Hydroxyethylpiperazine-N'-2-Ethanesulfonic Acid (HEPES; pH 7.3; #J848, VWR Life Science). In total, ten plaques each of G207-NKG2DBiTE and G207-ControlBiTE virus were picked. The resulting viral solutions in DMEM were added onto the Vero cells at dilutions ranging from 1: 100, 1: 50 and 1: 20, to dilute down to individual infectious viral particles.

Successful viral clones were then subjected to subsequent rounds of infection to ensure no remaining BAC plasmids were present (absence of RFP) and to elucidate clones that had better oncolytic activity. This round of infection allowed the assessment of viral fitness, infectivity, and cytotoxicity, as the viral particles were

now able to spread in solution and potentially infect the entire well, unlike with the transfection plaque agar assay. Some viral clones showed very poor infectivity, potentially due to mutations acquired in the viral genome during production, or not enough viral particles were collected from the plaque agar assay. However, other wells displayed multiple viral plaques within 1-3 days, suggesting the presence of multiple infectious viral particles in that well. All wells that showed the presence of virus showed no evidence of RFP expression, indicating complete removal of the BAC backbone and successful recombination. Ultimately, five wells of each virus were selected based on the following criteria: the presence of a single original plaque within the first few days (indicating a single originating infectious particle), the presence of GFP but not RFP (indicating successful excision of the BAC), growth of the original plaque and generation of secondary plaques (indicating the ability of the virus to produce infectious progeny and undergo subsequent rounds of infection), and the formation of clear plaques (indicating the cytopathic effect (CPE) of the virus). These wells were harvested and stored at -80 ˚C.

2.8.5 Assessment of BiTE production by G207-NKG2DBiTE and G207-ControlBiTE viruses

Vero cells were seeded in 15 mm dishes (#664160, Greiner BioOne) at $4x10^6$ cells/well, and infected the following day with the five clones of each virus (100 μL) diluted 1:50 into 5% DMEM containing 10 mM HEPES. Infections were left to progress over three days until 70% CPE was observed. Viral supernatant was collected and frozen; of the 4 mL collected, 200 μL was kept for western blotting analysis of C terminal 10xHis-tag expression, 200 μL was kept for functional assays, and the rest was stored at -80 ˚C.

To assess the production of functional NKG2D BiTE by the infected Vero cells, U87 cells were seeded in 96F plates at 2 x 10^4 cells/well, then treated with 20 μL of supernatant diluted with an additional 30 μL 2% RPMI containing 10mM HEPES. Four hours later, 1 x 10^5 PBMC-derived T cells were added in 2% RPMI containing 10 mM HEPES to a final volume of 100 μL. The final dilution of viral supernatants was therefore 1: 5 in 2% RPMI 10 mM HEPES. This was done for each viral clone, for both G207 NKG2D and G207 Control BiTE, and in triplicate. An untreated control was included, where uninfected U87 cells were co-cultured with T cells. U87 cells treated with T cells and 1 nM of concentrated NKG2D BiTE was used as a positive control. After 3 days, cells were harvested and stained for flow cytometry analysis.

2.9 Production and characterisation of G207-NKG2DBiTE and G207-ControlBiTE viruses

2.9.1 Amplification of armed G207 viruses

Clones N2 and B2 were selected to make stocks of G207-NKG2DBiTE and G207-ControlBiTE viruses, respectively. Each virus was expanded and purified separately to avoid any risk of contamination between batches. For viral expansion, Vero cells were seeded into ten 150 mm dishes (#639160, Greiner BioOne) at 8 x 10^6 cells/dish. The following day, seeding media was removed and replaced with 10 mL 5% FCS DMEM containing 10 mM HEPES and a 1:50 dilution of viral supernatant harvested from the 15 mm dish (from section 2.9.1). The infection progress was monitored over 3-5 days until all cells were GFP^+ and approximately 70% CPE was observed. Supernatant from each dish was collected and pooled, and any remaining adherent cells were scraped and added to the pooled

supernatant. A total of 100 mL of pooled supernatant/lysate was generated for each virus and stored in 2 x 50 mL falcon tubes (#AB036, Appleton), at -80 ˚C until virus purification.

2.9.2 Purification of armed G207 viruses

The G207 virus stock preparation process was adapted from Marconi et al., 2014 (Marconi & Manservigi, 2014). Recipes for solutions used in density gradients are provided in Table 7.1. In brief, the protocol involved the following steps:

1) Virus preparations were thawed in a water bath set to 37 ˚C before pelleting cell debris by centrifugation at 5251 x g for 10 mins at 4 ˚C
2) The supernatant from step 1) was added to Ultra-Clear ultracentrifuge tubes (Beckman Coulter, #326823). Tubes were placed in rotor SW32-Ti and centrifuged in an Optima XE-90 Ultracentrifuge (Beckman Coulter) at 20000 x rpm for 30 mins at 4 ˚C.
3) Meanwhile, cell pellets from step 1) were resuspended in a small amount of their own supernatant, before undergoing three rounds of freeze/thaw and sonication using an Ultrasonic cleaner (Hilsonic) to break apart cellular debris. This cell pellet fraction was then centrifuged at 1734 x g for 15 mins at 4 ˚C. This step was repeated until the supernatant was no longer turbid.
4) The ultracentrifuged supernatant from step 2) was removed, leaving a pellet of virus and cellular debris. This pellet was resuspended using the clarified supernatant from step 3), forming a suspension containing viral particles from both the cell pellet and supernatant from step 1), but having released viral particles from the debris by sonication.

5) The viral suspension from step 4) was added to a fresh ultracentrifuge tube, topped up with DPBS and ultracentrifuged using the same settings as step 2). After ultracentrifugation, the supernatant was removed and then 1.5 mL cold sterile DPBS was added to the pellet (without resuspending it). The tube was sealed with parafilm and placed on a rocker at 4 ˚C overnight to gently resuspend the pellet.
6) The following day, any remaining pellet was gently resuspended manually. The viral suspension was transferred to a fresh 15 mL falcon tube (#AB031, Appleton), treated with 4.5 μL sterile benzonase (#70664, EMD Millipore) and placed on a rotor at RT for 2 hours to degrade any cellular DNA, then sonicated to break up any remaining particulates.
7) The viral suspension was added to 8.5 mL of solution C, making solution E.
8) 5 mL of Solution D (containing OptiPrep Density Gradient Medium; #M1248, BioVision) was added to two fresh Ultra-Clear ultracentrifuge tubes (#344060, Beckman Coulter).
9) 5 mL of solution E (containing virus) was carefully layered onto each tube containing solution D (Opti-PREP gradient).
10) Remaining volume of the tube was topped off with solution F to balance tubes.
11) Ultra-Clear tubes containing viral density gradients were very carefully placed into ultracentrifuge tubes and put into an SW-40 Ti rotor, before being ultracentrifuged at 35,000 x rpm for 4 hours at 4 ˚C with zero braking (coast).
12) Following centrifugation, Ultra-Clear tubes were removed and held in a clamp stand against a black background. A discrete band was visible at the interphase of the OptiPrep layer, consisting of viral particles (Figure 2.5). To

collect intact virus particles, the tube was carefully punctured 1 cm below the lower band with a 21-gauge short needle (#AN*2138R1, Terumo) and the band was aspirated into a 5 mL syringe (Greiner-BioOne). The collected purified virus from the two tubes was then pooled into a fresh Ultra-Clear tube and then topped up with cold DPBS.

13) Virus was centrifuged in the SW-40 Ti rotor at 20,000 x rpm for 30 minutes at 4 ˚C.

14) Supernatant was removed, before adding 1 mL cold, sterile DPBS to the pellet without resuspending it. The tube was sealed with parafilm and then placed onto a rocker at 4 ˚C overnight to gently resuspend the pellet.

15) The following day, the virus was sonicated to break any remaining particulates, before being aliquoted into 50 μL aliquots, snap frozen on dry ice and stored at -80 ˚C.

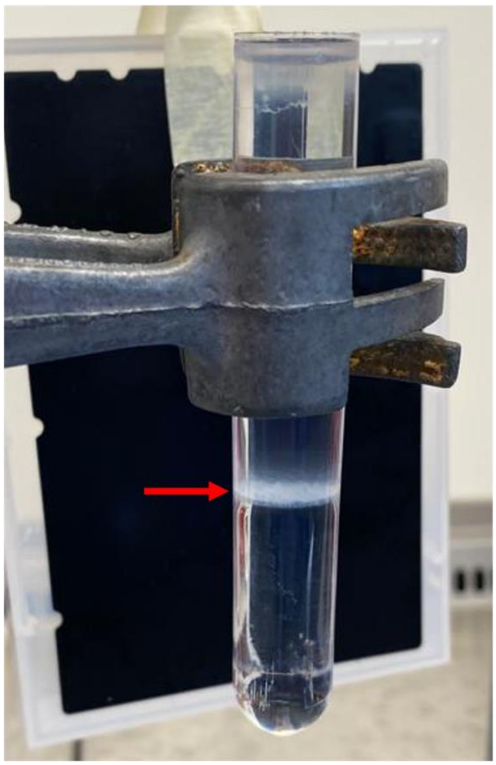

Figure 2.5 Interphase layer of oHSV-1 following density gradient ultracentrifugation
Representative image following density ultracentrifugation as described in step 12 above. The white interphase band visible on top of Solution D comprises of G207 oHSV-1 virus particles.

2.9.3 PicoGreen assay

The DNA concentration of purified G207 stock (viral genomes/mL) was quantified using the Quant-iT™ PicoGreen™ dsDNA Assay kit (#P7589, Invitrogen™). This kit contains a PicoGreen probe that selectively binds dsDNA and fluoresces upon binding. Stocks of G207 were diluted 1/10 and 1/100 in 1x TE buffer (Table 7.1) supplemented with 0.05% SDS (1x TES buffer) and heat treated (56 ˚C, 30 mins) to disrupt virus particle capsids. A standard curve was prepared by serially diluting 0.5 µg/mL bacteriophage λ-DNA in two-fold steps in 1x TES buffer. For each standard or sample, 50 µL was mixed with 50 µL PicoGreen™ reagent (1/200 dilution in 1x TE buffer) in solid black 96-well assay plates (#3925, Corning™). Fluorescence was measured using a Varioskan LUX plate reader at 485/535 nm (excitation/emission). Virus genome concentration was then calculated by

approximation of 0.5 ng of DNA equating to 3 x 10^6 HSV-1 viral particles (vp), as used by Ozuer et al. (Ozuer et al., 2003).

2.9.4 G207 titration by plaque-forming agar assay

Viruses were quantified by plaque agar assay. Vero cells were seeded at 1 x 10^6 cells/well in 6-well plates (#3516, Corning). The following day, seeding media was removed and replaced with 1 ml of serial 10-fold dilutions of each of the viruses, ranging from 10^{-3} to 10^{-9}. Infections were incubated for 4-6 hours at 37 °C, occasionally swirling the plate to ensure even distribution of the virus. The infection media was then removed and replaced with 4 mL of low-melting point agarose-DMEM mixture (Table 7.1). The agarose was allowed to set before returning plates to the incubator. After 4-5 days of incubation, individual plaques of GFP foci were counted for each dilution using a fluorescence microscope. The concentration of plaque forming units (PFU)/mL was determined for each dilution using the formula below. Experiment was conducted in triplicate, the mean of all dilutions and triplicate repeats was used as the final value in further experimental protocols.

$$Titer\left(\frac{PFU}{mL}\right) = \frac{Number\ of\ GFP\ foci}{volume\ of\ inoculum}$$

2.9.5 G207 infection assays

Infection was performed in RPMI containing 5% FCS and 10 mM HEPES pH 7.3, unless otherwise stated. The initial stage of infection was conducted in a lower volume of media to minimise the volume for the virus to diffuse through to reach target cells. After 4-6 hours, either volume was topped up to normal levels, or T cells were added.

Calculation of PFU/ml is described above. The infection dose for each experiment was based on the target cell seeding density and is given in further experimental protocols as the MOI. The MOI is defined as the ratio of infectious viral particles to infection targets, thus an MOI of 1 would equate to one infectious viral particle per cell.

2.9.6 Quantification of NKG2D BiTE production from G207-NKG2DBiTE virus-infected cell lines

A schematic of the timeline for the following experiment is shown in Figure 5.3. U87, A172 and Vero cells were seeded at 2 x 10^4 cells/well in 96F plates. The following day, cells were infected in triplicate with either G207-NKG2DBiTE or G207-ControlBiTE (as a negative control) at an MOI of 0, 0.001, 0.01 and 0.1 in a total volume of 100 μL 5% DMEM with 10 mM HEPES. The supernatants were pooled for each condition three days later. U87 cells were selected as the cell line to apply an NKG2D BiTE standard curve and interpolate the virally-produced BiTE activity against, to keep the T cell activation equivalent for the standard curve. U87 cells were seeded at 2 x 10^4 cells/well in a 96 well plate and the next day were treated with 50 μL of harvested viral supernatant from the three infected cell lines and co-cultured with 1 x 10^5 PBMC-derived T cells in 50 μL 5% RPMI with 10 mM HEPES, leaving a final dilution of 1:2 of the original viral supernatant containing the NKG2D or Control BiTE. For the standard curve, U87 cells were treated with increasing concentrations of recombinant NKG2D BiTE. After three days of BiTE or viral supernatant treatment, cells were harvested and analysed by flow cytometry. Three days was chosen as the assay length to prevent secondary rounds of infection by viruses in the supernatants.

2.9.7 U87 GSC infection conditions

For the experiment in section 5.3.7, U87 and patient derived GSCs were cultured in NBM (recipe in Table 7.1). U87 cultured in NBM have been demonstrated to display various markers of stemness, as well as form tumour spheres (Oh et al., 2017). Therefore, U87 cells were serially cultured in NBM until they formed non-adherent tumour spheres before dissociation for either surface staining of NKG2DLs or seeding for co-culture assays. After serial culture in DMEM or NBM, U87 cells were seeded, co-cultured with T cells and treated with virus or BiTE in 2% RPMI for the assay to ensure the co-culture media was controlled.

2.9.8 Quantification of soluble NKG2DLs

U87 cells were treated with G207-NKG2DBiTE, G207-ControlBiTE and G207 virus at an MOI of 0.1 or left uninfected for 72 hours before supernatants were collected. The concentration of soluble NKG2DLs (sNKG2DLs) in the culture supernatants was measured by sNKG2DL ELISA (MyBioSource #MBS744276) as per the manufacturer's instructions.

2.10 Patient-derived GBM samples

2.10.1 General statement

Patient-derived Glioblastoma tissue used in this thesis was released from The Oxford Brain Bank (OBB), Neuropathology, Level 1, West Wing, John Radcliffe Hospital, OX3 9DU, under the project "Evaluation of Oncolytic virus-based immunotherapy for brain cancer" (OBB 475). Samples were obtained with informed

consent from cancer patients at the John Radcliffe Hospital. Ethical approval for the study was gained from the institutional review board and research ethics committee in accordance with the UK Human Tissue Act 2004 and Declaration of Helsinki.

2.10.2 Primary GBM sample preparation

GBM tissue specimens were acquired by surgical resection. Two separate types of tissue were obtained from the same patient: a 5 mm^3 block of solid tissue derived from the tumour margin, and bulk tumour tissue obtained by cavitron ultrasonic surgical aspirator (CUSA). Both tissues were kept in 10% DMEM with P/S following surgery and during sample transit.

Both tissues were treated the same way for dissociation. Tissue was manually macerated using a scalpel blade before being mechanically and enzymatically dissociated into a single cell suspension using a Brain Tumour Dissociation Kit (#130-095-942), Miltenyi Biotech) with C tubes (#130-093-237, Miltenyi Biotech) and a GentleMACS Octo Dissociator (Miltenyi Biotech) according to the manufacturer's instructions. Following dissociation, cell suspension was passed through a 70 μm cell strainer (#352350, Falcon) and into a 50 mL falcon tube containing pre-warmed 10% DMEM and P/S. Cells were then centrifuged (300 x g, 10 mins) and resuspended in either 10% RPMI with P/S, NBM (Table 2.1) or MACS buffer for cell surface staining. Cells for culture were seeded into T25 flasks in the relevant media and incubated at 37 ˚C and 5% CO_2.

2.10.3 Primary GBM staining

Due to the inherent stress of sample acquisition and dissociation, surviving cells were cultured in 10% RPMI for 72 hours to allow the cells to recover, and to

remove dead cells and debris. After this recovery period, cells were harvested using non-enzymatic dissociation buffer and stained for flow cytometry analysis.

2.10.4 Primary GBM BiTE and virus assays

Primary GBM cells were cultured in 10% RPMI or NBM (Table 2.1) for two weeks to establish differentiated and GSC-like phenotypes, respectively. Cells were then seeded for BiTE and virus assays as described previously, with co-culture medium being changed to 10% RPMI for both cells upon the addition of BiTE, virus, or T cells.

2.11 Statistical tests

2.11.1 Tests of significance

Data processing and statistical analyses were performed using GraphPad Prism 9.3.1. When comparing two datasets, a Student's two-tailed t test was used. Where more than two variables were being compared, a one-way analysis of variance (ANOVA) test was used, either with Tukey's *post hoc* analysis, or with Dunnett's *post hoc* analysis if one control condition was being compared. For grouped datasets with multiple variables, a two-way ANOVA test was used with Dunnett's *post hoc* analysis compared to the control group. All data are presented alongside error bars indicating standard deviation (±SD) unless otherwise specified. The significance levels used were ns $p>0.05$, *$p\leq0.05$, **$p\leq0.01$, ***$p\leq0.001$ and ****$p\leq0.0001$. All *in vitro* experiments were performed in triplicate unless otherwise stated.

2.11.2 Bliss independence score

To assess synergy between treatments, the Bliss independence score was calculated (Q. Liu, Yin, Languino, & Altieri, 2018), using the following formula:

$$E_{Ind} = E_a + E_b - E_a E_b$$

$$\Delta E = E_{Obs} - E_{Ind}$$

E_{Ind} is the expected relative inhibition (in this case, cytotoxicity), calculated as a function of the cytotoxicity from the two treatments, E_a (TMZ and or radiation) and E_b (NKG2D BiTE or G207-NKG2DBiTE virus) used in isolation. E_{Ind} is compared to the actual observed value of cytotoxicity (E_{Obs}) when E_a and E_b are used in combination. If the difference (ΔE) between the observed and expected values is a positive value, then the relationship is deemed to be synergistic. If the difference is 0, then the variables are independent, whereas if the difference is a negative value, then the variables have an antagonistic relationship.

3 Targeting NKG2DLs with BiTEs

3.1 Introduction

The NKG2DL family comprises of eight different ligands in humans, including MICA, MICB, and ULBP1-6 (Figure 1.7). These ligands are minimally expressed on the surface of healthy cells, but expression is increased on the surface of stressed, virally infected, and malignantly transformed cells (reviewed in Baugh et al., 2020).

Reports on the level of surface expression of NKG2DLs on GBM cells and GSCs are almost as heterogenous as the tumours themselves. Pereboeva and colleagues reported no detectable expression of NKG2DLs in histological samples of normal human brain tissue, but strong signals for MICA, ULBP1, ULBP2, ULBP3 and ULBP4 in both human GBM and metastatic breast brain tumour slices (Pereboeva, Harkins, Wong, & Lamb, 2015). In contrast, Friese et al., describe constitutive surface expression of MICA, MICB, ULBP1, ULBP2 and ULBP3 on a range of widely used human glioma cell lines, including A172 and U87 cells, as well as on primary human glioma cells. The expression of each ligand varied between cell lines, but each cell line (including primary cells) was strongly positive for at least one ligand; by contrast, a non-neoplastic astrocytic cell line lacked surface NKG2DL expression (Friese et al., 2003). Furthermore, using human xenograft and syngeneic mouse models, the authors reported a selection *in vivo* for glioma-initiating cells with low MICA expression, suggesting an immune selection pressure against cells expressing high MICA (Friese et al., 2003). Chitadze et al., reported that primary human GBM cell lines cultured short-term were positive for surface

NKG2DL expression, albeit at low levels, and that expression was typically highest in patients that had previously undergone Stupp therapy (Stupp et al., 2005) but had recurrent GBM (Chitadze et al., 2017). They also reported that MICA and ULBP2 were the ligands expressed to the highest levels (Chitadze et al., 2017).

Co-staining of a range of human GBM cryo-sections for MICA, MICB, and ULBP1-3 demonstrated a strong staining signal in all samples, although a high degree of heterogeneity was observed, with NKG2DL-expressing cells rarely found together in clusters (Flüh et al., 2018). However, the authors frequently observed co-staining of NKG2DLs with glial fibrillary acidic protein (GFAP) rich areas of the tumour. To attempt to discern the NKG2DL expression patterns on GSCs, the sections were also stained for various stem cell markers but gave highly heterogenous results. Many NKG2DL-expressing cells were found to be positive for the transcription factor Krüppel-like factor 4 (Klf-4), but not all cells positive for stem cell markers expressed NKG2DLs and vice versa (Flüh et al., 2018). It is possible that level of NKG2DL expression may depend on the tumour grade, however. Eisele and colleagues reported increased expression of MICA, MICB and ULBP1-3 in human grade II astrocytomas compared to healthy brain, but MICA was decreased on higher grade gliomas, albeit with expression levels higher than normal brain (Eisele, 2006). Together these findings indicate the expression of NKG2DLs on GBM cells is highly variable, reflecting the heterogeneity and complexity of the tissue.

NKG2DLs have already been explored as possible targets for cancer immunotherapy. Some previous examples of cell based NKG2DL-targeted immunotherapy tested pre-clinically include sensitising tumour cells to the endogenous innate immune system (Shiraishi et al., 2016), use of allogeneic innate

adoptive cell therapy such as γδ T cells (Pereboeva et al., 2015) and the use of NKG2D-CAR-T cells (Spear, Barber, Rynda-Apple, & Sentman, 2013; Weiss, Weller, et al., 2018). Therapeutic proteins targeting NKG2DLs have also been investigated, such as NKG2D-Fc constructs to stimulate ADCC by NK cells (Hilpert et al., 2011; Raab et al., 2014), an NK cell engager to link the NKG2D receptor to target cells (Von Strandmann et al., 2006), and even a BiTE containing the murine NKG2D receptor linked to an anti-mouse CD3 scFv used in various murine epithelial tumour models (Märklin et al., 2019; T. Zhang & Sentman, 2011). These strategies have all demonstrated pre-clinical success. However, to our knowledge, bispecific proteins targeting human NKG2DLs have not been used in combination with oHSV-1 oncolytic virotherapy for GBM immunotherapy.

Based on these previous reports, we set out to develop our own immunotherapeutic proteins to also target NKG2DLs expressed on the surface of GBM cell lines. This chapter will focus on the design and evaluation of BiTEs designed to direct T cell cytotoxicity towards GBM cells expressing NKG2DLs and will assess their suitability to later encode into an oHSV-1 genome for tumour-specific expression.

3.2 Chapter hypothesis and aims

3.2.1 Hypothesis

We hypothesise that NKG2DLs expressed on GBM cell lines can be targeted with an NKG2D-containing BiTE.

3.2.2 Chapter aims

1) To assess the expression of NKG2DLs on a range of human cancer cell lines, patient-derived GBM cell lines, and primary GBM cells
2) To design, characterise and select an NKG2D BiTE candidate for cloning into the oHSV-1 genome
3) To determine the immunostimulatory and anti-cancer effects of NKG2D BiTE
4) Perform Immunophenotypic analysis primary GBM samples and assess NKG2D BiTE activity on these tissues

3.3 Results

3.3.1 Expression of surface NKG2DLs on cancer cell lines

In order to target cancer cells expressing surface NKG2DLs with immunotherapy, we first needed to assess the expression of these ligands on a range of cancer cell lines. The surface expression of MICA and MICB was assessed using a commercially available fluorescently labelled antibody. However, since there are eight different ligands that make up the NKG2D ligand family, we sought to use a method to detect expression of all eight ligands at once in a single staining process. Additionally, our targeting strategy of NKG2DLs for immunotherapy will be using the NKG2D receptor itself in a BiTE format to target all eight ligands and so it is important to assess the overall expression. However, no single antibodies exist that are capable of binding to all eight ligands. Therefore, a biotinylated recombinant human NKG2D receptor-Fc fusion protein (rhNKG2D-Fc) and Streptavidin-PE secondary were used (Materials and Methods section 2.3), which can bind all NKG2DLs, like during physiological interactions.

Two GBM cell lines, U87 and A172 were assessed for surface MICA and MICB using an anti-MICA/B-APC antibody and total NKG2DLs using the above-mentioned rhNKG2D-Fc-biotin with streptavidin-PE and respective isotype controls for flow cytometry analysis. Additionally, for comparison to other cancers, the colorectal carcinoma cell line, DLD-1, was also tested. All three cell lines were highly positive for MICA/B expression (Figure 3.1A) and showed very low non-specific staining with the isotype control. The relative surface expression for each cell line was measured in terms of mean fluorescence intensity (MFI) of the entire single cell population. All cell lines demonstrated specific staining for MICA/B (Figure 3.1B, C and D), and

very low non-specific signal was present with IgG2a isotype control, and all cell lines showed high MICA/B expression.

The percentage of cells expressing total NKG2DLs (Figure 3.1E) was less than the MICA/B$^+$ cells in Figure 3.1A, but still showed a high expression with 96%, 52% and 61% NKG2DL$^+$ DLD-1, U87 and A172 cells, respectively. However, the biotinylated recombinant human IgG1 isotype control and Streptavidin-PE secondary alone demonstrated non-specific signal compared to the unstained controls. The relative mean fluorescence intensity (RMFI) is shown in a table in Figure 3.1I, displaying the fold change of MFI from the MICA/B or NKG2D-Fc staining compared to the relevant isotype. Representative histograms of the flow cytometry data for MICA/B and NKG2DL staining can be seen in Appendix Figure 7.1A and B, respectively. Together, these results confirmed that these cancer cell lines express surface NKG2DLs, including MICA and MICB, which can be measured using flow cytometry staining with either a commercially available MICA/B antibody or the recombinant NKG2D-Fc protein. However, the NKG2D-Fc-Bio-Strep-PE system does generate a non-specific staining signal, and so needs to consistently be checked using the relevant controls in future experiments.

Given the aim of this thesis to develop a novel immunotherapy for GBM, U87 and A172 cells were selected for future use in assays given their expression of NKG2DLs.

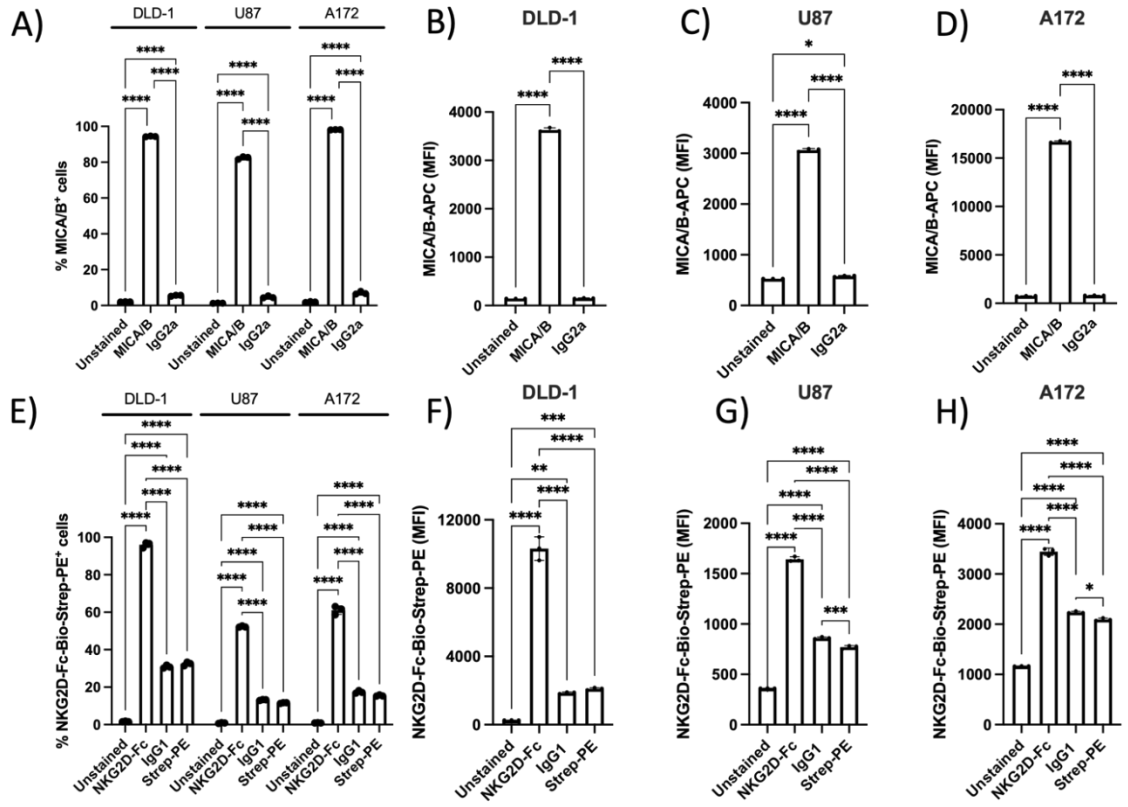

I)

Cell Line	MICA/B (RMFI)	MICA/B (%)	NKG2DL (RMFI)	NKG2DL (%)
U87	5.3	82	1.9	52
A172	20.5	98	1.5	61
DLD-1	23.9	94	5.5	96

Figure 3.1 Expression of surface MICA/B and total NKG2DLs on cancer cell lines.

Cancer cell lines DLD-1 (colorectal carcinoma), U87 (GBM) and A172 (GBM) cells were stained for flow cytometric analysis with either anti-MICA/B-APC or IgG2a-APC isotype or left unstained. (**A**) Percentage of cells positive for MICA/B or Isotype. (**B**) Relative surface expression of MICA/B compared to IgG2a isotype and unstained for DLD-1, (**C**) U87 and (**D**) A172 cells. (**E**) DLD-1, U87 and A172 cells were also stained for total surface NKG2DLs using biotinylated recombinant human NKG2D-Fc and Streptavidin-PE secondary (NKG2D-Fc-Bio-Strep-PE), biotinylated human IgG1 isotype (IgG1), or Streptavidin-PE secondary only (Strep-PE). Percentage of cells positive for NKG2D-Fc, IgG1 and Strep-PE compared to unstained. (**F**) Relative surface expression of total surface NKG2DLs compared to staining controls for DLD-1, (**G**) U87 and (**H**) A172 cells. Data represents mean percentage of positive cells (for (A) and (E)), or mean fluorescence intensity (MFI) (for (B-D) and (F-H)) of triplicate repeats ± S.D. Statistical significance was assessed by two-way ANOVA followed by Turkey's post hoc analysis. (ns $p>0.05$, *$p\leq0.05$, **$p\leq0.01$, ***$p\leq0.001$ and ****$p\leq0.0001$). (**I**) Table summarising MICA/B and NKG2DL staining for each cell line. Relative mean fluorescence intensity (RMFI) calculated as fold change of MICA/B or NKG2D-Fc MFI signal relative to the relevant isotype.

3.3.2 Comparison of different orientations for NKG2D BiTEs

Two different BiTE constructs were designed, either containing two NKG2DL-binding domains and one anti-CD3 scFv (NKG2D-αCD3-NKG2D), or two anti-CD3 scFv domains and a single NKG2DL-binding domain (αCD3-NKG2D-αCD3). Additionally, negative Control BiTEs were designed for each construct. These negative controls involved a mutating the stirrup loop (B5-B5' loop) of NKG2D, which turns the hydrophobic NKG2DL-binding pocket hydrophilic, and thus prevents recognition and binding to NKG2DLs (Figure 3.2). These Control BiTEs thus had the structure of NKG2D(B5)-αCD3-NKG2D(B5) and αCD3-NKG2D(B5)-αCD3 for the two respective BiTEs.

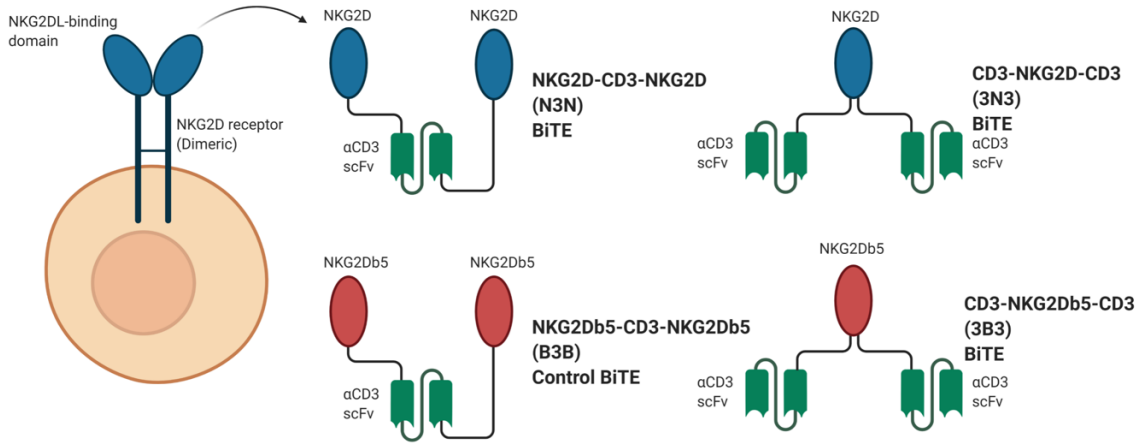

Figure 3.2 Schematic of NKG2D BiTE and mutant Control BiTE orientations
For the NKG2D-αCD3-NKG2D (N3N) BiTE, the ligand binding domain of the NKG2D receptor (monomeric) was used as a single protein domain capable of binding all eight human NKG2D ligands (NKG2DLs). This domain was linked via a GGGGS linker to an anti (α)-CD3 single chain variable fragment (scFv) (L2K), which binds to CD3ε on T cells. This αCD3 scFv was linked to another NKG2D domain via another GGGGS linker. Another BiTE was designed, using the same domains but in the orientation of αCD3-NKG2D-αCD3 (3N3). Non-binding Control BiTEs were also designed for each orientation but contained a mutation in the B5-B5' stirrup loop of the NKG2D domain, rendering the constructs unable to bind to NKG2DLs (B3B and 3B3). A signal peptide was added to the N terminus of each protein to ensure secretion, and a C terminal His-tag (not shown). Diagram created with BioRender.com.

To select a candidate BiTE for further use and to determine the specificity of the BiTEs, GBM cell lines A172 and U87 cells were treated with the functional and control BiTEs in both orientations alongside PBMC-derived T cells for 72 hours before harvesting and staining for flow cytometric analysis. T cell activation involves a broad phenotypic change in cellular expression markers such as CD69 and CD25. The percentage of T cells expressing these activation markers was measured in the presence and absence of target cells.

Baseline CD25 expression remained unchanged when T cells were treated with all BiTE constructs in monoculture (Figure 3.3A), suggesting neither BiTE was able to activate T cells in the absence of target cells. When treated with NKG2D-αCD3-NKG2D, CD25 expression significantly increased for A172 and U87 cell co-cultures and no significant increase was observed when treated with the corresponding Control BiTE (NKG2D(B5)-αCD3-NKG2D(B5)). Similarly, the αCD3-NKG2D-αCD3 BiTE also caused increased CD25 expression in co-cultures with A172 and U87 cells, although a similar increase was also observed with the corresponding Control BiTE (αCD3-NKG2D(B5)-αCD3). Interestingly, no significant increase in CD25 expression occurred in T cells in monoculture when treated with this Control BiTE (Figure 3.3A), suggesting its activity is dependent on cellular crosslinking, and not simple aggregation.

The CD69 expression data (Figure 3.3B) follows the same pattern as the CD25 expression, with specific upregulation in co-cultures with target cells treated with the NKG2D-αCD3-NKG2D but not the corresponding Control BiTE, and upregulation in co-cultures treated with either the αCD3-NKG2D-αCD3 BiTE or αCD3-NKG2D(B5)-αCD3 Control BiTE. Changes in CD69 expression appear to be more sensitive than CD25, as the baseline CD69 expression was lower in untreated T cells, compared

to the CD25 expression. This lower background CD69 expression enables the detection of a slight (but not significant) increase in $CD69^+$ T cells when monocultures were treated with either αCD3-NKG2D-αCD3 BiTE or its corresponding Control BiTE compared to untreated T cells in monoculture. Together, these data suggest that the BiTEs containing two αCD3 scFv domains (αCD3-NKG2D-αCD3 BiTE and αCD3-NKG2D(B5)-αCD3 Control BiTE) cause non-specific activation of T cells in the presence of target cells, as both CD25 and CD69 expression were similarly increased after treatment with these constructs in co-cultures, but not in monocultures. This could perhaps imply that the αCD3-NKG2D(B5)-αCD3 Control BiTE is still able to interact with target cells and induce T cell activation, unlike the NKG2D(B5)-αCD3-NKG2D(B5) Control BiTE, which induces no activation in the presence of target cells.

Therefore, given the observation that the NKG2D-αCD3-NKG2D BiTE caused a significant increase in both CD25 and CD69 expression on T cells when in co-culture with either A172 or U87 cells, but not when T cells were in monoculture, and that the corresponding NKG2D(B5)-αCD3-NKG2D(B5) Control BiTE did not cause any T cell activation, this pair of BiTEs were selected for further investigation in future experiments. Henceforth, for simplicity, the NKG2D-αCD3-NKG2D BiTE will be referred to as ‘NKG2D BiTE’, and the NKG2D(B5)-αCD3-NKG2D(B5) Control BiTE will be referred to as ‘Control BiTE’.

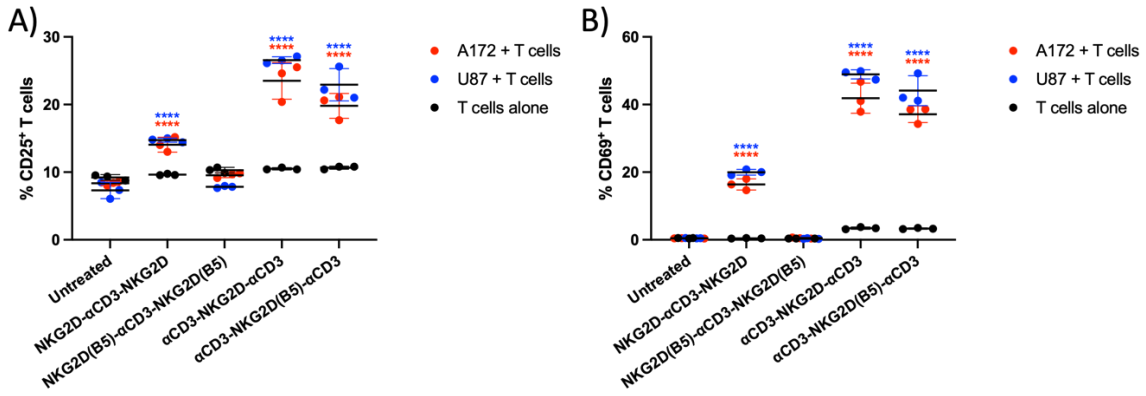

Figure 3.3 Assessment of T cell activation in response to both orientations of NKG2D BiTEs and Control BiTEs
PBMC-derived T cells were co-cultured with A172 cells (red), U87 cells (blue) or left in monoculture (black) at an E: T ratio of 5:1 and were treated with 0.5 nM of NKG2D-αCD3-NKG2D BiTE, NKG2D(B5)-αCD3-NKG2D(B5) Control BiTE, αCD3-NKG2D-αCD3 BiTE or αCD3-NKG2D(B5)-αCD3 Control BiTE or left untreated. After 72 hours, T cells were harvested and stained for activation markers for flow cytometric analysis to measure the percentage of (**A**) $CD25^+$ T cells and (**B**) $CD69^+$ T cells. Data represents mean percentage of positive T cells of triplicate repeats ± S.D. Statistical significance was assessed by two-way ANOVA followed by Bonferroni post hoc analysis. Significance was assessed versus untreated cells within the relevant group (ns $p>0.05$, *$p\leq0.05$, **$p\leq0.01$, ***$p\leq0.001$ and ****$p\leq0.0001$).

3.3.3 Investigating the dose-dependent response to NKG2D BiTE

Having selected the NKG2D BiTE for use in further assays, an optimal concentration of BiTE needed to be identified for future assays. A172 cells were selected to be the target cells for this assay as they grow and stay as a consistent monolayer over several days, unlike U87 cells which begin to cluster together. Therefore, a dose curve using A172 target cells was set up across a range of NKG2D BiTE concentrations for 96 hours, before harvesting the T cells and measuring surface expression of activation markers by flow cytometry. The time point of 96 hours was chosen to be the end point for this assay to enhance the sensitivity of detection of T cell activation at lower BiTE concentrations.

The percentage of T cells expressing CD25 (Figure 3.4A) and CD69 (Figure 3.4B) increased with increasing NKG2D BiTE concentration in a dose-dependent

manner, to a maximum of 64% CD25 and 91% CD69 at 25 nM NKG2D BiTE. No increases in either T cell activation marker were observed using NKG2D BiTE in monoculture at any concentration. This suggested that the NKG2D BiTE had no non-specific activation of T cells even at high concentrations.

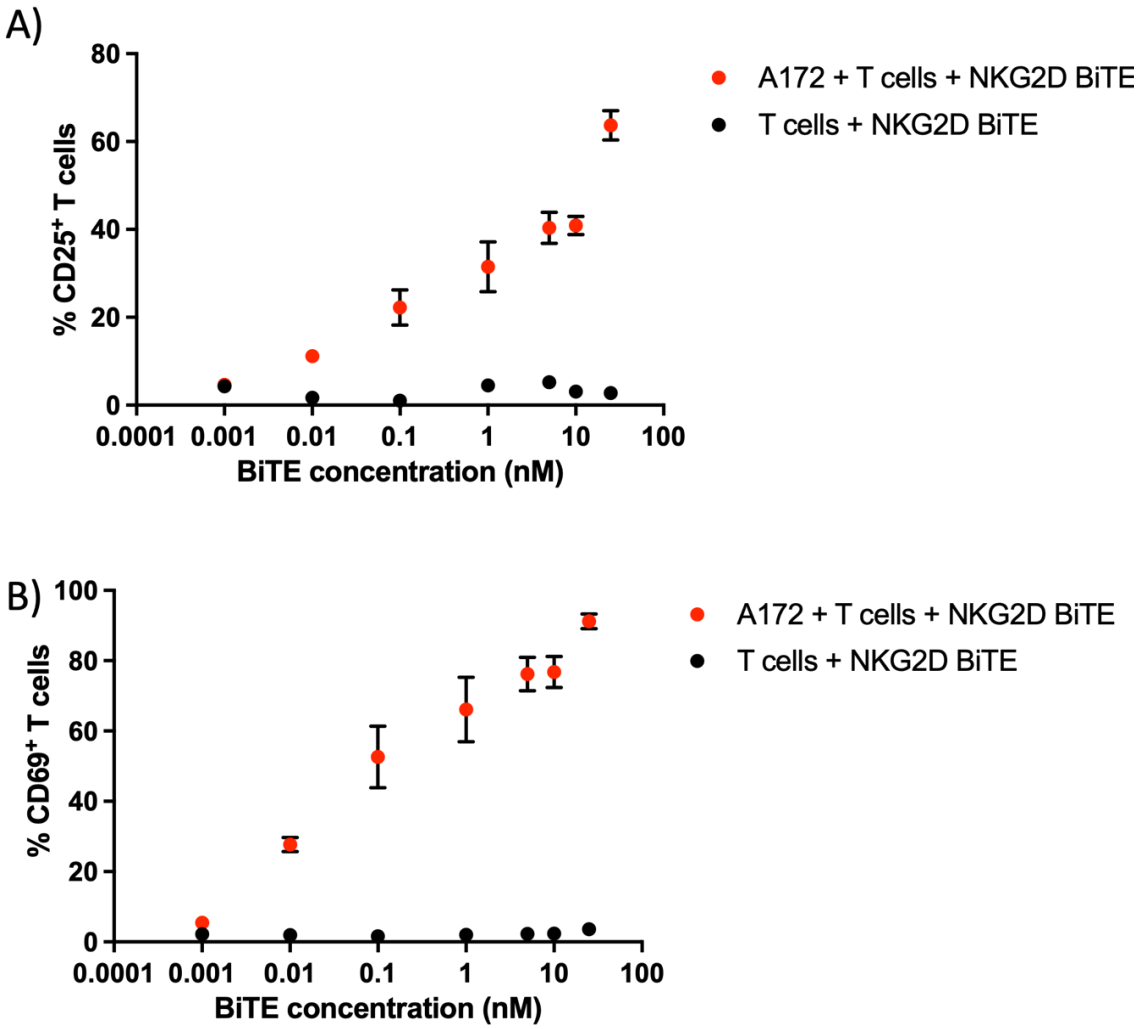

Figure 3.4 NKG2D BiTE activity dose curve
PBMC-derived T cells were either co-cultured with A172 cells (5:1 T cell: A172 ratio) treated with increasing concentrations of NKG2D BiTE (red), or in NKG2D BiTE-treated T cell monocultures (black) for 96 hours before assessing T cell activation markers (**A**) CD25 and (**B**) CD69 by flow cytometry. Each experiment was performed in triplicate. Data represents mean percentage of positive cells of triplicate repeats ± SD.

The concentration of NKG2D BiTE chosen for future assays was 1 nM, which resulted in 32% $CD25^+$ and 66% $CD69^+$ T cells after 96 hours. This concentration was selected as it achieved a high level of T cell activation, whilst using only a

sparing amount of the concentrated protein stock, thus allowing more separate uses from each batch of BiTE produced.

3.3.4 Evaluating NKG2D BiTE activity and T cell activation profile against GBM cell lines

Expression of CD107a or lysosomal associated membrane protein 1 (LAMP1), perforin, granzyme B and IFN-γ can also be used alongside CD25 and CD69 as means of measuring T cell activation. Since the NKG2D BiTE can bind to the CD3ε epitope, it does not discriminate between $CD4^+$ or $CD8^+$ T cells, and hence is able to activate both cell types in an antigen independent manner. Therefore, the expression of these various markers was assessed on both $CD4^+$ and $CD8^+$ T cells by flow cytometry.

GBM cell lines A172 and U87 cells co-cultured with PBMC-derived T cells and treated with either NKG2D BiTE, Control BiTE, CD3/CD28 Dynabeads for 72 hours before being harvested and stained for CD4, CD8, CD25, CD69, CD107a, perforin, granzyme B, intracellular IFN-γ and a viability dye for flow cytometric analysis. This enabled the measurement of expression of the various T cell activation markers on both $CD4^+$ and $CD8^+$ T cells. As well as co-cultures of each cell line with T cells, T cells were also treated alone in monoculture to further explore the specificity of the NKG2D BiTE and the dependence on target cells expressing NKG2DLs for T cell activation.

The NKG2D BiTE was able to activate both $CD4^+$ and $CD8^+$ T cells against both A172 and U87 cells, with increases in CD25 expression (Figure 3.5A) in response to the NKG2D BiTE. Similar increases were observed with CD69 expression (Figure 3.5B). As before, the NKG2D BiTE did not increase expression

of either CD25 or CD69 on T cells in the absence of target cells above the baseline expression, supporting a lack of non-specific activity of the NKG2D BiTE in the absence of target cells. The Control BiTE also did not trigger any noticeable T cell activation either in co-culture or in monoculture. CD3/CD28 Dynabeads, a positive control for T cell activation, caused greater CD25 and CD69 expression in co-cultures compared to the NKG2D BiTE and generally caused a greater activation of $CD4^+$ T cells compared to $CD8^+$ T cells.

The degranulation marker, CD107a, or LAMP-1, is a protein that is located on the outer leaflet of lysosomes but is trafficked to the outer leaflet of the plasma membrane during cytotoxic T cell and NK cell degranulation. CD107a is a commonly used marker for degranulation of immune cells, and so surface expression on $CD4^+$ and $CD8^+$ T cells was measured in response to NKG2D BiTE (Figure 3.5C). NKG2D BiTE- and Dynabead-mediated $CD8^+$ T cell activation resulted in significant increases in CD107a surface expression when in co-culture with target cells, but not in monoculture or with Control BiTE. Interestingly, a significant population of $CD107a^+CD4^+$ T cells was also detected, albeit at a lower proportion compared to the $CD107a^+CD8^+$ cells.

Another marker of cytotoxic T cell activation is the expression of perforin. Perforin is a glycoprotein that is released from cytolytic granules produced by cytotoxic T cells and NK cells and can polymerise to form pores in the plasma membrane of target cells. The intracellular expression of perforin on $CD4^+$ and $CD8^+$ T cells was therefore also measured in response to the NKG2D BiTE (Figure 3.5D). Perforin expression was absent in resting $CD4^+$ T cells, although it slightly increased in response to NKG2D BiTE and Dynabeads. In $CD8^+$ T cells however, expression increased significantly in NKG2D BiTE-treated co-cultures with A172 cells and U87

cells but not in T cell monocultures. Dynabeads had an even greater stimulatory effect on perforin expression in $CD8^+$ T cells.

Granzyme B, a serine protease also released from granules during cytolytic T cell and NK cell responses, activates caspase-dependent apoptosis in target cells after gaining entry via perforin pores. Granzyme B expression increases upon T cell activation, therefore, the intracellular expression of granzyme B was also measured on $CD4^+$ and $CD8^+$ T cells in response to NKG2D BiTE (Figure 3.5E). Like the perforin expression, intracellular granzyme B expression was absent in untreated $CD4^+$ T cells but was expressed in unstimulated $CD8^+$ T cells. This expression increased markedly in $CD8^+$ T cells in response to NKG2D BiTE in co-cultures with A172 cells and U87 cells, but not in monoculture. Interestingly, a significant increase in granzyme B^+ $CD4^+$ T cells was also observed when U87 co-cultures were treated with NKG2D BiTE, or Dynabeads in all cultures.

IFN-γ is a pro-inflammatory cytokine produced predominantly by $CD4^+$ T cells in response to activation and assists in various pro-inflammatory immune responses such as antigen presentation. The intracellular expression of IFN-γ was therefore measured in $CD4^+$ and $CD8^+$ T cells in response to the NKG2D BiTE (Figure 3.5F). Untreated $CD4^+$ T cells had a slightly higher baseline IFN-γ expression than $CD8^+$ T cells, although this remained below 2% for both cell types. Expression increased slightly in both $CD4^+$ and $CD8^+$ T cells in A172 co-cultures treated with NKG2D BiTE but did not reach statistical significance. However, U87 co-cultures treated with NKG2D BiTE significantly increased to 3.0% IFN-γ^+CD8^+ and 7.3% IFN-γ^+CD4^+ T cells. Significant increases in IFN-γ^+ $CD4^+$ and $CD8^+$ T cells were detected after Dynabead treatment for all culture conditions. The production of IFN-γ is typically

higher by the 'helper' $CD4^+$ T cells, whose main role is the production of cytokines to help direct the immune response.

Finally, the viability of the A172 and U87 cells was assessed in these co-cultures by a flow cytometric viability dye (Figure 3.5G). The viability of both cell lines was unaffected by co-culture with T cells or treatment with Control BiTE compared to untreated monocultures (85% and 91% for A172 and U87 cells, respectively). However, viability significantly decreased in response to NKG2D BiTE for A172 cells (24%) and U87 cells (54%).

In general, the NKG2D BiTE can activate both $CD4^+$ and $CD8^+$ T cells in the presence of both A172 and U87 cells, but not in the absence of target cells. Not only is this NKG2D BiTE-mediated activation of T cells able to induce the surface expression of various T cell activation markers such as CD25, CD69 and CD107a (Figure 3.5A, B and C, respectively), but it also increases the expression of various effector cytolytic proteins, such as perforin and granzyme B (Figure 3.5D and E, respectively), and pro-inflammatory cytokines such as IFN-γ (Figure 3.5F). Ultimately, this T cell activation in the presence of target cells leads to the direct killing of these target cells (Figure 3.5G).

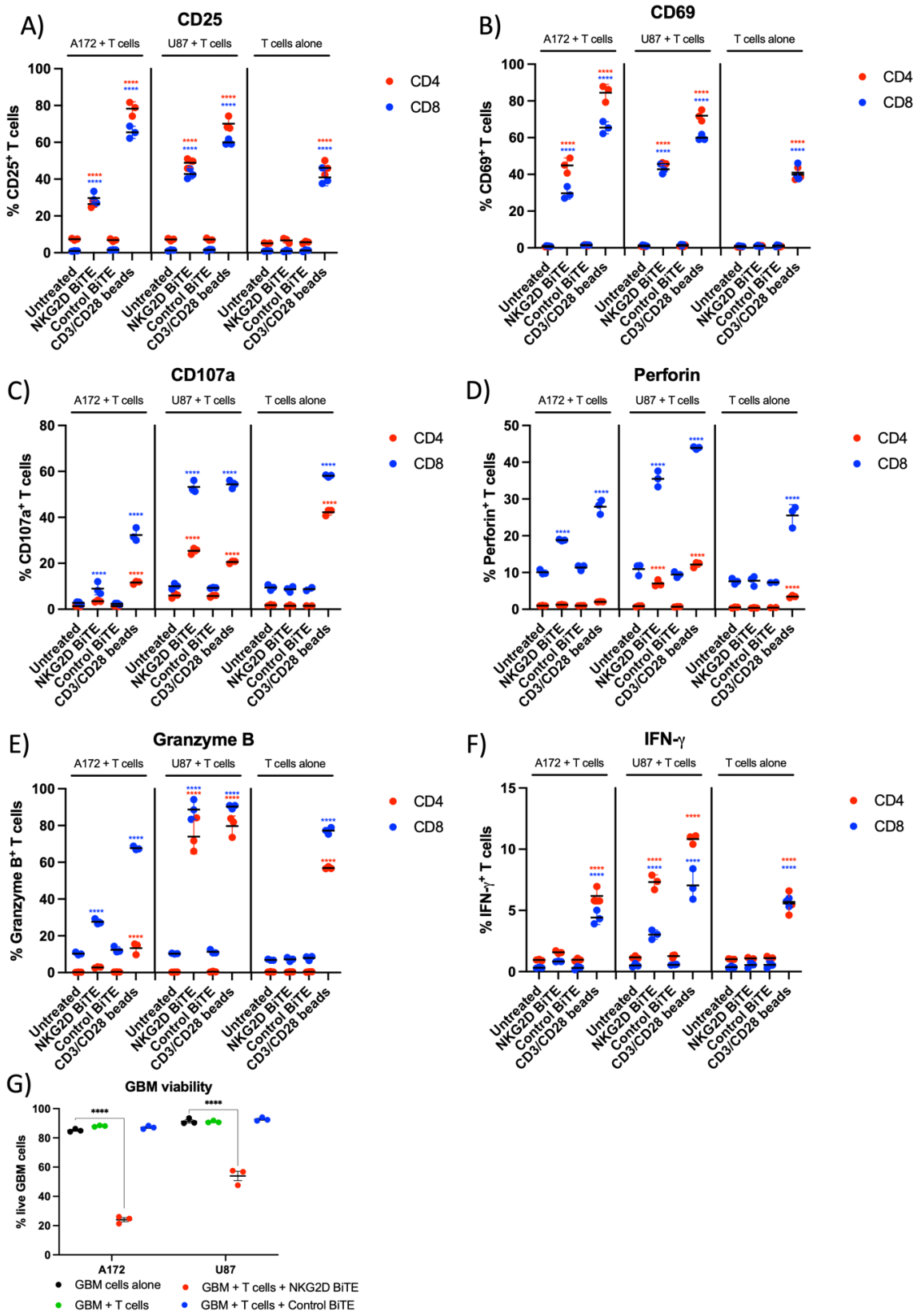

Figure 3.5 Characterisation of T cell activation in response to NKG2D BiTE
GBM cell lines A172 and U87 were treated with 1 nM NKG2D BiTE, 1 nM Control BiTE, CD3/CD28 Dynabeads or left untreated and co-cultured with PBMC-derived T cells at an E: T ratio of 5:1 for 72 hours before assessing expression of (**A**) CD25, (**B**) CD69, (**C**) CD107a, (**D**) perforin, (**E**) Granzyme B, (**F**) intracellular IFN-γ on both $CD4^+$ (red) and $CD8^+$ (blue) T cells by

flow cytometry. Data represents mean percentage of positive T cells of triplicate repeats ± S.D. (**G**) GBM cell viability was assessed from the same experiment using a viability dye by flow cytometry. GBM cell viability was assessed either as untreated cells in monoculture (black), untreated in co-culture with T cells (green), co-cultures treated with 1 nM NKG2D BiTE (red) or 1 nM Control BiTE (blue). Data represents the mean percentage of live GBM cells of triplicate repeats ± S.D. Statistical significance was assessed by two-way ANOVA followed by Bonferroni post hoc analysis. Significance was assessed versus untreated cells within the relevant group (ns $p>0.05$, *$p\leq0.05$, **$p\leq0.01$, ***$p\leq0.001$ and ****$p\leq0.0001$).

3.3.5 Assessing the specificity of the NKG2D BiTE compared to a BiTE targeting PD-L1

TAMs are one of the most common cells in the GBM TME, therefore we sought to investigate macrophage NKG2DL expression and any activity of the NKG2D BiTE towards macrophages compared to GBM cells. As a positive control for T cell activation against macrophages, an anti-PD-L1 BiTE developed in our laboratory which has been shown to activate T cells against PD-L1-expressing macrophages (Khalique et al., 2021) was also used at a pre-determined optimal concentration.

PBMC-derived monocytes were differentiated into macrophages and polarised with IFN-γ and LPS (‘M1’), IL-10 (‘M2c’) or left unpolarised (‘M0’) (Materials and Methods section 2.4.3). Macrophages were then harvested and stained for flow cytometric analysis of surface marker expression to verify polarisation or seeded for an NKG2D BiTE assay.

Macrophages have low MICA/B compared to PD-L1 expression

Macrophages were stained on day 6 to verify macrophage polarisation and surface marker expression (see timeline in Figure 3.6A). Macrophages were stained for: CD11b, as a pan-macrophage marker; CD80, as an M1 marker; CD206, as an M2c marker; PD-L1, as a positive control for PD-L1 BiTE activity; and MICA/B, to check for some NKG2DL expression. Macrophages were then analysed by flow cytometry for surface expression of these markers (Figure 3.6B). Unpolarised (M0)

macrophages showed low percentage of CD80 and CD206 expression, whereas M1 macrophages had greater than 99% CD80 expression but low CD206, indicating successful M1-like polarisation. M2c macrophages exhibited lower CD80 expression than M1 macrophages and had higher CD206 expression, suggesting an M2-like polarisation. All polarisations of macrophages (M0, M1 and M2c) displayed greater than 98% PD-L1 expression (Figure 3.6B), although relative expression was much greater on M1 cells in terms of MFI (Figure 3.6C).

All polarisations of macrophages exhibited low MICA/B expression, both in terms of percentage of positive cells (Figure 3.6B) and relative surface expression (Figure 3.6C).

Macrophages are not targeted by NKG2D BiTE but are targeted by PD-L1 BiTE

PBMC-derived T cells were co-cultured with autologous macrophages (M0, M1 and M2c), or U87 or A172 cells and treated with 40 nM PD-L1 BiTE, 1 nM NKG2D or Control BiTE or left untreated for 72 hours before assessing T cell CD25 and CD69 expression by flow cytometry (Figure 3.6E and F, respectively). T cells alone showed no increase in CD25 or CD69 expression in response to untreated M0, M1 or M2c macrophages, suggesting no antigen presentation and physiological T cell activation was taking place. There was also no background T cell activation in untreated co-cultures with U87 cells, A172 cells or T cells alone. Similarly, the Control BiTE did not activate the T cells in any co-cultures. However, when treated with PD-L1 BiTE, the CD25 expression (Figure 3.6E) was higher in co-cultures with macrophages compared to U87 or A172 cells. In contrast, the CD69 expression (Figure 3.6F) was higher on T cells in co-culture with U87 and A172 cells treated with NKG2D BiTE than with macrophages. CD69 is an early activation marker,

which peaks 24 hours after activation and then decreases, whereas CD25 expression peaks after 48-72 hours. Accordingly, these results might suggest that the PD-L1 BiTE activated the autologous T cells against the macrophages earlier than it did against the GBM cell lines. The PD-L1 BiTE also resulted in significant activation of T cells alone in monoculture but was lower than PD-L1 BiTE-treated co-cultures.

As expected, the NKG2D BiTE activated T cells in the presence of NKG2DL-expressing GBM cell lines. However, CD25 expression did not increase when T cells were cultured with NKG2D BiTE in the presence of M0, M1 or M2c macrophages, although there was a minor increase in CD69 expression. These findings suggest that while the NKG2D BiTE can activate T cells against target cells that express NKG2DLs, macrophages of various polarisation states lack sufficient NKG2DL expression to mediate activation.

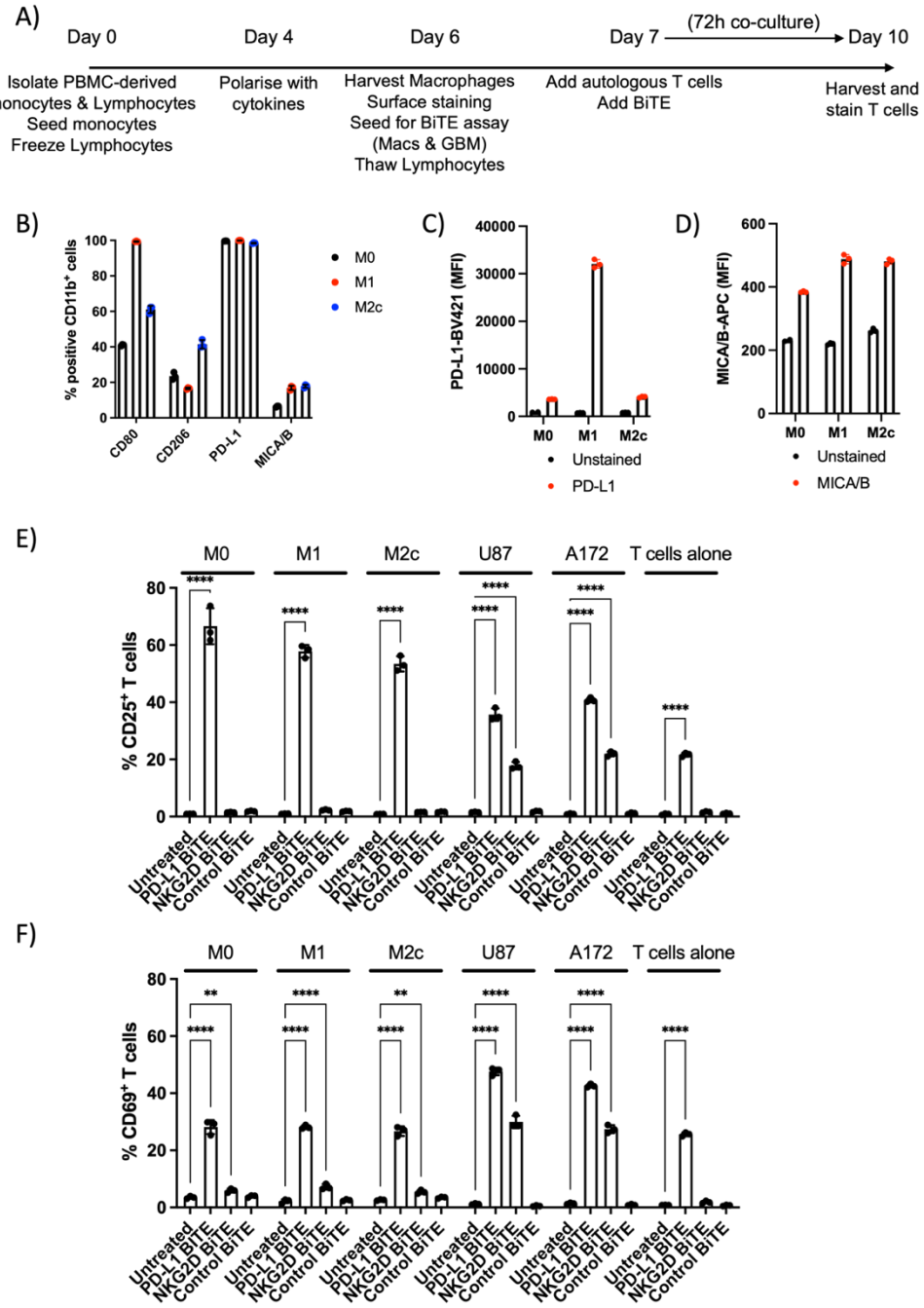

Figure 3.6 Assessing the specificity of NKG2D BiTE against macrophages
(**A**) Timeline of experimental setup. On day 0, human PBMC-derived monocytes and lymphocytes were isolated, and monocytes were differentiated into macrophages for 6 days. After 96 hours of differentiation, macrophages were either left unpolarized ('M0') or polarised with LPS and IFN-γ ('M1'), or IL-10 ('M2c') for the remaining 48 hours of differentiation. On day 6, macrophages or GBM cell lines A172 and U87 were seeded, or macrophages were stained for various surface markers. On day 7, macrophages and GBM cell lines were co-cultured with T cells at an E: T ratio of 5:1 and treated with 40 nM PD-L1 BiTE, 1 nM NKG2D BiTE or 1 nM Control BiTE for 72 hours before harvesting and staining for T cell activation markers and flow cytometric analysis. (**B**) Flow cytometric surface expression of CD80, CD206, PD-L1 and MICA/B on 'M0' (black), 'M1' (red) and 'M2c' (blue) macrophages. Data represents the mean percentage of positive CD11b$^+$ cells of triplicate repeats ± S.D. (**C**) Relative expression of PD-L1 (red) and (**D**) MICA/B (red) on CD11b$^+$ cells compared to unstained cells (black) by flow cytometry. Data represents the mean of mean fluorescence intensity (MFI) values of triplicate

repeats ± S.D. (**E**) Percentage of $CD25^+$ and (**E**) $CD69^+$ T cells in co-cultures with 'M0', 'M1', and 'M2c' macrophages or U87 and A172 GBM cell lines, or T cells in monoculture treated with PD-L1 BiTE, NKG2D BiTE or Control BiTE or left untreated. Data represents the mean percentage of positive cells of triplicate repeats ± S.D. Statistical significance was assessed by two-way ANOVA followed by Bonferroni post hoc analysis. Significance was assessed versus untreated cells within the relevant group (ns $p>0.05$, *$p\leq0.05$, **$p\leq0.01$, ***$p\leq0.001$ and ****$p\leq0.0001$).

3.3.6 Activated T cells express NKG2DLs

Surface NKG2DL expression is low or absent on most healthy cells unless they are undergoing cellular stress. However, T cells have been reported to express surface NKG2DLs, including MICA, upon engagement with CD3 or CD28, but not resting T cells (Molinero, Fuertes, Rabinovich, Fainboim, & Zwirner, 2002). This could potentially have the consequence of allowing the NKG2D BiTE to target T cells against each other, mediating a process known as 'fratricide'.

We therefore sought to confirm whether T cells express NKG2DLs upon stimulation for ourselves. Human PBMC-derived T cells were either treated with CD3/CD28 Dynabeads or left untreated for 48 hours before harvesting and staining for CD4, CD8 and MICA/B, or total NKG2DLs for analysis by flow cytometry (Figure 3.7).

Surface MICA/B was absent on both resting $CD4^+$ and $CD8^+$ T cells when untreated (Figure 3.7A and B), which increased significantly on both cell types upon stimulation with CD3/CD28 Dynabeads, with greater increases on $CD4^+$ T cells than $CD8^+$ T cells. The relative total surface NKG2DL expression across the T cell population also significantly increased (Figure 3.7C) upon stimulation with CD3/CD28 Dynabeads compared to untreated resting T cells.

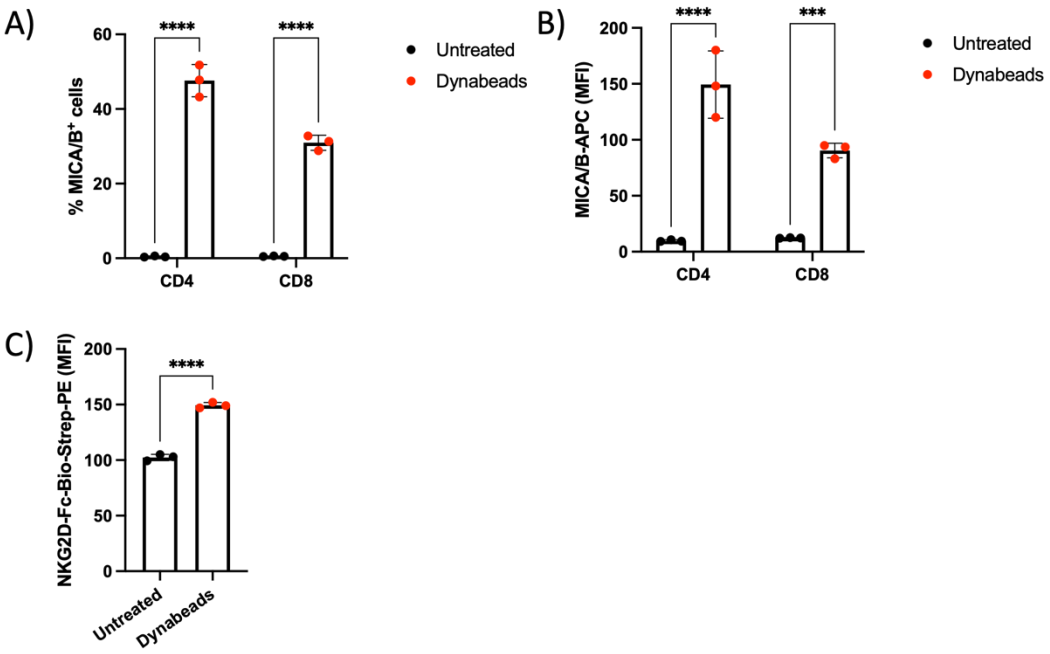

Figure 3.7 Surface NKG2DL expression on activated and resting T cells
Human PBMC-derived T cells were treated with 1 μg/well CD3/CD28 Dynabeads (red) or left untreated with no beads (black) for 48 hours before being stained for CD4, CD8 and surface MICA expression for flow cytometry analysis. (**A**) The percentage of MICA/B$^+$ CD8$^+$ and CD4$^+$ T cells and (**B**) Relative surface expression of MICA/B on CD8$^+$ and CD4$^+$ T cells after stimulation with CD3/CD28 Dynabeads or no bead treatment. Data represents the mean percentage of MICA/B$^+$ cells, or mean fluorescence intensity (MFI) of triplicate repeats ± S.D. Statistical significance was assessed by two-way ANOVA followed by Bonferroni post hoc analysis. (**C**) T cells were also stained for total surface NKG2DLs using biotinylated recombinant human NKG2D-Fc and Streptavidin-PE secondary (NKG2D-Fc-Bio-Strep-PE). Data represents the MFI of triplicate repeats ± S.D. Statistical significance was assessed by unpaired t test. (ns $p>0.05$, *$p\leq0.05$, **$p\leq0.01$, ***$p\leq0.001$ and ****$p\leq0.0001$).

These findings indicate that T cells increase their surface NKG2DL expression upon activation, in line with other findings in the literature. However, basal expression on resting T cells is absent. The lack of NKG2DL expression on resting T cells may explain the absence of NKG2D BiTE activity when T cells are cultured without target cells, as seen in Figure 3.5.

3.3.7 Determining surface expression of NKG2DLs in primary ex vivo GBM samples

While they serve as a useful model system, the surface NKG2DLs expression on clonal cell lines, such as U87 and A172 cells, may not likely to fully represent the heterogeneity and complexity of surface expression of a real human GBM tumour. Therefore, the surface NKG2DL expression on primary human GBM tissue was assessed.

Human GBM tissue from a single GBM patient was obtained using cavitron ultrasonic surgical aspirator (CUSA) during surgical resection. Solid tissue was mechanically dissociated to isolate a single-cell suspension (Materials and Methods section 2.10) and stained for surface MICA/B or total NKG2DL expression for flow cytometric analysis (Figure 3.8).

Surface expression of MICA/B (Figure 3.8A) was undetectable on the patient derived GBM cells. However, there was a small but significant increase in MFI when stained with NKG2D-Fc compared to the IgG1 isotype and Strep-PE staining controls, indicating the expression of some surface NKG2DLs. Together, these results suggest the human GBM cells lack MICA/B expression, but may express other ligands, such as ULBP1-6.

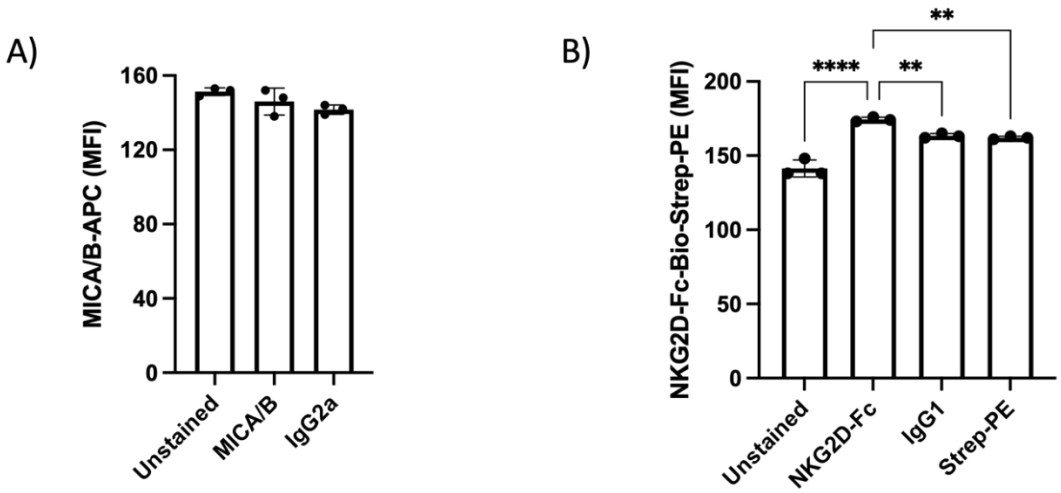

Figure 3.8 Surface NKG2DL expression on primary human GBM cells.
Human GBM tissue obtained by cavitron ultrasonic surgical aspirator (CUSA) was dissociated and stained for flow cytometric analysis with (**A**) anti-MICA/B-APC or IgG2a-APC isotype or left unstained. (**B**) Cells were also stained for total surface NKG2DLs using biotinylated recombinant human NKG2D-Fc and Streptavidin-PE secondary (NKG2D-Fc-Bio-Strep-PE), biotinylated human IgG1 isotype (IgG1), Streptavidin-PE secondary only (Strep-PE) or left unstained. Data represent the mean fluorescence intensity (MFI) of triplicate repeats ± S.D. Statistical significance was assessed by one-way ANOVA followed by Bonferroni post hoc analysis. Significance was assessed versus MICA/B or NKG2D-Fc-stained cells (ns $p>0.05$, *$p\leq0.05$, **$p\leq0.01$, ***$p\leq0.001$ and ****$p\leq0.0001$). Patient sample n=1.

3.3.8 Immunophenotyping primary GBM tissue

The overall strategy for the NKG2D BiTE immunotherapy is for it to be encoded into an oHSV-1 to enable tumour selective, local expression of the BiTE directly *in situ*. The aim is then for the NKG2D BiTE to activate endogenous TILs, regardless of TCR specificity, whether it is a $CD4^+$ or $CD8^+$ T cell, and independent of HLA-restricted antigen presentation by the target cell. This T cell activation should then induce target cell death, anti-tumour immune responses and T cell proliferation within the tumour.

We sought to identify the proportions of TILs, TAMs, and tumour cells in a primary human GBM sample. The same human CUSA-derived GBM tissue from Figure 3.8 was stained for CD3 (as a marker of TILs) and CD11b (as a marker of TAMs) before analysis by flow cytometry. Additionally, GBM cells were identified by

staining with epidermal growth factor receptor (EGFR). The percentages of live $CD3^+$ cells, $CD11b^+$, $EGFR^+$ and remaining cells not positive for these markers (Other) is shown in Figure 3.9.

The sample did contain some T cells, but very few (<3%), while $CD11b^+$ cells made up around 11% of the total live cells in the sample (Figure 3.9). 33% of cells were $EGFR^+$, suggesting that these may be tumour cells, although the heterogeneity of GBM may mean this is not an accurate representation of the real number of tumour cells, as many more tumour cells are likely to be hidden in the "Other" category.

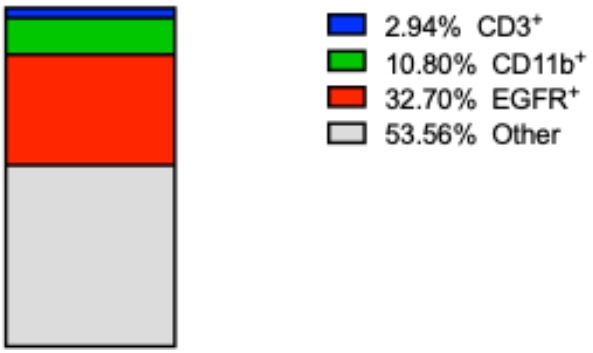

Figure 3.9 Immune profile of human GBM tissue
Human GBM tissue obtained by cavitron ultrasonic surgical aspirator (CUSA) was dissociated and stained for various cell markers for flow cytometric analysis. Area on bar represents mean percentage of $CD3^+$ (blue), $CD11b^+$ (green), Epidermal growth factor receptor $(EGFR)^+$ (red) positive cells, and remaining cells (grey) of the total live cell population from triplicate repeats. Patient sample n=1

3.4 Discussion

The results in this chapter focusses on the exploration of NKG2DL-targeted BiTE immunotherapy for GBM, highlighting the levels of expression of NKG2DLs on GBM cells, macrophages, and T cells, as well as characterising the NKG2D BiTE activity. The hypothesis posed in this chapter is that GBM cells expressing NKG2DLs could be targeted with a BiTE to activate T cells and direct cytotoxicity towards the GBM cells.

Firstly, it was demonstrated that a range of cancer cell lines express NKG2DLs. The data in Figure 3.1 show the surface expression of MICA/B and total NKG2DLs on GBM cell lines U87 and A172, as well as colorectal DLD-1 cells. Each cell line exhibited high MICA/B expression, with A172 cells having higher levels than U87 cells. The expression of NKG2DLs on A172 and U87 cells has been previously reported and is in line with the results observed here in Figure 3.1, with A172 cells having high MICA/B signal and slightly lower for ULBP1, ULBP2 and ULBP3. U87 cells also displayed high MICA/B expression, but lower than A172 cells, while ULBP1 and ULBP2 expression was similar to A172 cells and ULBP3 was higher (Friese et al., 2003). The expression of these ligands was also tested across a range of other commonly used GBM cell lines, and five primary human GBM cell lines, all of which expressed at least one NKG2DL, and with MICA/B typically being the highest expressed (Friese et al., 2003).

There appears to be a slight contradiction between the data in Figure 3.1A and E, whereby all cell lines tested have very high expression of MICA/B (94%, 82% and 98% for DLD-1, U87 and A172, respectively), but lower expression of total NKG2DLs for GBM cells (52% and 61% for U87 and A172, respectively), but not DLD-1 cells. If the staining efficiencies were equivalent for MICA/B and total

NKG2DL, one would expect the expression of total NKG2DL to be higher as it would include the MICA/B$^+$ cells, and also any others that express ULBP1-6. However, it is likely that the staining efficiencies are not equivalent. The MICA/B antibody is a commercially-available mouse anti-human MICA/B, conjugated to APC fluorophore, and so is likely to be high affinity, and only requires one cycle of staining. The NKG2D-Fc-biotin staining system requires a relatively low affinity NKG2D receptor that also requires a secondary staining step with streptavidin-PE, and so the staining process involves additional washing cycles. Therefore, the MICA/B staining is more efficient, whereas the total NKG2DL staining is likely to be an underestimate.

Having confirmed the GBM cell lines expressed NKG2DLs, BiTEs targeting these ligands were constructed and characterised to identify the optimal orientation of BiTE construct. In the comparison of the two different orientations of NKG2D BiTE (NKG2D-αCD3-NKG2D and αCD3-NKG2D-αCD3) in Figure 3.3, the data suggested there may be some non-specific activation of T cells using the αCD3-NKG2D-αCD3 construct. The CD25 expression data (Figure 3.3A) would suggest this T cell activation is dependent on GBM target cells as no increase is observed in T cell monocultures. However, the CD69 data (Figure 3.3B) may indicate that some non-specific T cell activation still occurs in the absence of target cells. This non-specific activation of T cells may be due to one of two possibilities: 1) the double αCD3 scFv constructs are binding to CD3 in *trans* between two T cells, or 2) in *cis* on the same T cell, triggering CD3 clustering in a target cell-independent manner, or 3) the mutation in the NKG2D(B5) domain has not fully abrogated the binding ability of the NKG2D domain, and thus the αCD3-NKG2D(B5)-αCD3 Control BiTE is still able to bind to NKG2DLs and trigger T cell activation in a similar manner to

the αCD3-NKG2D-αCD3 BiTE. Given the same mutation was introduced into the NKG2D(B5)-αCD3-NKG2D(B5) Control BiTE, which did not trigger any T cell activation, it is likely that the former possibility is most likely.

Based on the target cell-independent T cell activation with the αCD3-NKG2D-αCD3, the NKG2D-αCD3-NKG2D orientation was identified as the optimal construct for further characterisation. Further exploration into the activity profile of NKG2D BiTE-activated T cells in Figure 3.5 revealed that not only are both $CD4^+$ and $CD8^+$ T cells activated in response to NKG2D BiTE, but they are also both capable of expressing pro-inflammatory IFN-γ as well as cytolytic proteins such as granzyme B and perforin. This may indicate that $CD4^+$ T cells, traditionally only considered to provide 'help' to cytotoxic $CD8^+$ T cells in the form of cytokines, may be able to directly perform some of the cytotoxic effector functions that these $CD8^+$ T cells would perform when activated by the NKG2D BiTE. Conversely, $CD8^+$ T cells are shown here to also be able to produce IFN-γ alongside the $CD4^+$ T cells. Taken together, these suggest that the NKG2D BiTE could work to activate any tumour infiltrating T cells, independent of their TCR specificity, HLA status of the target cell, and independent of whether it is a $CD4^+$ or $CD8^+$ T cell. This activation is not only able to direct cytotoxicity towards target cells expressing NKG2DLs, but also help to create a more pro-inflammatory tumour microenvironment with the production of IFN-γ. Other studies using BiTEs have demonstrated similar findings, generating cytotoxic $CD4^+$ and IFN-γ-producing $CD8^+$ T cells (Freedman et al., 2017; Khalique et al., 2021).

We next sought to investigate the reactivity of the NKG2D BiTE towards macrophages, considering microglia/macrophages are some of the most abundant stromal cells in the GBM TME (Morantz et al., 1979). Macrophages were polarised

in Figure 3.6B with IFN-γ with LPS or IL-10 to stimulate classically activated, pro-inflammatory macrophages and alternatively activated, anti-inflammatory macrophages, respectively. The use of these cytokines to stimulate macrophage phenotypes has been well established, however the measurement of surface marker expression, such as CD80 and CD206, is likely to be an oversimplification (reviewed in Metchnikoff & Prize, 2015). This matter is discussed further in the discussion for the next chapter in section 4.4. Nevertheless, the markers of CD80 and CD206 were used here in Figure 3.6B as a simple and quick confirmation that the different cytokine treatments had driven a phenotypic change in the macrophages, albeit perhaps an oversimplification.

In assessing the specificity of the NKG2D and PD-L1 BiTEs towards macrophages compared to GBM cell lines (Figure 3.6E and F), both BiTEs were found to activate T cells in the presence of GBM cell lines, but only the PD-L1 BiTE activated T cells against macrophages. This would suggest that the low MICA/B expression on macrophages (Figure 3.6B and D) is not enough for the NKG2D BiTE to activate T cells at the concentration used in this experiment of 1 nM. The two different BiTEs were used at their respective optimal concentrations: the NKG2D BiTE used at 1 nM was determined in the dose curve in Figure 3.4, whereas the PD-L1 BiTE concentration of 40 nM was determined previously (Khalique et al., 2021). The use of two different concentrations may explain the discrepancies in activity of the two BiTEs against macrophages and GBM cell lines, and that perhaps the 1 nM NKG2D BiTE is too low to activate T cells against macrophages. Likewise, the PD-L1 BiTE may not show as much activation if used at 1 nM. Nevertheless, 1 nM NKG2D BiTE was able to effectively activate T cells against GBM cell lines which express higher levels of NKG2DLs but not against macrophages which

express lower levels, thus demonstrating the specificity of the BiTE towards cells expressing relatively high surface NKG2DLs. This may be due to the inability for the NKG2D BiTE to successfully form an immunological synapse with cells expressing low NKG2DLs, like macrophages.

The expression of NKG2DLs on monocyte-derived macrophages and their subsequent sensitivity to NK cell-mediated lysis has previously been described. Nedvetski and colleagues reported increased macrophage NKG2DL expression following treatment with 200 ng/mL LPS, which sensitised them to NK cell lysis, but not with 100 ng/mL LPS (Nedvetzki et al., 2007). These findings align with the results in Figure 3.6, whereby macrophages polarised to a classically activated M1-like phenotype with 10 ng/mL LPS and 25 ng/mL IFN-γ had a low MICA surface expression and were not sensitive to the NKG2D BiTE, possibly because the concentration of LPS was far lower than the levels needed to induce NKG2DL expression (Nedvetzki et al., 2007).

In terms of NKG2DL expression on cells in the brain parenchyma, Pereboeva et al. report moderate constitutive surface expression of MICA and some ULBP2 in resting primary human astrocytes *in vitro*, but only demonstrated a slight cytotoxicity in co-culture with γδ T cells (Pereboeva et al., 2015). They also reported by histology a low level of MULT-1 (a murine NKG2DL) in normal mouse brains (Pereboeva et al., 2015). Other studies investigating NKG2DL expression in human GBM tissue revealed that NKG2DLs rarely coincided with CD11b or von Willebrand factor (vWF), indicating that tumour associated microglia and endothelia are rarely positive for NKG2DLs (Flüh et al., 2018). These observations and the data in Figure 3.6 suggest, therefore, that the NKG2D BiTE may not activate T cells against

microglia/macrophages, astrocytes or endothelia in the brain parenchyma or in GBM due to their reported low NKG2DL expression.

The NKG2D BiTE does not activate T cells in the absence of target cells expressing NKG2DLs, however the PD-L1 BiTE demonstrated target cell-independent T cell activation (Figure 3.6E and F). This has previously been reported by Khalique et al., who noted that several T cells expressed PD-L1, and thus the PD-L1 BiTE activated T cells in the absence of other target cells (Khalique et al., 2021). The authors also reported that when activated by the PD-L1 BiTE, T cell viability decreased in the presence of target cells but not in the absence of target cells. This decrease in viability was therefore concluded to be due to activation induced cell death (AICD) rather than fratricide (direct lysis of T cells by other T cells) (Khalique et al., 2021). It remains unclear whether this autoreactivity with the PD-L1 BiTE was due to the BiTE binding and activating in *cis* (binding to PD-L1 and CD3 on the same cell), or in *trans* (crosslinking two different cells).

T cells have been reported to express some surface NKG2DLs upon activation (Molinero et al., 2002; Nausch & Cerwenka, 2008). Furthermore, the data in Figure 3.7 demonstrates an increase in both $CD4^+$ and $CD8^+$ T cells upon stimulation with CD3/CD28 Dynabeads. However Flüh et al., noted that in human GBM sections, NKG2DLs were rarely expressed on cells stained for CD3γ (Flüh et al., 2018). Furthermore, based on the data in Figure 3.7, resting T cells did not express surface NKG2DLs. Together, these findings may indicate that resting T cells lack enough NKG2DL expression for the NKG2D BiTE to activate them (Figure 3.6E and F), and that TILs in GBM are also unlikely to be autoreactive with the NKG2D BiTE. However, it is possible that once the T cells do become activated with the NKG2D BiTE, they may start to become autoreactive due to activation-induced NKG2DL

upregulation. In a study using NKG2D-CAR-T cells, fratricide was observed due to transient stress inducing CAR-T cell NKG2DL expression during production and freeze-thawing of the engineered cells (Breman et al., 2018). The authors investigated the use of PI3K inhibitors to prevent the transient expression of NKG2DLs on the CAR-T cells, or the use of an NKG2D-neutralising antibody, both of which reduced fratricide during manufacture of the NKG2D-CAR-T cells (Breman et al., 2018). This may suggest that TILs could undergo fratricide with the NKG2D BiTE once they have been initially activated and is a subject for further investigation.

The use of bispecific proteins to target T cells against cells with NKG2DL expression has been explored elsewhere. Zhang and Sentman developed a BiTE which involved a C terminal anti-mouse-CD3ε scFv linked to the ligand binding domain of murine NKG2D receptor (T. Zhang & Sentman, 2011). This construct is essentially the murine version of the NKG2D BiTE used here, but only contains a single NKG2D domain, unlike the NKG2D-αCD3-NKG2D BiTE. The NKG2D ligand binding domain binds to each NKG2DL with different affinities, but generally in the μM range (Raulet et al., 2013), and so generally has a lower affinity than scFvs or other immunotherapeutics that involve ligand binding, such as antibodies. The NKG2D BiTE used here, which contains two NKG2D domains, may therefore offer an advantage over similar BiTEs that use a single NKG2D domain as it may allow for greater avidity, despite the relatively low affinity.

The number of TILs in GBM is considered to be lower than most other solid tumours, partly due to restriction posed by the BBB (Orrego et al., 2018). This is in line with the findings in Figure 3.9, with relatively few of the cells obtained from the single patient GBM sample being $CD3^+$. One major potential limitation of the NKG2D BiTE immunotherapy is the lack of TILs in the tumour microenvironment for the

NKG2D BiTE to activate. This will be discussed in more detail in the main discussion (Section 6), but in brief, the advantage of the NKG2D BiTE is that it has the potential to activate any and every T cell in the vicinity of the tumour cells, providing there is NKG2D BiTE and NKG2DL expression. Therefore, these TILs are not restricted to TCR specificity, target cell HLA expression, or whether the T cell is $CD4^+$ or $CD8^+$. Furthermore, BiTE-mediated activation has been shown to induce T cell proliferation (Freedman et al., 2017; Khalique et al., 2021). Therefore, we hypothesise that activation of GBM TILs by the NKG2D BiTE is likely to trigger T cell proliferation *in situ*, thus amplifying the number of TILs in the tumour microenvironment.

The data shown in this chapter using clinical GBM material is from a single patient sample, and so does not reflect the heterogeneity of GBM tumours. When more samples become available, this study will be extended.

3.5 Conclusions

The results of this chapter indicate that the NKG2D BiTE is effective at activating both $CD4^+$ and $CD8^+$ T cells towards target cells that express NKG2DLs but does not activate T cells in the absence of target cells, therefore confirming the initial hypothesis for this chapter, stated in section 3.2.1. Furthermore, the NKG2D BiTE is able not only to activate T cells to generate a highly activated anti-tumour phenotype, but it is also able to direct cytotoxicity towards GBM target cells. Meanwhile, the Control BiTE, which is unable to bind to NKG2DLs but can still bind to CD3 on T cells, is unable to trigger T cell activation. The NKG2D BiTE was therefore selected to be used for further experiments to potentially encode into an oncolytic virus for tumour-selective delivery in GBM tumours, and to also investigate

the interactions between current GBM chemotherapy and radiotherapy and NKG2D BiTE activity.

4 Combining NKG2D BiTE with oHSV-1 and conventional GBM therapy

4.1 Introduction

As discussed in section 1.4.2.1, conventional GBM therapy involves surgical resection to remove the bulk tumour mass followed by concomitant radiotherapy and temozolomide (TMZ) chemotherapy, (known as Stupp therapy (Stupp et al., 2005)). TMZ and radiation therapy both induce DNA damage, either by directly alkylating DNA residues and inducing base mispairing (S. Y. Lee, 2016) or inducing DNA strand breakage with ionising radiation (Baskar et al., 2014), in the hope of triggering apoptosis in any remaining cancerous cells. However, GBM tumours invariably recur and often acquire resistance to these therapies, rendering them ineffective.

Cancer cells frequently exhibit increased NKG2DL expression compared to healthy cells due to chronic activation of the DDR and sustained proliferative signalling, and the ATM/ATR-mediated DNA damage checkpoint plays a key role in this upregulation (Gasser et al., 2005). Additionally, p53 and the cGAS/STING pathways have been implicated in inducing NKG2DL expression in various model systems (Lam et al., 2014; Textor et al., 2011). These mechanisms are discussed in more detail in section 1.8.4.1. Therefore, a clear link between DNA damage and NKG2DL expression has been established.

Based on the link between DNA damage and NKG2DL expression, it is unsurprising that DNA damage induced by radiation and TMZ further upregulates NKG2DL expression in GBM cancer cells, as well as other inducers of DNA damage in other tumours. For example, Weiss et al. explored the effects of TMZ and radiation on NKG2DL expression on murine GBM cells and demonstrated that NKG2DLs were further upregulated after TMZ and radiation, and that upregulation was dependent on ATM (Weiss, Schneider, et al., 2018). Furthermore, the authors reported that TMZ and radiation treatment enhanced the immunogenicity of GBM cells and imparted a survival benefit in murine syngeneic orthotopic GBM models, an effect which was dependent on the innate NKG2D response (Weiss, Schneider, et al., 2018).

In a study by Lamb et al., immunodeficient mice with orthotopic patient-derived xenografted GBM cells were treated with engineered TMZ-resistant γδ T cells and demonstrated additive survival benefit when used alongside TMZ (Lamb et al., 2021). Furthermore, Weiss et al. demonstrated synergistic activity when using an NKG2D-CAR-T cell in combination with a sublethal dose of radiation in a murine syngeneic glioma model, owing to the increased NKG2DL expression following radiation (Weiss, Weller, et al., 2018). These studies indicate that TMZ and radiotherapy may also synergise with NKG2D BiTE activity.

Systemic administration of BiTEs is challenging due to rapid clearance (Stork et al., 2009) and potential on-target, off-tumour effects (discussed in section 1.3.6), and the BBB poses an additional barrier to BiTE delivery for GBM (discussed in section 1.4.2.4). Therefore, we propose to encode the NKG2D BiTE into the genome of the oHSV-1 G207 to achieve local delivery of the BiTE directly within the GBM TME.

However, when considering G207 oHSV-1 as a delivery vector for the NKG2D BiTE, it is important to address the relationship between viruses and the NKG2D response. The NKG2D receptor and ligands are a crucial part of the innate immune response to virus-infected cells as well as malignantly transformed cells. Many viruses exploit various strategies to evade the NKG2DL immune response, such as retaining ligands intracellularly, directing ligands for proteasomal degradation, miRNA-mediated destabilisation of mRNA transcripts and shedding of surface proteins (Baugh et al., 2020). However, both cancer cells and viruses have evolved an array of means to downregulate these NKG2DLs and subvert the NKG2D immune response in attempts to evade the NKG2D immune response, showing a remarkable degree of convergent evolution (Baugh et al., 2020).

Despite the numerous mechanisms convergently evolved by viruses and cancers to evade the NKG2D response, such as downregulating expression of certain ligands, it is unlikely that a virus or cancer cell can prevent the surface expression of all eight NKG2DLs. As discussed in section 1.8.5, ligand diversity makes total immune evasion as a result of viral gene products or a mutation during malignant transformation far more unlikely (Eagle & Trowsdale, 2007; Zingoni et al., 2018).

Based on the data from Chapter 3 demonstrating the ability of the NKG2D BiTE to specifically activate both $CD4^+$ and $CD8^+$ T cells in an TCR-independent manner to induce lysis of GBM cells, in this chapter we explore whether the G207 oHSV-1 is a suitable vector for NKG2D BiTE therapy, and seek to find ways to complement conventional GBM therapy of TMZ and radiation with the NKG2D BiTE.

4.2 Chapter hypothesis and aims

4.2.1 Hypothesis

We hypothesise that conventional GBM therapy of TMZ and radiation will enhance NKG2D BiTE activity.

4.2.2 Chapter aims

1) To investigate the relationship between oHSV-1 infection and surface NKG2DL expression on GBM cell lines
2) To assess the impact of TMZ and radiation on NKG2DL expression in GBM cells and macrophages
3) To determine the anti-tumour effects of TMZ and radiation pre-treatment on NKG2D BiTE activity
4) To investigate the effects of NKG2D BiTE-conditioned medium on macrophage immunophenotype

4.3 Results

4.3.1 Effects of oHSV infection on expression of NKG2DLs in infected cells

The overall strategy for this thesis is to deliver the NKG2D BiTE to GBM cells by using an oHSV-1 as a vector; it is, therefore, prudent to investigate the relationship between oHSV-1 infection and NKG2DL expression in cancer cells. To investigate this, U87 and A172 cells were infected with increasing multiplicities of infection (MOIs) of the oHSV-1, G207, before staining for surface MICA/B and total NKG2DLs by flow cytometry 72 hours later (Figure 4.1).

The G207 genome encodes GFP under control of the *ICP6* promoter, enabling quantitative assessment of infected cells. Therefore, using flow cytometry, the percentage of infected (GFP^+) U87 and A172 cells was measured following infection at a range of MOIs (Figure 4.1A and B, respectively). U87 cells were highly permissive to G207 infection (Figure 4.1A), while A172 cells were less permissive (Figure 4.1B).

The virally-encoded GFP not only enables the quantification of infected cells, but it also allows the distinction between infected (GFP^+) and uninfected (GFP^-) populations during flow cytometric analysis and thus allows the measurement of expression of MICA/B and NKG2DLs on infected and uninfected cells. Therefore, we measured the relative surface expression (MFI) of MICA/B on U87 and A172 cells (Figure 4.1C and D, respectively) and total NKG2DLs (Figure 4.1E and F, respectively) on infected (GFP^+) and uninfected (GFP^-) cells.

G207 infection decreases surface MICA/B expression in U87 and A172 GBM cell lines

When U87 cells were treated with G207, there was a dose-dependent downregulation in relative MICA/B expression, with decreased expression in both the infected and uninfected populations compared to uninfected controls (MOI 0) (Figure 4.1C). This downregulation was more pronounced in the GFP^+ infected population of U87 cells. A172 cells also demonstrated MICA/B downregulation in infected cells, but the global downregulation (in GFP^- cells) was only observed at an MOI of 5 (when a significant proportion of A172 cells were GFP^+), but not at lower MOIs (Figure 4.1D). This could be due to the low percentage of GFP^+ A172 cells at these lower MOIs compared to U87 cells.

Both cell lines demonstrate a global MICA/B downregulation when the levels of infection are high (MOI 0.1, 1 and 5 for U87 cells, but only MOI 5 for A172 cells) compared to the baseline expression on cells in the absence of any virus (MOI 0). This could reflect non-productive virus entry into those cells, or perhaps result from a paracrine-acting factor secreted by the infected cells.

Total NKG2DL expression remains unchanged in infected U87 cells but decreases in A172 cells

The relative total surface NKG2DL expression on U87 cells (Figure 4.1E) did not follow the same pattern as the MICA/B expression; NKG2DL expression remained unchanged in both infected and uninfected cells at all MOIs compared to uninfected controls. By contrast, the total relative NKG2DL expression on A172 cells (Figure 4.1F) did significantly decrease in infected cells compared to the uninfected cells. At MOI 0.1, there appeared to be a significant increase in total surface NKG2DL expression compared to uninfected cells, although these results may be unreliable given only 2% of the A172 cells were GFP^+ at MOI 0.1.

Together, these results suggest that in both U87 and A172 cells, G207 infection resulted in a downregulation of surface MICA/B, with a striking decrease in infected GFP$^+$ cells but also a modest decrease in uninfected GFP$^-$ cells. However, in U87 cells, the total NKG2DL expression did not change in infected or uninfected cells compared to baseline expression, whereas A172 cells still demonstrated a decrease in total NKG2DL expression in infected cells.

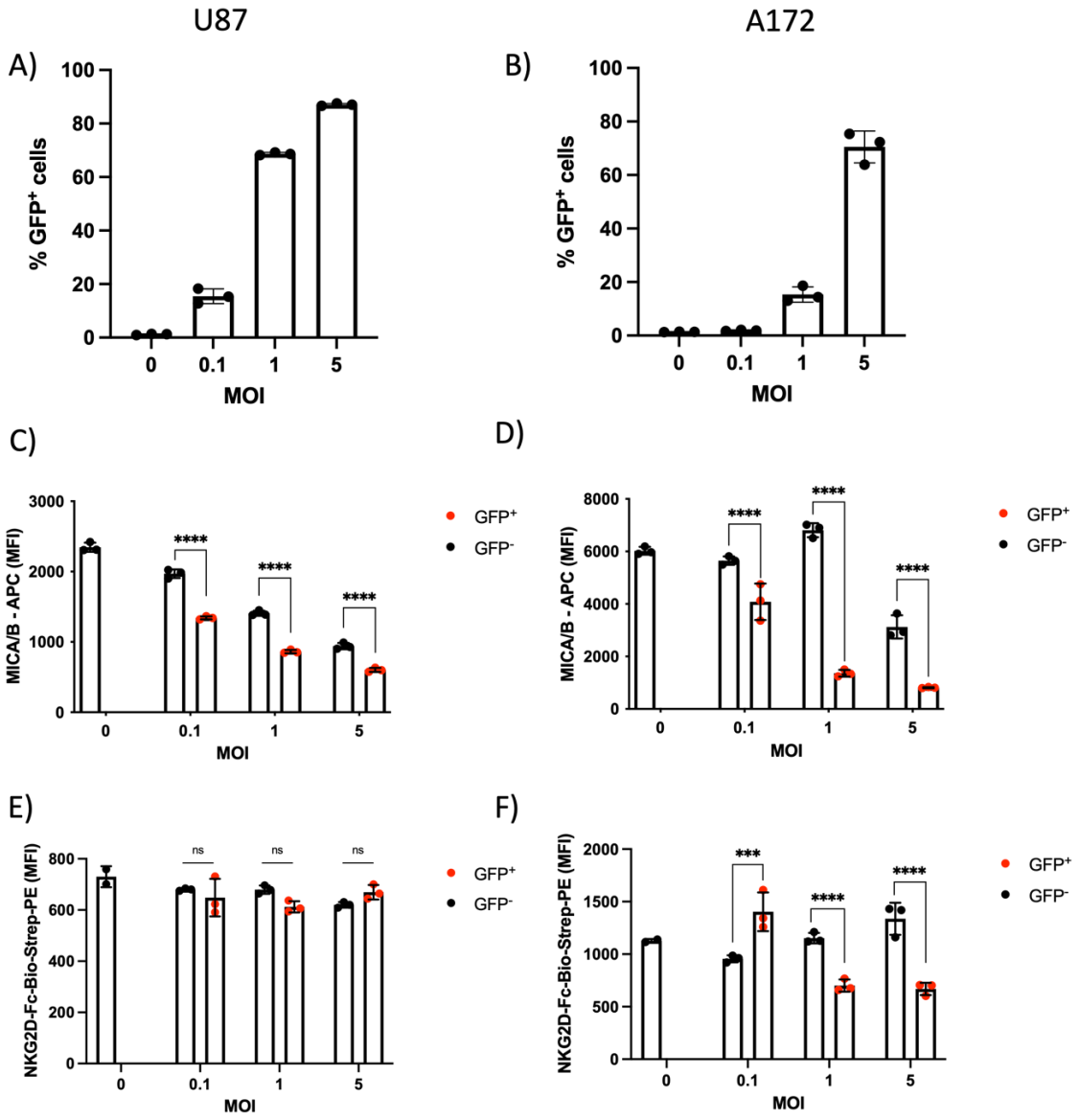

Figure 4.1 Effects of infection with G207 oHSV-1 on surface NKG2DL expression

U87 (left) and A172 (right) cells were seeded in 24 well plates and infected with G207 oHSV-1 at a multiplicity of infection (MOI) of 0, 0.1, 1 or 5. 72 hours after infection, cells were harvested and stained for flow cytometry analysis. Cells infected with G207 could be traced by flow cytometry due to virally-encoded GFP expression. (**A**) The percentage of GFP^+ U87 and (**B**) A172 cells 72 hours after infection with G207 oHSV-1. Data represents mean percentage of GFP^+ cells of triplicate repeats ± S.D. (**C**) Wells of U87 cells and (**D**) A172 cells infected with G207 oHSV-1 were stained for surface MICA/B-APC. (**E**) Wells of U87 cells and (**F**) A172 cells infected with G207 oHSV-1 were stained for total surface NKG2DLs using biotinylated recombinant human NKG2D-Fc and Streptavidin-PE secondary (NKG2D-Fc-Bio-Strep-PE). Relative surface expression of MICA/B or total NKG2DLs for the infected (GFP^+, red) and uninfected (GFP^-, black) was measured for each MOI. Data represents mean fluorescence intensity (MFI) of triplicate repeats ± S.D. Statistical significance was assessed by two-way ANOVA followed by Bonferroni post hoc analysis. Significance was assessed versus GFP^- cells at each MOI (ns $p>0.05$, *$p\leq0.05$, **$p\leq0.01$, ***$p\leq0.001$ and ****$p\leq0.0001$).

4.3.2 Combining G207 oHSV-1 and NKG2D BiTE immunotherapies

Given the observation that surface NKG2DLs, such as MICA/B, are downregulated on cells infected with the G207 virus (Figure 4.1), we investigated whether G207 infection induced shedding of NKG2DLs from infected U87 cells (Appendices section 7.1.4) and revealed no significant increase in soluble NKG2DLs. We next sought to investigate whether G207 infection impacted NKG2D BiTE activity when treated simultaneously. Therefore, we simultaneously treated U87 and A172 cells with G207 virus and NKG2D BiTE in co-culture with T cells (Materials and Methods section 2.5.1).

G207 virus treatment alone causes a modest dose-dependent cytotoxicity

The viability of U87 and A172 cells after simultaneous G207 and NKG2D BiTE treatment was assessed by flow cytometry (Figure 4.2A and B, respectively). For both U87 and A172 cells, G207 treatment alone had a modest dose-dependent effect on viability when in monocultures or co-cultures with T cells but no BiTE. These results indicate that in both cell lines, the G207 virus has a modest direct cytolytic effect at lower MOIs (0.1 and 1), increasing slightly at MOI 5. Furthermore, these results show that infected GBM cell lines in co-culture with T cells does not

further decrease the viability of the cells, suggesting that there is no detectable T cell-mediated cytotoxicity towards infected cells.

G207 treatment has an additive cytotoxic effect with NKG2D BiTE in U87 cells, but limits BiTE activity in A172 cells at high MOIs

Both cell lines showed dramatic viability decreases when in uninfected (MOI 0) co-cultures with T cells and treated with NKG2D BiTE compared to no BiTE (Figure 4.2A and B). As seen in previous figures (Figure 3.5G), A172 cell viability was more sensitive to NKG2D BiTE (Figure 4.2B) than U87 cells (Figure 4.2A). For U87 cells, G207 treatment demonstrated a significant dose-dependent additive cytotoxic effect when also treated with NKG2D BiTE (Figure 4.2A). However, A172 cells did not follow this same pattern (Figure 4.2B); even in the absence of G207 at MOI 0, viability was low following NKG2D BiTE treatment, which decreased subtly at MOI 0.1 and 1, and increased at MOI 5. These results together suggest that the NKG2D BiTE can trigger T cell-mediated cytotoxicity of both GBM cell lines even with G207 infection, and that combination of virus and NKG2D BiTE have an additive effect in killing GBM cells. However, at a high MOI in A172 cells, the NKG2D BiTE begins to lose its efficacy, suggesting that in these cells the viral-mediated downregulation of surface NKG2DLs affects the BiTE activity.

Simultaneous NKG2D BiTE and G207 treatment limits infection in U87 cells but not A172 cells

The percentage of live G207-infected GFP^+ U87 and A172 cells was determined by flow cytometry (Figure 4.2C and D, respectively). As expected, G207 treatment caused a dose-dependent increase in the percentage of live GFP^+ cells

for both U87 (Figure 4.2C) and A172 cells (Figure 4.2D) in monocultures and co-cultures without BiTE. U87 cells showed greater infection at lower MOIs than A172 cells, highlighting their greater permissiveness to G207 infection.

The dose-dependent increase of GFP^+ A172 cells also increased in NKG2D BiTE-treated co-cultures (Figure 4.2D). In contrast, however, the percentage of GFP^+ U87 cells was suppressed in infected co-cultures treated with NKG2D BiTE compared to the other conditions. These results suggest the NKG2D BiTE activity may be limiting G207 spread by killing U87 cells before the infection can progress enough for detection by GFP.

Simultaneous G207 and NKG2D BiTE treatment limits T cell activation with A172 cells, but not U87 cells

The activation of T cells in co-culture with infected U87 and A172 cells and NKG2D BiTE treatment was measured by CD25 expression using flow cytometry (Figure 4.2E). For both cell lines, T cells were not activated in the absence of NKG2D BiTE, independent of increasing G207 infection. T cells were only activated in the presence of the NKG2D BiTE, suggesting that any T cell activation is specifically due to NKG2D BiTE, and not G207 cross-reactivity or presentation of viral antigens and cross-reactivity. Furthermore, Control BiTE (data not shown) did not induce any T cell activation.

When treated with NKG2D BiTE, T cell activation in co-cultures with U87 cells and NKG2D BiTE was unaffected by G207 virus at an MOI of 0.1 and 1, although a slight but significant decrease was observed at MOI 5. A172 cells however, showed a significant dose-dependent decrease in T cell activation with increasing MOI of

G207, suggesting that increasing G207 infection was limiting the activity of NKG2D BiTE.

These observations are in alignment with those made in Figure 4.1 regarding the effects of G207 infection and total surface NKG2DL expression. In U87 cells, surface NKG2DL expression was unaffected by G207 infection, and thus T cell activation remains broadly unaffected by G207 infection except at MOI 5. In contrast, G207 infection decreased A172 cell NKG2DL expression, leading to decreased NKG2D BiTE-mediated T cell activation as the proportion of infected cells increased with MOI.

Together, these findings provide evidence that G207 oHSV-1 is a suitable candidate for arming to express NKG2D BiTE and is likely to activate T cell against GBM cells (see results chapter 5).

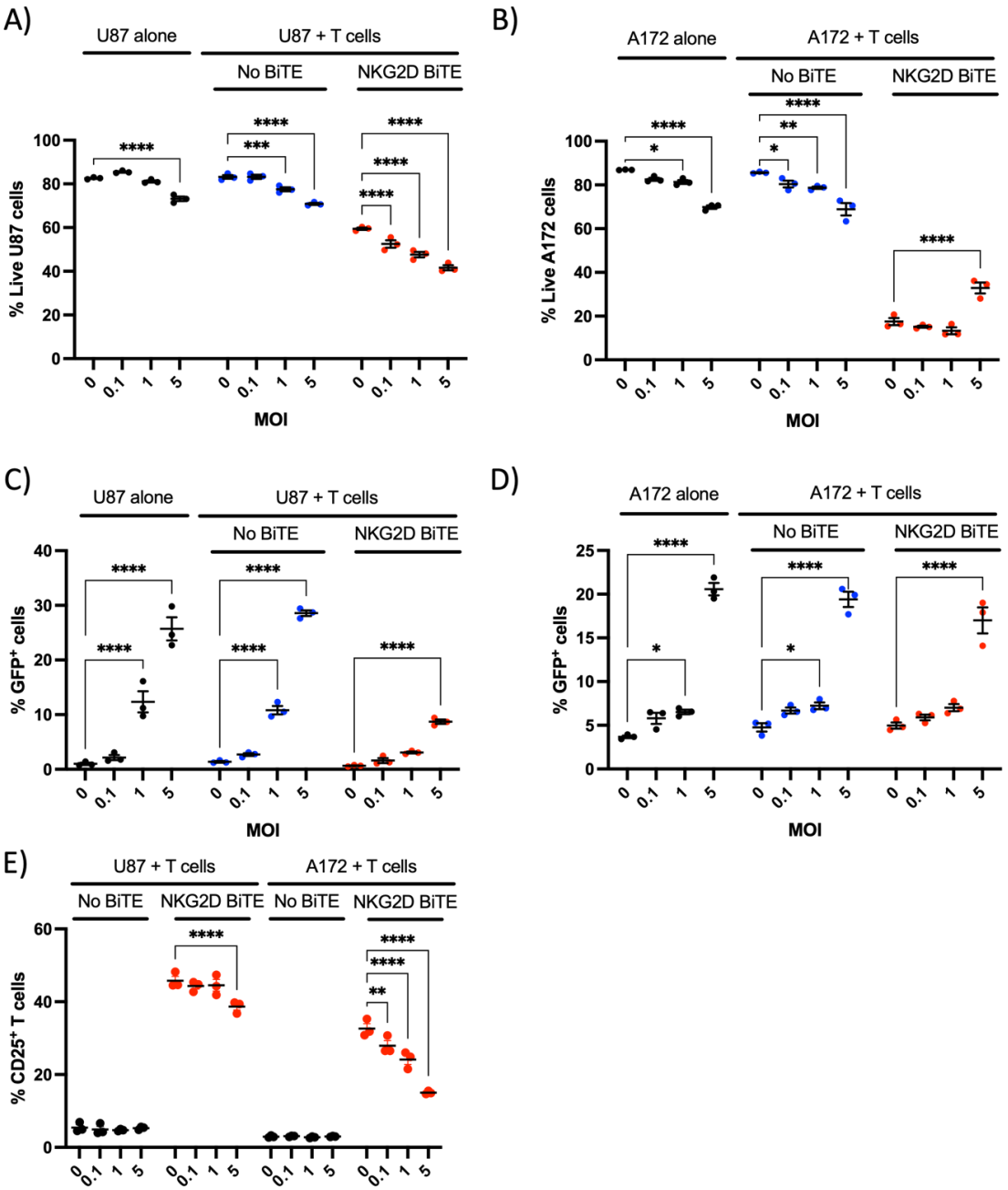

Figure 4.2 Combination of G207 oHSV-1 with NKG2D BiTE and T cells in GBM cell lines

U87 and A172 cells were seeded in 96 well plates and infected with G207 oHSV-1 at a multiplicity of infection (MOI) of 0, 0.1, 1 or 5. 4 hours after infection, PBMC-derived T cells were added at an E: T ratio of 5: 1 and treated with either no BiTE or 1 nM NKG2D BiTE. 96 hours after infection and treatment, all cells (including dead non-adherent cells in the media) were harvested and stained for flow cytometric analysis. (**A**) U87 and (**B**) A172 cells were stained with a flow cytometric viability dye. (**C**) Live U87 and (**D**) A172 cells infected with G207 could be traced by flow cytometry due to the expression of virally-encoded GFP. Data represents the mean percentage of live or GFP⁺ cells from triplicate repeats ± S.D from infected monocultures (black), infected co-cultures (blue) or infected co-cultures treated with NKG2D BiTE (red). (**E**) T cells from co-cultures were stained for activation marker CD25. Data represents the mean percentage of CD25⁺ cells from triplicate repeats ± S.D from infected co-cultures with U87 and A172 cells treated with no BiTE (black) or NKG2D BiTE (red). Statistical

significance was assessed by two-way ANOVA followed by Bonferroni post hoc analysis. Significance was assessed versus uninfected (MOI 0) cells within the relevant group (ns $p>0.05$, *$p\leq0.05$, **$p\leq0.01$, ***$p\leq0.001$ and ****$p\leq0.0001$).

4.3.3 TMZ chemotherapy increases surface NKG2DL expression on GBM cells

The aim of the work carried out in this thesis is to develop an immunotherapy using NKG2D BiTEs that can complement conventional GBM therapy of TMZ and radiation (Stupp et al., 2005). Therefore, we sought to investigate the effects of TMZ on surface NKG2DL expression by treating U87 and A172 cells with increasing concentrations of TMZ or DMSO vehicle control before assessing surface MICA/B expression 72 hours later by flow cytometry (Materials and Methods section 2.5.2) (Figure 4.3).

The effects on the viability of U87 and A172 cells were determined by the percentage of live cells in the flow cytometry analysis (Figure 4.3A and B respectively) in response to increasing doses of TMZ or DMSO. U87 cells were relatively resistant to TMZ, with no change in the percentage of live cells in response to increasing doses of TMZ or DMSO compared to untreated cells (Figure 4.3A). A172 cells, however, were sensitive to TMZ (Figure 4.3B), with significant decreases in the percentage of live cells in response to the increasing TMZ concentrations compared to untreated cells. This effect was specific to TMZ, as the cells treated with the equivalent DMSO vehicle control showed no decrease in viability compared to untreated cells.

The relative surface expression (MFI) of MICA/B on U87 and A172 cells was measured by flow cytometry (Figure 4.3C and D, respectively). U87 cells demonstrated subtle increases in relative surface expression of MICA/B with increasing TMZ compared to untreated cells (Figure 4.3C). However, U87 cells

treated with equivalent volumes of DMSO vehicle control also caused increases in MICA/B MFI at higher concentrations, although TMZ had a greater effect. These results suggest that TMZ treatment subtly increases relative surface expression and percentage of MICA/B$^+$ cells; however, these effects are not entirely specific to the TMZ alone, as the DMSO vehicle control also caused small increases in MICA/B expression.

A172 cells also showed increasing relative MICA/B expression (Figure 4.3D) with increasing TMZ concentration. However, DMSO treatment caused greater increases than TMZ, and became significantly higher at 200 µM, suggesting that DMSO solvent may be having the dominant effect in increasing MICA/B expression on A172 cells. However, the A172 cell viability was highly sensitive to TMZ (Figure 4.3B), but not DMSO. These effects observed in the surface expression may be due to the reduction in live cells at these higher concentrations.

Together, these results may indicate that, while U87 cells are resistant to TMZ treatment, the cells increase surface MICA/B expression, whereas A172 cells are sensitive to TMZ treatment, and die without increasing MICA/B expression.

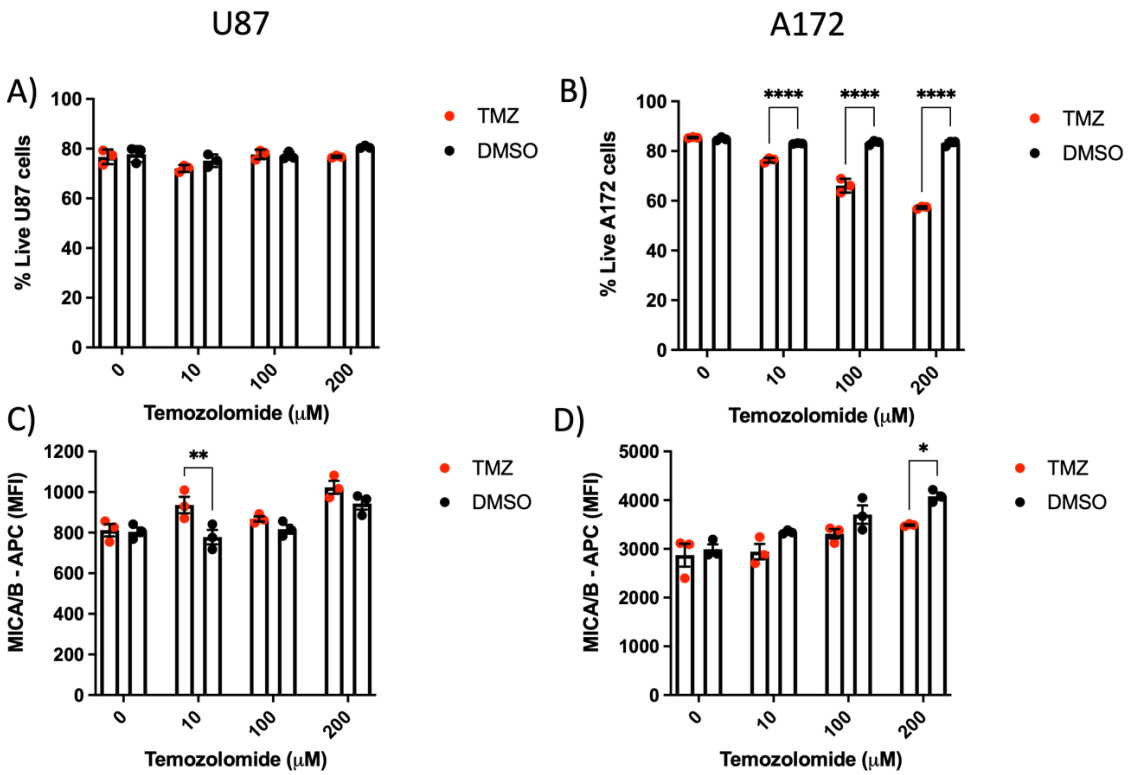

Figure 4.3 Effect of TMZ on surface MICA/B expression on GBM cell lines
U87 (left) and A172 (right) cells were seeded in individual T25 flasks in 10% DMEM and treated with 10, 100 or 200 μM TMZ (red) or the equivalent volume of DMSO vehicle control (black). 72 hours after treatment, all cells (including dead non-adherent cells in the media) were harvested with non-enzymatic dissociation buffer and stained for flow cytometric analysis. (**A**) U87 and (**B**) A172 cells were stained with a flow cytometric viability dye. Data represents the mean percentage of live cells of triplicate repeats ± S.D. (**C**) U87 and (**D**) A172 cells were stained for surface MICA/B-APC. Data represents the mean fluorescence intensity (MFI) of triplicate repeats ± S.D. Statistical significance was assessed by two-way ANOVA followed by Bonferroni post hoc analysis. Significance was assessed versus 0 μM TMZ or DMSO (ns $p>0.05$, * $p\leq0.05$, ** $p\leq0.01$, *** $p\leq0.001$ and **** $p\leq0.0001$).

4.3.4 Radiation increases surface NKG2DL expression on GBM cells

Alongside TMZ chemotherapy, GBM patients are often given radiation therapy of 2 Gy each weekday for six weeks (Stupp et al., 2005). Having observed the increase in surface MICA/B expression on GBM cell lines after TMZ treatment in Figure 4.3, we next sought to investigate what effect radiation would have on the surface expression of NKG2DLs.

U87 and A172 cells were irradiated with increasing doses of radiation before assessing surface MICA/B and total NKG2DLs by flow cytometry 24- and 48-hours post-irradiation (Materials and Methods section 2.5.2).

The viability of irradiated U87 and A172 cells was assessed by flow cytometry (Figure 4.4A and B). Radiation caused a modest dose-dependent decrease in U87 cell viability 24- and 48-hours post-irradiation (Figure 4.4A). Meanwhile, A172 cells were more sensitive to radiation treatment than U87 cells (Figure 4.4B), with greater dose-dependent decreases in viability at both time points.

The relative surface expression of MICA/B on U87 and A172 cells is shown in Figure 4.4C and D, respectively. The MFI of MICA/B significantly increased in a dose-dependent manner on U87 cells (Figure 4.4C) at both timepoints. However, while the relative expression of MICA/B on A172 cells also significantly increased in a dose-dependent manner at 24 hours, relative expression decreased at 48 hours (Figure 4.4D).

Total NKG2DL relative expression on U87 and A172 cells is shown in Figure 4.4E and F, respectively. Like the MICA/B data in in Figure 4.4C, relative total NKG2DL expression increased in a dose-dependent manner for U87 cells (Figure 4.4E) at both timepoints. However, in contrast to the MICA/B data in Figure 4.4D, the total relative NKG2DL expression on A172 cells (Figure 4.4F) increased at both 24 and 48 hours.

The decrease in surface MICA/B expression on A172 cells at 48 hours with increasing radiation dose (Figure 4.4D) may be due to the cytotoxicity associated with the radiation, as can be observed in Figure 4.4B. However, this explanation does not fully address the issue, as at 24 hours, the viability of A172 cells does decrease in a dose-dependent manner similar to 48 hours, albeit not as much as

48 hours. This apparent decrease in surface MICA/B on irradiated A172 cells is masked by the increased expression of total NKG2DLs (Figure 4.4F) with increasing radiation dose, suggesting that perhaps other NKG2DLs such as ULBP1-6 are also upregulated to account for the loss of MICA/B. Alternatively, the MICA/B surface expression data at 48 hours could be anomalous, as it does not fit with the total NKG2DL expression at that time point or the MICA/B expression at 24 hours.

These data in Figure 4.4 support the hypothesis that DNA damage induced by radiation triggers an upregulation in surface NKG2DLs, such as MICA/B. While U87 cells are more resistant to radiation than A172 cells, both cell lines increased surface NKG2DL expression.

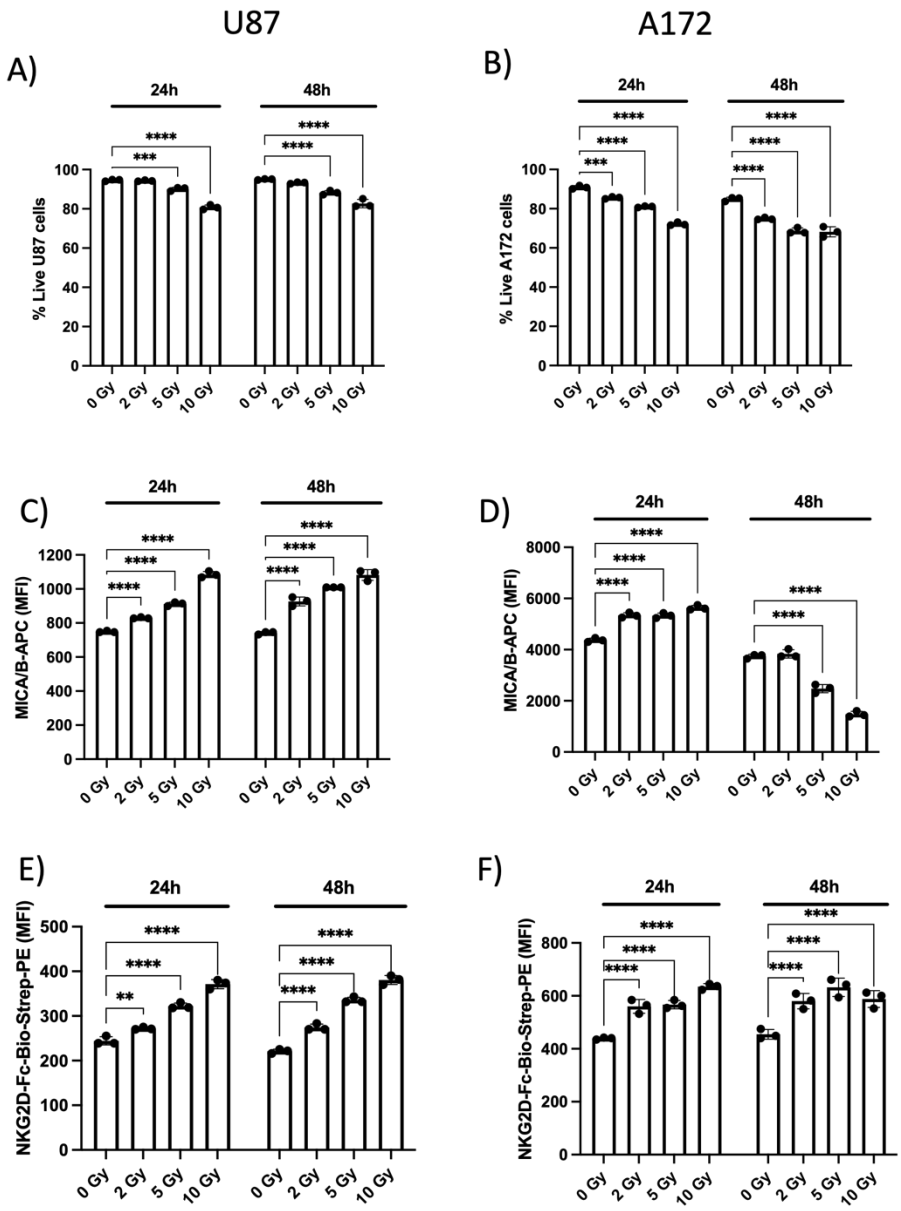

Figure 4.4 Effects of radiation on NKG2DL expression on GBM cell lines.
U87 (left) and A172 (right) cells were seeded in individual T25 flasks in 10% DMEM and irradiated with either 0 Gy, 2 Gy, 5 Gy or 10 Gy. 24 and 48 hours after irradiation, all cells (including dead non-adherent cells in the media) were harvested with non-enzymatic dissociation buffer and stained for flow cytometric analysis. (**A**) U87 and (**B**) A172 cells were stained with a flow cytometric viability dye. Data represents the mean percentage of live cells of triplicate repeats ± S.D. (**C**) U87 and (**D**) A172 cells were stained for surface MICA/B-APC, or (**E**-**F**) biotinylated recombinant human NKG2D-Fc and Streptavidin-PE secondary (NKG2D-Fc-Bio-Strep-PE). Data represents the mean fluorescence intensity (MFI) of triplicate repeats ± S.D. Statistical significance was assessed by two-way ANOVA followed by Bonferroni post hoc analysis. Significance was assessed versus 0 Gy at each timepoint (ns $p>0.05$, *$p\leq0.05$, **$p\leq0.01$, ***$p\leq0.001$ and ****$p\leq0.0001$).

4.3.5 Pre-treatment of U87 cells with TMZ and radiation enhances NKG2D BiTE-mediated T cell activation

Based on the experimental evidence discussed earlier, TMZ (Figure 4.3) and radiation (Figure 4.4) induced an increase in surface NKG2DLs on GBM cell lines. We also investigated the effects of a combination of TMZ and radiation and a combination (Appendices Figure 7.2). We next sought to investigate whether this increase in surface ligands enhanced the sensitivity towards the NKG2D BiTE. Optimisation of the pre-treatment doses revealed that A172 cells were too sensitive to pre-treatment, but U87 cells could tolerate 50 μM TMZ and 2 Gy radiation (Appendices section 7.1.2 for detail).

Pre-treatment of 50 μM TMZ and 2 Gy in combination increases U87 NKG2DL expression

Based on the dosage optimisation from Appendices section 7.1.2, U87 cells were exposed to 50 μM TMZ and 2 Gy radiation and stained for total surface NKG2DL expression by flow cytometry (Figure 4.5). U87 cells with no pre-treatment displayed clear expression of NKG2DLs, with an increased MFI compared to staining controls. This NKG2DL expression then significantly increased in response to all pre-treatments except DMSO alone.

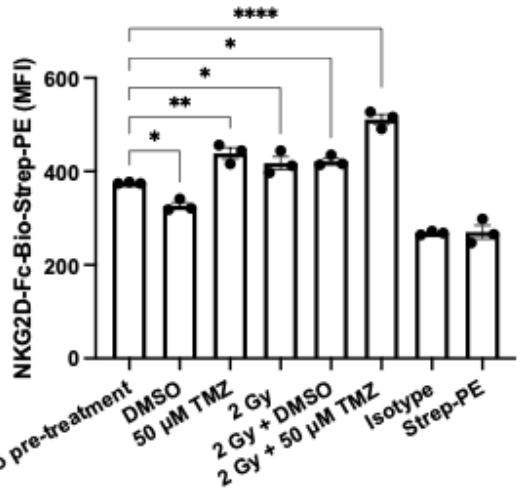

Figure 4.5 Surface expression of NKG2DLs on U87 cells pre-treated with conventional GBM therapies

U87 cells were treated with a single dose of 50 μM temozolomide (TMZ) or equivalent vehicle control (DMSO), or a single dose of 2 Gray (Gy) radiation either alone or in combination with 50 μM TMZ (2 Gy + TMZ) or vehicle control (2 Gy + DMSO), or left untreated (no pre-treatment). 48 hours after treatment, cells were dissociated with non-enzymatic dissociation buffer and stained with biotinylated recombinant human NKG2D-Fc protein as a primary, followed by streptavidin-PE secondary (NKG2D-Fc-Bio-Strep-PE). A biotinylated recombinant human IgG1 isotype was used as a control (Isotype), and secondary staining alone (Strep-PE). Relative NKG2DL expression was measured by flow cytometry. Data represents the mean of Mean fluorescence intensity (MFI) values of triplicate repeats ± S.D. Statistical significance was assessed by one-way ANOVA followed by Bonferroni post hoc analysis. Significance was assessed versus no pre-treatment (ns $p>0.05$, *$p\leq0.05$, **$p\leq0.01$, ***$p\leq0.001$ and ****$p\leq0.0001$).

Pre-treatment with TMZ and radiation enhances NKG2D BiTE-mediated T cell activation

U87 cells were pre-treated for 72 hours as described in Figure 4.5, before being co-cultured with T cells and treated with NKG2D BiTE, Control BiTE, or left untreated for a further 72 hours. BiTE activity was then assessed by flow cytometry. Two doses of BiTE were chosen for this experiment, 0.1 nM, and 1 nM; 1 nM has been determined to be an optimal BiTE concentration (Figure 3.4). However, this concentration may activate the T cells to the extent that subtle differences in activity may be missed. Therefore, a sub-optimal concentration of 0.1 nM was also used in the hope of detecting slight increases in T cell activity.

Given that $CD8^+$ T cells express the NKG2D receptor, we first sought to address whether pre-treatment sensitised U87 cells to T cell activation in the absence of NKG2D BiTE. Increased surface NKG2DL expression on U87 cells did not induce NKG2D BiTE-independent T cell activation, as T cell CD25 (Figure 4.6A) and CD69 expression (Figure 4.6B) in co-cultures with U87 cells in the absence of BiTE were low and remained unchanged with pre-treatments. Furthermore, treatment with 0.1 nM or 1 nM of Control BiTE did not cause any T cell activation and remained unchanged with pre-treatment.

The NKG2D BiTE activated T cells at the low concentration of 0.1 nM, with an increase in the percentage of $CD25^+$ T cells (Figure 4.6A) without pre-treatment, compared to baseline expression in untreated co-cultures. This CD25 expression using 0.1 nM NKG2D BiTE was further increased only when the U87 cells were pre-treated with TMZ or 2 Gy + TMZ. These observations were supported with the CD69 expression (Figure 4.6B), whereby co-cultures treated with sub-optimal BiTE concentration significantly increased CD69 expression following TMZ and 2 Gy + TMZ pre-treatment, compared to no pre-treatment. However, other pre-treatments of DMSO, 2 Gy and 2 Gy + DMSO caused a significant decrease in $CD69^+$ T cells.

At the higher concentration of NKG2D BiTE of 1 nM, CD25 expression again increased in TMZ and 2 Gy + TMZ pre-treated co-cultures compared to no pre-treatment; meanwhile, DMSO, 2 Gy and 2 Gy + DMSO all caused significant decreases in CD25 expression (Figure 4.6A). However, the percentage of $CD69^+$ T cells (Figure 4.6B) decreased significantly in response to all pre-treatments, which could possibly be explained by pre-treatment triggering earlier BiTE-mediated T cell activation, so CD69 expression had already peaked and begun to decline again by the end point of the assay.

Together these findings suggest that at 0.1 nM NKG2D BiTE, pre-treatment of TMZ or 2 Gy + TMZ enhanced T cell activation in response to NKG2D BiTE in terms of both CD25 and CD69 expression, thus extending the therapeutically effective concentration of the NKG2D BiTE. However, at the higher concentration of 1 nM, while CD25 expression still increased slightly after pre-treatment with TMZ and 2 Gy + TMZ, the CD69 expression was lower on those same T cells than no pre-treatment, perhaps indicating earlier T cell activation kinetics.

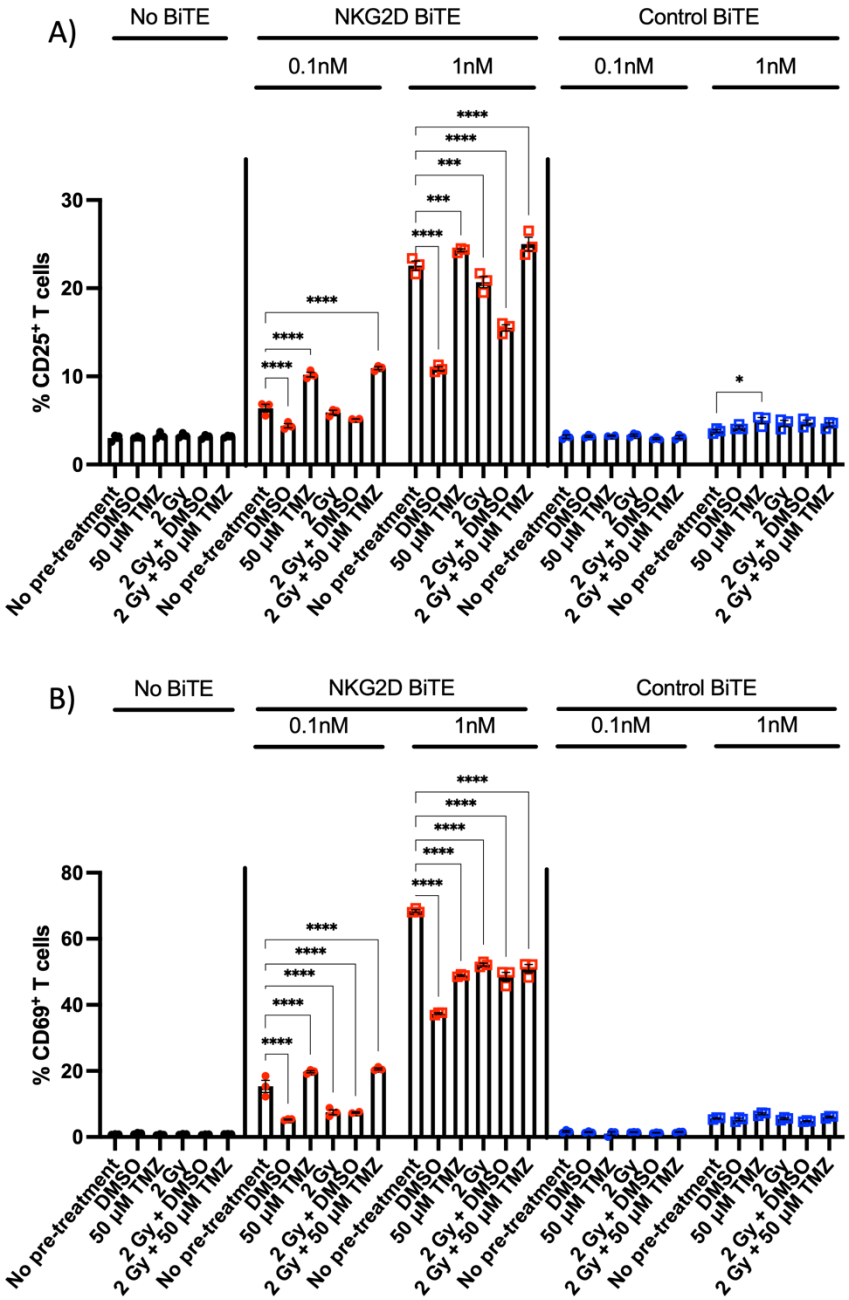

Figure 4.6 Conventional GBM therapy pre-treatment enhances NKG2D BiTE-mediated T cell activation

U87 cells were treated with a single dose of 50 μM temozolomide (TMZ) or equivalent vehicle control (DMSO), or a single dose of 2 Gray (Gy) radiation either alone (2 Gy) or in combination with 50 μM TMZ (2 Gy + TMZ) or vehicle control (2 Gy + DMSO) or left untreated (no pre-treatment). 72 hours after pre-treatment, U87 cells were seeded in co-cultures with PBMC-derived T cells at an E: T ratio of 5:1 and treated with 0.1 nM or 1 nM NKG2D BiTE (red, filled circles and hollow squares, respectively), 0.1 or 1 nM Control BiTE (blue, filled circles and hollow squares, respectively) or left untreated (black). After co-culturing for 72 hours, T cells were harvested, stained and the percentage of (**A**) $CD25^+$ and (**B**) $CD69^+$ T cells was measured by flow cytometry. Data represents the mean percentage of positive cells of triplicate repeats ± S.D. Statistical significance was assessed by two-way ANOVA followed by Bonferroni post hoc analysis. Significance was assessed versus no pre-treatment within the relevant group (ns $p>0.05$, *$p\leq0.05$, **$p\leq0.01$, ***$p\leq0.001$ and ****$p\leq0.0001$).

4.3.6 Pre-treatment synergises with NKG2D BiTE-mediated cytotoxicity of U87 cells

Alongside T cell activation, U87 viability was also measured by flow cytometry. Pre-treatment alone had cytotoxic effects on U87 cells, causing significantly decreased U87 cell viability in monoculture, and in untreated or Control BiTE-treated co-cultures (Figure 4.7A).

The sub-optimal NKG2D BiTE concentration caused no cytotoxicity in co-cultures without pre-treatment (Figure 4.7A); however, viability significantly decreased after pre-treatment with TMZ, 2 Gy and 2 Gy + TMZ. This viability decrease with 0.1 nM NKG2D BiTE and pre-treatment was greater than the effects of pre-treatment alone, as seen in co-cultures with no BiTE or Control BiTE, suggesting that U87 cells are normally insensitive to 0.1 nM NKG2D BiTE, but pre-treatment increases the cytotoxic concentration range of the NKG2D BiTE.

At the optimal concentration of NKG2D BiTE, the viability of the U87 cells decreased in co-cultures without pre-treatment compared to no BiTE or Control BiTE equivalents (Figure 4.7A), indicating that at 1 nM, the NKG2D BiTE was causing a direct cytotoxic effect on U87 cells, unlike at 0.1 nM. This viability then significantly decreased further with TMZ and 2 Gy + TMZ pre-treatment compared to no pre-treatment. The combined cytotoxic effect of the 1 nM NKG2D BiTE with TMZ and 2 Gy + TMZ pre-treatment was more pronounced than the effects of the same pre-treatments in co-cultures with no BiTE or 1 nM Control BiTE.

The findings in Figure 4.7A suggest that the pre-treatment of 50 μM TMZ and 2 Gy + 50 μM TMZ extends the effective concentration of the NKG2D BiTE, as it can trigger T cell-mediated killing of U87 cells at 0.1 nM only when these cells have been pre-treated. At this sub-optimal concentration, when U87 cells have not had

TMZ or 2 Gy + TMZ pre-treatment, the NKG2D BiTE does not cause any cytotoxicity versus no BiTE or Control BiTE. Furthermore, at the optimal concentration, the NKG2D BiTE shows some cytotoxic effect without pre-treatment, which is significantly enhanced following TMZ or 2 Gy + TMZ pre-treatment.

To further interrogate this relationship between TMZ and radiation pre-treatment and the NKG2D BiTE, the viability data from Figure 4.7A was used to elucidate any evidence of synergy using the Bliss Independence model (Q. Liu et al., 2018) (Materials and Methods section 2.11.2). In brief, the Bliss Independence model compares the expected values of two variables in combination, assuming they operate independently, with the observed experimental values. If the observed experimental value is greater than the expected value, then the variables are deemed to be synergistic; if the observed value is lower than the expected, they are deemed antagonistic; if the observed value equals the expected, they are independent.

The Bliss independence values for the cytotoxicity data is shown in Figure 4.7B. The combinations of 50 μM TMZ with 0.1 nM and 1 nM NKG2D BiTE were 0.03 and 0.18, respectively, indicating a slight synergistic relationship between these variables, which increased with a greater concentration of NKG2D BiTE. The combination of 2 Gy + 50 μM TMZ with 0.1 nM and 1 nM NKG2D BiTE achieved Bliss Independence scores of 0.08 and 0.14, respectively, again indicating a synergistic relationship that increased with higher NKG2D BiTE concentrations. However, 2 Gy combined with 0.1 nM and 1 nM NKG2D BiTE achieved Bliss Independence scores of 0.01 and -0.12, respectively, indicating an independent and even antagonistic relationship between radiation alone and NKG2D BiTE.

The results in Figure 4.7 together suggest that pre-treatment of U87 cells with relatively low doses of conventional GBM therapies of 50 μM TMZ and 2 Gy radiation does not induce a substantial amount of cytotoxicity on their own but can act in concert with NKG2D BiTE immunotherapy to activate T cells and kill target cells to a greater extent than any of the therapies alone. Furthermore, the pre-treatment can extend the effective concentration range of the NKG2D BiTE, enabling it to kill and activate T cells at lower concentrations. Finally, TMZ and 2 Gy + TMZ can achieve synergy with the NKG2D BiTE immunotherapy.

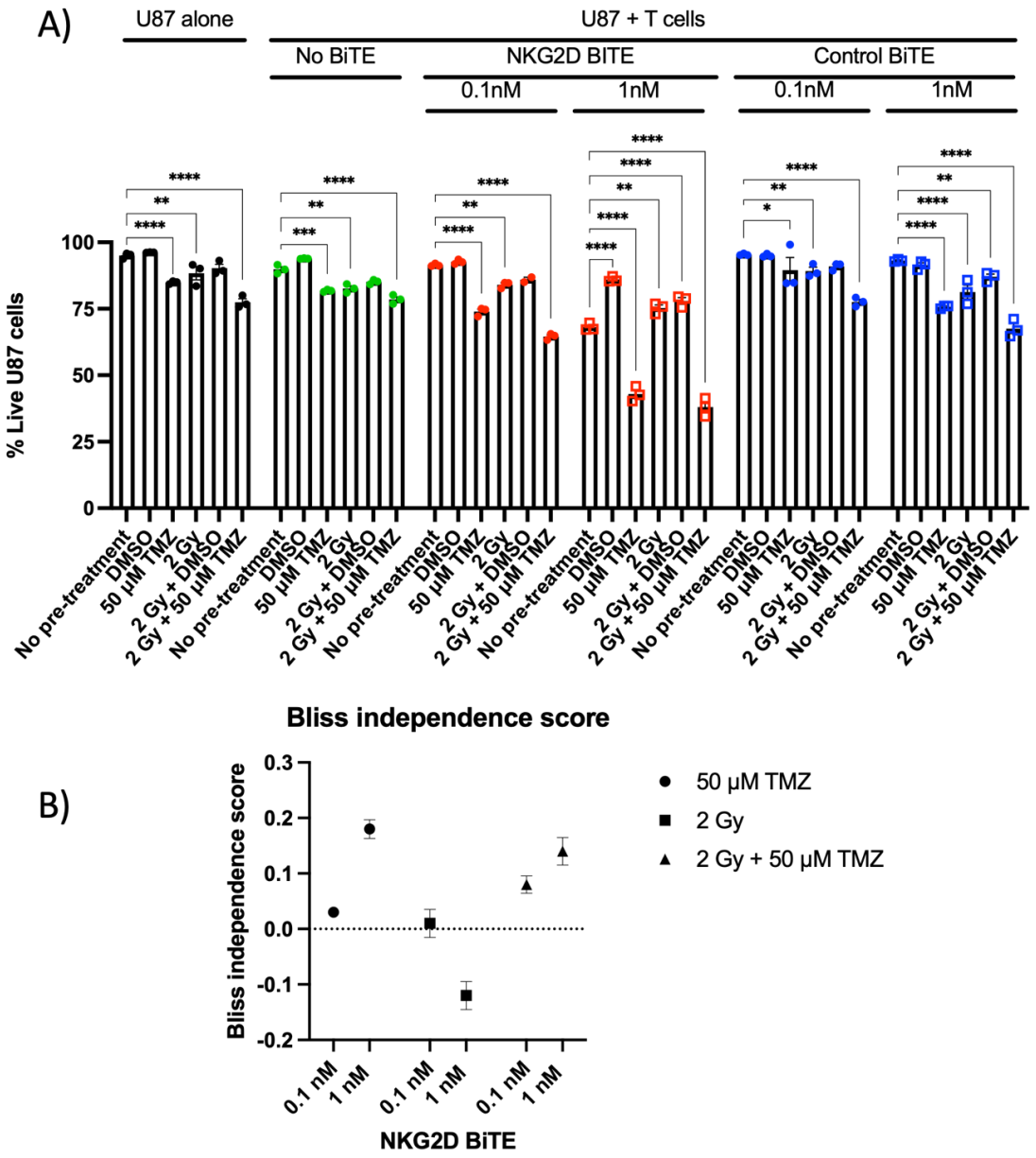

Figure 4.7 Conventional GBM therapy pre-treatment synergises with NKG2D BiTE to mediate decrease in U87 viability

U87 cells were treated with a single dose of 50 μM temozolomide (TMZ) or equivalent vehicle control (DMSO), or a single dose of 2 Gray (Gy) radiation either alone (2 Gy) or in combination with 50 μM TMZ (2 Gy + TMZ) or vehicle control (2 Gy + DMSO) or left untreated (no pre-treatment). 72 hours after pre-treatment, U87 cells were seeded and kept in untreated monocultures (black), untreated co-cultures with PBMC-derived T cells (green), or treated co-cultures with 0.1 nM or 1 nM NKG2D BiTE (red, filled circle and hollow squares, respectively), 0.1 or 1 nM Control BiTE (blue, filled circle and hollow squares, respectively). Co-cultures with PBMC-derived T cells had an E: T ratio of 5:1. After 72 hours, U87 cells were harvested and stained with a flow cytometric viability dye (**A**). Data represents the percentage of viable U87 cells of triplicate repeats ± S.D. Statistical significance was assessed by two-way ANOVA followed by Bonferroni post hoc analysis. Significance was assessed versus no pre-treatment within the relevant group (ns $p>0.05$, *$p\leq0.05$, **$p\leq0.01$, ***$p\leq0.001$ and ****$p\leq0.0001$). (**B**) Bliss independence score (BIS) was calculated using the viability data to determine the presence of synergy between the various treatments (BIS >0, synergy; BIS = 0, independent; BIS <0, antagonistic).

4.3.7 Pre-treatment does not sensitise macrophages to NKG2D BiTE immunotherapy

Given the data indicating that increased NKG2DL expression on GBM cells in response to TMZ and radiation may have increased sensitivity to NKG2D BiTE, we next sought to investigate the effects of this pre-treatment on macrophages, since TAMs can make up a significant proportion of the stromal cells in GBM (Morantz et al., 1979). Human PBMC-derived macrophages were pre-treated with the same regimen as described above (50 μM TMZ, 2 Gy radiation or a combination), then co-cultured with autologous T cells and treated with 1 nM NKG2D BiTE for a further 72 hours, at which point T cell activity was assessed by flow cytometry. In addition, 48 hours following pre-treatment, when the macrophages were re-seeded, surface MICA/B and NKG2DLs were also measured.

Pre-treatment of macrophages slightly increases NKG2DL expression

Macrophages pre-treated with radiation and TMZ were stained for surface expression of MICA/B and NKG2DLs. To address the potential issue of the rhNKG2D-Fc protein binding to FcγRs, macrophages were administered with a blocking agent for FcγRs before staining, and the equivalent isotype and Strep-PE secondary staining controls were included.

The surface expression of MICA/B slightly but significantly increased following all pre-treatments except 2 Gy alone (Figure 4.8A). However, the expression of MICA/B was confined to a small percentage of cells; fewer than 4% of untreated macrophages had surface MICA/B, which significantly increased to a maximum of only 7.5% following pre-treatment (Figure 4.8B).

The relative surface expression of all NKG2DLs followed a similar pattern to the MICA/B data, in that all pre-treatments induced a slight but significant increase in surface expression (Figure 4.6C). The MFI increased from the baseline in pre-treated macrophages but was not much greater than the staining controls of biotinylated IgG1 isotype and Strep-PE secondary, suggesting a strong contribution from non-specific Strep-PE staining towards this background signal.

These observations are further supported by the data in Figure 4.8D, which shows the percentage of macrophages expressing NKG2DLs did significantly increase in response to pre-treatment but is confined to a very small population of cells (maximum of 3.9%).

Taken together, the results in Figure 4.8 suggest that baseline expression of NKG2DLs is very low on macrophages at baseline Although expression does increase slightly in response to TMZ and radiation, it is confined to a very small fraction of the population.

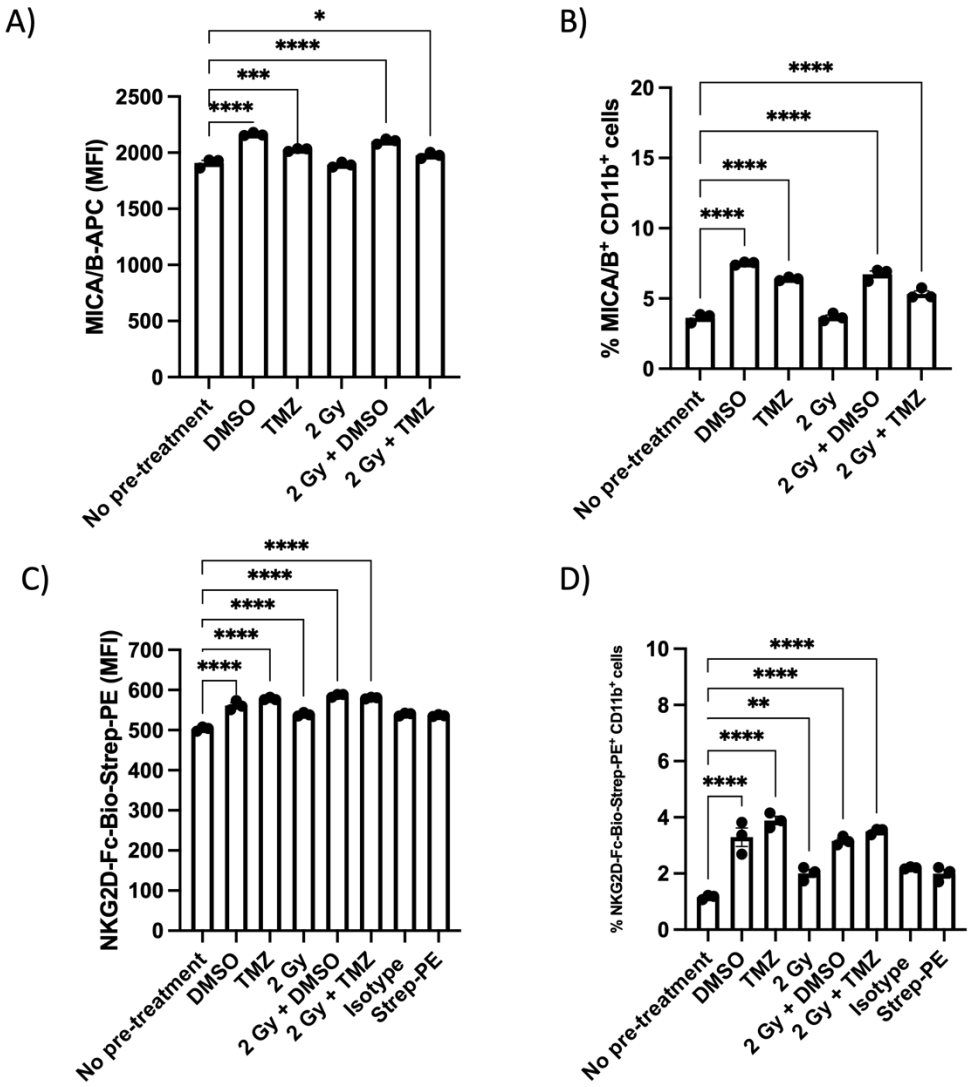

Figure 4.8 NKG2DL expression on PBMC-derived macrophages after conventional GBM pre-treatment

PBMC-derived macrophages were treated with a single dose of 50 μM temozolomide (TMZ) or equivalent vehicle control (DMSO), or a single dose of 2 Gray (Gy) radiation either alone (2 Gy) or in combination with 50 μM TMZ (2 Gy + TMZ) or vehicle control (2 Gy + DMSO), or left untreated (no pre-treatment). 48 hours after treatment, cells were dissociated with non-enzymatic dissociation buffer and stained for CD11b and either MICA/B-APC or biotinylated recombinant human NKG2D-Fc protein as a primary, followed by streptavidin-PE secondary for flow cytometric analysis (NKG2D-Fc-Bio-Strep-PE). (A) Relative macrophage surface expression of MICA/B and (C) total NKG2DLs. Data represents mean fluorescence intensity (MFI) of triplicate repeats ± S.D. (B) Percentage of MICA/B$^+$ CD11b$^+$ macrophages and (D) NKG2D-Fc-Bio-Strep-PE$^+$ CD11b$^+$ macrophages. Data represents the mean percentage of positive cells of triplicate repeats ± S.D. Statistical significance was assessed by one-way ANOVA followed by Bonferroni post hoc analysis. Significance was assessed versus no pre-treatment (ns $p>0.05$, *$p\leq0.05$, **$p\leq0.01$, ***$p\leq0.001$ and ****$p\leq0.0001$).

Pre-treatment of macrophages does not trigger NKG2D BiTE-mediated T cell activation

We have previously demonstrated that macrophages do not activate autologous T cells when treated with NKG2D BiTE, likely owing to their low NKG2DL expression (Figure 3.6). We therefore next sought to investigate whether the slight increase in NKG2DL expression on macrophages pre-treated with TMZ and radiation (Figure 4.8) increased sensitivity and T cell activity to the NKG2D BiTE, as observed with U87 cells (Figure 4.6).

Expression of both CD25 and CD69 remained low on T cells in co-culture with macrophages in the absence of BiTE, which remained unchanged with different pre-treatments (Figure 4.9B and C). There was no change in the T cell CD25 expression after the addition of NKG2D or Control BiTE, confirming macrophages were not targeted by the NKG2D BiTE. However, a slight increase in the percentage of $CD69^+$ T cells was observed when they were treated with NKG2D BiTE and Control BiTE compared to untreated co-cultures. This CD69 expression is likely to be because of non-specific BiTE activity as the Control BiTE also slightly activated T cells in this setting. However, pre-treatment of macrophages had no effect on T cell activation in the presence of NKG2D or Control BiTE.

The data in Figure 4.8 and Figure 4.9 suggest that pre-treatment of macrophages with TMZ, radiation or a combination slightly increases their surface expression of NKG2DLs. However, this expression is still at a low enough level such that they are unable to activate T cells in response to the NKG2D BiTE.

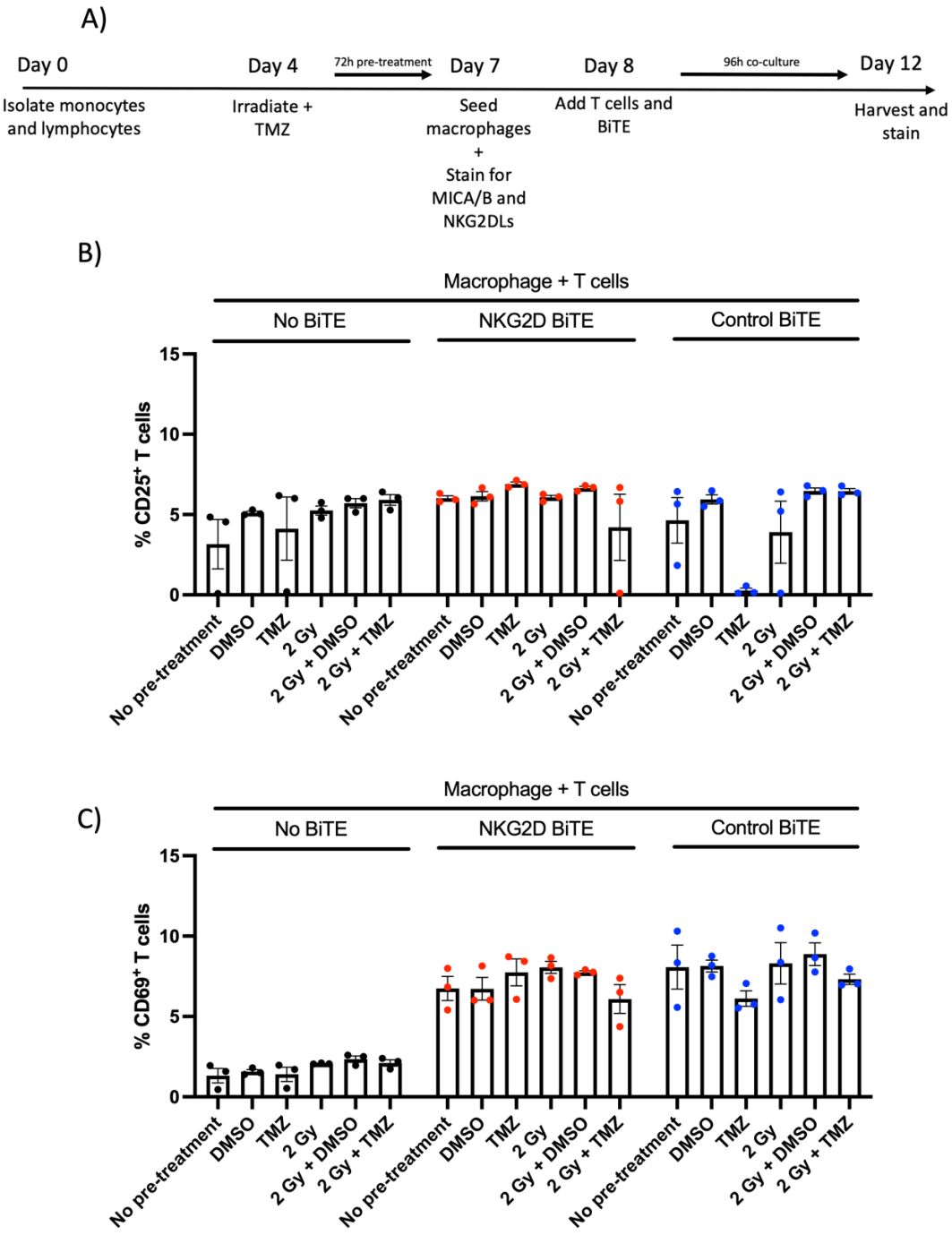

Figure 4.9 Autologous T cell activation in co-culture with autologous PBMC-derived macrophages after conventional GBM pre-treatment

(**A**) Timeline of experiment. PBMC-derived macrophages were pre-treated with a single dose of 50 μM temozolomide (TMZ) or equivalent vehicle control (DMSO), or a single dose of 2 Gray (Gy) radiation either alone (2 Gy) or in combination with 50 μM TMZ (2 Gy + TMZ) or vehicle control (2 Gy + DMSO), or left untreated (no pre-treatment). 72 hours after pre-treatment, macrophages were seeded in co-cultures with autologous PBMC-derived T cells at an E: T ratio of 5:1 and treated with 1 nM NKG2D BiTE (red), 1 nM Control BiTE (blue) or left untreated (black). After co-culturing for 72 hours, T cells were harvested, stained and the percentage of (**B**) $CD25^+$ and (**C**) $CD69^+$ T cells was measured by flow cytometry. Data represents the mean percentage of positive cells of triplicate repeats ± S.D. Statistical significance was assessed by two-way ANOVA followed by Bonferroni post hoc analysis. Significance was assessed

versus no pre-treatment within the relevant group (ns $p>0.05$, *$p\leq0.05$, **$p\leq0.01$, ***$p\leq0.001$ and ****$p\leq0.0001$).

4.3.8 NKG2D BiTE activity triggers macrophage polarisation via soluble mediators

TAMs make up a considerable proportion of the immune component in GBM tumours (Morantz et al., 1979), and frequently exhibit immunosuppressive phenotypes (Ding et al., 2014). Considering this, re-polarising these TAMs towards a more pro-inflammatory phenotype is often a goal for GBM immunotherapy.

We therefore sought to investigate whether T cell activation mediated by the NKG2D BiTE could redirect macrophages from an immunosuppressive phenotype towards a pro-inflammatory one. To address this issue, PBMC-derived macrophages were cultured in normal medium or in patient-derived immunosuppressive ascites fluid obtained from the peritoneal cavity of cancer patients, which can contain many highly immunosuppressive constituents and drive an immunosuppressive macrophage phenotype (See Materials and Methods section 2.4.10). Normal and ascites-polarised macrophages were then further cultured in conditioned media from U87 and autologous T cell co-cultures treated with NKG2D BiTE for a further 48 hours before the expression of classically-activated macrophage marker, CD80, was assessed by flow cytometry. Timelines for the experiment are shown in Figure 4.10A.

NKG2D BiTE- and CD3/CD28 Dynabead-treated T cells produced immunostimulatory conditioned media

To generate conditioned media to treat the macrophages, U87 and T cells (autologous to the macrophages) were treated with NKG2D BiTE, Control BiTE or

CD3/CD28 Dynabeads for 96 hours; BiTE treatments were allowed to extend until 96 hours to provide a longer timeframe for any pro-inflammatory mediators to accumulate in the conditioned media. T cell activation by NKG2D BiTE and Dynabeads was confirmed by assessing T cell CD25 and CD69 expression by flow cytometry (Figure 4.10B and C, respectively). As expected, CD25 and CD69 expression increased when T cells were co-cultured with NKG2D BiTE and U87 target cells, but not in the absence of target cells, whereas treatment with Dynabeads induced T cell activation in co-culture and monoculture. The percentage of $CD69^+$ T cells did slightly increase above the untreated baseline when in the presence of Control BiTE, both in co-culture with U87 cells and in monoculture of T cells alone, suggesting there may be a small amount of non-specific activation of T cells arising from the Control BiTE in this assay (Figure 4.10C). This non-specific activity with the Control BiTE may be due to the longer timeframe of the assay of 96 hours.

Ascites-polarised macrophages have low CD80 expression which increases following stimulation with IFN-γ and LPS

After being cultured in the BiTE conditioned media for 48 hours, macrophages were harvested and stained for surface expression of CD80. The relative macrophage CD80 expression after culture in the various conditioned media is shown in Figure 4.10D.

The relative CD80 expression was very low at baseline after being cultured in 2% RPMI for both X-VIVO and ascites-polarised macrophages but was lower in ascites-polarised macrophages (Figure 4.10D). As a positive control, macrophages treated with additional pro-inflammatory stimuli of IFN-γ and LPS, resulting in

significant CD80 upregulation in both X-VIVO and ascites-polarised macrophages, demonstrating that macrophages polarised in either X-VIVO medium or ascites fluid could still be re-programmed to become pro-inflammatory macrophages.

Conditioned media from BiTE- and Dynabead-activated T cells increases CD80 expression on unpolarised and ascites-polarised macrophages

Macrophage CD80 expression remained unchanged when cultured in conditioned media from U87 cells alone, untreated T cells alone, or untreated U87 + T cell co-cultures (Figure 4.10D). Conditioned media from U87 + T cell co-cultures treated with NKG2D BiTE induced a significant upregulation in CD80 expression in both X-VIVO- and ascites-polarised macrophages. The conditioned media from Dynabead-treated T cells, both in co-cultures and alone, also significantly increased macrophage CD80 expression in both sets of macrophages.

The macrophages also showed a slight increase in CD80 expression when in Control BiTE-conditioned media, both for ascites- and normal media-differentiated macrophages (Figure 4.10D), likely reflecting the slight non-specific T cell activation with Control BiTE (Figure 4.10C).

The results in Figure 4.10D show that conditioned media from NKG2D BiTE or Dynabead-activated T cells caused an increase in CD80 expression on macrophages in a pattern that closely correlates to the CD69 expression in Figure 4.10C. Furthermore, this CD80 increase occurred on both unpolarised macrophages (initially cultured in X-VIVO) and immunosuppressive macrophages (initially cultured in ascites fluid). However, the macrophages initially polarised in ascites fluid consistently had lower CD80 expression compared to the X-VIVO-cultured cells, demonstrating the immunosuppressive nature of the ascites fluid.

Nevertheless, these ascites-polarised macrophages were still able to be re-programmed to increase CD80 expression and move towards a pro-inflammatory phenotype in response to conditioned media from activated T cells. Overall, the activation of T cells in response to NKG2D BiTE or Dynabeads results in the production of soluble mediators that can increase CD80 expression on unpolarised and immunosuppressive macrophages.

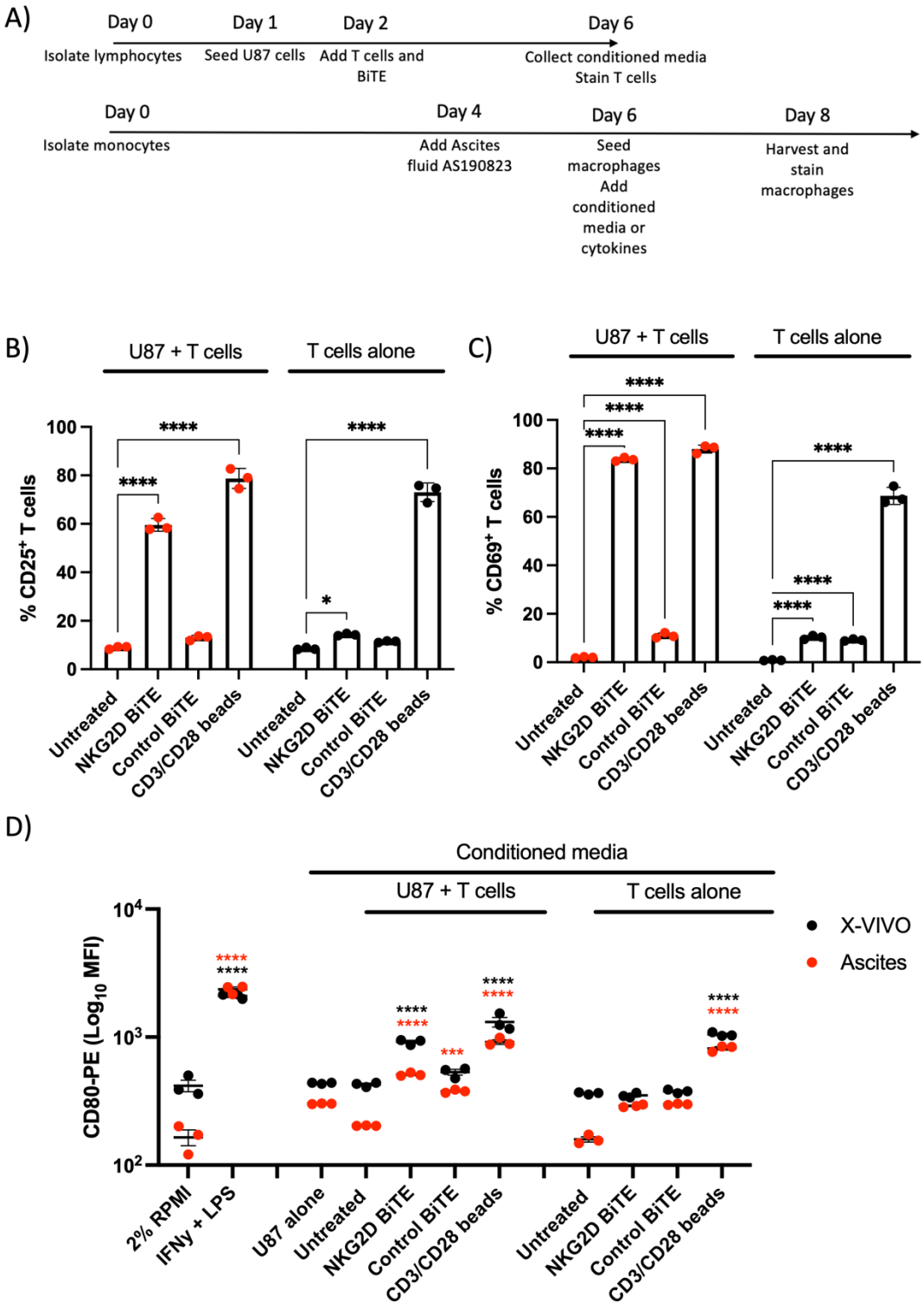

Figure 4.10 Effects of NKG2D BiTE-conditioned media on macrophage polarisation

(**A**) Timeline of experiment. Autologous PBMC-derived monocytes and lymphocytes were isolated on day 0. Monocytes were differentiated into macrophages in low adherence T175 flasks for 4 days in X-VIVO medium containing 2% human serum (HS). On day 4, the medium was replaced with either fresh 2% HS X-VIVO or heterologous patient-derived ascites fluid (AS190823) for an additional 2 days. Meanwhile, U87 cells were co-cultured with the T cells at an E: T ratio of 5:1 and treated with 1 nM NKG2D BiTE, 1 nM Control BiTE, CD3/CD28

Dynabeads. After 96 hours of T cell and U87 co-culture, T cells were harvested, stained and the percentage of (**B**) $CD25^+$ and (**C**) $CD69^+$ T cells was measured by flow cytometry. Data represents the mean percentage of positive cells of triplicate repeats ± S.D. On day 6 post PBMC isolation and macrophage polarisation, macrophages were re-seeded and exposed to a 1:1 mix of seeding media (2% FCS RPMI) and conditioned media from the U87 + T cell co-cultures. As a positive control, macrophages were also treated with IFN-γ and LPS. After a further 48 hours of culture in conditioned media, macrophages were dissociated and stained for CD11b and CD80 for flow cytometric analysis. (**D**) Relative CD80 expression on $CD11b^+$ macrophages after being initially differentiated in X-VIVO (black) or ascites fluid (red), followed by polarisation in conditioned media. Data represents the mean Log_{10} CD80-PE MFI of triplicate repeats ± S.D. Statistical significance was assessed by two-way ANOVA followed by Bonferroni post hoc analysis. Significance was assessed versus 2% RPMI within the initial differentiation conditions (ns $p>0.05$, *$p\leq0.05$, **$p\leq0.01$, ***$p\leq0.001$ and ****$p\leq0.0001$).

4.4 Discussion

This chapter aimed to explore how various factors affect the expression of NKG2DLs, ranging from G207 infection to TMZ and radiation, and how these perturbations in expression impact the activity of the NKG2D BiTE. This chapter culminates with the observations that conventional GBM therapy has the potential to synergise with NKG2D BiTE immunotherapy by increasing anti-glioma effects without targeting other cells in the TME, such as TAMs. Furthermore, the activity of the NKG2D BiTE may help shift the balance of the TME away from immunosuppression.

The data in this chapter demonstrates that G207 infection does decrease the expression of some NKG2DLs (Figure 4.1), but that the NKG2D BiTE is still effective despite this (Figure 4.2). The expression of NKG2DLs on the surface of cells infected with G207 in Figure 4.1 raises a few questions. For instance, why does surface MICA/B decrease in infected cells yet total NKG2DL expression remains unchanged between infected and uninfected cells? This discrepancy could perhaps be explained by an increase in the surface expression of other NKG2DLs, such as ULBP1-6 to compensate for the decrease in MICA/B, thus making the total NKG2DL expression remain essentially unchanged.

The expression of NKG2DLs is closely linked to cell stress associated with the DDR and sustained proliferative signalling (Cerboni et al., 2014). Wild type HSV-1 has been demonstrated to activate the DDR (Shirata et al., 2005) and the PI3K/Akt pathway (Hsu et al., 2010), and so G207 oHSV-1 is likely also to induce these same pathways and trigger an upregulation in NKG2DL expression. This may therefore result in U87 cells upregulating the expression of NKG2DLs, including ULBP1-6.

Suppose the G207 is specifically downregulating MICA/B surface expression as an immune evasion strategy, but also inadvertently triggering the upregulation of other NKG2DLs. In that case, this may result in the observations in Figure 4.1, whereby total surface NKG2DLs remain unchanged, but MICA/B decrease with infection. This could be investigated further by staining for each NKG2DL individually.

The downregulation of surface MICA/B specifically by G207 (Figure 4.1) has not been previously reported. Many examples of virus downregulation of NKG2DLs as immune evasion strategies have been reported (reviewed in Baugh et al., 2020), with several being employed by members of the *Herpesviridae* family, especially HCMV. However, few studies have looked at the effects of HSV-1 on NKG2DL expression. Campbell et al. described a decrease in total MICA, ULBP2 and ULBP3, and a decrease in surface ULBP1 on non-cancerous ARPE-19 epithelial cells, human foreskin fibroblasts and 293T human embryonic kidney cells upon infection with WT HSV-1 (T. M. Campbell et al., 2015). Meanwhile, Schepis et al. reported a downregulation in surface expression of MICA and ULBP2 only, with total protein remaining unchanged on U373 astroglioma and HeLa epithelial tumour cell lines. This downregulation was attributed to a late viral gene product retaining the proteins intracellularly (Schepis et al., 2009) (adapted from Baugh *et al.* 2020). The inconsistencies in the literature demonstrate that the precise mechanistic details, and even which ligands are downregulated, is somewhat contentious and may depend on the cells used for the experiment. This is also further demonstrated in Figure 4.1 in the different expression patterns between the two cell lines.

As described in section 1.8.5, having eight different NKG2DLs, each of which can instigate an immune response by an immune effector cell with the NKG2D receptor, may allow a degree of functional redundancy, and reduces the chances of

complete immune evasion of the NKG2D response by a virus or cancer cell (Zingoni et al., 2018). This may reflect the observations in Figure 4.2, that the NKG2D BiTE retains its activity towards cells infected with G207, despite downregulation of NKG2DLs.

This chapter also explores the effects of TMZ and radiation pre-treatment on NKG2DL expression. A172 cells were highly sensitive to TMZ Figure 4.3, with a significant dose-dependent decrease in viability with increasing TMZ. These results are in line with findings elsewhere in the literature, which reveal A172 cells to be highly sensitive to TMZ, with an IC_{50} of around 14 μM TMZ (Perazzoli, Prados, Ortiz, Caba, & Cabeza, 2015). Meanwhile, U87 cells were much more resistant to TMZ than A172 cells in Figure 4.3. The IC_{50} values for U87 cells have been widely reported but vary greatly depending on the time and method of viability assessment; in a systematic review, Poon et al. reported a median IC_{50} value of 230 μM for U87 cells with TMZ for 72 hours, but with an inter quartile range of 34 – 650 μM (Poon, Bruce, Simpson, Hannan, & Brennan, 2021). The TMZ doses used in this thesis for were therefore below this median IC_{50} for U87 cells.

The effects of TMZ and radiation on NKG2DL expression in GBM has also been explored previously. Lamb et al. described significant upregulation in MICA/B, ULBP1, 2 and 4 in U87 cells up to 24 hours after treatment with 100 μM TMZ (Lamb et al., 2013). Similar observations were made using other GBM cell lines, with increasing surface NKG2DL expression within the range of 10 – 200 μM TMZ and a particular increase between 30 – 80 μM (Weiss, Schneider, et al., 2018). Furthermore, this concentration range of 30 - 80 μM was reported to be the approximate serum concentration in patients undergoing Stupp therapy (Weiss, Schneider, et al., 2018), while, Rosso et al. reported between 2.9 – 6.7 μg/mL (15

– 34 μM) TMZ in human glioma tumours (Rosso et al., 2009). Following 2 Gy radiation, increases in MICA, MICB, ULBP2 and ULBP3 transcription in GBM cell lines has been reported (Weiss, Schneider, et al., 2018). Additionally, Flüh et al. described an increase in NKG2DL mRNA levels in T98G and U251MG GBM cell lines when in GSC-like conditions and treated with TMZ, although this was using 500 μM TMZ (Flüh et al., 2018). Therefore, pre-treatment regimen of 50 μM and 2 Gy in the assays in this chapter are within clinically relevant ranges, and the findings here are in concordance with the literature (Weiss, Schneider, et al., 2018).

The results in Figure 4.6 demonstrate an increased T cell activation with NKG2D BiTE following pre-treatment of U87 target cells with TMZ, radiation and a combination. However, there was also a significant decrease in T cell activation following pre-treatment with the vehicle control, DMSO. It has been previously demonstrated that even low amounts of DMSO can significantly inhibit $CD4^+$ T cell activation (Holthaus et al., 2018). Therefore, the decrease of T cell activation in Figure 4.6 with DMSO pre-treatment may be due to the effects of small contaminating amounts of DMSO remaining in the well.

We demonstrate in this chapter evidence of potentiation of BiTE activity by enhancing the expression of target ligands in response to pre-treatment. Enhancing BiTE activity by increasing target ligand expression has been reported previously by Khalique et al., (Khalique et al., 2021). Studies using a BiTE targeting PD-L1 demonstrated increased T cell activation and target cell lysis when used in immunosuppressive ascites fluid which drove increased surface expression of PD-L1 on target cells, and even overcame the immunosuppressive effects of the ascites fluid itself (Khalique et al., 2021).

We also demonstrated evidence that NKG2D BiTE-mediated T cell activation resulted in the production of soluble mediators capable of increasing CD80 expression on macrophages (Figure 4.10). The measurement of pro-inflammatory macrophages by CD80 expression in Figure 4.10 is perhaps an oversimplification, as also with the classification of macrophages in Figure 3.6B in the previous chapter. Nevertheless, CD80 is widely regarded as a marker of classically activated macrophages, despite their complexity and plasticity (Metchnikoff & Prize, 2015). This is also demonstrated here by the high CD80 expression in Figure 4.10 when macrophages were treated with IFN-γ and LPS. Therefore, the results in Figure 4.10 provide an indication that the BiTE-conditioned media is driving macrophage polarisation towards a pro-inflammatory phenotype. However, this data could be made more robust with single-cell sequencing data on the macrophages across various phenotypic markers, to reveal a wider shift from anti-inflammatory to pro-inflammatory cell signatures.

We have yet to specifically address what the soluble factors were in the conditioned media that drove increased CD80 expression. However, we can infer from the data in the previous chapter that the NKG2D BiTE induces IFN-γ production from both $CD4^+$ and $CD8^+$ T cells when activated by BiTE (Figure 3.5F), which may be one of the key cytokines driving this macrophage phenotype. Other cytokines, alongside IFN-γ, could also be involved, such as IP-10 and TNF-α which have previously been shown to be secreted by T cells upon stimulation by BiTE (Freedman et al., 2017; Khalique et al., 2021).

4.5 Conclusions

Conventional therapy for GBM of TMZ and radiation is currently insufficient, as tumours invariably recur, often with resistance, leading to very short survival statistics for patients. Therefore, there is a desperate un-met need to enhance this current strategy, with novel therapeutic options that complement TMZ and radiation treatment. We have demonstrated in this chapter that the NKG2D BiTE-mediated T cell activity is enhanced by pre-treatment of sublethal doses of TMZ and radiation, synergising together to increase target cell lysis, confirming our initial hypothesis stated in section 4.2.1. Furthermore, we have demonstrated that this pre-treatment does not sensitise other non-malignant cells that may be found in the GBM TME, such as macrophages, to the NKG2D BiTE, and that NKG2D BiTE activity may help to create a less immunosuppressive TME. Finally, we demonstrate that G207 oHSV-1 will be a suitable vector to express the NKG2D BiTE in GBM, as the NKG2D BiTE retains its activity in the presence of G207-infected GBM cells.

5 Arming oHSV-1 with NKG2D BiTE for use alongside conventional GBM therapy

5.1 Introduction

oHSV-1 has been investigated extensively as an anti-cancer agent. The large HSV-1 genome (~150 kb), 30 kb of which is non-essential, has allowed genetic engineering to produce multiple generations of cancer-selective oHSV-1 variants which are safe for use in humans. Furthermore, HSV-1 induces a lytic cell death, releasing many pro-inflammatory DAMPs and PAMPs, making oHSV-1 an attractive tool for selectively infecting and killing cancer cells. Finally, the large genome capacity of oHSV-1 allows the insertion of transgenes into the genome, enabling expression of therapeutic molecules directly within the TME. These characteristics have led to oHSV-1 being among the most studied and clinically advanced OVs to date.

Given current standard of care therapies for GBM (debulking surgery followed by concomitant TMZ and radiation (Stupp et al., 2005)) have not progressed in many years, there is a great un-met need for effective GBM therapies. The slow progress in GBM patient survival statistics, combined with the resistant nature of recurrent GBM towards TMZ and radiotherapy, and the issue of delivering therapeutics into the tumour across the BBB in therapeutically effective doses has led to a focus on novel immunotherapies, particularly oHSV-1. Stereotactic administration of oHSV-1 directly within the GBM tumour during debulking surgery offers a unique strategy

for GBM therapy: a therapeutic capable of self-amplification *in situ*. Therefore, oHSV-1 has been widely investigated for GBM OV therapy, both pre-clinically and clinically (Table 1.3).

oHSV-1 can be 'armed' to express payloads directly within the TME that would otherwise be too potent to administer systemically. T-VEC, armed to express GM-CSF, is the most clinically advanced OV, and was given FDA approval for the treatment of metastatic melanoma in 2015 (Conry et al., 2018; Kaufman et al., 2010). Other oHSV-1 candidates have also been armed to express many different payloads, ranging from cytokines (Burton et al., 2018; Cheema et al., 2013; Kaufman et al., 2010), full length antibodies (B. Xu et al., 2021), BiTEs (Khalique et al., 2021) and other molecules.

Multiple generations of oHSV-1 have been generated to date using genetic modification of WT strains of HSV-1, all of which include the deletion of both copies of the gene *γ34.5*, which encodes ICP34.5 (Chou et al., 1990; MacLean et al., 1991). ICP34.5 is essential for HSV-1 neurovirulence, and its deletion endows cancer-selectivity for oHSV-1 (discussed in detail in section 1.6.2). G207, the oHSV-1 used in this thesis, is further engineered to gain cancer-selectivity by introducing deletions in ICP6, the oHSV-1 RR, rendering the G207 dependent on actively dividing cells with high dNTP pools (Mineta et al., 1995).

In the context of combination therapy of G207 with conventional GBM therapy, G207 has been evaluated pre-clinically and clinically alongside radiation. In a murine orthotopic GBM model using U87 cells, Markert et al. showed a majority of increased long-term survivors when treated with G207 and two fractions of 5 Gy radiation, which was improved compared to G207 or radiation alone (J. M. Markert, Yancey Gillespie, Weichselbaum, Roizman, & Whitley, 2000). Furthermore, in

human patients with recurrent malignant glioma, nine recurrent glioma patients were given a single stereotactic dose of G207 into the tumour margin before receiving 5 Gy radiation 24 hours later (J. M. Markert et al., 2014). The authors reported good safety profiles, and six out of nine patients reported with stable disease or partial response, and three patients showed radiographic responses (J. M. Markert et al., 2014).

However, GBM is a highly heterogeneous tumour, comprising of sub-populations of GSCs, with stem-cell like phenotypes capable of self-renewal and resistance; and differentiated GBM cells. Early generations of oHSV-1, including G207 (Mineta et al., 1995) used in this thesis, have been shown to effectively infect and lyse differentiated GBM cells, but GSCs remain non-permissive to G207 (Kanai et al., 2012), therefore, posing a barrier to G207 GBM therapy. Recently, G47Δ (DELYTACT), an enhanced successor to G207 with enhanced potency in GSCs, received approval for treatment of malignant glioma in Japan in 2021 (Daiichi Sankyo, 2021), demonstrating the necessity to improve GSC targeting in GBM OV therapy.

Much of the research into GBM in vitro involves the use of cell lines, which serve as a useful and reproducible model. However, these cell lines often fail to recapitulate many of the characteristics of real GBM. Hence, the use of patient-derived GBM cells cultured in the presence of growth factors has been demonstrated to result in more clinically representative GSCs, maintaining heterogeneity, molecular aberrations and genotypes (J. Lee et al., 2006).

Given its extensive clinical history and safety profile (also alongside radiation (J. M. Markert et al., 2014)), G207 oHSV-1 may be suitable vector to express the NKG2D BiTE for GBM OV therapy.

5.2 Chapter hypothesis and aims

5.2.1 Hypothesis

We hypothesise that an oHSV-1 (G207) expressing the NKG2D BiTE will deliver functional BiTE *in situ* and combine with TMZ and radiotherapy to kill GBM cells.

5.2.2 Aims

1) To engineer the G207 virus to express the NKG2D and Control BiTEs
2) To demonstrate the G207-NKG2DBiTE virus works in concert alongside conventional GBM therapy in GBM cell lines
3) To demonstrate the ability of the G207-NKG2DBiTE virus to overcome limitations in GSC oHSV-1 therapy
4) To demonstrate the G207-NKG2DBiTE virus is effective in clinically relevant human GBM tissue

5.3 Results

5.3.1 Design and engineering of oHSV expressing NKG2D BiTE

Previous chapters have demonstrated the ability of the NKG2D BiTE to activate T cells and trigger GBM cell lysis (Figure 3.5) and that it still maintains its activity in cells infected with G207 oHSV-1 (Figure 4.2). It therefore seems plausible that the BiTE may function well when encoded into the virus, and accordingly, in this chapter the sequences for the NKG2D BiTE (NKG2D-αCD3-NKG2D) and Control BiTE (NKG2Db5-αCD3-NKG2Db5) were inserted into the G207 genome, under control of the cytomegalovirus (CMV) promoter.

The overall process of cloning the NKG2D BiTE and Control BiTE into the G207 backbone was carried out following the protocol first described by Terada et al. using the HSVQuik platform (Terada et al., 2006). A simplified schematic of the HSVQuik platform can be seen in Figure 2.3, along with a detailed description of the protocol and strategy in section 2.8 (adapted from Terada et al., 2006).

As described in section 2.8, the BACs containing the G207-NKG2DBiTE or G207-ControlBiTE genomes were co-transfected into Vero cells alongside a plasmid expressing Cre recombinase (Figure 2.3D). Successful recombination events resulted in excision of the BAC plasmid backbone and the generation of the G207-BiTE genome. Transfected cells with successful recombination events could be identified by the presence of GFP (in the G207 genome) but the absence of RFP (in the BAC backbone). Successfully transfected and recombined viral clones produced infectious viral particles from the transfected Vero cells (Figure 2.3E), which were collected for further assessment.

5.3.2 Characterisation of G207-NKG2DBiTE and G207-ControlBiTE clones

Following transfection of the fHSVQuik-1-NKG2D and Control BiTE sequences, several plaques of G207-NKG2DBiTE and G207-ControlBiTE, respectively, were formed. These were isolated and subjected to further rounds of amplification and assessment of viral fitness and purity. This was narrowed down to five potential clones for each virus, N1-5 and B1-5 for G207-NKG2DBiTE and G207-ControlBiTE viruses, respectively.

While these initial rounds of amplification and infection allowed for a qualitative assessment of viral infectivity and fitness, it did not elucidate any information on the expression or function of the encoded NKG2D or Control BiTEs. Therefore, the next stage involved assessing of the NKG2D or Control BiTE protein expression, ensuring the proteins can be expressed, are the correct length, and are functional (in the case of the NKG2D BiTE).

Vero cells were infected with dilutions of each viral clone for three days. The unconcentrated viral supernatants were then assessed by SDS-PAGE and western blot for the production of NKG2D or Control BiTE and to ensure the BiTEs were being secreted correctly (Materials and Methods section 2.8.5). Due to the relatively low protein concentration in the supernatants, the western blots required long exposure times to visualise the correct band corresponding to NKG2D or Control BiTE. A faint band can be observed in clones N2 and B2 at ~70 kDa (expected size 63 kDa) (Figure 5.1A and B, red arrow), and is the same size as the positive BiTE control band, which suggests the presence of the NKG2D and Control BiTEs. However, the band for the Control BiTE is very faint, indicating a very low concentration of BiTE. In both western blots, non-specific bands can be observed

in lanes 1-5 but not in the serum control or BiTE positive control (Figure 5.1A and B), indicating a viral protein that may be causing non-specific binding of the anti-His-Tag antibody. Additionally, a band appears at around 60 kDa in supernatants, most likely a non-specific detection protein in FCS due to its presence in the serum control.

To screen for clones producing functional NKG2D BiTE, T cell activation in the presence of target cells can be used with G207-NKG2DBiTE virus clone supernatants. However, given the Control BiTE cannot bind to target cells, assessment of Control BiTE production from different clones by this method is not possible. Nevertheless, assessment of virus infectivity, viral oncolysis and non-specific T cell activation by different clones of G207-ControlBiTE virus can still be compared.

U87 cells were treated with virus supernatants from each G207-NKG2DBiTE and G207-ControlBiTE virus clone and co-cultured with PBMC-derived T cells. A positive control was also set up using the concentrated NKG2D BiTE from previous chapters. To determine the activity of the NKG2D BiTE in the original viral supernatant and not BiTE produced from secondary rounds of infection, the experiment was terminated after three days. The clones were then assessed by flow cytometry based on their T cell activation (CD25 and CD69 expression), target cell infectivity (GFP expression) and cytotoxicity (cell viability dye).

Comparison of T cell activation by G207-NKG2DBiTE viral clones

In Figure 5.1C, G207-NKG2DBiTE clones N1, N2, N3 and N5 significantly increased CD25 expression, with clones N1 and N2 showing the greatest expression, and clone N4 showing no T cell activation at all above baseline.

Encouragingly, none of the G207-ControlBiTE clones induced any CD25 expression above the baseline, suggesting that neither the Control BiTE nor the G207 virus itself activated the T cells. The percentage of $CD69^+$ T cells (Figure 5.1D) showed a similar pattern, with G207-NKG2DBiTE clones N1, N2, N3 and N5 activating T cells, but no activation being observed for clone N4 and all five G207-ControlBiTE clones. The T cell activation demonstrated that clone N2 had the greatest activation, therefore suggesting that this clone had the most NKG2D BiTE activity in the original viral supernatant.

Comparison of G207-NKG2DBiTE viral clone infectivity and BiTE production

The supernatants of all clones for both viruses contained infectious viral particles that could infect the U87 cells and cause GFP expression (Figure 5.1E). Within the G207-NKG2DBiTE clones, clones N1, N2, N3 and N5 all demonstrated a similar level of infected cells; however, clone N4 had a markedly lower percentage of infected cells. Interestingly, all the G207-ControlBiTE clones showed high GFP expression, similar to or greater than those of the G207-NKG2DBiTE clones.

The observation that the levels of infection with the G207-ControlBiTE clones were generally higher than those of the G207-NKG2DBiTE clones further confirms that the G207 virus itself did not trigger any T cell activation; the lack of T cell activation with G207-ControlBiTE clones (that had greater levels of GFP^+ cells than G207-NKG2DBiTE clones) confirms that any T cell activation was BiTE-dependent. Furthermore, the G207-NKG2DBiTE clone N2 (which displayed the greatest T cell activation) did not have a significantly higher level of infection compared to the other G207-NKG2DBiTE clones (such as N1) suggesting that the NKG2D BiTE produced from clone N2 was indeed functional and produced at a higher level than the other

clones. This observation is in line with the western blot data in Figure 5.1A, whereby clone N2 had the greatest expression out of the five G207-NKG2DBiTE clones.

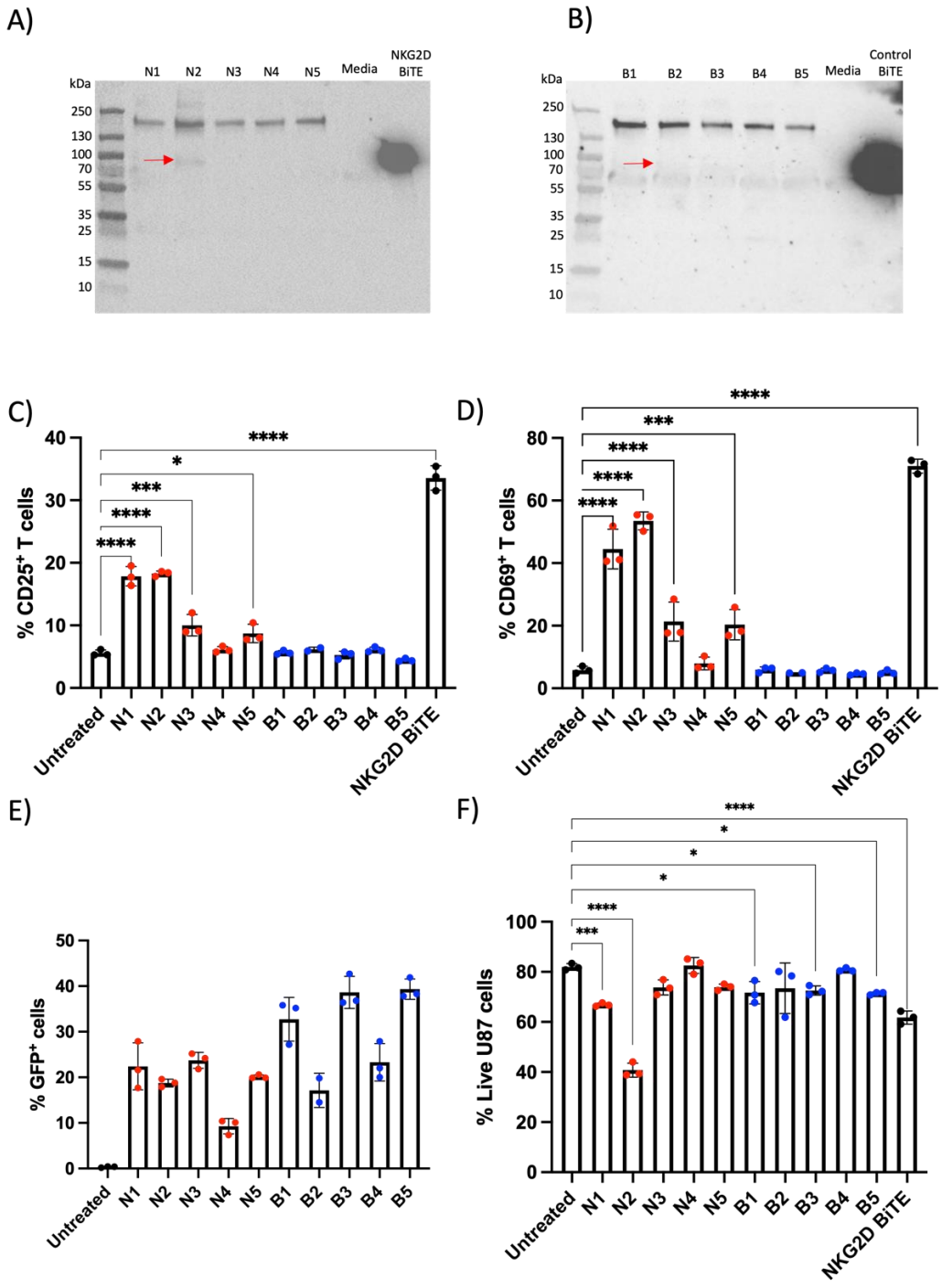

Figure 5.1 Selection of G207-NKG2DBiTE and G207-ControlBiTE viral clones
(**A**) Western blots of raw supernatants of Vero cells infected with G207-NKG2DBiTE clones N1-5 or (**B**) G207-ControlBiTE clones B1-5. Membranes were probed with a mouse anti-His-Tag primary antibody and horse anti-mouse HRP conjugated secondary. Uninfected media controls and concentrated NKG2D or Control BiTE were included as negative and positive controls, respectively. Red arrows indicate present of NKG2D or Control BiTE. (**C**) U87 cells

were treated with raw supernatants from Vero cells infected with G207-NKG2DBiTE clones N1-5 (red) or G207-ControlBiTE clones B1-5 (blue), or left untreated (black) or treated with 1 nM NKG2D BiTE, and were co-cultured with PBMC-derived T cells at an E: T ratio of 5:1. After 3 days of co-culture, cells were harvested and stained for flow cytometry analysis, assessing percentage of $CD25^+$ and (**D**) $CD69^+$ T cells, (**E**) percentage of GFP^+ U87 cells and (**F**) percentage of live U87 cells using a flow cytometric viability dye. Data represents mean percentage of positive T cells, GFP^+ cells or viable cells of triplicate repeats ± S.D. Statistical significance was assessed by two-way ANOVA followed by Bonferroni post hoc analysis. Significance was assessed versus untreated cells within the relevant group (ns $p>0.05$, *$p\leq0.05$, **$p\leq0.01$, ***$p\leq0.001$ and ****$p\leq0.0001$).

The western blots in Figure 5.1A and B suggest that G207-NKG2DBiTE clone N2 produces more BiTE than the G207-ControlBiTE clone B2, as this protein band is very faint. This is also in line with observations during transfections of 293-Ad cells to produce free BiTE, whereby under identical transfection conditions the yield of NKG2D BiTE is often noticeably greater than that of the Control BiTE (data not shown). The lower production of the Control BiTE from the G207-ControlBiTE virus compared to the NKG2D BiTE was ultimately not considered to be too much of a concern, as previous experiments have demonstrated that the Control BiTE does not induce T cell activation, even when in equimolar concentration to the NKG2D BiTE (Figure 3.5).

Comparison of G207-NKG2DBiTE viral clone cytotoxicity

The viability of the U87 cells was determined using a fluorescent viability dye for flow cytometry (Figure 5.1F) and allowed the assessment of the cytotoxic effects of both the G207 virus itself and the NKG2D BiTE. The viability of infected U87 cells was generally lower than untreated U87 cells for all clones, including the G207-ControlBiTE clones, highlighting the direct oncolytic activity of the G207 virus. The G207-NKG2DBiTE clones generally showed a similar level of viability compared to the G207-ControlBiTE clones. This suggests that although most G207-NKG2DBiTE

clones could activate T cells, as seen in Figure 5.1C and D, T cell cytotoxicity had not yet been induced. This may be due to the time course of the experiment, as cells had only been co-cultured for 72 hours; given the low amount of NKG2D BiTE present in the viral supernatants used, there may not be enough to exhibit cytotoxicity within this timeframe. The exception was G207-NKG2DBiTE clone N2, which demonstrated a significant decrease in cell viability compared to untreated U87 cells and was greater than the other G207-NKG2DBiTE clones. This is unsurprising given that clone N2 had the highest T cell activation compared to others. Interestingly, clone N2 caused lower viability than treatment with 1 nM NKG2D BiTE alone, despite having lower T cell activation, suggesting that the combination of the G207 virus and the NKG2D BiTE was more cytotoxic to the U87 cells than the G207 virus alone (exemplified by the G207-ControlBiTE clones) or the NKG2D BiTE alone.

The G207-NKG2DBiTE clone N2 was ultimately selected for larger-scale production due to the detectable protein band for NKG2D BiTE by western blot, the greatest ability to activate T cells, a robust infectivity of U87 cells, and the greatest cytotoxic potency. The G207-ControlBiTE clone B2 was selected for expansion due to its ability to express control BiTE with no induction of T cell activation, whilst it also demonstrated infectivity and oncolytic activity. These virus clones were expanded, purified and titred as described in Materials and Methods sections 2.9.

5.3.3 Functional testing of G207-NKG2DBiTE and G207-ControlBiTE viruses

Incorporation of constructs into viral genomes may hinder oncolytic activity. Hence, constructs were titred and their oncolytic activity compared to the original

G207 virus was confirmed (Appendices section 7.1.3). In addition, shedding of NKG2DLs from the cell surface is a common immune evasion tactic by many cancers and even some viruses (Baugh et al., 2020). Therefore, we also explored whether G207-NKG2DBiTE infection affected shedding of NKG2DLs from U87 cells, and demonstrated infection had no significant effect on NKG2DL shedding (Appendices section 7.1.4).

We next investigated the kinetics and potency of the NKG2D BiTE produced by the purified and titrated G207-NKG2DBiTE virus. To assess the activity of the NKG2D and Control BiTEs expressed by their respective G207 viruses, we analysed T cell activation, infectivity and target cell viability using flow cytometry. U87 cells were infected with G207-NKG2DBiTE or G207-ControlBiTE at a range of MOIs, and were co-cultured with T cells for 4, 6 and 11 days. Four days post-infection was chosen as the first time point because experiments using free NKG2D BiTE would significantly activate T cells by 72-96 hours. The typical G207 life cycle is around 72 hours. Therefore, the timepoint of four days post-infection should give an idea of the NKG2D BiTE activity after a single round of G207 infection and oncolysis.

G207-NKG2DBiTE and G207-ControlBiTE viruses both demonstrated similar levels of infection (determined by the percentage of GFP^+ cells) across the range of time points and MOIs, which increased in a dose-dependent manner (Figure 5.2A). However, at higher MOIs, the percentage of GFP^+ cells decreased slightly by day 11 for both viruses, but more so with G207-NKG2DBiTE virus. This possibly reflects the direct viral oncolysis and BiTE-mediated cytotoxicity over time reducing the numbers of live GFP^+ cells measured by flow cytometry.

T cells were only activated when in co-cultures with U87 cells infected with G207-NKG2DBiTE virus, with both CD69 and CD25 expression increasing with MOI and over time (Figure 5.2B and C, respectively). On day 4, the percentage of $CD69^+$ T cells increased in a dose-dependent manner, suggesting that at this early time point the increasing levels of virus infection resulted in increased NKG2D BiTE production, and hence an increase in T cell activation. As expected, the G207-ControlBiTE virus did not significantly activate T cells at any time point or MOI compared to uninfected controls. This confirmed that the purified G207-ControlBiTE virus was not able to trigger T cell activation due to non-specific activity of the Control BiTE or the presence of the G207 virus.

At later time points, the linear dose-response was lost; at higher MOIs of G207-NKG2DBiTE virus on day 6 and day 11, the CD69 expression (Figure 5.2C) begins to decrease compared to lower MOIs. This could be due to high levels of virus triggering oncolysis of the infected cells, meaning fewer live U87 cells for the NKG2D BiTE to activate the T cells against. Another potential explanation for the decrease in T cell activation at high MOIs could be due to a downregulation in surface NKG2DLs in infected cells. The findings in section 4.3.1 indicate that G207 infection in U87 cells triggers a dose-dependent downregulation of surface MICA/B expression in both GFP^+ (infected) and GFP^- (uninfected bystander cells) (Figure 4.1C). However, total surface NKG2DLs remained unchanged in infected U87 cells (Figure 4.1E). Therefore, the decrease in T cell activity here in Figure 5.2B and C could be due to downregulation in MICA/B, and perhaps a decrease in total NKG2DLs that were not detected by the rhNKG2D-Fc-Bio-Strep-Pe flow cytometry assay. Nevertheless, despite this, the data in Figure 4.2 showed that the NKG2D

BiTE was still able to activate T cells and kill target cells even if these ligands had partially been downregulated.

Crucially, the overall desired function of the G207-NKG2DBiTE virus is to kill GBM cells, and so it is important to assess its ability to reduce the viability of U87 cells. The viability of the infected U87 cells in this experiment was measured by a flow cytometry viability dye.

At day 4, neither virus showed any change in viability at any MOI compared to uninfected cells. These findings suggest that at this early timepoint, although the NKG2D BiTE is specifically activating T cells, and that the G207 virus itself has infected a large proportion of the cells, it is still too early to detect T cell- or virus-mediated cytotoxicity.

By day 6, the cytotoxic effects of the G207-NKG2DBiTE virus are detectable. (Figure 5.2D). The G207-ControlBiTE virus still does not show any significant decrease in viability compared to the uninfected cells, even at MOI 5. This indicates that although the proportion of infected cells is relatively high, no detectable viral-mediated reduction in viability has occurred yet. However, at day 6, there was a significant reduction of viability in G207-NKG2DBiTE virus-infected cells. Given the G207-ControlBiTE virus caused no significant decrease in viability at this timepoint, despite similar levels of infection, it suggests that this is due to NKG2D BiTE and T cell-mediated cytotoxicity, in concordance with the T cell activity data.

By day 11, the oncolytic activity of the G207 virus itself became apparent, with significant dose-dependent decreases in viability with both the G207-NKG2DBiTE and G207-ControlBiTE viruses (Figure 5.2D). The decrease in viability with G207-NKG2DBiTE virus was greater than the G207-ControlBiTE virus. The cytotoxicity of

G207 virus combined with NKG2D BiTE is best exemplified at MOIs of 0.05 and 0.5 at day 11, whereby the G207-NKG2DBiTE virus caused a viability reduction of 39% and 51%, respectively, compared to uninfected cells, whereas the G207-ControlBiTE virus caused a 19% and 43% reduction, respectively.

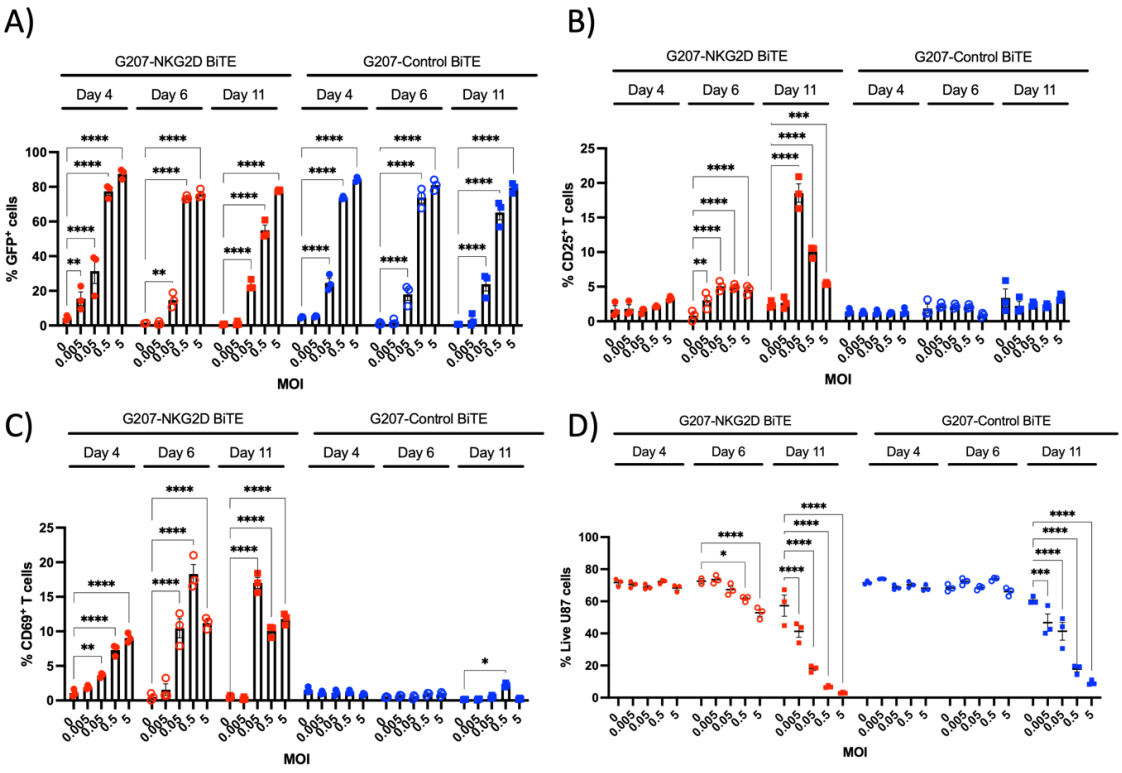

Figure 5.2 Time course and dose response of G207-NKG2DBiTE and G207-ControlBiTE viruses

U87 cells were infected with increasing multiplicity of infections (MOIs) of either G207-NKG2DBiTE (red) or G207-ControlBiTE (blue) ranging from MOI 0.005 to 5 before being co-cultured with PBMC-derived T cells at an E: T ratio of 5:1 for 4, 6 and 11 days. Cells were then harvested, stained and analysed for (**A**) GFP expression, (**B**) CD25, and (**C**) CD69 expression by flow cytometry. (**D**) U87 cell viability was assessed from the same experiment using a viability dye by flow cytometry. Data represents mean percentage of positive T cells, GFP^+ cells or viable cells of triplicate repeats ± S.D. Statistical significance was assessed by two-way ANOVA followed by Bonferroni post hoc analysis. Significance was assessed versus untreated cells within the relevant group (ns $p>0.05$, *$p\leq0.05$, **$p\leq0.01$, ***$p\leq0.001$ and ****$p\leq0.0001$).

The kinetics of U87 cell death when infected with increasing doses of G207-NKG2DBiTE or G207-ControlBiTE virus in Figure 5.2D seem to be relatively slow. By day 6, the G207-ControlBiTE virus caused no noticeable decrease in cell viability

compared to uninfected cells or compared to an earlier timepoint at day 4. Meanwhile, the G207-NKG2DBiTE virus had a significant decrease in viability at MOIs of 0.5 and 5 compared to uninfected cells or earlier timepoints, which is likely to be due to the activity of the NKG2D BiTE and T cell activation (Figure 5.2B and C).

Together, these findings confirm that activity of the NKG2D BiTE is retained in the G207 clone N2 following large scale purification, and that the T cell activity is specifically due to the NKG2D BiTE, not the G207 virus. Additionally, these results show that the combination of the direct oncolytic activity of the G207 virus and the NKG2D BiTE expressed by the infected cells can act together to kill GBM cells. Finally, the efficacy of the virus infection and viral oncolysis of the infected cells, combined with the NKG2D BiTE-mediated cytotoxicity is encouraging, as it seems the virus can infect the cells efficiently (at higher MOIs) and early (within four days), and begin producing the NKG2D BiTE at a functional dosage which can trigger T cell-mediated lysis of target cells (within six days) before the virus begins to cause oncolysis of the infected cells. This is a reassuring observation as it means that the infected cells will continue to produce the NKG2D BiTE and act as a protein 'factory' without the G207 virus killing the host cell before enough functional BiTE can be produced. Furthermore, the relatively slow kinetics of BiTE-mediated killing may allow more time for BiTE production before the producer cell is killed.

5.3.4 Quantification of NKG2D BiTE production from G207-NKG2DBiTE-infected cell lines

To compare the NKG2D BiTE activity produced from the G207-NKG2DBiTE virus to the free recombinant NKG2D BiTE, it was important to measure the

concentration of BiTE produced from infected cells. Since the NKG2D BiTE and Control BiTE contain C terminal 10xHis-Tags, the ideal measurement method would be by His-Tag ELISA. Unfortunately, however, His-Tag ELISAs using viral supernatants containing G207 viral particles generates a high background (data not shown), even with the use of a parental G207 not expressing any His-Tagged proteins, suggesting an artefact of the virus causes a non-specific signal in the His-Tag ELISA.

Therefore, the concentration of NKG2D BiTE produced from G207-NKG2DBiTE virally-infected cells was measured using a standard curve of T cell activation generated using known concentrations of recombinant NKG2D BiTE. Since Control BiTE cannot activate T cells, the concentration could not be assessed using this method. NKG2D BiTE production was compared across U87 and A172 GBM cell lines, while Vero cells were used as a positive control due to their high permissiveness to G207 infection. Cells were infected with G207-NKG2DBiTE or G207-ControlBiTE (as a negative control) across a range of MOIs before supernatants were collected from each well and pooled for each condition.

U87 cells were selected as a standardised cell line to apply an NKG2D BiTE-mediated T cell activation curve and interpolate the virally-produced BiTE activity against. U87 cells were treated with the harvested viral supernatants from the three infected cell lines and co-cultured with T cells. A standard curve was established by co-cultures with a range of recombinant NKG2D BiTE concentrations. Co-cultures were incubated together for three days before assessing T cell activity and target cell viability by flow cytometry. See Figure 5.3A for a schematic timeline and Materials and Methods section 2.9.6 for a protocol of the experiment.

The standard curves of T cell activation in response to free NKG2D BiTE are plotted in Figure 5.3B and C, displaying the percentage of $CD25^+$ and $CD69^+$ T cells, respectively. Both standard curves generated a sigmoidal curve of T cell activation; the percentage of $CD69^+$ T cells plateaued between 10 and 25 nM at around 80%, but the CD25 standard curve did not reach a plateau, likely due to the kinetics of CD25 expression. The CD69 standard curve was also more sensitive than CD25 at lower NKG2D BiTE concentrations. Therefore, due to the increased range in T cell activation and sensitivity at lower NKG2D BiTE concentrations, the CD69 standard curve was selected for interpolation.

The activation of the T cells after co-culture with U87 cells treated with supernatants from G207-NKG2DBiTE- or G207-ControlBiTE-infected cell lines can be seen in Figure 5.3D and E for CD25 and CD69 expression, respectively. As expected, the G207-ControlBiTE supernatant did not cause any T cell activation at any MOI.

The G207-NKG2DBiTE supernatants did not cause any T cell activation at the lowest MOI used (0.001) in any cell line. At an MOI of 0.01, the supernatants from G207-NKG2DBiTE-infected Vero cells caused significant increases in both CD25 and CD69 expression, meanwhile, infected U87 cell supernatants only induced significant CD69 upregulation. However, at an MOI of 0.1, both infected Vero and U87 cell supernatants significantly increased CD25 and CD69 expression, and was greater in U87 cell supernatants, indicating a higher concentration of NKG2D BiTE. Supernatants from G207-NKG2DBiTE-infected A172 cells did not induce T cell activation at any MOI, possibly due to poor BiTE production from the infected A172 cells or due to low infection of the A172 cells.

The cytotoxic activity of the NKG2D BiTE in the various supernatants was assessed by flow cytometry (Figure 5.3F). As expected, the G207-ControlBiTE supernatants did not cause any cytotoxicity. Also, in concordance with the prior observations in Figure 5.3D and E, supernatants from A172 cells infected with G207-NKG2DBiTE did not induce any cytotoxicity. However, significant decreases in viability were observed in G207-NKG2DBiTE supernatants from U87 and Vero cells infected at MOI 0.1. However, no noticeable effect on viability was observed at lower MOIs, correlating with the low T cell activation.

The percentage of $CD69^+$ T cells was used to interpolate the original NKG2D BiTE concentrations in the supernatants of U87, A172 and Vero cells infected with different MOIs of the G207-NKG2DBiTE virus, factoring in any dilutions made (Figure 5.3G). Due to the lack of T cell activation observed at all MOIs for A172s, and MOI 0.001 for U87 and Vero cells, the estimated concentration of NKG2D BiTE was 0 nM. At an MOI 0.01, U87 and Vero cell supernatants produced 0.03 nM and 0.2 nM of NKG2D BiTE over 72 hours, respectively. Finally, at an MOI 0.1, U87 cell supernatants contained 0.5 nM NKG2D BiTE and Vero cell supernatants contained 0.3 nM NKG2D BiTE.

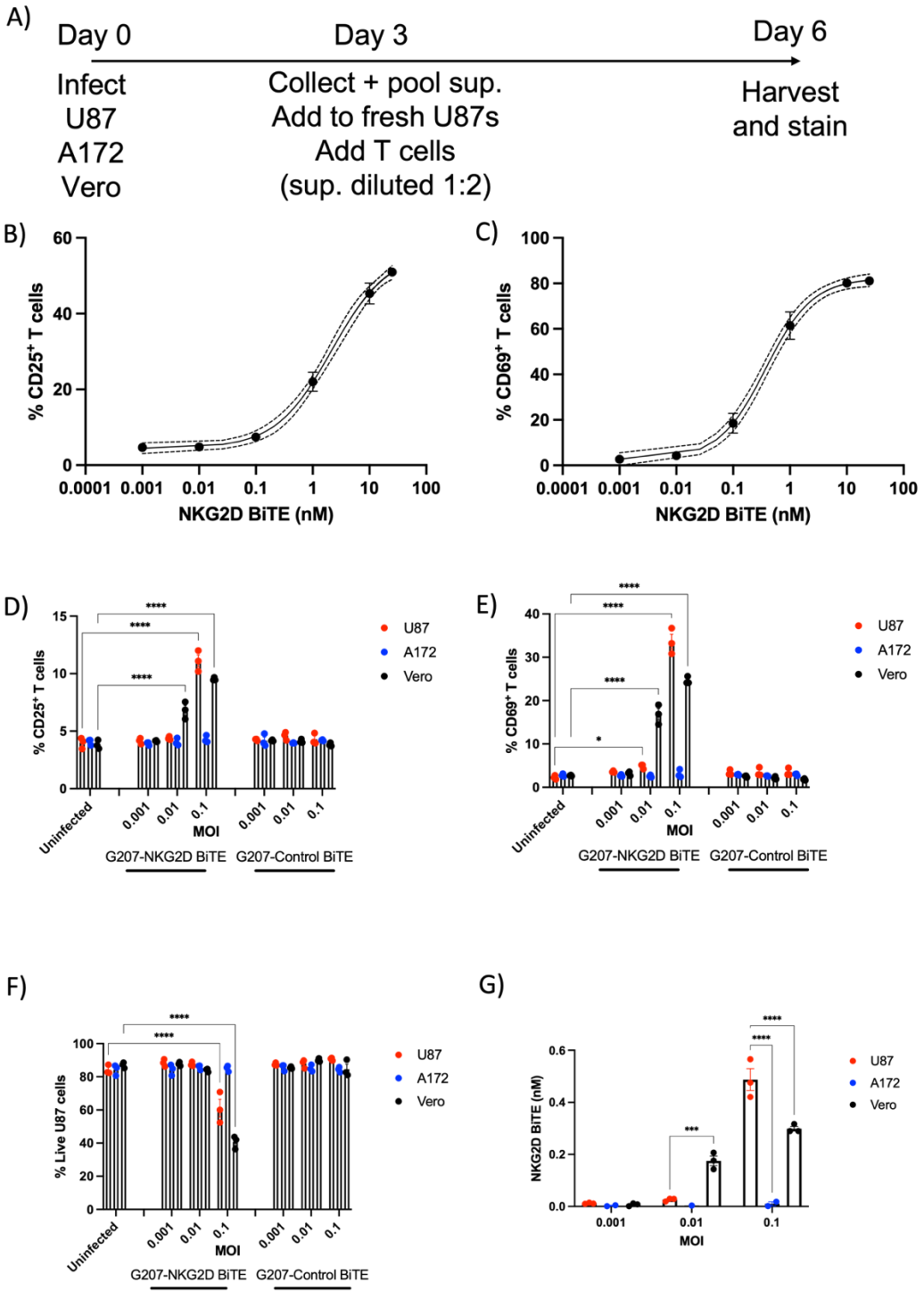

Figure 5.3 Quantification of functional NKG2D BiTE production from cell lines infected with G207-NKG2DBiTE

(**A**) Timeline of experimental setup. U87, A172 and Vero cells were infected with G207-NKG2DBiTE (red) or G207-ControlBiTE (blue) at a multiplicity of infection (MOI) 0.001, 0.01 and 0.1 for 72 hours. Infected supernatants were then collected and added to freshly seeded U87 cells alongside PBMC-derived T cells at an E: T ratio of 5:1. Cells were co-cultured for a further 72 hours before being harvested and stained for flow cytometric analysis. (**B**) T cells were co-cultured with U87 cells treated with a standard curve of 0.001, 0.01, 0.1, 1, 10 and 25 nM free NKG2D BiTE for 72 hours before being harvested and stained for percentage of $CD25^+$ and (**C**) $CD69^+$ cells and assessed by flow cytometry. (**D**) Percentage of T cells positive for CD25 and (**E**) CD69, or (**F**) percentage of live U87 cells in co-cultures treated with G207-

NKG2DBiTE or G207-ControlBiTE infected supernatants from U87 (red), A172 (blue) or Vero (black) cells as assessed by flow cytometry. Data represents mean percentage of positive cells of triplicate repeats ± S.D. (**G**) Interpolated concentrations of NKG2D BiTE produced into the supernatant of infected U87 (red), A172 (blue) or Vero (black) cells based on CD69 expression from (E) and the standard curve in (C). Statistical significance was assessed by two-way ANOVA followed by Bonferroni post hoc analysis. Significance was assessed versus uninfected cells within the relevant group (ns $p>0.05$, *$p\leq0.05$, **$p\leq0.01$, ***$p\leq0.001$ and ****$p\leq0.0001$).

5.3.5 Pre-treatment of TMZ and radiation enhances G207-NKG2DBiTE virus activity

We next sought to use viruses to exploit the findings in Chapter 4, whereby GBM cells pre-treated with conventional GBM therapy of radiation and TMZ increase NKG2DL expression (Figure 4.5), T cell activation (Figure 4.6) and sensitivity to NKG2D BiTE-mediated cytotoxicity (Figure 4.7). The same experimental setup was used as in section 4.3.5. In brief, U87 cells were pre-treated with a low dose of TMZ, radiation or a combination, or left untreated. After 72 hours of pre-treatment, U87 cells were infected with G207, G207-NKG2DBiTE or G207-ControlBiTE at an MOI of 0.1, or left uninfected, before being co-cultured with T cells or left in monoculture for a further three days. GFP expression, CD25 and CD69 expression and U87 cell viability were then assessed by flow cytometry. Additionally, an independent means of assessing cytotoxicity was performed to validate the findings; supernatant was collected from the cultures to determine U87 cytotoxicity by an LDH release assay. An experimental timeline is shown in Figure 5.5A.

Despite decreasing G207 infection levels, pre-treatment enhances G207-NKG2DBiTE-mediated T cell activation

We firstly assessed the effect of pre-treatments on the G207 virus infectivity. The percentage of live GFP^+ U87 cells was measured by flow cytometry. To determine the relationship between the viruses and the pre-treatments alone without the interference of NKG2D BiTE and T cell activity, the viral infection level was measured in infected U87 monocultures. The three viruses, G207, G207-NKG2DBiTE and G207-ControlBiTE all demonstrated high levels of infection in the U87 cells with no pre-treatment (Figure 5.4B).

Pre-treatment with TMZ, radiation or a combination caused a significant decrease in the percentage of live GFP^+ cells for all three viruses (Figure 5.4B). TMZ pre-treatment reduced the percentage of GFP^+ cells more than radiation alone, and the combination together caused an even greater decrease. These findings suggests that the pre-treatment of U87 cells with TMZ and radiation, even at sub-lethal doses, causes either a reduction in permissiveness of U87 cells to G207 infection or the percentage of live cells able to support G207 infection.

The percentage of $CD25^+$ and $CD69^+$ T cells co-cultured with uninfected U87 cells did not increase when pre-treated, confirming that increased NKG2DL expression did not trigger BiTE-independent, NKG2D-dependent T cell activation (Figure 5.4C and D). T cells were only activated when in co-culture with U87 cells infected with G207-NKG2DBiTE virus, although this activation was lower than in previous experiments using free NKG2D BiTE, likely due to the kinetics of infection and BiTE expression, and the lower concentration of NKG2D BiTE (approximately 0.5 nM), as estimated in Figure 5.3G.

T cell CD25 and CD69 expression increased significantly in pre-treated co-cultures infected with G207-NKG2DBiTE virus (Figure 5.4C and D, respectively). CD69 expression significantly increased from 8% with no pre-treatment to 14% in TMZ pre-treated, 10% in 2 Gy pre-treated and 13% in 2 Gy + TMZ pre-treated cells. Similar increases were observed in CD25 expression, increasing from 4% in cells with no pre-treatment to 7% in TMZ pre-treated and 7% in 2 Gy + TMZ pre-treated. However, 2 Gy alone did not cause a significant increase in CD25 expression (Figure 5.4C). These results were consistent with the findings in Figure 4.6, whereby the U87 cells pre-treated with TMZ, 2 Gy or a combination increased activated T cells with NKG2D BiTE treatment.

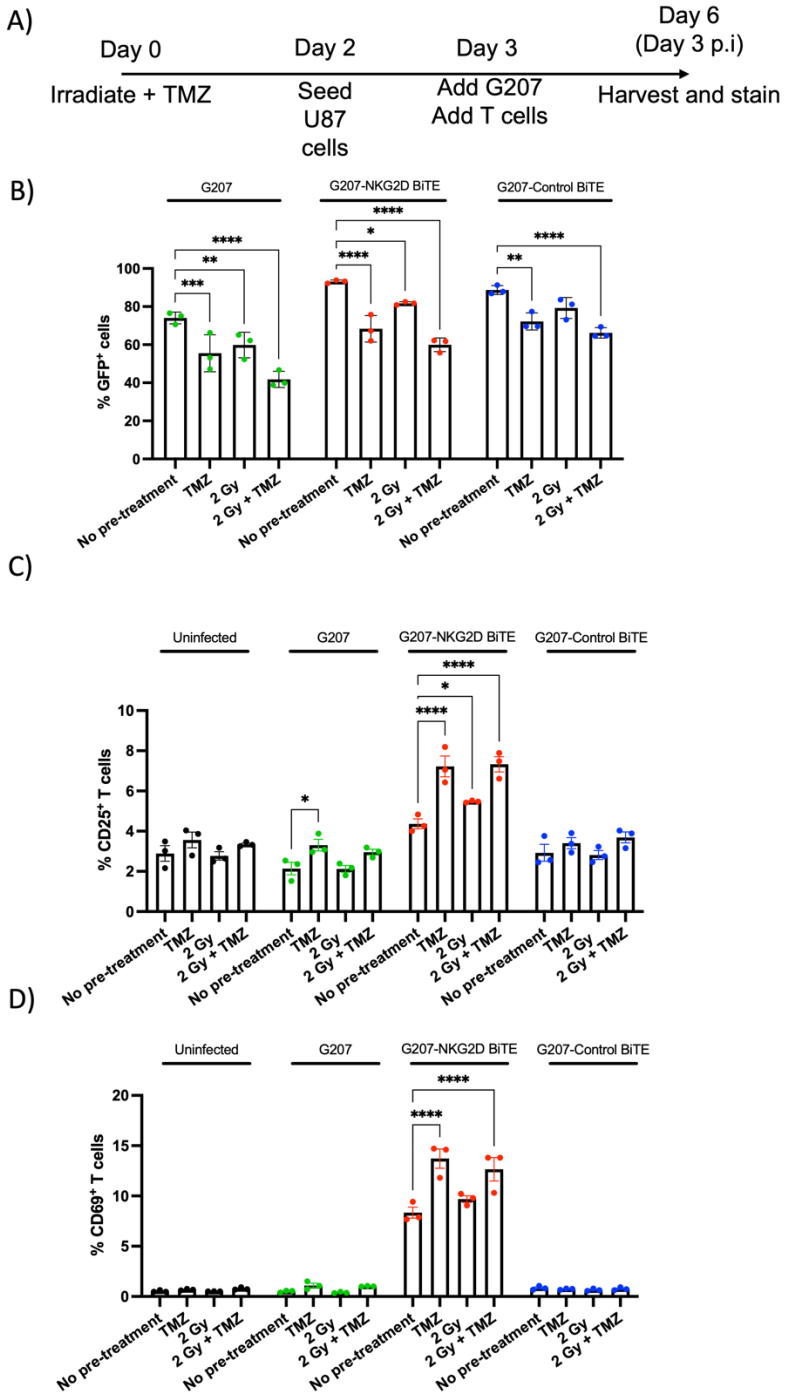

Figure 5.4 Assessment of the effects of combination of TMZ and radiation pre-treatment on G207-NKG2DBiTE virus infectivity and T cell activation

(**A**) Timeline of experimental set up. U87 cells were treated with 50 μM temozolomide (TMZ), a single dose of 2 Gray (Gy) radiation either alone (2 Gy) or in combination with 50 μM TMZ (2 Gy + TMZ) or left untreated (no pre-treatment). 72 hours after pre-treatment, U87 cells were seeded and infected with parental G207 (green), G207-NKG2DBiTE (red) or G207-ControlBiTE (blue) at a multiplicity of infection (MOI) of 0.1 or left uninfected (black). 4 hours after infection, PBMC-derived T cells were added at an E: T ratio of 5:1. After co-culturing for 72 hours, cells were harvested, stained and the percentage of (**B**) GFP^+ U87 cells, (**C**) $CD25^+$ and (**D**) $CD69^+$ T cells was measured by flow cytometry. Data represents mean percentage of positive cells from triplicate repeats ± S.D. Statistical significance was assessed by two-way

ANOVA followed by Bonferroni post hoc analysis. Significance was assessed versus no pre-treatment within the relevant group (ns $p>0.05$, *$p\leq0.05$, **$p\leq0.01$, ***$p\leq0.001$ and ****$p\leq0.0001$).

Pre-treatment alone has only a modest effect on uninfected U87 cell viability

The viability of U87 cells in uninfected co-cultures significantly decreases from 94% with no pre-treatment to 83%, 84% and 73 with TMZ, 2 Gy and 2 Gy + TMZ, respectively (Figure 5.5A). This trend was also similar in uninfected monocultures of U87 and T cells (Appendices Figure 7.6A), reflecting a modest but significant decrease in U87 viability in response to pre-treatment. An alternative representation of the data is shown in Figure 5.5B, comparing each the viability of each virus with each pre-treatment.

Only infection with G207-NKG2DBiTE virus decreases U87 cell viability

Infection with any of the G207 viruses in monoculture without pre-treatments had very little effect on U87 cell viability (Appendices Figure 7.6A). Furthermore, non-pre-treated co-cultures of T cells with U87 cells infected with G207 or G207-ControlBiTE also showed no loss of viability compared to uninfected co-cultures (Figure 5.5A). However, co-cultures infected with G207-NKG2DBiTE virus showed some BiTE-dependent cytotoxicity, with 78% viability compared to 94% viability in the corresponding uninfected co-culture. These results suggest that the G207 virus itself was having little direct oncolytic activity on its own, and that in the absence of pre-treatment, any cytotoxicity was NKG2D BiTE-dependent. This effect can also be seen across each pre-treatment in Figure 5.5B.

Pre-treatment enhances sensitivity to G207 oncolysis

Pre-treatment increased the sensitivity to G207 viral oncolysis, with 72%, 83% and 71% viability when U87 monocultures were infected with G207 and pre-treated with TMZ, 2 Gy and 2 Gy + TMZ, respectively, compared to 92% with no pre-treatment (Appendices Figure 7.6A). The cytotoxic effect of pre-treatments and G207 infection were also greater than for pre-treatment alone. This pattern was observed across all G207 viruses (Figure 5.5B), suggesting that the pre-treatment was sensitising the U87 cells to G207-mediated oncolysis.

Pre-treatment significantly enhances U87 sensitivity to G207-NKG2DBiTE-mediated cytotoxicity

Pre-treatment caused significant decreases in viability when U87 and T cell co-cultures were infected with G207-NKG2DBiTE virus. U87 cell viability decreased from 78% with no pre-treatment to 45% and 40% when pre-treated with TMZ and 2 Gy + TMZ, respectively, although 2 Gy pre-treatment did not have a significant effect (Figure 5.5A). This decrease was far greater than by pre-treatment alone or with either G207 or G207-ControlBiTE viruses (Figure 5.5B), indicating that pre-treatment with TMZ or 2 Gy + TMZ increased the NKG2D BiTE-dependent lysis of U87 cells.

The results in Figure 5.5A show a decrease in cell viability in U87 cells pre-treated with TMZ or 2 Gy + TMZ compared to no pre-treatment when infected with G207-NKG2DBiTE virus and in co-culture with T cells. These results are encouraging since Figure 5.4B suggests that TMZ and 2 Gy + TMZ pre-treatment significantly decreases the percentage of GFP^+ cells compared to no pre-treatment. This would suggest that either there is an additive effect of the virus oncolytic activity

and TMZ or 2 Gy + TMZ pre-treatment together to kill U87 cells despite the lower levels of virally-infected cells, or that the combination of pre-treatment and G207 virus may be too cytotoxic for the U87 cells, resulting in cell lysis and under-representation of infection (by the percentage of live GFP^+ cells) as determined by flow cytometry.

Combination therapy of pre-treatment and G207-NKG2DBiTE is synergistic

A Bliss independence test (Q. Liu et al., 2018) was performed to further investigate the relationship between conventional therapy pre-treatment and G207-NKG2DBiTE immunotherapy and to determine whether the combination therapy achieved a synergistic or additive effect. The percentage of live U87 cells in co-cultures were used for Bliss independence analysis. The Bliss independence scores of TMZ, 2 Gy and 2 Gy + TMZ pre-treated cells infected with G207-NKG2DBiTE in co-culture were calculated. As with the analysis and findings earlier in Figure 4.7, Bliss independence scores of >0 are deemed synergistic, whereas a score of 0 suggests the two variables are independent of each other, and a score <0 is antagonistic. The Bliss independence scores in Figure 5.5C indicate that the relationship between TMZ and 2 Gy + TMZ pre-treatments and G207-NKG2DBiTE is synergistic, with 0.19 and 0.1, respectively. However, 2 Gy pre-treatment alone appears to be antagonistic, with a Bliss independence score of -0.06.

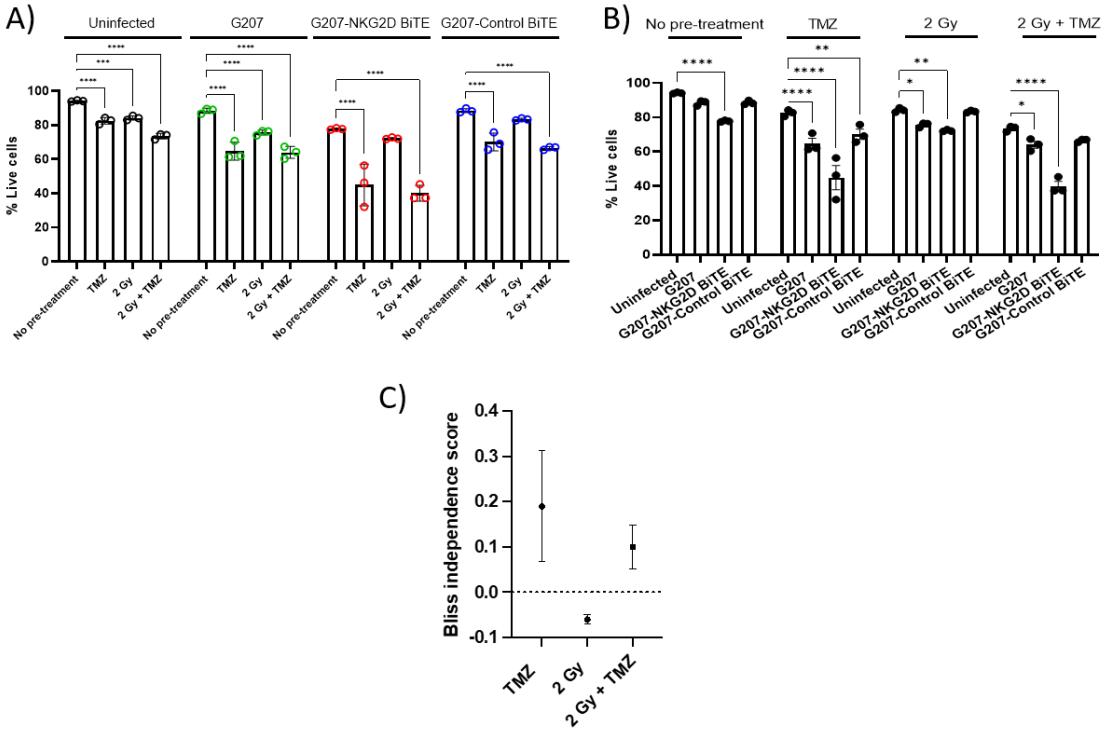

Figure 5.5 Conventional GBM therapy pre-treatment synergises with G207-NKG2DBiTE virus to decrease U87 viability

(**A**) U87 cells were pre-treated with 50 μM temozolomide (TMZ), a single dose of 2 Gray (Gy) radiation alone (2 Gy) or in combination with 50 μM TMZ (2 Gy + TMZ) or left untreated (no pre-treatment). 72 hours after pre-treatment, U87 cells were infected with parental G207 (green), G207-NKG2DBiTE (red) or G207-ControlBiTE (blue) at a multiplicity of infection (MOI) of 0.1 or left uninfected (black). 4 hours after infection, PBMC-derived T cells were added at an E: T ratio 5:1. After culturing for 72 hours, cells were harvested, stained and percentage of live U87 cells was assessed using a flow cytometric viability dye. Data represents mean percentage of live U87 cells from triplicate repeats ± S.D. Statistical significance was assessed by two-way ANOVA followed by Bonferroni post hoc analysis. Significance was assessed versus no pre-treatment within the relevant group. (**B**) Alternative representation of the data from (A) where significant was assessed versus Uninfected for each pre-treatment group. (ns p>0.05, *p≤0.05, **p≤0.01, ***p≤0.001 and ****p≤0.0001) (**C**) The Bliss independence score (BIS) was calculated using the viability data to determine the presence of synergy between the various treatments (BIS >0, synergy; BIS = 0, independent; BIS <0, antagonistic).

Validating the findings that pre-treatment enhances G207-NKG2DBiTE virus activity by LDH assay

Alongside measuring the viability of U87 cells by flow cytometry, cytotoxicity was measured by LDH release assay using supernatants collected from an independent experiment following the same experimental set-up, and the full data including cytotoxicity of monocultures is shown in Appendices Figure 7.6B.

The data assessing cytotoxicity by LDH release (Figure 5.6A and B) show the same overall pattern as the flow cytometry data in Figure 5.5A and B. Firstly, the G207 viruses alone did not induce much cytotoxicity. Infection of monocultures with G207, G207-NKG2DBiTE, and G207-ControlBiTE viruses induced small increases in cytotoxicity compared to uninfected (Appendices Figure 7.6B). Low cytotoxicity was also maintained in co-cultures with T cells when infected with G207 or G207-ControlBiTE viruses but is increased with the G207-NKG2DBiTE virus (29%) (Figure 5.6B).

The cytotoxic effects of pre-treatments are visible with all co-culture and virus conditions (Figure 5.6B). TMZ, radiation and 2 Gy + TMZ pre-treatment induced slight increases of cytotoxicity in U87 cells in monoculture, with TMZ and 2 Gy + TMZ having the greatest effects (Appendices Figure 7.6B). This trend was also maintained across all viruses in both mono- and co-cultures (Figure 5.6B).

Pre-treatment synergises with G207-NKG2DBiTE-mediated U87 cell lysis – confirmation by LDH assay

Co-cultures infected with G207-NKG2DBiTE virus, however, induced significantly more cytotoxicity when cells were pre-treated with TMZ (50%), 2 Gy (35%) or 2 Gy + TMZ (52%), compared to no pre-treatment (29%), indicating enhanced NKG2D BiTE-mediated lysis of U87 cells that had been pre-treated.

As in Figure 5.5C, a Bliss Independence score was calculated for these LDH data to assess the synergy between the treatments (Figure 5.6C). The Bliss independence scores for TMZ, 2 Gy and 2 Gy + TMZ were 0.19, 0.02 and 0.17, respectively, indicating that all pre-treatment combinations synergised with the

G207-NKG2DBiTE virus, with 2 Gy + TMZ having the greatest effect. However, the Bliss Independence score for 2 Gy pre-treatment was not statistically significant.

Two distinct and independent assays were used to measure the ability of the G207-NKG2DBiTE to kill U87 cells pre-treated with TMZ and radiation. Figure 5.5 uses a flow cytometry viability dye, which relies on the principle that live cells are impermeable to the viability dye, but dead cells are permeable. This is essentially a means of directly counting live cells in a sample, and exclusion of dead cells which take up the dye. Meanwhile, Figure 5.6 uses an LDH release assay, which measures the release of cytoplasmic LDH enzymes into the supernatant and is a measure of cell lysis. Despite these two different means of measuring NKG2D BiTE activity, the findings from the LDH release assay are highly concurrent with the flow cytometry data, and the Bliss Independence scores are similar (Figure 5.5C andFigure 5.6C). The Bliss Independence scores follow the same trend for TMZ and 2 Gy + TMZ pre-treatments, both showing synergy with the G207-NKG2DBiTE virus. However, the 2 Gy pre-treatment in Figure 5.6C (LDH assay) is trending towards synergistic but does not reach significance, meanwhile it is slightly antagonistic in Figure 5.5C (flow cytometry). This discrepancy may be due to the differences in sensitivities of the two methods in measuring cell viability and cytotoxicity. Additionally, these discrepancies may be due to the cell of origin for the LDH release, as some LDH may have been released from the T cells in the co-cultures.

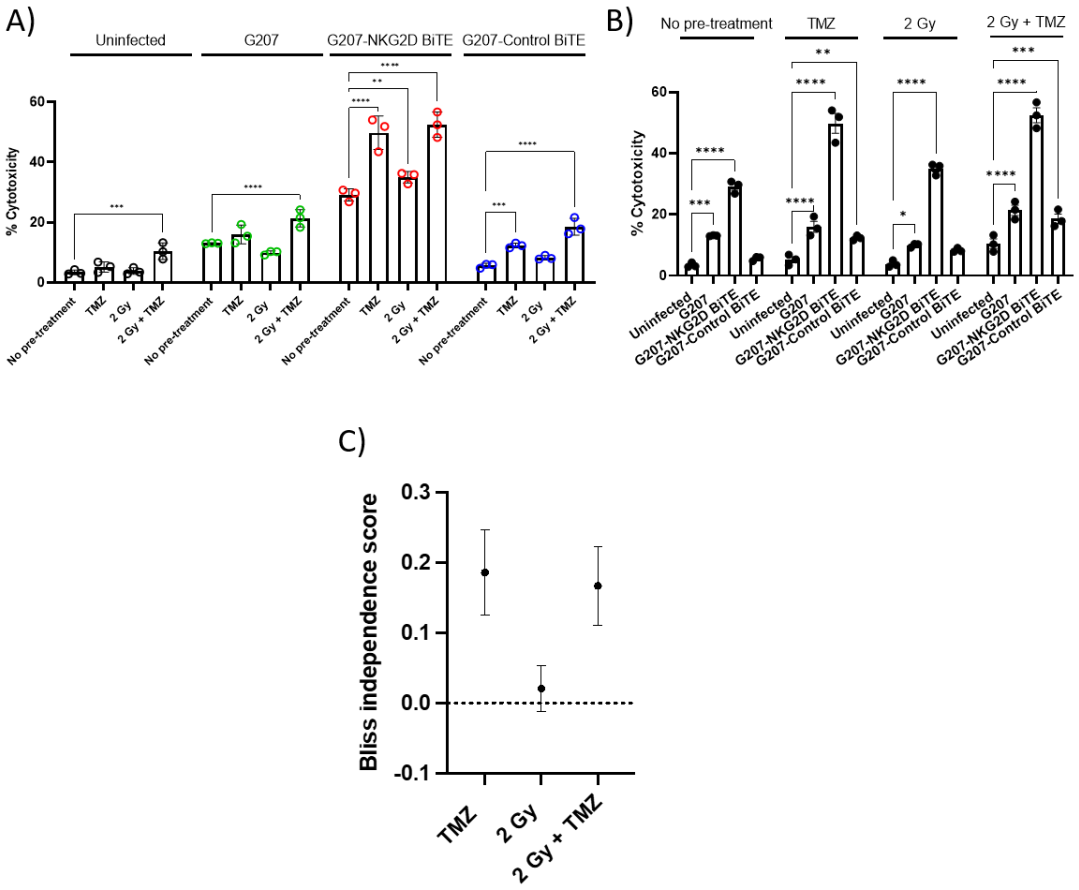

Figure 5.6 Conventional GBM therapy pre-treatment synergises with G207-NKG2DBiTE virus to increase U87 cytotoxicity.

(**A**) U87 cells were pre-treated with 50 μM temozolomide (TMZ), a single dose of 2 Gray (Gy) radiation alone (2 Gy) or in combination with 50 μM TMZ (2 Gy + TMZ) or left untreated (no pre-treatment). 72 hours after pre-treatment, U87 cells were infected with parental G207 (green), G207-NKG2DBiTE (red) or G207-ControlBiTE (blue) at a multiplicity of infection (MOI) of 0.1 or left uninfected (black). 4 hours after infection, PBMC-derived T cells were added at an E: T ratio of 5:1. After culturing for 72 hours, cell culture supernatants were harvested, and the relative toxicity was assessed by lactate dehydrogenase (LDH) release assay. Relative cytotoxicity for each treatment was calculated compared to lysis controls of U87 cells in monoculture. Data represents mean relative cytotoxicity from triplicate repeats ± S.D. Statistical significance was assessed by two-way ANOVA followed by Bonferroni post hoc analysis. Significance was assessed versus no pre-treatment within the relevant group (ns $p>0.05$, *$p\leq0.05$, **$p\leq0.01$, ***$p\leq0.001$ and ****$p\leq0.0001$). (**B**) Alternative representation of the data from (A) where significant was assessed versus Uninfected for each pre-treatment group. (ns $p>0.05$, *$p\leq0.05$, **$p\leq0.01$, ***$p\leq0.001$ and ****$p\leq0.0001$) (**C**) Bliss independence score (BIS) was calculated using the viability data to determine the presence of synergy between the various treatments (BIS >0, synergy; BIS = 0, independent; BIS <0, antagonistic).

5.3.6 Comparing TMZ and radiation pre-treatment versus concomitant treatment alongside G207-NKG2DBiTE virotherapy

The standard of care for GBM patients undergoing Stupp therapy consists of a total of 60 Gy radiation, divided over 6 weeks, with five daily doses of 2 Gy each week (6 x 5 x 2 Gy) and concomitant daily TMZ of 75 mg/m^2 during the course of radiotherapy. This is then followed up with six cycles of adjuvant TMZ chemotherapy at 150-200 mg/m^2 for five days each monthly cycle (Stupp et al., 2005). This treatment regimen is typically administered after debulking surgery.

The proposed route of delivery of the G207-NKG2DBiTE virus is via intratumoural stereotactic administration directly into the surgical cavity during debulking surgery (J. M. Markert et al., 2014). Therefore, if the G207-NKG2DBiTE virus immunotherapy is to fit alongside current Stupp therapy, then it is important to investigate the effects of concomitant TMZ and radiation on the activity of the G207 virus, NKG2D BiTE and cytotoxicity.

We therefore sought to investigate the effects of concomitant treatment of TMZ and radiation on G207-NKG2DBiTE immunotherapy compared to pre-treatment. See Figure 5.8A for an experimental timeline. To do this, U87 cells were either pre-treated with 2 Gy + 50 μM TMZ or given no pre-treatment. After 72 hours of pre-treatment, U87 cells were infected with G207-NKG2DBiTE virus or left uninfected, and co-cultured with T cells. To achieve concomitant TMZ treatment, a single dose of TMZ was administered during infection, since replenishing the TMZ in the media each day would remove virus, BiTE, T cells and accumulating LDH from the cell culture supernatants. Therefore, single doses of increasing concentration were administered during infection to simulate an accumulating daily dose of TMZ. For

concomitant radiotherapy, co-cultures were treated with 2 Gy radiation on three consecutive days to simulate the daily 2 Gy radiation in the Stupp regimen. 96 hours post-infection, cell supernatants were collected for LDH release assays to assess U87 cell cytotoxicity. A summary of the experimental timeline and the various doses and treatment combinations is in Figure 5.7.

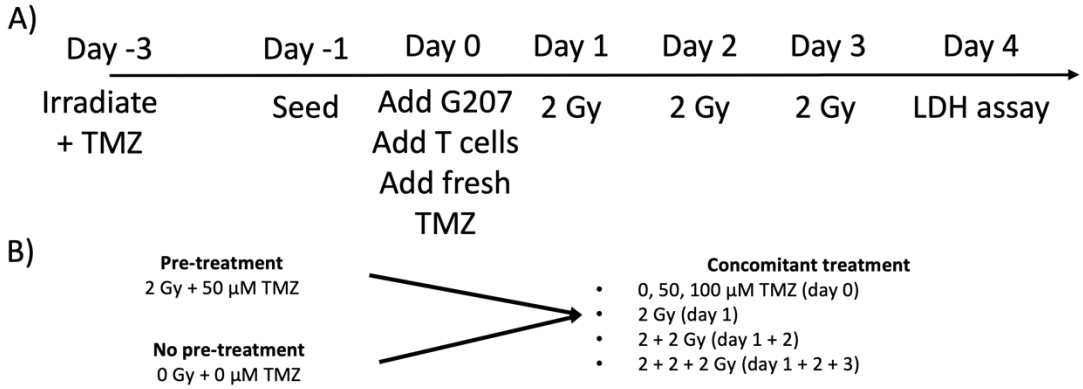

Figure 5.7 Overview of experimental set up for concomitant TMZ and radiation with G207-NKG2DBiTE immunotherapy

(**A**) Timeline of experimental set up. U87 cells were pre-treated with 50 μM temozolomide (TMZ) and a single dose of 2 Gray (Gy) radiation or given no pre-treatment. 72 hours after pre-treatment, U87 cells were seeded and infected with G207-NKG2DBiTE at a multiplicity of infection (MOI) of 0.1, followed by the addition of PBMC-derived T cells at an E: T ratio 5: 1 four hours later. Co-cultures were also treated with 0, 50 or 100 μM fresh concomitant TMZ. 24 hours after infection, co-cultures were exposed to concomitant radiation of 2 Gy, which was repeated each day for 3 days. 96 hours after infection, cell culture supernatants were harvested, and cell cytotoxicity was assessed by lactate dehydrogenase (LDH) release assay. (**B**) Summary of the treatment combinations of U87 cells. Cells were either pre-treated or given no pre-treatment and given concomitant TMZ and radiation alongside infection with G207-NKG2DBiTE.

The comparison of relative cytotoxicity of concomitantly treated U87 cells infected with G207-NKG2DBiTE virus following pre-treatment and no pre-treatment is shown in Figure 5.8A and B, respectively. The G207-NKG2DBiTE-infected co-culture data from Figure 5.8A and B are presented in a more condensed format in Figure 5.8C, allowing direct comparison between pre-treated and non-pre-treated cells.

Pre-treatment causes greater cytotoxicity of G207-NKG2DBiTE virus than no pre-treatment

The first two columns in Figure 5.8C, (no concomitant treatment) show a general consistent trend of increased cytotoxicity when the U87 cells have been pre-treated prior to infection with G207-NKG2DBiTE virus compared to no pre-treatment. This difference did not reach statistical significance although the general trend was maintained across all concomitant treatment variations, with pre-treatment trending towards greater cytotoxicity than no pre-treatment, although only reaching statistical significance at concomitant 2 Gy + 0 μM TMZ and 2 + 2 Gy + 0 μM TMZ.

Only cells that have experienced no pre-treatment are sensitive to concomitant TMZ treatment

Pre-treated uninfected U87 cells experienced greater cytotoxicity compared to no pre-treatment (Figure 5.8A), but this remained unchanged when these pre-treated co-cultures were also exposed to concomitant TMZ or radiation. However, when U87 cells experienced no pre-treatment (Figure 5.8B), they showed a slight increase in cytotoxicity with concomitant TMZ but not radiation.

The cytotoxicity of 100 μM concomitant TMZ towards uninfected U87 cells was roughly the same, independent of pre-treatment (Figure 5.8B). This may suggest that for uninfected U87 cells, around 20% of the cells are sensitive to TMZ and die, and this occurs either from pre-treatment or from concomitant TMZ.

When infected with G207-NKG2DBiTE virus, the cytotoxicity of pre-treated U87 cells does not change with concomitant radiation or 50 μM TMZ but does

significantly increase with 100 μM concomitant TMZ (Figure 5.8A). However, infected U87 cells that had no pre-treatment (Figure 5.8B) show a dose-dependent response to concomitant TMZ, but not radiation. This may suggest that the additional cytotoxicity and benefit gained by pre-treatment is perhaps slightly negated during concomitant TMZ therapy, and that concomitant TMZ may increase sensitivity to NKG2D BiTE in a similar way to pre-treatment.

Concomitant radiation gives no significant benefit to cytotoxicity

In contrast to the TMZ dose-dependent increase in cytotoxicity for non-pre-treated cells as discussed above, concomitant radiation did not have any enhancing effect on cytotoxicity for cells that were either pre-treated or not (Figure 5.8A and B, respectively). The effects of concomitant radiation were very slight, with no noticeable increase in cytotoxicity at any concentration of TMZ, whether the cells were infected with G207-NKG2DBiTE virus or not. There was even a slight general trend towards decreasing cytotoxicity as the cumulative dose of radiation increased (Figure 5.8A), although this did not reach statistical significance.

The cytotoxicity induced by pre-treatment and concomitant 0 Gy + 100 μM TMZ was greater (83%) than pre-treatment and concomitant 2 + 2 + 2 Gy + 100 μM TMZ (73%) (Figure 5.8A); this is somewhat surprising as the latter of the combined treatment regimens involves a further combined 6 Gy of radiation to the former, and so one might expect the latter to have triggered the most U87 cell lysis.

Furthermore, concurrent TMZ seemed to have a more significant impact on U87 cytotoxicity than concurrent radiation. Concurrent radiation did not increase cytotoxicity at all, and even started to slightly decrease cytotoxicity. This may suggest that the radiation is affecting T cell activity and may be limiting their ability

to activate with the NKG2D BiTE to kill U87 cells. One of the goals of this experiment was to investigate the effect of concomitant Stupp therapy on G207-NKG2DBiTE virus therapy, and whether TMZ and radiation might dampen the effects of G207-NKG2DBiTE therapy by interfering with the G207 virus itself or the T cells. Based on the results in Figure 5.8, it appears that concomitant TMZ and radiation has no detectable negative impact on G207-NKG2DBiTE therapy. However, this could be investigated further by looking in more detail specifically at T cell activation and viability by flow cytometry.

One of the goals of this experiment was to identify the optimal balance of pre-treatment and concomitant treatment to complement the G207-NKG2DBiTE immunotherapy. While this experiment lacks any T cell activation data (due to the size and complexity of the experiment), the optimal conditions should be picked based on maximum induced cytotoxicity. Based on this assumption, the optimal conditions for G207-NKG2DBiTE immunotherapy would be 2 Gy + 50 μM pre-treatment followed by 100 μM concurrent TMZ (but no concurrent radiation), which induced the highest relative cytotoxicity out of all conditions tested with 83% (Figure 5.8A). This combination was greater than the same conditions without pre-treatment (Figure 5.8B), which induced 75% cytotoxicity, and greater than conditions that had the most amount of conventional therapy (pre-treatment with 2 + 2 + 2 Gy and 100 μM TMZ), which achieved 73% cytotoxicity.

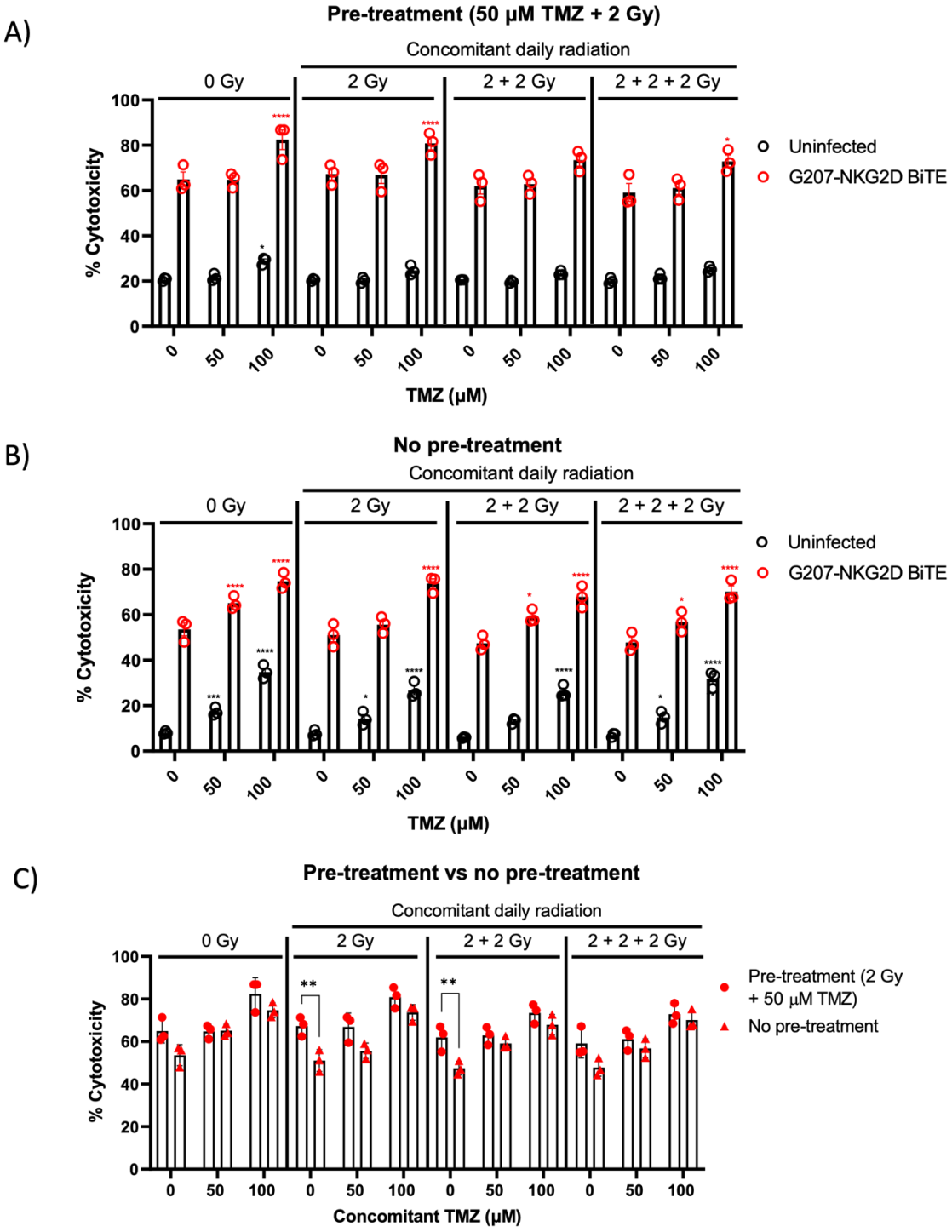

Figure 5.8 Investigating the effects of concomitant TMZ and radiation on G207-NKG2DBiTE immunotherapy.

(**A**) U87 cells were pre-treated with 50 μM temozolomide (TMZ) and a single dose of 2 Gray (Gy) radiation or (**B**) given no pre-treatment. 72 hours after pre-treatment, U87 cells were seeded and infected with G207-NKG2DBiTE (red) at a multiplicity of infection (MOI) of 0.1 or left uninfected (black). Four hours after infection, PBMC-derived T cells were added at an E: T ratio of 5: 1. Cells were also treated with 0, 50 or 100 μM fresh concomitant TMZ. 24 hours after infection, cells were exposed to concomitant radiation of 2 Gy, which was repeated each day for 3 days. 96 hours after infection, cell culture supernatants were harvested, and cell cytotoxicity was assessed by lactate dehydrogenase (LDH) release assay (Promega). Data

shows relative mean percentage of cytotoxicity 96 hours after infection. The relevant data from (A) and (B) are presented in (**C**), comparing pre-treatment (red circles) and no pre-treatment (red triangles) of co-cultures infected with G207-NKG2DBiTE virus. Relative percentage cytotoxicity assessed by LDH release assay at 96 hours post infection. Data represents mean percentage of cytotoxicity relative to 100% lysis control of triplicate repeats ± S.D. Statistical significance was assessed by two-way ANOVA followed by Bonferroni post hoc analysis. Significance was assessed versus no concomitant treatment for (A) and (B) or compared to pre-treatment in (C) (ns $p>0.05$, *$p\leq0.05$, **$p\leq0.01$, ***$p\leq0.001$ and ****$p\leq0.0001$).

5.3.7 GSCs are non-permissive to G207 virus but are sensitive to NKG2D BiTE

GSCs pose a significant obstacle to GBM therapy. They have been demonstrated to be an obstacle towards GBM oHSV-1 oncolytic virotherapy, as many ICP34.5-deleted mutant oHSV-1 viruses are ineffective in GSCs (Peters et al., 2018). Therefore, we sought to investigate the effect of G207-NKG2DBiTE virus on GSCs.

To develop a simple *in vitro* model of GSC-like conditions, U87 cells were cultured in NBM supplemented with EGF and fibroblast growth factor (FGF) (described in more detail in methods section 2.9.7) for one week, until cells became semi-adherent tumour spheres. These GSC-like U87 cells were then compared to normally bulk-differentiated U87 tumour cells, cultured in DMEM supplemented with 10% FCS, which maintained an adherent, single cellular monolayer.

Firstly, we investigated whether GSC-like U87 cells had different NKG2DL expression; therefore, NKG2DL and MICA/B expression were measured on GSC-like and differentiated U87 cells by flow cytometry. Surface MICA/B expression was slightly but significantly lower on GSC-like U87 cells (Figure 5.9A), although there was no significant difference in the relative total NKG2DL expression (Figure 5.9B). These findings suggest that NKG2DL expression on GSC-like U87 cells is similar

to differentiated U87 cells, although the GSC-like phenotype has a slightly lower MICA/B expression.

The activity of G207-NKG2DBiTE virus was then compared in GSC-like and differentiated U87 cells. Cells were infected with G207-NKG2DBiTE or G207-ControlBiTE virus, or left uninfected, before being co-cultured with T cells for 96 hours. The permissiveness of the two cell types to G207 infection was assessed by the percentage of GFP^+ U87 cells, as well as T cell activation and U87 viability by flow cytometry.

GSC-like U87 cells are non-permissive to G207-NKG2DBiTE virus infection, resulting in no BiTE-mediated T cell activation or cytotoxicity

Differentiated U87 cells demonstrated high levels of GFP^+ cells when treated with either G207-NKG2DBiTE or G207-ControlBiTE virus, however, no significant increase in GFP^+ cells was detected in the GSC-like U87 cells compared to uninfected controls (Figure 5.9C). These findings indicate that the GSC-like U87 cells were non-permissive to G207 virus, in contrast to the differentiated U87 cells (Figure 5.9C).

The T cell activation data in Figure 5.9D shows a significant increase in the percentage of $CD69^+$ T cells when differentiated U87 cells were infected with G207-NKG2DBiTE virus compared to uninfected co-cultures, but not with G207-ControlBiTE virus. This increase in CD69 expression was only observed in differentiated U87 cells infected with G207-NKG2DBiTE virus, but not in GSC-like U87 cells.

Both viruses caused a slight decrease in viability in both phenotypes of U87 cells compared to uninfected controls (Figure 5.9E). However, G207-ControlBiTE

virus infections showed no difference in viability between differentiated or GSC-like U87 cells, suggesting the decrease was due to the presence of the virus, despite the apparently low level of infection in GSC-like U87 cells. However, when the differentiated U87 cells were infected with G207-NKG2DBiTE virus, the viability decreased further than for GSC-like U87 cells or differentiated cells infected with G207-ControlBiTE virus. These results indicate that the NKG2D BiTE itself was causing a cytotoxic effect only on the differentiated U87 cells, but not GSC-like cells.

Taking the results from Figure 5.9C-E together, differentiated U87 cells were readily infected with both G207-NKG2DBiTE and G207-ControlBiTE viruses, which resulted in production of functional NKG2D BiTE, T cell activation and target cell lysis. However, GSC-like U87 cells did not infect well with the G207 virus, and so likely produced very little NKG2D BiTE, thus resulting in no detectable T cell activation or NKG2D BiTE-mediated cell lysis. These findings indicate that GSCs are insensitive to G207 virus.

GSC-like U87 cells are sensitive to free NKG2D BiTE

To investigate whether the NKG2D BiTE itself could induce GSC-like cell cytotoxicity, we decided to use free NKG2D BiTE in the same experimental set up as above but without the G207 virus. Differentiated U87 cells or GSC-like U87 cells were treated with 1 nM NKG2D BiTE, 1 nM Control BiTE or left untreated and co-cultured with T cells before assessing T cell activation and live U87 cells by flow cytometry.

The NKG2D BiTE induced significant increases in $CD25^+$ and $CD69^+$ T cells (Figure 5.9F and G, respectively) in co-cultures with U87 cells in both U87 cell phenotypes, but not with Control BiTE. Both CD25 and CD69 expression was

greater on T cells in co-cultures with GSC-like U87 cells than with differentiated U87 cells. The Control BiTE also induced a slight but significant increase in $CD69^+$ T cells (Figure 5.9G), which likely indicates some non-specific BiTE activity after 96 hours of treatment.

The viability of both GSC-like and differentiated U87 cells decreased significantly when treated with NKG2D BiTE compared to untreated or Control BiTE (Figure 5.9H). The decrease in viable cells after NKG2D BiTE treatment was greater for GSC-like U87 cells (42% decrease relative to untreated) than for differentiated U87 cells (35% decrease relative to untreated). The Control BiTE also resulted in a slight reduction in viability compared to untreated co-cultures with the GSC-like U87 cells, which may be due to the non-specific T cell activation induced by the Control BiTE observed in Figure 5.9F and G.

Together, the results from Figure 5.9F-H using NKG2D BiTE demonstrate that the BiTE can activate T cells and direct cytotoxicity towards differentiated U87 cells (cultured in 10% DMEM), but also towards GSC-like U87 cells (cultured in NBM). The data in Figure 5.9C-E demonstrates that GSC-like U87 cells were not permissive to G207 and did not produce functional NKG2D BiTE, but were still sensitive to the NKG2D BiTE itself in Figure 5.9F-H. Meanwhile, differentiated U87 cells were sensitive to both G207-NKG2DBiTE virus and NKG2D BiTE itself.

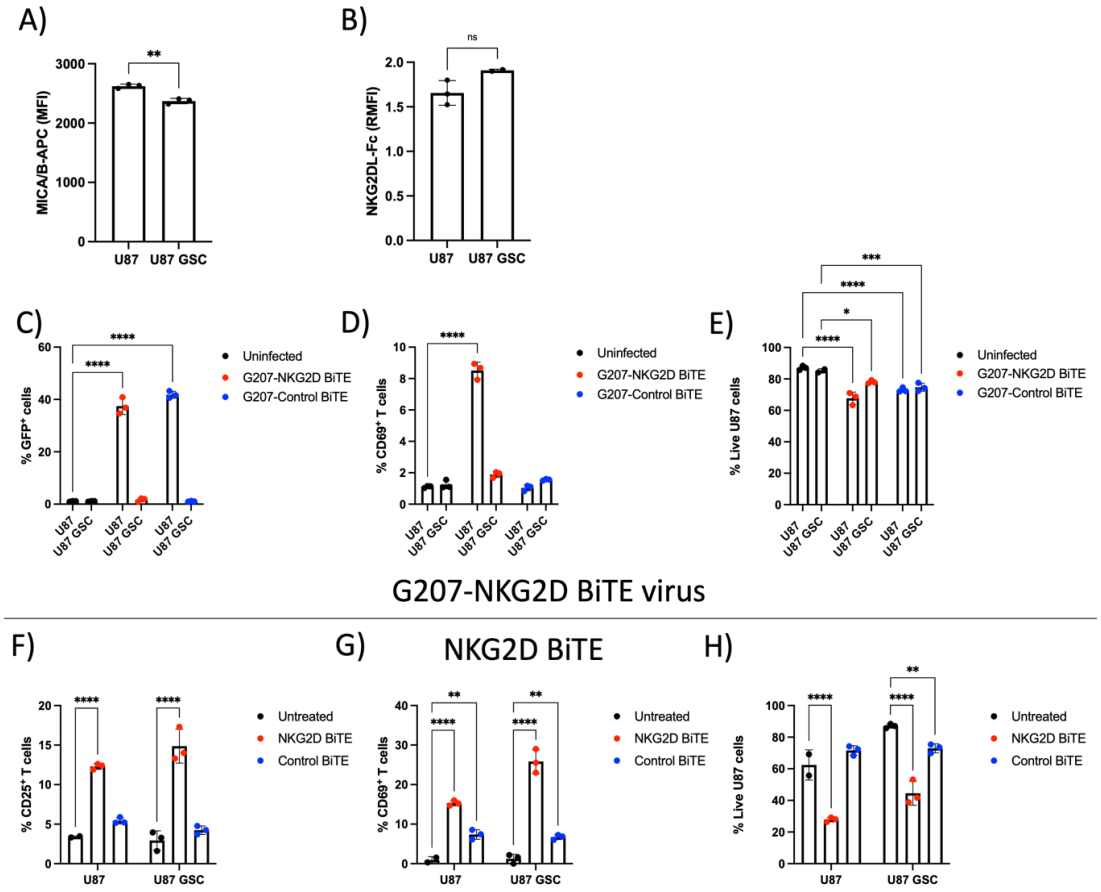

Figure 5.9 Activity of G207-NKG2DBiTE and free NKG2D BiTE against differentiated versus GSC-like U87 cells

U87 cells were cultured either normally in DMEM supplemented with 10% FCS (U87) to promote cancer cell differentiation; or in neurobasal medium (NBM) supplemented with recombinant human fibroblast growth factor (FGF) and epidermal growth factor (EGF), to promote a glioma stem cell-like (U87 GSC) phenotype. Differentiated and GSC-like U87 cells were stained with MICA/B-APC or biotinylated recombinant human NKG2D-Fc protein as a primary, followed by streptavidin-PE secondary for flow cytometric analysis secondary (NKG2D-Fc-Bio-Strep-PE). (**A**) Relative surface expression of MICA/B. Data represents mean fluorescence intensity (MFI) of triplicate repeats ± S.D. (**B**) Relative surface expression of total NKG2DLs. Data represents relative mean fluorescence intensity (RMFI) of triplicate repeats, relative to Isotype staining control ± S.D. Statistical significance was assessed by unpaired t test. Differentiated U87 cells or GSC-like U87 cells were infected with G207-NKG2DBiTE (red) or G207-ControlBiTE (blue) at an MOI of 0.1 or left uninfected (black), before being co-cultured with PBMC-derived T cells at an E: T ratio of 5:1 in RPMI supplemented with 2% FCS. After 96 hours of co-culture, cells were harvested, stained and percentage of (**C**) GFP^+ U87 cells, (**D**) $CD69^+$ T cells and (**E**) live U87 cells was measured by flow cytometry. Uninfected differentiated or GSC-like U87 cells were also treated with 1 nM NKG2D BiTE (red), Control BiTE (blue) or left untreated (black), and co-cultured with T cells as described above. 96 hours after co-culture, cells were harvested, and the percentage of (**F**) $CD25^+$ T cells, (**G**) $CD69^+$ T cells, and (**H**) live U87 cells was measured by flow cytometry. Data represents mean percentage of positive cells from triplicate repeats ± S.D. Statistical significance was assessed by two-way ANOVA followed by Bonferroni post hoc analysis. Significance was assessed versus untreated within the relevant culture medium (ns $p>0.05$, *$p\leq0.05$, **$p\leq0.01$, ***$p\leq0.001$ and ****$p\leq0.0001$).

5.3.8 Primary GBM cells are permissive to G207-NKG2DBiTE virus and targeted by NKG2D BiTE

We have demonstrated the ability of the NKG2D BiTE and the G207-NKG2DBiTE virus in activating T cells and directing cytotoxicity towards GBM cell lines. We next sought to investigate the effects of the BiTE and G207 virus in a more clinically relevant setting, using fresh human GBM tissue.

Primary human GBM cells derived from human tissue from a single patient (Materials and Methods section 2.10.2) were cultured in 10% RPMI to encourage differentiated GBM cell behaviour or NBM to encourage GSC-like cell behaviour. The cells were then incubated with G207-NKG2DBiTE or G207-ControlBiTE virus and co-cultured with heterologous PBMC-derived T cells for 96 hours, before assessing the percentage of GFP^+ GBM or GSC-like cells, $CD69^+$ T cells, and viable GBM or GSC-like cells by flow cytometry.

Patient-derived GSCs are less permissive to G207-NKG2DBiTE infection than differentiated GBM cells

Differentiated primary GBM cells were readily infected with both viruses, with many GFP^+ cells; but no infection was detected in primary GSC-like cells (Figure 5.10A). These results suggest that differentiated primary GBM cells are more permissive to the G207 virus than primary GSC-like cells and are reminiscent of those in Figure 5.9C, which shows low infectivity of GSC-like U87 cells compared to differentiated U87 cells.

CD69 expression (Figure 5.10B) was significantly greater following infection with G207-NKG2DBiTE virus in both cell types compared to uninfected controls and G207-ControlBiTE, with a greater increase in CD69 expression occurring for

differentiated primary GBM cells. This suggests that the NKG2D BiTE is being produced from infected primary GBM cells, and that it can activate T cells. The greater T cell activation in co-cultures with primary differentiated GBM cells reflects greater infectivity by the NKG2DBiTE virus. Nevertheless, the T cell activation in co-cultures with primary GSC-like cells shows that functional levels of NKG2D BiTE can be produced even when infection levels are low – gauged by GFP expression (Figure 5.10A). Due to the equal levels of infection of the two viruses in GBM cells we can conclude that that the T cell activation observed in Figure 5.10B is due to the NKG2D BiTE produced from infected cells, and not a response to the G207 virus itself.

Both viruses induced a similar decrease in differentiated primary GBM cell viability (Figure 5.10C), suggesting that this cytotoxic effect was due to the G207 virus itself and not the encoded BiTEs. In contrast, the G207-ControlBiTE virus showed no effect on GSC-like cell viability, whereas the G207-NKG2DBiTE virus slightly but significantly decreased the GSC-like cell viability, indicating NKG2D BiTE-mediated cytotoxicity.

Patient-derived GSCs are targeted by free NKG2D BiTE

Alongside infection with BiTE-encoded viruses, we sought to explore the activity of free NKG2D BiTE. The BiTE demonstrated a clear ability to activate T cells in the presence of both differentiated primary GBM cells and GSC-like cells with significant increases in CD25 (Figure 5.10D) and CD69 expression (Figure 5.10E) upon treatment with NKG2D BiTE compared to untreated. T cell activation was more pronounced in co-cultures with differentiated GBM cells (CD25, 35%;

CD69, 26%), than in culture with GSC-like cells (CD25, 14%; CD69, 17%) The Control BiTE did not induce any T cell activation in culture with either cell type

Treatment with free NKG2D BiTE also caused a slight but significant decrease in differentiated primary GBM cell viability (Figure 5.10F) compared to untreated, although it had no effect on primary GSC-like cells, where Control BiTE caused a significant increase in viability. These results contrast with those described above for the BiTE-encoded viruses and require further exploration to determine whether the effect is real, and perhaps reflect differences in local BiTE production.

These data clearly demonstrate NKG2D BiTE activity towards patient-derived GBM cells. This is in slight contrast to the findings in Figure 3.8, which suggest very low MICA/B expression and only slight total NKG2DL expression. Nevertheless, these results demonstrate NKG2D BiTE activity against clinically relevant human GBM tissue and show that the BiTE can direct T cell activation and cytotoxicity towards primary human GBM cells, both differentiated bulk tumour cells and GSC-like cells. Furthermore, we have demonstrated that the primary differentiated GBM cells are infectable with G207-NKG2DBiTE, and so may serve as a BiTE ‘factory’ to produce NKG2D BiTE *in situ* in the GBM TME, which can then target the G207-resistant GSC populations.

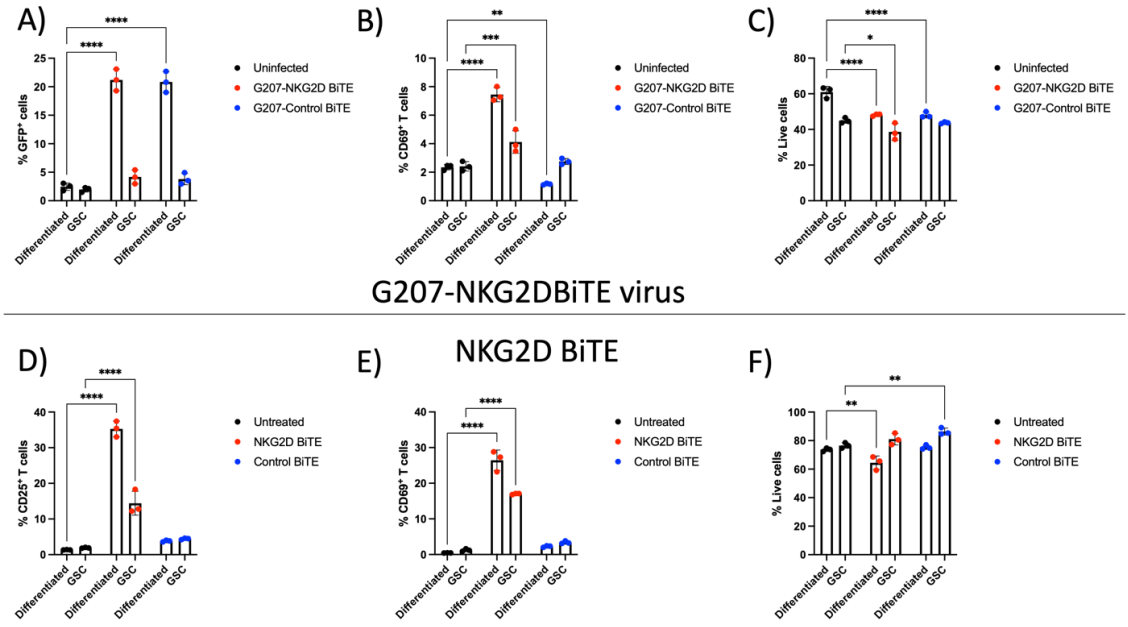

Figure 5.10 G207-NKG2DBiTE virus infects human primary GBM cells and triggers NKG2D BiTE-mediated T cell activation

Human GBM tissue obtained by cavitron ultrasonic surgical aspirator (CUSA) was dissociated and cultured in either neurobasal medium (NBM) supplemented with recombinant human fibroblast growth factor (FGF) and epidermal growth factor (EGF) to encourage a glioma stem cell-like (GSC) phenotype, or in RPMI containing 10% FCS to encourage a differentiated phenotype (Differentiated). Primary GBM cells were infected with G207-NKG2DBiTE (red) or G207-ControlBiTE (blue) virus at a multiplicity of infection (MOI) of 0.1 or left uninfected (black). Cells were co-cultured with PBMC-derived T cells at an E: T ratio of 5:1) for 96 hours before assessing the percentage of (**A**) GFP^+ GBM cells (**B**) $CD69^+$ T cells, (**C**) and GBM cell viability using a flow cytometric viability dye. Uninfected primary GBM cells were also treated with 1 nM NKG2D BiTE (red) or 1 nM Control BiTE (blue) or left untreated (black) and co-cultured with PBMC-derived T cells for 72 hours before assessing the percentage of (**D**) $CD25^+$ and (**E**) $CD69^+$ T cells or (**F**) CUSA cell viability. Data represents the mean percentage of positive GBM cells of triplicate repeats ± S.D. Statistical significance was assessed by two-way ANOVA followed by Bonferroni post hoc analysis. Significance was assessed versus untreated or uninfected cells within the relevant group (ns $p>0.05$, *$p\leq0.05$, **$p\leq0.01$, ***$p\leq0.001$ and ****$p\leq0.0001$). Patient sample n=1.

5.4 Discussion

This chapter focuses on the production of an oHSV-1 encoding the NKG2D BiTE to explore its potential utility in the treatment of GBM. The oHSV-1 used here, G207, has been extensively clinically evaluated, with a good safety profile but somewhat lacking in efficacy (J. M. Markert et al., 2009, 2014; J. Markert et al., 2000). The hypothesis posed in this chapter is that the efficacy of the G207 oHSV-1 virus could be improved by expressing NKG2D BiTE, for use alongside conventional GBM therapy of radiation and TMZ.

In this results chapter, we have successfully engineered G207 to express the NKG2D BiTE and demonstrated increased cytotoxicity compared to its parental virus counterpart. The G207-NKG2DBiTE virus not only triggers enhanced cytotoxicity towards GBM cells compared to G207-ControlBiTE virus (Figure 5.2), which is potentiated further following TMZ and radiation pre-treatment (Figure 5.5 and Figure 5.6), the G207-NKG2DBiTE virus also provides a potential strategy to eradicate GSCs (Figure 5.9 and Figure 5.10).

Although we have demonstrated enhanced cytotoxicity of the G207-NKG2DBiTE virus in combination with TMZ and radiation (Figure 5.4 and Figure 5.5), most of the enhanced cytotoxicity was NKG2D BiTE-dependent, with little contribution from the G207 virus itself. Furthermore, the GFP expression data (Figure 5.4B) indicates a decline in infected GFP^+ cells following pre-treatment of 2 Gy radiation compared to non-irradiated controls. This contrasts with reports in the literature.

As described in section 5.1, G207 has demonstrated enhanced activity pre-clinically and clinically when administered 24 hours before radiation. The

mechanism underlying the enhancement of G207 activity *in vivo* and *in vitro* when administered 24 hours before radiation revealed three main pathways that may contribute towards the augmentation (Sunil J. Advani, Mezhir, Roizman, & Weichselbaum, 2006). Firstly, DNA damage induced by radiation was shown to increase RR activity in dividing cells (Chabes & Thelander, 2000). In human colorectal carcinoma cells, host cell RR activity was doubled up to 24 hours following 2.5 Gy radiation, which potentiated G207 replication (Stanziale et al., 2002). Secondly, the cellular homolog of ICP34.5, growth arrest and DNA damage protein 34 (GADD34), which normally recruits PP1α to dephosphorylate eIF-2α to enable translation initiation, was shown to be upregulated in a number of cancer cells when irradiated and infected with G207 (Adusumilli et al., 2005; Jarnagin et al., 2006; S. H. Kim et al., 2005). Thirdly, the p38 pathway, was shown to be activated following irradiation, which greatly increase the gene expression of viral late genes (Mezhir et al., 2005; Zachos, Clements, & Conner, 1999). Therefore, the combined effects of radiation on G207 oHSV-1 results in: increased cellular RR activity, leading to greater production of cellular dNTPs which helps to compensate for G207 ICP6 deletion; increased GADD34-mediated dephosphorylation of eIF-2α, which antagonises the PKR translation shut-off response and compensates for G207 ICP34.5 deletion; and increased p38 activity, which boosts G207 late viral gene expression. Together, these effects of radiation lead to increased G207 replication and activity in irradiated cancer cells.

The discrepancies observed between the results in this chapter, indicating radiation pre-treatment limited G207 infection levels, and those reported in the literature, indicating a potentiation of G207 activity when followed by radiation, may be due to the timeline of the assay. The experiment in Figure 5.4 involved pre-

treatment with radiation 72 hours before infection, whereas the experiments described above by others typically within 24 hours of irradiation, or radiating a few hours following infection (Adusumilli et al., 2014; Jarnagin et al., 2006; S. H. Kim et al., 2005; Mezhir et al., 2005). The goal of the experiments performed in Figure 5.4 and Figure 5.5 were to assess the effects of radiation and TMZ pre-treatment on NKG2D BiTE activity, and not G207 replication, and hence cells were allowed to recover for three days before infection, to ensure that viral infection was equivalent across the pre-treatments. This suggests that perhaps the effects of radiation that would enhance G207 replication and infection, such as increased GADD34 and RR activity, may have subsided by the time the G207 virus was added. Additionally, the assay was terminated three days after initial infection to assess T cell activity (and limit subsequent rounds of viral infection); but perhaps allowing the assay to progress for longer may have revealed a potentiation of G207 infection after irradiation in subsequent infection cycles.

Similarly, the experiment in Figure 5.8 used concomitant radiation alongside G207 infection; the first dose of concomitant radiation was administered 24 hours after initial infection, and GBM cell lysis was determined by LDH release. Unfortunately, GFP expression was not measured for this experiment due to the size and complexity, but the LDH release data in Figure 5.8A did not show any increased cytotoxicity when G207 infected U87 cells were given concomitant radiation. Again, perhaps if the experiment was left for longer, then the beneficial effects of radiation on G207 infection and replication may become visible.

As well as radiotherapy, GBM patients also receive TMZ chemotherapy. The data in Figure 5.4, Figure 5.5, and Figure 5.6 indicate that G207-NKG2DBiTE-mediated T cell activation and killing of U87 cells is significantly increased when the

cells were pre-treated with TMZ or TMZ with radiation. However, concurrent treatment of TMZ and radiation may have a more damaging effect on the G207-NKG2DBiTE immunotherapy than the benefits of inducing increased NKG2DL expression. Glioblastoma patients undergoing radiation and TMZ therapy were reported to have significant lymphopenia in PBMCs, with significant reductions in the number of $CD4^+$ T cells, as well as $CD8^+$ cells following therapy (Fadul et al., 2011). In addition to the depletion of immune cells after GBM Stupp therapy, Chitadze and colleagues report a significant decrease in the number of peripheral blood $CD4^+$ and $CD8^+$ T cells following dexamethasone steroid treatment, given to reduce brain oedema for GBM patients (Chitadze et al., 2017).

Additionally, a study using the oHSV-1 G47Δ armed to express IL-12 to promote an anti-tumour response in a mouse immunocompetent GBM model demonstrated that concurrent administration of TMZ *in vivo* abrogated the beneficial immune response generated by the virus and IL-12 (Saha, Rabkin, & Martuza, 2020). The authors reported this abrogation to be due to significant decreases in both $CD4^+$ and $CD8^+$ TILs and splenocytes when mice were treated even with a low dose (7.5 mg/mL) of TMZ (Saha et al., 2020). Attempts to overcome the sensitivity towards TMZ by immune effector cells targeting NKG2DLs in glioblastoma have been investigated. Lamb et al. noted that TMZ was highly toxic towards γδ T cells, and so engineered γδ T cells to express MGMT, thus conferring TMZ-resistance for allogenic cell therapy for murine GBM models (Lamb et al., 2013).

When put together, the evidence of lymphopenia in GBM patients after TMZ and radiotherapy (Fadul et al., 2011), the reduction in TILs and efficacy with concurrent TMZ therapy alongside oHSV-1 immunotherapy in murine glioma models (Saha et al., 2020), and the data in Figure 5.8 suggesting limited benefits of

concurrent TMZ and radiation build a case towards a potentially different treatment regime with G207-NKG2DBiTE virus. These findings may lead to the conclusion that that pre-treatment of TMZ and radiation prior to surgical debulking and G207-NKG2DBiTE administration may provide the initial boost of increased NKG2DL expression, and then cessation of concurrent TMZ and radiation after surgery may allow for sustained TIL activity and prevent lymphopenia.

The data in Figure 5.9 suggest that the NKG2D BiTE activated T cells and caused more cytotoxicity with GSC-like U87 cells than differentiated U87 cells. This is in line with observations made by Oh et al., whereby GSC-like U87 cells cultured in NBM were more sensitive to NK cell lysis than differentiated U87 cells (Oh et al., 2017). While the data in Figure 5.9A demonstrated significantly higher MICA/B expression in differentiated U87 cells, the total NKG2DL expression trended towards being greater on GSC-like U87 cells, although this did not reach statistical significance (Figure 5.9B). This may be in line with the observations by Oh et al., who also reported increased total ULBP1 and ULBP3 mRNA and protein expression by western blot in GSC-like U87 cells than differentiated cells (Oh et al., 2017), and hence may explain the lower MICA/B expression, but slightly increased ULBP1 and ULBP3 on GSC-like U87 cells in Figure 5.9.

GSCs pose an significant obstacle to GBM therapy, often displaying resistance towards TMZ and radiotherapy (Bao et al., 2006; Qiu et al., 2014) that leads to post-treatment repopulation of the tumour with resistant cells (J. Chen et al., 2012). Alongside this resistance to conventional GBM therapy, GSCs limit the activity of oHSV-1. Peters et al. demonstrated that G207, with deletion of both copies of *γ34.5*, was able to translate true late (TL) proteins in bulk differentiated GBM cells, but was unable to in GSCs (Peters et al., 2018). This restriction of TL protein synthesis was

attributed to be because of a global inhibition of translation in GSCs when infected with G207, but early and 'leaky' late viral proteins could still be expressed (Peters et al., 2018). These findings are in line with the data in Figure 5.9 and Figure 5.10, whereby differentiated U87 or primary GBM cells were permissive to G207-NKG2DBiTE virus infection, but GSC-like cells displayed very low GFP expression, indicating poor permissiveness to the G207 virus.

GFP is encoded in the G207 viral genome within the *ICP6* locus (Terada et al., 2006), and so is driven by the *ICP6* promoter. The *ICP6* promoter is described as 'leaky' early (Sze & Herman, 1992), which should therefore allow translation of GFP in GSCs, based on the observations by Peters et al. that early and 'leaky' late genes could be translated (Peters et al., 2018). However, in the GSC-like U87 cells and primary GSC-like cells, the percentage of GFP^+ was not significantly increased compared to uninfected cells (Figure 5.9C and Figure 5.10A, respectively). The low percentage of GFP^+ cells may be explained by GSCs inhibiting G207 TL protein synthesis, thus limiting the number of viral genomes in the GSCs compared to differentiated GBM cells, thus resulting in fewer copies of the *GFP* gene, and thus lower GFP protein expression. This GFP lower expression may then not cross the threshold for detection by flow cytometry.

Nevertheless, despite the poor infectivity of GSCs by G207-NKG2DBiTE virus, the differentiated GBM cells were permissive and produced functional NKG2D BiTE. One could therefore infer that in a heterogeneous tumour cell population, containing sub-populations of differentiated GBM cells and GSCs, treatment with the G207-NKG2DBiTE virus would infect the bulk differentiated tumour cells (but not GSCs). This could then produce functional NKG2D BiTE that could direct T cell cytotoxicity towards the G207-resisitant GSCs, as well as the differentiated tumour cells.

Therefore, these data imply that the G207-NKG2DBiTE virus could provide a strategy for eliminating the GSC population that typically acts as a barrier to most GBM therapies.

5.5 Conclusions

GBMs are highly heterogeneous tumours, with sub-populations of GSCs and differentiated GBM cells. The resistant nature of GSCs to conventional GBM therapy as well as oncolytic virotherapy have made them a target for novel immunotherapies. The data in this chapter provides evidence that the G207-NKG2DBiTE virus is a promising candidate for GBM oncolytic virotherapy. Firstly, we have demonstrated the G207-NKG2DBiTE virus is able to infect GBM cells and produce functional BiTE which can activate T cells and direct cytotoxicity towards target cells. Furthermore, the G207 virus can infect the bulk differentiated GBM cells, which would enable localised production of the NKG2D BiTE within the tumour. This *in situ* expression of the NKG2D BiTE should enable TILs to direct cytotoxicity towards the GSC populations in the tumour and eradicate them. Finally, use of G207-NKG2DBiTE immunotherapy alongside radiation and TMZ increases the sensitivity of the target GBM cells to the BiTE, further increasing T cell activation and GBM cell cytotoxicity, confirming our initial hypothesis for this chapter, stated in section 5.2.1.

6 Thesis overview, final discussion, and conclusions

6.1 Thesis summary

GBM patient outcomes remain bleak, with little treatment advancement made in recent years. GBM is a highly complex disease, and its immunosuppressive, heterogeneous, infiltrative and therapy-resistant nature heavily influence a median survival time of only 14.6 months, despite TMZ chemotherapy and radiotherapy (McFaline-Figueroa & Lee, 2018). Therefore, there is a desperate need for novel therapeutic approaches for GBM.

One class of GBM therapies demonstrating great potential are OVs. While several different OVs have been developed and investigated in the context of GBM (Stavrakaki, Dirven, & Lamfers, 2021), oHSV-1 are the most clinically advanced (Nguyen & Saha, 2021), with the oHSV-1 G47Δ (DELYTACT) being approved for malignant glioma treatment in Japan (Daiichi Sankyo, 2021). The oHSV-1 G207 has been explored extensively in clinical trials for GBM and has demonstrated some encouraging results, but lacked overall efficacy (J. M. Markert et al., 2014). Therefore, the overall research goal of this thesis was to develop a novel method to enhance G207 oncolytic virotherapy of GBM in a strategy that could complement the current standard of care of TMZ and radiotherapy.

Given the success of engineering OVs to locally express BiTEs to direct T cell cytotoxicity towards target cells in the TME demonstrated by others in the field

(Freedman et al., 2017; Yu et al., 2014), this thesis explored the potential of arming G207 with BiTEs to enhance GBM immunotherapy. NKG2DLs were chosen as target ligands for a BiTE, since these components of the innate immune system could provide cancer-selective targets to focus T cell attack, that might become further upregulated when tumour cells are stressed during therapy (Baugh et al., 2020). In Chapter 3, a BiTE targeting NKG2DLs upregulated on GBM cells was characterised, demonstrating the ability to activate T cells independent of TCR specificity, HLA status or T cell subtype against GBM cell lines expressing NKG2DLs (Figure 3.3). The NKG2D BiTE was able to induce strong pro-inflammatory and cytotoxic responses from both $CD4^+$ and $CD8^+$ T cells, with increased expression of activation markers (CD25 and CD69), cytotoxic effector markers and molecules (CD107a, perforin and granzyme B) and pro-inflammatory cytokines (IFN-γ), culminating in GBM cell cytotoxicity (Figure 3.5). The NKG2D BiTE also demonstrated selectivity towards GBM cells expressing NKG2DLs, but not towards macrophages which lacked sufficient NKG2DLs for BiTE activity (Figure 3.6). Furthermore, resting T cells were shown to lack NKG2DL expression, although expression significantly increased following stimulation with anti-CD3/CD28 beads (Figure 3.7), confirming the observations that NKG2D BiTE does not activate resting T cells in the absence of target cells, due to the lack of T cell NKG2DL expression. However, whether the NKG2D BiTE activates resting T cells against stimulated T cells has not yet been addressed and is a matter for further investigation.

The results from Chapter 3 warranted further investigation into the relationship between NKG2DL expression and NKG2D BiTE activity. In Chapter 4, to develop the rationale for encoding the NKG2D BiTE into the G207 genome, the relationship between G207 infection and surface NKG2DL was explored. Given reports in the

literature that WT HSV-1 downregulated MICA/B in some cell lines (T. M. Campbell et al., 2015; Schepis et al., 2009), it was therefore also possible that G207 oHSV-1 would also downregulate MICA/B, and potentially limit the activity of the NKG2D BiTE. Subsequently, GBM cell lines infected with G207 demonstrated clear MICA/B downregulation, and cell line-dependent downregulation of total NKG2DLs (Figure 4.1), although this did not significantly affect the activity of the NKG2D BiTE towards these infected cells unless infected at a high MOI (Figure 4.2). This confirmed that G207 was a suitable virus to encode the NKG2D BiTE.

Additionally, following reports in the literature that DNA damage induced by TMZ and radiation caused increased NKG2DL expression on GBM cells (Lamb et al., 2013; Weiss, Schneider, et al., 2018; Weiss, Weller, et al., 2018), GBM cell lines, A172 and U87, demonstrated increased NKG2DLs following TMZ, radiation and a combination (Figure 4.3, Figure 4.4 and Figure 4.5). Furthermore, when pre-treated with sublethal doses of TMZ and radiation (50 μM and 2 Gy, respectively), this increased NKG2DL expression sensitised U87 cells to the NKG2D BiTE, resulting in enhanced T cell activation and cytotoxicity (Figure 4.6 and Figure 4.7). Pre-treatment also extended the effective concentration range of the NKG2D BiTE, allowing it to activate T cells even at a suboptimal concentration (0.1 nM) (Figure 4.6), synergising with NKG2D BiTE to induce U87 cell cytotoxicity (Figure 4.7). However, although pre-treatment also slightly increased expression of NKG2DLs on macrophages (Figure 4.8), the level of expression was still insufficient to be targeted by the NKG2D BiTE (Figure 4.9). These findings suggested that NKG2D BiTE immunotherapy might therefore be enhanced in patients undergoing TMZ and radiation, possibly without targeting other immune cells in the GBM TME.

Finally, T cells activated by NKG2D BiTE demonstrated the release of soluble mediators, likely IFN-γ, which induced increased expression of the pro-inflammatory macrophage marker, CD80, on immunosuppressive macrophages (Figure 4.10), and so suggests that NKG2D BiTE may begin to counteract the immunosuppressive TME in GBM.

Following on from the results of the previous chapters, the NKG2D BiTE was successfully encoded into the G207 genome in Chapter 5, and stocks of the G207-NKG2DBiTE and G207-ControlBiTE viruses were purified and characterised. The G207-NKG2DBiTE virus demonstrated good infectivity in U87 cells and elicited a dual mode of action for GBM cytotoxicity, by inducing direct oncolysis and NKG2D BiTE-mediated killing (Figure 5.2). The synergy following TMZ and radiation pre-treatment was also demonstrated using the G207-NKG2DBiTE virus, with enhanced T cell activation and U87 cell cytotoxicity compared to G207 or G207-ControlBiTE viruses, or pre-treatment alone (Figure 5.4, Figure 5.5 and Figure 5.6). Pre-treatment caused greater G207-NKG2DBiTE-mediated cytotoxicity, and this increased further with concomitant TMZ, whereas concomitant radiation had little benefit (Figure 5.8). These findings give further evidence that G207-NKG2DBiTE immunotherapy may complement the TMZ and radiation treatment regimens currently used for GBM, that usually lack sufficient potency to eradicate the tumour on their own.

The final sections of this thesis focus on GSCs, a sub-population of cells found in GBM that are capable of self-renewal and display resistant phenotypes to various therapies, including G207 infection (Kanai et al., 2012). One of the major limiting factors of G207 use in GBM clinical trials is thought to be the non-permissiveness of GSCs to G207 infection (Peters et al., 2018). Therefore, the activity of G207-

NKG2DBiTE virus against GSC-like U87 cells and patient derived GSC cells was investigated. We confirmed the poor permissiveness of GSCs to G207 infection compared to differentiated U87 or primary GBM cells (Figure 5.9 and Figure 5.10). Despite this, the differentiated GBM cells remained permissive to G207-NKG2DBiTE virus and produced functional NKG2D BiTE which triggered BiTE-mediated T cell activation and killing of GSC-like U87 and primary GSCs (Figure 5.9 and Figure 5.10).

These findings unveil a potentially novel strategy of targeting GSCs that has not been explored previously to our knowledge; using the G207-NKG2DBiTE virus to deliver the NKG2D BiTE to the GBM TME via infection of permissive differentiated GBM cells, which could then target TILs towards the non-permissive GSC sub-populations.

6.2 Final discussion

G207-NKG2DBiTE is an attractive candidate for further exploration in GBM immunotherapy. The G207 virus itself has been extensively tested in clinical settings and showed some promising signs of efficacy but has also highlighted issues for future oHSV-1 candidates to address, such as the need to effectively target GSCs. Nevertheless, the data in this thesis provides evidence that NKG2D BiTE immunotherapy would be well suited to complement current G207 and Stupp GBM therapy (Stupp et al., 2005) and could potentially address the current limitations of the G207 virus.

The data in this thesis present an exciting strategy for targeting NKG2DLs upregulated on GBM cells using the G207 virus to deliver the BiTE for localised expression. Although the data in this thesis are novel and could represent a

potentially beneficial new therapy option for GBM that may overcome current obstacles, it is not without its limitations. One major limitation of the experiments used throughout this thesis is that the T cells used in co-cultures with GBM cells were from PBMC-derived lymphocytes from healthy donors. These T cells are unlikely to be representative of the T cells in GBM patients. For instance, it has been demonstrated that GBM cells produce gangliosides capable of inducing apoptosis in T cells (Mahata et al., 2015). Furthermore, glioma patients have been shown to have fewer peripheral $CD3^+$ cells compared to healthy controls, which decreases further with glioma grade (P. Y. Chen et al., 2019), and that GBM TILs commonly express exhaustion markers (P. Y. Chen et al., 2019). Furthermore, patients undergoing Stupp therapy or steroid treatment (Stupp et al., 2005) reportedly have significant lymphopenia (Chitadze et al., 2017; Fadul et al., 2011). These reports in the literature therefore contrast with the use of healthy PBMC-derived T cells for this thesis, which were cultured in conditions that do not impede activation. Additionally, in all experiments in this thesis, T cells were co-cultured with target cells at a ratio of 5: 1, with no other immunosuppressive obstacles such as TAMs or ECM to interfere with target cell and T cell interactions. Therefore, while these co-culture assays have served as controlled platforms for proof of principle studies that require high sensitivity, they likely do not reflect the physiological interactions in GBM.

A potential future direction could involve using either autologous PBMC-derived T cells from the GBM patients, or to isolate $CD3^+$ cells from the disaggregated GBM tissue itself and use these physiologically relevant T cells for BiTE assays. This could be extended further by using a technique currently under development from our group involving incubating fresh slices of tumour tissue with free BiTE or OV expressing a BiTE. Assessment of immune activation and

cytotoxicity can then be obtained either measuring IFN-γ and LDH release into the supernatant, by staining for T cell activation markers via IHC, or by disaggregating the sample and staining for flow cytometry analysis. This technique thus utilises the live tumour cells *in situ* to be infected with OV and be targeted by the BiTE and TILs in the tumour slice, thus creating a more realistic model for assessing BiTE function.

The use of orthotopic GSC murine models have been explored extensively in the field of GBM OV therapy, both using murine GSCs in immunocompetent mice (Kleijn et al., 2014; Saha et al., 2017) and human GSCs in immunodeficient mice (Wakimoto et al., 2009). These models generate clinically relevant GBM that begin to recapitulate the GBM TME and can provide valuable information about the interactions between the virus, the GSCs and the immune response. However, there is little cross-reactivity between human and mouse NKG2D and their ligands (Y. Kim, Born, Bléry, & Steinle, 2020), and so would require either using humanised mice or engineering G207 expressing murine NKG2D BiTE. In light of this, the experiments in this thesis have pursued the use of human GBM tissue.

One potential limitation of NKG2D BiTE immunotherapy for GBM, and many other GBM immunotherapy strategies in general, is the somewhat limited number of TILs. This is highlighted in the immunophenotyping of the patient derived GBM sample (Figure 3.9), which contained fewer than 3% $CD3^+$ cells. It is also possible that these TILs from the sample were from the margins of the tissue, and perhaps over-represent the immune infiltration in the tumour core; unfortunately, no spatial information from the sample was obtained. To ensure the efficacy of the NKG2D BiTE, TILs are essential. Although, NKG2D BiTE therapy may be more successful than other strategies that rely on antigen-specific responses, as the NKG2D BiTE will activate any T cell, independent of its TCR specificity, HLA status of the target

cells, or whether it is $CD4^+$ or $CD8^+$. Furthermore, previous experiments using BiTEs have demonstrated T cell proliferation following BiTE activation (Freedman et al., 2017), and so NKG2D BiTE-mediated activation may trigger TIL expansion in the GBM TME, increasing the number of effector cells for BiTE therapy.

OVs also act as an immune stimulant in the GBM TME, as described in section 1.7, with increased pro-inflammatory signatures and TILs observed after OV therapy in mouse models and human tissue with a number of different OVs (Bernstock et al., 2019; Cheema et al., 2013; Van Den Bossche et al., 2018; van Putten et al., 2022). This could be further enhanced by encoding cytokines into the OV, such as with G47Δ-mIL-12, which increased TILs and IFN-γ production in orthotopic GSC models (Cheema et al., 2013; Saha et al., 2017).

Despite these potential limitations however, G207-NKG2DBiTE could also be expanded to other settings. For instance, G207 is currently being trialled for paediatric brain tumours alongside radiotherapy (Bernstock et al., 2020; Waters et al., 2017), and increased NKG2DLs have been reported in paediatric low grade gliomas, but not in high grade paediatric glioma (Haberthur et al., 2016). Therefore, G207-NKG2DBiTE virus may have further application in paediatric brain tumours as well as adult GBM.

We have demonstrated in section 5.3.7 and 5.3.8 that GSCs can trigger NKG2D BiTE-mediated T cell activation, despite being non-permissive to G207 infection, and so may provide an effective strategy to eradicate GSCs. A limitation of our study is that the only sources of GSCs used were from the U87 cell line, cultured from differentiated cells into GSC-like cell in NBM (Figure 5.9) or primary human GBM cells from a single patient that were also grown in NBM (Figure 5.10). This is unlikely to represent the degree of heterogeneity in GBM, and so more

patient-derived samples need to be analysed with the G207-NKG2DBiTE virus once they become available.

GSCs have several characteristics that may protect them from other immunotherapies but may still be targeted by the NKG2D BiTE. For instance, GSCs have been shown to downregulate MHC-I molecules (W. Yang et al., 2020), and may thus be protected from antigen-specific immune responses, potentially making a GBM cancer vaccine strategy unsuitable. Meanwhile, GSCs have been reported to express NKG2DLs (Flüh et al., 2018), and be effectively targeted with NKG2D-CAR-T cells (D. Yang et al., 2019), as well as the NKG2D BiTE used in this thesis (Figure 5.9 and Figure 5.10). Furthermore, the expression on GSCs, and bulk tumour cells, has been shown to be increased following Stupp therapy (Chitadze et al., 2017). Whether GSCs can be further sensitised to NKG2D BiTE following radiation and TMZ is yet to be investigated but is a research priority.

Despite the inability of G207 to infect GSCs, we have provided compelling evidence that G207-NKG2DBiTE virus can act as a delivery vector to infect differentiated GBM cells and produce NKG2D BiTE that can then target the sub-population of GSCs. However, if the G207-NKG2DBiTE virus was to prove ineffective in a clinical setting, perhaps due to insufficient infection to produce effective BiTE concentrations, then a more potent virus could be used to deliver the NKG2D BiTE. An example of a more potent oHSV-1 is G47Δ (DELYTACT), which recently gained approval for treatment of malignant glioma in Japan (Daiichi Sankyo, 2021), and has demonstrated the ability to successfully infect GSCs (Peters et al., 2018). Additionally, G47Δ has demonstrated the capacity to be armed with transgenes (Saha et al., 2017), therefore, it may be the next logical step for advancing the potency of oHSV-1-encoded NKG2D BiTE therapy.

Conversely, using the slightly underpowered G207 (compared to G47Δ) for NKG2D BiTE delivery to the GBM TME may provide an unsuspected advantage. For the experiments in chapter 5 using G207-NKG2DBiTE virus, an MOI of 0.1 was mostly used. This was to allow a significant proportion of the cells to remain uninfected initially so they could be targeted by the NKG2D BiTE being produced from the infected cells. However, when higher MOIs were used (MOI of 0.5 or 5) in U87 cells (Figure 5.2B and C), the T cell activation was decreased compared to MOI of 0.05. Despite this lower BiTE activity, the U87 cell viability was lower at MOI 0.5 and 5 compared to 0.05 (Figure 5.2D), indicating that at higher MOIs, the G207 virus was causing a direct oncolytic effect that superseded the NKG2D BiTE activity. The high MOIs may have caused significant viral oncolysis such that the cells were not viable to produce NKG2D BiTE any longer, or perhaps the high infection caused a downregulation of MICA/B (as observed in Figure 4.1) that rendered the NKG2D BiTE unable to bind to target cells. These observations demonstrate that there is a fine balance to be struck between the level of viral infection and BiTE production, and that if the level of infection is too great, it may impact the production of the BiTE. Therefore, there is a possibility that using G47Δ to express the NKG2D BiTE may tip the balance too far in the direction of viral oncolysis compared to G207, thus reducing the longevity and efficacy of the NKG2D BiTE. One could perhaps consider it as like a ‘Goldilocks’ scenario: G207 alone is not potent enough to eradicate GBM (“too cold”); G47Δ-NKG2DBiTE may prove too potent and undermine the potential of the NKG2D BiTE (“too hot”); but the G207-NKG2DBiTE virus may strike the right balance for viral oncolysis and BiTE delivery (“just right”).

Beyond oHSV-1 vectors to deliver the NKG2D BiTE for GBM therapy, other OVs could also be explored (Table 1.2). Delta24-RGD, an engineered oncolytic

adenovirus, has shown promising results in phase I clinical trials for recurrent GBM patients when administered using convection enhanced delivery (van Putten et al., 2022). Treatment with Delta24-RGD led to increases in pro-inflammatory cytokines in the CSF and brain interstitial fluid, as well as an increase in $CD4^+$, $CD8^+$ and NK cells in the CSF (van Putten et al., 2022). Furthermore, in subcutaneous tumours and *in vitro* using U87 cells, Delta24-RGD showed increased anti-tumour efficacy alongside radiation, but not in orthotopic glioma models (Lamfers et al., 2007). Meanwhile, in murine glioma models, Delta24-RGD demonstrated increased survival when also treated with TMZ compared to untreated controls, although this was not significantly improved compared to virus alone, and TMZ treatment reduced the number of $CD8^+$ TILs (Kleijn et al., 2017). Delta24-RGD has also previously been used as a vector to express other transgenes locally (Jiang et al., 2017; Rivera-Molina et al., 2019). Together, based on its recent clinical success in GBM, its induction of pro-inflammatory responses and immune cells, its use alongside TMZ and its capacity to encode transgenes, Delta24-RGD may also be a highly suitable vector to encode the NKG2D BiTE.

Moving beyond GBM, another adenovirus that would be well suited to express the NKG2D BiTE is EnAd. EnAd is a chimeric oncolytic adenovirus that has previously shown pre-clinical success with arming to express BiTEs (Freedman et al., 2018, 2017; Scott et al., 2019). While EnAd lacks a proven track record in GBM, it has shown success in epithelial tumour models, including in pre-clinical malignant ascites models (Scott et al., 2020), and it is currently being investigated in clinical trial for rectal cancer in combination with radiotherapy (O'Cathail et al., 2020). Furthermore, Pokrovska et al*.,* demonstrated synergy between EnAd and radiation *in vitro* and enhanced survival *in vivo* when given EnAd and radiation compared to

radiation alone (Pokrovska et al., 2020). Therefore, arming EnAd to express the NKG2D BiTE to use alongside radiotherapy in epithelial cancers is an exciting prospect, given the demonstrated synergy between radiation and EnAd (Pokrovska et al., 2020), and the NKG2D BiTE shown here in this thesis. EnAd-NKG2DBiTE is currently being investigated in our group.

The expression of NKG2DLs has widely been reported on a number of cancer types, including leukaemia (Salih et al., 2003), colorectal carcinoma (Watson et al., 2006), hepatocellular carcinoma (Jinushi et al., 2003), melanoma (Vetter et al., 2002), pancreatic carcinoma (Duan et al., 2011), breast carcinoma (de Kruijf et al., 2012) and glioma (Friese et al., 2003), but their expression on healthy cells is mostly absent (Schrambach et al., 2007). Given NKG2DL expression is mechanistically tied to various general phenotypes associated with cell stress and malignancy, such as the DDR and excessive proliferation (Gasser et al., 2005; Jung et al., 2012; Tokuyama et al., 2011), it would be difficult for cancer cells to avoid these general cancer-associated phenotypes (Hanahan & Weinberg, 2011). Cancers have evolved a number of means to avoid the subsequent immune response to NKG2DL expression by dysregulating the NKG2D response downstream of the induction of NKG2DL expression, such as ligand shedding or immune subversion (Table 1.5) (Baugh et al., 2020). Despite these downstream immune evasion tactics, the root of the cause for NKG2DL expression remains: the cancer phenotype itself. Perhaps with additional augmentation to prevent these immune evasion tactics, such as inhibition of NKG2DL shedding with MMP inhibitors (Shiraishi et al., 2016), NKG2DLs may serve as attractive pan-cancer antigens.

NKG2DLs have been investigated as a cancer immunotherapy target extensively using ACT approaches, such as NKG2D-CAR-T cells and engineered

TMZ-resistant γδ T cells (Lamb et al., 2013; Weiss, Weller, et al., 2018). However, these systemically administered cellular approaches for targeting NKG2DLs may potentially lead to on-target, off-tumour reactions if there were other cells in the body currently experiencing cell stress and had upregulated NKG2DLs. For instance, if the patient is also receiving radiotherapy and chemotherapy, it is possible that other healthy tissues perhaps on the path of the radiation beam, may upregulate NKG2DLs, and so trigger adoptive cell reactivity. These potential issues are less likely to impact the activity of the G207-NKG2DBiTE virus, as expression of the NKG2D BiTE will be restricted to the tumour due to virus selectivity.

This thesis was focussed on adapting an armed oHSV-1 to enhance conventional GBM therapy of TMZ and radiation. However, increasing NKG2DL expression on cancer cells for NKG2D BiTE immunotherapy is not necessarily restricted to using TMZ and radiation. For instance, inhibitors of histone deacetylases (HDAC) have been explored extensively for use in cancer therapy, and exert anti-cancer effects via a range of mechanisms (Eckschlager, Plch, Stiborova, & Hrabeta, 2017). HDAC inhibitors were shown to specifically induce NKG2DL expression in human hepatocellular carcinoma cells, sensitising them to NK cell lysis, but not in primary hepatocytes (Armeanu et al., 2005). Likewise, proteasome inhibitors have been shown to increase NKG2DL expression in a range of cell lines (Valés-Gómez, Chisholm, Cassady-Cain, Roda-Navarro, & Reyburn, 2008). Therefore, HDAC inhibitors could also be explored for use in combination with NKG2D BiTE immunotherapy.

Shedding of NKG2DLs from the surface of cancer cells is observed in a number of cancer types, and may be a means of immune evasion (Table 1.5) (Baugh et al., 2020), although we did not detect high levels of shedding from U87

cells (Appendices section 7.1.4). To address the issue of shedding NKG2DLs, chemical inhibitors of ADAM17, MMP-2 and MMP-9 have been demonstrated to restore surface NKG2DL expression on hepatocellular carcinoma and gastric cancer cells, re-sensitising them to NK cell lysis (Arai et al., 2018; Shiraishi et al., 2016). Similarly, antibodies have been generated against the α3 domain of MICA and MICB, blocking the proteolytic cleavage site, thus maintaining high MICA/B expression on a range of cancer cells that typically shed their ligands, resulting in inhibited tumour growth in melanoma mouse models (Ferrari de Andrade et al., 2018). These anti-cleavage site antibodies could potentially be encoded into an OV alongside the NKG2D BiTE to act in concert.

Other transgenes could also be encoded into an OV to further enhance NKG2DL expression. One specific example could be to use the oncolytic virus as a gene therapy vector to deliver short interfering RNA (siRNA) within the cancer cell, knocking down ADAM10 and ADAM17 expression, and thus prevent NKG2DL shedding. The cumulative effects of heightened NKG2DL expression normally associated with cancer cells, alongside virus-induced NKG2DL expression, with further siRNA-mediated inhibition of NKG2DL shedding could drastically increase the likelihood of immune detection and cancer cell lysis (Baugh et al., 2020).

The data in Chapter 4 suggests that G207 infection triggers downregulation of MICA/B, and total NKG2DLs in some GBM cell lines. If this became an issue in some patients, or if a patient's GBM cells did not express high levels of NKG2DLs, this could be addressed by further 'arming' the oHSV-1 used to deliver the NKG2D BiTE. Wirsching et al. engineered an oHSV-1 to express human ULBP3 which showed efficacy in a genetically engineered murine model of IDH WT GBM (Wirsching et al., 2019). However, the authors reported a novel, non-canonical

mechanism which was myeloid-dependent, suggesting a potential role for ULBP3 interacting with myeloid cells (Wirsching et al., 2019). Nevertheless, their study demonstrates the potential of encoding NKG2DLs into the oHSV-1 genome to be expressed alongside the NKG2D BiTE. This would ensure maintained surface NKG2DLs (particularly MICA or MICB) to overcome any downregulation by G207, or to increase the NKG2DL expression selectively in infected cancer cells, and thus ensure target ligands are present for the NKG2D BiTE. However, in the context of the 'Goldilocks' scenario stated above, this may then tip the scales too far in favour of cytotoxicity towards the infected cells themselves ("too hot"), due to increased ULBP3 expression. This could potentially result in the NKG2D BiTE limiting the infectivity of G207 as T cells are directed to kill the cells before a complete viral lifecycle can occur.

This thesis demonstrates G207-NKG2DBiTE virus could have potential clinical impact in the future. Before any clinical translation can take place, further questions need to be addressed, however. One key matter to address is the effect of TMZ and radiation on GSCs and whether it also sensitises them further to NKG2D BiTE, and is a matter of research priority. Additionally, more understanding is required of the expression of each of the NKG2DL during G207 infection and TMZ + radiotherapy, beyond simply MICA/B. Finally, an important future direction is to further extend the study using more clinically relevant material, including patient-derived GBM cell lines and fresh GBM surgical tissue.

To enable possible clinical translation in the future, other important questions need to be addressed. For instance, are stressed (but non-malignant) cells targeted by the NKG2D BiTE, particularly in the healthy brain parenchyma following radiotherapy and TMZ? This could be investigated with orthotopic murine GBM

models treated with TMZ with radiotherapy and a re-engineered NKG2D BiTE to target murine NKG2DLs and CD3. Also, further investigation into a clinically relevant dosing schedule and treatment regimen of G207-NKG2DBiTE alongside TMZ and radiotherapy would be required both *in vitro* and in orthotopic murine models, to evaluate whether concomitant Stupp therapy could feasibly work alongside G207-NKG2DBiTE immunotherapy in patients.

6.3 Concluding remarks

GBM is a highly challenging tumour to treat using conventional methods. Oncolytic virotherapy is an emerging therapeutic option and holds a great deal of potential, however, current strategies using the oHSV-1 G207 have lacked the potency to eradicate the tumour. The data in this thesis provides a novel means of enhancing G207 virotherapy for GBM with the virally-encoded NKG2D BiTE. Alongside the direct oncolytic activity of G207 itself, the localised expression of NKG2D BiTE in the tumour enables T cell-directed cytotoxicity towards transformed cells expressing pan-cancer antigens, NKG2DLs.

Current strategies for GBM therapy involve TMZ and radiation to induce tumour cell apoptosis, but tumours almost invariably recur and become resistant, suggesting they lack the direct cytotoxic potency to achieve tumour elimination. However, the G207-NKG2D BiTE may complement this treatment strategy, as the sublethal pre-treatment of GBM cells with radiation and TMZ may serve to further sensitise them to increased NKG2D BiTE activity.

Furthermore, GSCs are a stubborn obstacle that must be overcome to achieve successful GBM therapy to prevent recurrence. While GSCs are non-permissive to the G207 virus, they remain targetable with the NKG2D BiTE. Therefore, the G207-

NKG2DBiTE virus may serve as a gene therapy vector to achieve tumour-specific NKG2D BiTE expression which may then aid in the elimination of these GSCs.

G207-NKG2DBiTE virus is an exciting and novel immunotherapeutic approach in the treatment of GBM and could feasibly be translated into patients alongside conventional therapies to improve outcomes.

References

Adusumilli, P. S., Chan, M.-K., Chun, Y. S., Hezel, M., Chou, T.-C., Rusch, V. W., & Fong, Y. (2014). Cisplatin-induced GADD34 upregulation potentiates oncolytic viral therapy in the treatment of malignant pleural mesothelioma. *Cancer Biology & Therapy*, *5*(1), 48–53. https://doi.org/10.4161/cbt.5.1.2237

Adusumilli, P. S., Stiles, B. M., Chan, M. K., Chou, T. C., Wong, R. J., Rusch, V. W., & Fong, Y. (2005). Radiation therapy potentiates effective oncolytic viral therapy in the treatment of lung cancer. *Annals of Thoracic Surgery*, *80*(2), 409–417. https://doi.org/10.1016/j.athoracsur.2005.01.048

Advani, S. J., Sibley, G. S., Song, P. Y., Hallahan, D. E., Kataoka, Y., Roizman, B., & Weichselbaum, R. R. (1998). Enhancement of replication of genetically engineered herpes simplex viruses by ionizing radiation: A new paradigm for destruction of therapeutically intractable tumors. *Gene Therapy*, *5*(2), 160–165. https://doi.org/10.1038/sj.gt.3300546

Advani, Sunil J., Mezhir, J. J., Roizman, B., & Weichselbaum, R. R. (2006). ReVOLT: radiation-enhanced viral oncolytic therapy. *International Journal of Radiation Oncology Biology Physics*, *66*(3), 637–646. https://doi.org/10.1016/j.ijrobp.2006.06.034

Aldrak, N., Alsaab, S., Algethami, A., Bhere, D., Wakimoto, H., Shah, K., … Zaidan, N. (2021). Oncolytic herpes simplex virus-based therapies for cancer. *Cells*, *10*(6), 1–17. https://doi.org/10.3390/cells10061541

Allez, M., Tieng, V., Nakazawa, A., Treton, X., Pacault, V., Dulphy, N., … Toubert, A. (2007). CD4+NKG2D+ T Cells in Crohn's Disease Mediate Inflammatory and Cytotoxic Responses Through MICA Interactions. *Gastroenterology*, *132*(7), 2346–2358. https://doi.org/10.1053/j.gastro.2007.03.025

Andtbacka, R. H. I., Collichio, F., Harrington, K. J., Middleton, M. R., Downey, G., Öhrling, K., & Kaufman, H. L. (2019). Final analyses of OPTiM: A randomized phase III trial of talimogene laherparepvec versus granulocyte-macrophage colony-stimulating factor in unresectable stage III-IV melanoma. *Journal for ImmunoTherapy of Cancer*, *7*(1), 1–11. https://doi.org/10.1186/s40425-019-0623-z

Arai, J., Goto, K., Tanoue, Y., Ito, S., Muroyama, R., Matsubara, Y., … Kato, N. (2018). Enzymatic inhibition of MICA sheddase ADAM17 by lomofungin in hepatocellular carcinoma cells. *International Journal of Cancer*, *143*(10), 2575–2583. https://doi.org/10.1002/ijc.31615

Armeanu, S., Bitzer, M., Lauer, U. M., Venturelli, S., Pathil, A., Krusch, M., … Salih, H. R. (2005). Natural Killer Cell–Mediated Lysis of Hepatoma Cells via Specific Induction of NKG2D Ligands by the Histone Deacetylase Inhibitor Sodium Valproate. *Cancer Research*, *65*(14), 6321–6329. https://doi.org/10.1158/0008-5472.CAN-04-4252

Arnone, C. M., Polito, V. A., Mastronuzzi, A., Carai, A., Diomedi, F. C., Antonucci, L., … Del Bufalo, F. (2021). Oncolytic adenovirus and gene therapy with EphA2-BiTE for the treatment of pediatric high-grade gliomas. *Journal for ImmunoTherapy of Cancer*, *9*(5). https://doi.org/10.1136/jitc-2020-001930

Arruebo, M., Vilaboa, N., Sáez-Gutierrez, B., Lambea, J., Tres, A., Valladares, M., & González-Fernández, Á. (2011). Assessment of the evolution of cancer treatment therapies. *Cancers*, *3*(3), 3279–3330. https://doi.org/10.3390/cancers3033279

Ashiru, O., Bennett, N. J., Boyle, L. H., Thomas, M., Trowsdale, J., & Wills, M. R. (2009). NKG2D Ligand MICA Is Retained in the cis-Golgi Apparatus by Human Cytomegalovirus Protein UL142. *Journal of Virology*, *83*(23), 12345–12354. https://doi.org/10.1128/JVI.01175-09

Bacon, L., Eagle, R. A., Meyer, M., Easom, N., Young, N. T., & Trowsdale, J. (2004). Two Human ULBP/RAET1 Molecules with Transmembrane Regions Are Ligands for NKG2D. *The Journal of Immunology*, *173*(2), 1078–1084. https://doi.org/10.4049/jimmunol.173.2.1078

Badie, B., Schartner, J., Prabakaran, S., Paul, J., & Vorpahl, J. (2001). Expression of Fas ligand by microglia: Possible role in glioma immune evasion. *Journal of Neuroimmunology*, *120*(1–2), 19–24. https://doi.org/10.1016/S0165-5728(01)00361-7

Baeuerle, P. A., & Reinhardt, C. (2009). Bispecific T-cell engaging antibodies for cancer therapy. *Cancer Research*. https://doi.org/10.1158/0008-5472.CAN-09-0547

Bao, S., Wu, Q., McLendon, R. E., Hao, Y., Shi, Q., Hjelmeland, A. B., … Rich, J. N. (2006). Glioma stem cells promote radioresistance by preferential activation of the DNA damage response.

Nature, *444*(7120), 756–760. https://doi.org/10.1038/nature05236

Barrow, A. D., Martin, C. J., & Colonna, M. (2019). The natural cytotoxicity receptors in health and disease. *Frontiers in Immunology*, *10*(MAY), 1–20. https://doi.org/10.3389/fimmu.2019.00909

Bartkova, J., Hořejší, Z., Koed, K., Krämer, A., Tort, F., Zieger, K., … Bartek, J. (2005). DNA damage response as a candidate anti-cancer barrier in early human tumorigenesis. *Nature*, *434*(7035), 864–870. https://doi.org/10.1038/nature03482

Baskar, R., Dai, J., Wenlong, N., Yeo, R., & Yeoh, K. W. (2014). Biological response of cancer cells to radiation treatment. *Frontiers in Molecular Biosciences*, *1*(NOV), 1–9. https://doi.org/10.3389/fmolb.2014.00024

Baskar, R., Lee, K. A., Yeo, R., & Yeoh, K. W. (2012). Cancer and radiation therapy: Current advances and future directions. *International Journal of Medical Sciences*, *9*(3), 193–199. https://doi.org/10.7150/ijms.3635

Bauer, S. (1999). Activation of NK Cells and T Cells by NKG2D, a Receptor for Stress-Inducible MICA. *Science*, *285*(5428), 727–729. https://doi.org/10.1126/science.285.5428.727

Baugh, R., Khalique, H., & Seymour, L. W. (2020). Convergent Evolution by Cancer and Viruses in Evading the NKG2D Immune Response. https://doi.org/10.3390/cancers12123827

Bauman, Y., Nachmani, D., Vitenshtein, A., Tsukerman, P., Drayman, N., Stern-Ginossar, N., … Mandelboim, O. (2011). An Identical miRNA of the Human JC and BK Polyoma Viruses Targets the Stress-Induced Ligand ULBP3 to Escape Immune Elimination. *Cell Host & Microbe*, *9*(2), 93–102. https://doi.org/10.1016/j.chom.2011.01.008

Ben-Meir, K., Twaik, N., & Baniyash, M. (2018). Plasticity and biological diversity of myeloid derived suppressor cells. *Current Opinion in Immunology*, *51*, 154–161. https://doi.org/10.1016/j.coi.2018.03.015

Bergers, G., & Benjamin, L. E. (2003). Tumorigenesis and the angiogenic switch. *Nature Reviews Cancer*, *3*(6), 401–410. https://doi.org/10.1038/nrc1093

Bernstock, J. D., Bag, A. K., Fiveash, J., Kachurak, K., Elsayed, G., Chagoya, G., … Friedman, G. K. (2020). Design and Rationale for First-in-Human Phase 1 Immunovirotherapy Clinical Trial of Oncolytic HSV G207 to Treat Malignant Pediatric Cerebellar Brain Tumors. *Human Gene Therapy*, *31*(19–20), 1132–1139. https://doi.org/10.1089/hum.2020.101

Bernstock, J. D., Vicario, N., Rong, L., Valdes, P. A., Choi, B. D., Chen, J. A., … Friedman, G. K. (2019). A novel in situ multiplex immunofluorescence panel for the assessment of tumor immunopathology and response to virotherapy in pediatric glioblastoma reveals a role for checkpoint protein inhibition. *OncoImmunology*, *8*(12). https://doi.org/10.1080/2162402X.2019.1678921

Bhatia, A., & Kumar, Y. (2014). Cellular and molecular mechanisms in cancer immune escape: A comprehensive review. *Expert Review of Clinical Immunology*. https://doi.org/10.1586/1744666X.2014.865519

Bloch, O., Crane, C. A., Kaur, R., Safaee, M., Rutkowski, M. J., & Parsa, A. T. (2013). Gliomas Promote Immunosuppression through Induction of B7-H1 Expression in Tumor-Associated Macrophages, (8), 3165–3176. https://doi.org/10.1158/1078-0432.CCR-12-3314

Borchers, M. T., Harris, N. L., Wesselkamper, S. C., Vitucci, M., & Cosman, D. (2006). NKG2D ligands are expressed on stressed human airway epithelial cells. *American Journal of Physiology-Lung Cellular and Molecular Physiology*, *291*(2), L222–L231. https://doi.org/10.1152/ajplung.00327.2005

Boutet, P., Agüera-González, S., Atkinson, S., Pennington, C. J., Edwards, D. R., Murphy, G., … Valés-Gómez, M. (2009). Cutting Edge: The Metalloproteinase ADAM17/TNF-α-Converting Enzyme Regulates Proteolytic Shedding of the MHC Class I-Related Chain B Protein. *The Journal of Immunology*, *182*(1), 49–53. https://doi.org/10.4049/jimmunol.182.1.49

Breman, E., Demoulin, B., Agaugué, S., Mauën, S., Michaux, A., Springuel, L., … Steenwinckel, V. (2018). Overcoming Target Driven Fratricide for T Cell Therapy. *Frontiers in Immunology*, *9*(December), 1–11. https://doi.org/10.3389/fimmu.2018.02940

Brown, M. C., Holl, E. K., Boczkowski, D., Dobrikova, E., Mosaheb, M., Chandramohan, V., … Nair, S. K. (2017). Cancer immunotherapy with recombinant poliovirus induces IFN-dominant activation of dendritic cells and tumor antigen-specific CTLs. *Science Translational Medicine*, *9*(408), 1–17. https://doi.org/10.1126/scitranslmed.aan4220

Bryceson, Y. T., Ljunggren, H.-G., & Long, E. O. (2009). Minimal requirement for induction of natural cytotoxicity and intersection of activation signals by inhibitory receptors. *Blood*, *114*(13), 2657–2666. https://doi.org/10.1182/blood-2009-01-201632

Burton, C., Das, A., McDonald, D., Vandergrift III, W. A., Patel, S. J., Cachia, D., & Bartee, E. (2018). Oncolytic myxoma virus synergizes with standard of care for treatment of glioblastoma

multiforme. *Oncolytic Virotherapy*, *Volume 7*, 107–116. https://doi.org/10.2147/OV.S179335

Caldwell, C. C., Kojima, H., Lukashev, D., Armstrong, J., Farber, M., Apasov, S. G., & Sitkovsky, M. V. (2001). Differential Effects of Physiologically Relevant Hypoxic Conditions on T Lymphocyte Development and Effector Functions. *The Journal of Immunology*, *167*(11), 6140–6149. https://doi.org/10.4049/jimmunol.167.11.6140

Campbell, J. A., Trossman, D. S., Yokoyama, W. M., & Carayannopoulos, L. N. (2007). Zoonotic orthopoxviruses encode a high-affinity antagonist of NKG2D. *Journal of Experimental Medicine*, *204*(6), 1311–1317. https://doi.org/10.1084/jem.20062026

Campbell, T. M., McSharry, B. P., Steain, M., Slobedman, B., & Abendroth, A. (2015). Varicella-Zoster Virus and Herpes Simplex Virus 1 Differentially Modulate NKG2D Ligand Expression during Productive Infection. *Journal of Virology*, *89*(15), 7932–7943. https://doi.org/10.1128/JVI.00292-15

Cao, W., Xi, X., Wang, Z., Dong, L., Hao, Z., Cui, L., … He, W. (2008). Four novel ULBP splice variants are ligands for human NKG2D. *International Immunology*, *20*(8), 981–991. https://doi.org/10.1093/intimm/dxn057

Carayannopoulos, L. N., Naidenko, O. V., Fremont, D. H., & Yokoyama, W. M. (2002). Cutting Edge: Murine UL16-Binding Protein-Like Transcript 1: A Newly Described Transcript Encoding a High-Affinity Ligand for Murine NKG2D. *The Journal of Immunology*, *169*(8), 4079–4083. https://doi.org/10.4049/jimmunol.169.8.4079

Carelle, N., Piotto, E., Bellanger, A., Germanaud, J., Thuillier, A., & Khayat, D. (2002). Changing patient perceptions of the side effects of cancer chemotherapy. *Cancer*, *95*(1), 155–163. https://doi.org/10.1002/cncr.10630

Cassady, K. A. (2005). Human Cytomegalovirus TRS1 and IRS1 Gene Products Block the Double-Stranded-RNA-Activated Host Protein Shutoff Response Induced by Herpes Simplex Virus Type 1 Infection. *Journal of Virology*, *79*(14), 8707–8715. https://doi.org/10.1128/JVI.79.14.8707-8715.2005

Cassady, K. A., Gross, M., & Roizman, B. (1998). The Herpes Simplex Virus US11 Protein Effectively Compensates for the γ134.5 Gene if Present before Activation of Protein Kinase R by Precluding Its Phosphorylation and That of the α Subunit of Eukaryotic Translation Initiation Factor 2. *Journal of Virology*, *72*(11), 8620–8626. https://doi.org/10.1128/jvi.72.11.8620-8626.1998

Cerboni, C., Fionda, C., Soriani, A., Zingoni, A., Doria, M., Cippitelli, M., & Santoni, A. (2014). The DNA Damage Response: A Common Pathway in the Regulation of NKG2D and DNAM-1 Ligand Expression in Normal, Infected, and Cancer Cells. *Frontiers in Immunology*, *4*(JAN), 1–7. https://doi.org/10.3389/fimmu.2013.00508

Cerboni, C., Neri, F., Casartelli, N., Zingoni, A., Cosman, D., Rossi, P., … Doria, M. (2007). Human immunodeficiency virus 1 Nef protein downmodulates the ligands of the activating receptor NKG2D and inhibits natural killer cell-mediated cytotoxicity. *Journal of General Virology*, *88*(1), 242–250. https://doi.org/10.1099/vir.0.82125-0

Cerwenka, A., Bakker, A. B. ., McClanahan, T., Wagner, J., Wu, J., Phillips, J. H., & Lanier, L. L. (2000). Retinoic Acid Early Inducible Genes Define a Ligand Family for the Activating NKG2D Receptor in Mice. *Immunity*, *12*(6), 721–727. https://doi.org/10.1016/S1074-7613(00)80222-8

Cerwenka, A., Baron, J. L., & Lanier, L. L. (2001). Ectopic expression of retinoic acid early inducible-1 gene (RAE-1) permits natural killer cell-mediated rejection of a MHC class I-bearing tumor in vivo. *Proceedings of the National Academy of Sciences*, *98*(20), 11521–11526. https://doi.org/10.1073/pnas.201238598

Chabes, A., & Thelander, L. (2000). Controlled protein degradation regulates ribonucleotide reductase activity in proliferating mammalian cells during the normal cell cycle and in response to DNA damage and replication blocks. *Journal of Biological Chemistry*, *275*(23), 17747–17753. https://doi.org/10.1074/jbc.M000799200

Chabner, B. A., & Roberts, T. G. (2005). Chemotherapy and the war on cancer. *Nature Reviews Cancer*, *5*(1), 65–72. https://doi.org/10.1038/nrc1529

Chalupny, N. J., Rein-Weston, A., Dosch, S., & Cosman, D. (2006). Down-regulation of the NKG2D ligand MICA by the human cytomegalovirus glycoprotein UL142. *Biochemical and Biophysical Research Communications*, *346*(1), 175–181. https://doi.org/10.1016/j.bbrc.2006.05.092

Chambers, R., Gillespie, G. Y., Soroceanu, L., Andreansky, S., Chatterjee, S., Chou, J., … Whitley, R. J. (1995). Comparison of genetically engineered herpes simplex viruses for the treatment of brain tumors in a scid mouse model of human malignant glioma. *Proceedings of the National Academy of Sciences of the United States of America*, *92*(5), 1411–1415. https://doi.org/10.1073/pnas.92.5.1411

Cheema, T. A., Wakimoto, H., Fecci, P. E., Ning, J., Kuroda, T., Jeyaretna, D. S., … Rabkin, S. D. (2013). Multifaceted oncolytic virus therapy for glioblastoma in an immunocompetent cancer stem cell model. *Proceedings of the National Academy of Sciences of the United States of America*, *110*(29), 12006–12011. https://doi.org/10.1073/pnas.1307935110

Chen, J., Li, Y., Yu, T. S., McKay, R. M., Burns, D. K., Kernie, S. G., & Parada, L. F. (2012). A restricted cell population propagates glioblastoma growth after chemotherapy. *Nature*, *488*(7412), 522–526. https://doi.org/10.1038/nature11287

Chen, P. Y., Wu, C. Y. J., Fang, J. H., Chen, H. C., Feng, L. Y., Huang, C. Y., … Lin, C. Y. (2019). Functional Change of Effector Tumor-Infiltrating CCR5+CD38+HLA-DR+CD8+ T Cells in Glioma Microenvironment. *Frontiers in Immunology*, *10*(October), 1–14. https://doi.org/10.3389/fimmu.2019.02395

Chen, Q., Wu, J., Ye, Q., Ma, F., Zhu, Q., Wu, Y., … Qin, C. F. (2018). Treatment of human glioblastoma with a live attenuated Zika virus vaccine candidate. *MBio*, *9*(5), 1–13. https://doi.org/10.1128/mBio.01683-18

Cheng, P. H., Wechman, S. L., McMasters, K. M., & Zhou, H. S. (2015). Oncolytic replication of E1b-deleted adenoviruses. *Viruses*, *7*(11), 5767–5779. https://doi.org/10.3390/v7112905

Chiocca, E. A., Nakashima, H., Kasai, K., Fernandez, S. A., & Oglesbee, M. (2020). Preclinical Toxicology of rQNestin34.5v.2: An Oncolytic Herpes Virus with Transcriptional Regulation of the ICP34.5 Neurovirulence Gene. *Molecular Therapy - Methods and Clinical Development*, *17*(June), 871–893. https://doi.org/10.1016/j.omtm.2020.03.028

Chitadze, G., Flüh, C., Quabius, E. S., Freitag-Wolf, S., Peters, C., Lettau, M., … Kabelitz, D. (2017). In-depth immunophenotyping of patients with glioblastoma multiforme: Impact of steroid treatment. *OncoImmunology*, *6*(11), e1358839. https://doi.org/10.1080/2162402X.2017.1358839

Chitadze, G., Lettau, M., Luecke, S., Wang, T., Janssen, O., Fürst, D., … Kabelitz, D. (2016). NKG2D- and T-cell receptor-dependent lysis of malignant glioma cell lines by human γδ T cells: Modulation by temozolomide and A disintegrin and metalloproteases 10 and 17 inhibitors. *OncoImmunology*, *5*(4), e1093276. https://doi.org/10.1080/2162402X.2015.1093276

Choi, B. D., Yu, X., Castano, A. P., Bouffard, A. A., Schmidts, A., Larson, R. C., … Maus, M. V. (2019). CAR-T cells secreting BiTEs circumvent antigen escape without detectable toxicity. *Nature Biotechnology*, *37*(9), 1049–1058. https://doi.org/10.1038/s41587-019-0192-1

Chou, J., Kern, E. R., Whitley, R. J., & Roizman, B. (1990). Mapping of Herpes Simplex Virus-1 Neurovirulence to γ 1 34.5, a Gene Nonessential for Growth in Culture. *Science*, *250*(4985), 1262–1266. https://doi.org/10.1126/science.2173860

Chung, R. Y., Saeki, Y., & Chiocca, E. A. (1999). B- myb Promoter Retargeting of Herpes Simplex Virus γ34.5 Gene-Mediated Virulence toward Tumor and Cycling Cells . *Journal of Virology*, *73*(9), 7556–7564. https://doi.org/10.1128/jvi.73.9.7556-7564.1999

Clemente, C. G., Mihm, M. C., Bufalino, R., Zurrida, S., Collini, P., & Cascinelli, N. (1996). Prognostic value of tumor infiltrating lymphocytes in the vertical growth phase of primary cutaneous melanoma. *Cancer*, *77*(7). https://doi.org/10.1002/(SICI)1097-0142(19960401)77:7<1303::AID-CNCR12>3.0.CO;2-5

Cloughesy, T. F., Landolfi, J., Vogelbaum, M. A., Ostertag, D., Elder, J. B., Bloomfield, S., … Walbert, T. (2018). Durable complete responses in some recurrent high-grade glioma patients treated with Toca 511 + Toca FC. *Neuro-Oncology*, *20*(10), 1383–1392. https://doi.org/10.1093/neuonc/noy075

Coley, W. B. (1895). THE TREATMENT OF INOPERABLE MALIGNANT TUMORS WITH THE TOXINS OF ERYSIPELAS AND BACILLUS PRODIGIOSUS. *The American Journal of the Medical Sciences*, *110*(5), 608. https://doi.org/10.1097/00000441-189511000-00038

Coniglio, S. J., Eugenin, E., Dobrenis, K., Stanley, E. R., West, B. L., Symons, M. H., & Segall, J. E. (2012). Microglial stimulation of glioblastoma invasion involves epidermal growth factor receptor (EGFR) and colony stimulating factor 1 receptor (CSF-1R) signaling. *Molecular Medicine (Cambridge, Mass.)*, *18*(1), 519–527. https://doi.org/10.2119/molmed.2011.00217

Conry, R. M., Westbrook, B., McKee, S., & Norwood, T. G. (2018). Talimogene laherparepvec: First in class oncolytic virotherapy. *Human Vaccines & Immunotherapeutics*, *14*(4), 839–846. https://doi.org/10.1080/21645515.2017.1412896

Corrales, L., McWhirter, S. M., Dubensky, T. W., & Gajewski, T. F. (2016). The host STING pathway at the interface of cancer and immunity. *Journal of Clinical Investigation*, *126*(7), 2404–2411. https://doi.org/10.1172/JCI86892

Cosman, D., Müllberg, J., Sutherland, C. L., Chin, W., Armitage, R., Fanslow, W., … Chalupny, N. J. (2001). ULBPs, Novel MHC Class I–Related Molecules, Bind to CMV Glycoprotein UL16 and

Stimulate NK Cytotoxicity through the NKG2D Receptor. *Immunity*, *14*(2), 123–133. https://doi.org/10.1016/S1074-7613(01)00095-4

Crane, C. A., Austgen, K., Haberthur, K., Hofmann, C., Moyes, K. W., Avanesyan, L., … Lanier, L. L. (2014). Immune evasion mediated by tumor-derived lactate dehydrogenase induction of NKG2D ligands on myeloid cells in glioblastoma patients. *Proceedings of the National Academy of Sciences*, *111*(35), 12823–12828. https://doi.org/10.1073/pnas.1413933111

Crane, C. A., Han, S. J., Barry, J. J., Ahn, B. J., Lanier, L. L., & Parsa, A. T. (2010). TGF-downregulates the activating receptor NKG2D on NK cells and CD8+ T cells in glioma patients. *Neuro-Oncology*, *12*(1), 7–13. https://doi.org/10.1093/neuonc/nop009

Cribaro, G. P., Saavedra-López, E., Romarate, L., Mitxitorena, I., Díaz, L. R., Casanova, P. V., … Barcia, C. (2021). Three-dimensional vascular microenvironment landscape in human glioblastoma. *Acta Neuropathologica Communications*, *9*(1), 1–20. https://doi.org/10.1186/s40478-020-01115-0

Cully, M., You, H., Levine, A. J., & Mak, T. W. (2006). Beyond PTEN mutations: the PI3K pathway as an integrator of multiple inputs during tumorigenesis. *Nature Reviews Cancer*, *6*(3), 184–192. https://doi.org/10.1038/nrc1819

da Fonseca, A. C. C., Wang, H., Fan, H., Chen, X., Zhang, I., Zhang, L., … Badie, B. (2014). Increased expression of stress inducible protein 1 in glioma-associated microglia/macrophages. *Journal of Neuroimmunology*, *274*(1–2), 71–77. https://doi.org/10.1016/j.jneuroim.2014.06.021

Dahlstrand, J., Collins, V. P., & Lendahl, U. (1992). Expression of the class VI intermediate filament nestin in human central nervous system tumors. *Cancer Research*, *52*(19), 5334–5341. article. Retrieved from http://www.ncbi.nlm.nih.gov/pubmed/1382841

Daiichi Sankyo. (2021). Press Release DELYTACT ® Oncolytic Virus G47Δ Approved in Japan for Treatment of Patients with Malignant Glioma, 3–5. Retrieved from www.daiichisankyo.com.

das Neves, S. P., Delivanoglou, N., & Da Mesquita, S. (2021). CNS-Draining Meningeal Lymphatic Vasculature: Roles, Conundrums and Future Challenges. *Frontiers in Pharmacology*, *12*(April), 1–17. https://doi.org/10.3389/fphar.2021.655052

de Kruijf, E. M., Sajet, A., van Nes, J. G. H., Putter, H., Smit, V. T. H. B. M., Eagle, R. A., … Kuppen, P. J. K. (2012). NKG2D ligand tumor expression and association with clinical outcome in early breast cancer patients: an observational study. *BMC Cancer*, *12*(1), 24. https://doi.org/10.1186/1471-2407-12-24

DeCordova, S., Shastri, A., Tsolaki, A. G., Yasmin, H., Klein, L., Singh, S. K., & Kishore, U. (2020). Molecular Heterogeneity and Immunosuppressive Microenvironment in Glioblastoma. *Frontiers in Immunology*, *11*(July), 1–18. https://doi.org/10.3389/fimmu.2020.01402

Deli, M. A., Ábrahám, C. S., Kataoka, Y., & Niwa, M. (2005). Permeability studies on in vitro blood-brain barrier models: Physiology, pathology, and pharmacology. *Cellular and Molecular Neurobiology*, *25*(1), 59–127. https://doi.org/10.1007/s10571-004-1377-8

Dhatchinamoorthy, K., Colbert, J. D., & Rock, K. L. (2021). Cancer Immune Evasion Through Loss of MHC Class I Antigen Presentation. *Frontiers in Immunology*, *12*(March). https://doi.org/10.3389/fimmu.2021.636568

Di Paolo, N. C., Miao, E. A., Iwakura, Y., Murali-Krishna, K., Aderem, A., Flavell, R. A., … Shayakhmetov, D. M. (2009). Virus Binding to a Plasma Membrane Receptor Triggers Interleukin-1α-Mediated Proinflammatory Macrophage Response In Vivo. *Immunity*, *31*(1), 110–121. https://doi.org/10.1016/j.immuni.2009.04.015

Di Tomaso, T., Mazzoleni, S., Wang, E., Sovena, G., Clavenna, D., Franzin, A., … Maccalli, C. (2010). Immunobiological Characterization of Cancer Stem Cells Isolated from Glioblastoma Patients. *Clinical Cancer Research*, *16*(3), 800–813. https://doi.org/10.1158/1078-0432.CCR-09-2730

Di, Y., Seymour, L., & Fisher, K. (2014). Activity of a group B oncolytic adenovirus (ColoAd1) in whole human blood. *Gene Therapy*, *21*(4), 440–443. https://doi.org/10.1038/gt.2014.2

Diefenbach, A., Jamieson, A. M., Liu, S. D., Shastri, N., & Raulet, D. H. (2000). Ligands for the murine NKG2D receptor: expression by tumor cells and activation of NK cells and macrophages. *Nature Immunology*, *1*(2), 119–126. https://doi.org/10.1038/77793

Diefenbach, A., Jensen, E. R., Jamieson, A. M., & Raulet, D. H. (2001). Rae1 and H60 ligands of the NKG2D receptor stimulate tumour immunity. *Nature*, *413*(6852), 165–171. https://doi.org/10.1038/35093109

Ding, P., Wang, W., Wang, J., Yang, Z., & Xue, L. (2014). Expression of Tumor-Associated Macrophage in Progression of Human Glioma. *Cell Biochemistry and Biophysics*, *70*(3), 1625–1631. https://doi.org/10.1007/s12013-014-0105-3

Dock, G. (1904). the Influence of Complicating Diseases Upon Leukæmia.*. *The American Journal of the Medical Sciences*. https://doi.org/10.1097/00000441-190412740-00001

Duan, X., Deng, L., Chen, X., Lu, Y., Zhang, Q., Zhang, K., … Sun, W. (2011). Clinical significance of the immunostimulatory MHC class I chain-related molecule A and NKG2D receptor on NK cells in pancreatic cancer. *Medical Oncology*, *28*(2), 466–474. https://doi.org/10.1007/s12032-010-9480-9

Dubinski, D., Wölfer, J., Hasselblatt, M., Schneider-Hohendorf, T., Bogdahn, U., Stummer, W., … Grauer, O. M. (2016). CD4+ T effector memory cell dysfunction is associated with the accumulation of granulocytic myeloid-derived suppressor cells in glioblastoma patients. *Neuro-Oncology*, *18*(6), 807–818. https://doi.org/10.1093/neuonc/nov280

Dubois, L. G., Campanati, L., Righy, C., Dâ€™Andrea-Meira, I., Spohr, T. C. L. de S. e, Porto-Carreiro, I., … Moura-Neto, V. (2014). Gliomas and the vascular fragility of the blood brain barrier. *Frontiers in Cellular Neuroscience*, *8*(December), 1–13. https://doi.org/10.3389/fncel.2014.00418

Dunn, C., Chalupny, N. J., Sutherland, C. L., Dosch, S., Sivakumar, P. V., Johnson, D. C., & Cosman, D. (2003). Human Cytomegalovirus Glycoprotein UL16 Causes Intracellular Sequestration of NKG2D Ligands, Protecting Against Natural Killer Cell Cytotoxicity. *Journal of Experimental Medicine*, *197*(11), 1427–1439. https://doi.org/10.1084/jem.20022059

Dunn, G. P., Bruce, A. T., Ikeda, H., Old, L. J., & Schreiber, R. D. (2002). Cancer immunoediting: from immunosurveillance to tumor escape. *Nature Immunology*, *3*(11), 991–998. https://doi.org/10.1038/ni1102-991

Dvorak, H. F. (2003). How tumors make bad blood vessels and stroma. *American Journal of Pathology*, *162*(6), 1747–1757. https://doi.org/10.1016/S0002-9440(10)64309-X

Dyer, A., Di, Y., Calderon, H., Illingworth, S., Kueberuwa, G., Tedcastle, A., … Seymour, L. W. (2017). Oncolytic Group B Adenovirus Enadenotucirev Mediates Non-apoptotic Cell Death with Membrane Disruption and Release of Inflammatory Mediators. *Molecular Therapy - Oncolytics*, *4*(March), 18–30. https://doi.org/10.1016/j.omto.2016.11.003

Eagle, R. A., Traherne, J. A., Hair, J. R., Jafferji, I., & Trowsdale, J. (2009). ULBP6/RAET1L is an additional human NKG2D ligand. *European Journal of Immunology*, *39*(11), 3207–3216. https://doi.org/10.1002/eji.200939502

Eagle, R. A., & Trowsdale, J. (2007). Promiscuity and the single receptor: NKG2D. *Nature Reviews Immunology*, *7*(9), 737–744. https://doi.org/10.1038/nri2144

Eckschlager, T., Plch, J., Stiborova, M., & Hrabeta, J. (2017). Histone deacetylase inhibitors as anticancer drugs. *International Journal of Molecular Sciences*, *18*(7), 1–25. https://doi.org/10.3390/ijms18071414

Eisele, G. (2006). TGF- and metalloproteinases differentially suppress NKG2D ligand surface expression on malignant glioma cells. *Brain*, *129*(9), 2416–2425. https://doi.org/10.1093/brain/awl205

Enk, J., Levi, A., Weisblum, Y., Yamin, R., Charpak-Amikam, Y., Wolf, D. G., & Mandelboim, O. (2016). HSV1 MicroRNA Modulation of GPI Anchoring and Downstream Immune Evasion. *Cell Reports*, *17*(4), 949–956. https://doi.org/10.1016/j.celrep.2016.09.077

Erra Díaz, F., Dantas, E., & Geffner, J. (2018). Unravelling the interplay between extracellular acidosis and immune cells. *Mediators of Inflammation*. https://doi.org/10.1155/2018/1218297

Esteso, G., Guerra, S., Valés-Gómez, M., & Reyburn, H. T. (2017). Innate immune recognition of double-stranded RNA triggers increased expression of NKG2D ligands after virus infection. *Journal of Biological Chemistry*, *292*(50), 20472–20480. https://doi.org/10.1074/jbc.M117.818393

Esteso, G., Luzón, E., Sarmiento, E., Gómez-Caro, R., Steinle, A., Murphy, G., … Reyburn, H. T. (2014). Altered MicroRNA Expression after Infection with Human Cytomegalovirus Leads to TIMP3 Downregulation and Increased Shedding of Metalloprotease Substrates, Including MICA. *The Journal of Immunology*, *193*(3), 1344–1352. https://doi.org/10.4049/jimmunol.1303441

Fadul, C. E., Fisher, J. L., Gui, J., Hampton, T. H., Côté, A. L., & Ernstoff, M. S. (2011). Immune modulation effects of concomitant temozolomide and radiation therapy on peripheral blood mononuclear cells in patients with glioblastoma multiforme. *Neuro-Oncology*, *13*(4), 393–400. https://doi.org/10.1093/neuonc/noq204

Fajardo, C. A., Guedan, S., Rojas, L. A., Moreno, R., Arias-Badia, M., De Sostoa, J., … Alemany, R. (2017). Oncolytic adenoviral delivery of an EGFR-targeting t-cell engager improves antitumor efficacy. *Cancer Research*, *77*(8), 2052–2063. https://doi.org/10.1158/0008-5472.CAN-16-1708

Farassati, F., Yang, A. D., & Lee, P. W. K. (2001). Oncogenes in Ras signalling pathway dictate host-cell permissiveness to herpes simplex virus 1. *Nature Cell Biology*, *3*(8), 745–750. https://doi.org/10.1038/35087061

Ferguson, M. S., Lemoine, N. R., & Wang, Y. (2012). Systemic delivery of oncolytic viruses: Hopes and hurdles. *Advances in Virology*, *2012*. https://doi.org/10.1155/2012/805629

Ferrari de Andrade, L., Tay, R. E., Pan, D., Luoma, A. M., Ito, Y., Badrinath, S., … Wucherpfennig, K. W. (2018). Antibody-mediated inhibition of MICA and MICB shedding promotes NK cell–driven tumor immunity. *Science*, *359*(6383), 1537–1542. https://doi.org/10.1126/science.aao0505

Fielding, C. A., Aicheler, R., Stanton, R. J., Wang, E. C. Y., Han, S., Seirafian, S., … Tomasec, P. (2014). Two Novel Human Cytomegalovirus NK Cell Evasion Functions Target MICA for Lysosomal Degradation. *PLoS Pathogens*, *10*(5), e1004058. https://doi.org/10.1371/journal.ppat.1004058

Fielding, C. A., Weekes, M. P., Nobre, L. V., Ruckova, E., Wilkie, G. S., Paulo, J. A., … Wilkinson, G. W. G. (2017). Control of immune ligands by members of a cytomegalovirus gene expansion suppresses natural killer cell activation. *ELife*, *6*, 1–27. https://doi.org/10.7554/eLife.22206

Fischer, K., Hoffmann, P., Voelkl, S., Meidenbauer, N., Ammer, J., Edinger, M., … Kreutz, M. (2007). Inhibitory effect of tumor cell-derived lactic acid on human T cells. *Blood*, *109*(9). https://doi.org/10.1182/blood-2006-07-035972

Fisher, K., Hazini, A., & Seymour, L. W. (2021). Tackling HLA Deficiencies Head on with Oncolytic Viruses. *Cancers*, *13*(4), 719. https://doi.org/10.3390/cancers13040719

Flügel, A., Labeur, M. S., Grasbon-Frodl, E. M., Kreutzberg, G. W., & Graeber, M. B. (1999). Microglia only weakly present glioma antigen to cytotoxic T cells. *International Journal of Developmental Neuroscience*, *17*(5–6), 547–556. https://doi.org/10.1016/S0736-5748(99)00020-9

Flüh, C., Chitadze, G., Adamski, V., Hattermann, K., Synowitz, M., Kabelitz, D., & Held-Feindt, J. (2018). NKG2D ligands in glioma stem-like cells: expression in situ and in vitro. *Histochemistry and Cell Biology*, *149*(3), 219–233. https://doi.org/10.1007/s00418-018-1633-5

Freedman, J. D., Duffy, M. R., Lei-Rossmann, J., Muntzer, A., Scott, E. M., Hagel, J., … Fisher, K. D. (2018). An Oncolytic Virus Expressing a T-cell Engager Simultaneously Targets Cancer and Immunosuppressive Stromal Cells. *Cancer Research*, *78*(24), 6852–6865. https://doi.org/10.1158/0008-5472.CAN-18-1750

Freedman, J. D., Hagel, J., Scott, E. M., Psallidas, I., Gupta, A., Spiers, L., … Seymour, L. W. (2017). Oncolytic adenovirus expressing bispecific antibody targets T-cell cytotoxicity in cancer biopsies. *EMBO Molecular Medicine*, *9*(8), 1067–1087. https://doi.org/10.15252/emmm.201707567

Friedberg, J. W. (2005). Unique toxicities and resistance mechanisms associated with monoclonal antibody therapy. *Hematology / the Education Program of the American Society of Hematology. American Society of Hematology. Education Program*, 329–334. https://doi.org/10.1182/asheducation-2005.1.329

Friese, M. A., Platten, M., Lutz, S. Z., Naumann, U., Aulwurm, S., Bischof, F., … Weller, M. (2003). MICA/NKG2D-mediated immunogene therapy of experimental gliomas. *Cancer Research*, *63*(24), 8996–9006. Retrieved from http://www.ncbi.nlm.nih.gov/pubmed/14695218

Friese, M. A., Wischhusen, J., Wick, W., Weiler, M., Eisele, G., Steinle, A., & Weller, M. (2004). RNA Interference Targeting Transforming Growth Factor-β Enhances NKG2D-Mediated Antiglioma Immune Response, Inhibits Glioma Cell Migration and Invasiveness, and Abrogates Tumorigenicity In vivo. *Cancer Research*, *64*(20), 7596–7603. https://doi.org/10.1158/0008-5472.CAN-04-1627

Fuertes, M. B., Girart, M. V., Molinero, L. L., Domaica, C. I., Rossi, L. E., Barrio, M. M., … Zwirner, N. W. (2008). Intracellular Retention of the NKG2D Ligand MHC Class I Chain-Related Gene A in Human Melanomas Confers Immune Privilege and Prevents NK Cell-Mediated Cytotoxicity. *The Journal of Immunology*, *180*(7), 4606–4614. https://doi.org/10.4049/jimmunol.180.7.4606

Fueyo, J., Gomez-Manzano, C., Alemany, R., Lee, P. S., McDonnell, T. J., Mitlianga, P., … Kyritsis, A. P. (2000). A mutant oncolytic adenovirus targeting the Rb pathway produces anti-glioma effect in vivo. *Oncogene*, *19*(1), 2–12. https://doi.org/10.1038/sj.onc.1203251

Galon, J., Costes, A., Sanchez-Cabo, F., Kirilovsky, A., Mlecnik, B., Lagorce-Pagès, C., … Pagès, F. (2006). Type, Density, and Location of Immune Cells Within Human Colorectal Tumors Predict Clinical Outcome. *Science*, *313*(5795), 1960–1964. https://doi.org/10.1126/science.1129139

García-Romero, N., Palacín-Aliana, I., Esteban-Rubio, S., Madurga, R., Rius-Rocabert, S., Carrión-Navarro, J., … Ayuso-Sacido, A. (2020). Newcastle Disease Virus (NDV) Oncolytic Activity in Human Glioma Tumors Is Dependent on CDKN2A-Type I IFN Gene Cluster Codeletion. *Cells*, *9*(6), 1–17. https://doi.org/10.3390/cells9061405

Gardell, J. L., Matsumoto, L. R., Chinn, H., DeGolier, K. R., Kreuser, S. A., Prieskorn, B., … Crane, C. A. (2020). Human macrophages engineered to secrete a bispecific T cell engager support antigen-dependent T cell responses to glioblastoma. *Journal for Immunotherapy of Cancer*, *8*(2), 1–14. https://doi.org/10.1136/jitc-2020-001202

Garrido, F., Perea, F., Bernal, M., Sánchez-Palencia, A., Aptsiauri, N., & Ruiz-Cabello, F. (2017). The escape of cancer from T cell-mediated immune surveillance: HLA class I loss and tumor tissue architecture. *Vaccines*. https://doi.org/10.3390/vaccines5010007

Gascard, P., & Tlsty, T. D. (2016). Carcinoma-associated fibroblasts: Orchestrating the composition of malignancy. *Genes and Development*. https://doi.org/10.1101/gad.279737.116

Gasser, S., Orsulic, S., Brown, E. J., & Raulet, D. H. (2005). The DNA damage pathway regulates innate immune system ligands of the NKG2D receptor. *Nature*, *436*(7054), 1186–1190. https://doi.org/10.1038/nature03884

Geiger, R., Rieckmann, J. C., Wolf, T., Basso, C., Feng, Y., Fuhrer, T., … Lanzavecchia, A. (2016). L-Arginine Modulates T Cell Metabolism and Enhances Survival and Anti-tumor Activity. *Cell*, *167*(3), 829-842.e13. article. https://doi.org/10.1016/j.cell.2016.09.031

Ghonime, M. G., Jackson, J., Shah, A., Roth, J., Li, M., Saunders, U., … Cassady, K. A. (2018). Chimeric HCMV/HSV-1 and Δγ134.5 oncolytic herpes simplex virus elicit immune mediated antigliomal effect and antitumor memory. *Translational Oncology*, *11*(1), 86–93. https://doi.org/10.1016/J.TRANON.2017.10.005

Goldsmith, K., Chen, W., Johnson, D. C., & Hendricks, R. L. (1998). Infected cell protein (ICP)47 enhances herpes simplex virus neurovirulence by blocking the CD8+ T cell response. *Journal of Experimental Medicine*, *187*(3), 341–348. https://doi.org/10.1084/jem.187.3.341

Goldstein, D. J., & Weller, S. K. (1988). Herpes simplex virus type 1-induced ribonucleotide reductase activity is dispensable for virus growth and DNA synthesis: isolation and characterization of an ICP6 lacZ insertion mutant. *Journal of Virology*, *62*(1), 196–205. https://doi.org/10.1128/jvi.62.1.196-205.1988

Gong, J., & Mita, M. M. (2014). Activated Ras signaling pathways and reovirus oncolysis: An update on the mechanism of preferential reovirus replication in cancer cells. *Frontiers in Oncology*, *4 JUN*(June), 1–7. https://doi.org/10.3389/fonc.2014.00167

Gorgoulis, V. G., Vassiliou, L.-V. F., Karakaidos, P., Zacharatos, P., Kotsinas, A., Liloglou, T., … Halazonetis, T. D. (2005). Activation of the DNA damage checkpoint and genomic instability in human precancerous lesions. *Nature*, *434*(7035), 907–913. https://doi.org/10.1038/nature03485

Gras Navarro, A., Kmiecik, J., Leiss, L., Zelkowski, M., Engelsen, A., Bruserud, Ø., … Chekenya, M. (2014). NK Cells with KIR2DS2 Immunogenotype Have a Functional Activation Advantage To Efficiently Kill Glioblastoma and Prolong Animal Survival. *The Journal of Immunology*, *193*(12), 6192–6206. https://doi.org/10.4049/jimmunol.1400859

Groh, V. (1998). Recognition of Stress-Induced MHC Molecules by Intestinal Epithelial T Cells. *Science*, *279*(5357), 1737–1740. https://doi.org/10.1126/science.279.5357.1737

Groh, V., Bahram, S., Bauer, S., Herman, A., Beauchamp, M., & Spies, T. (1996). Cell stress-regulated human major histocompatibility complex class I gene expressed in gastrointestinal epithelium. *Proceedings of the National Academy of Sciences of the United States of America*, *93*(22), 12445–12450. https://doi.org/10.1073/pnas.93.22.12445

Groh, V., Rhinehart, R., Randolph-Habecker, J., Topp, M. S., Riddell, S. R., & Spies, T. (2001). Costimulation of CD8αβ T cells by NKG2D via engagement by MIC induced on virus-infected cells. *Nature Immunology*, *2*(3), 255–260. https://doi.org/10.1038/85321

Groh, V., Wu, J., Yee, C., & Spies, T. (2002). Tumour-derived soluble MIC ligands impair expression of NKG2D and T-cell activation. *Nature*, *419*(6908), 734–738. https://doi.org/10.1038/nature01112

Gromeier, M., Alexander, L., & Wimmer, E. (1996). Internal ribosomal entry site substitution eliminates neurovirulence in intergeneric poliovirus recombinants. *Proceedings of the National Academy of Sciences of the United States of America*, *93*(6), 2370–2375. https://doi.org/10.1073/pnas.93.6.2370

Guan, Y., Li, W., Hou, Z., Han, Q., Lan, P., Zhang, J., … Zhang, C. (2016). HBV suppresses expression of MICA/B on hepatoma cells through up-regulation of transcription factors GATA2 and GATA3 to escape from NK cell surveillance. *Oncotarget*, *7*(35), 56107–56119.

https://doi.org/10.18632/oncotarget.11271
Guerra, N., Tan, Y. X., Joncker, N. T., Choy, A., Gallardo, F., Xiong, N., … Raulet, D. H. (2008). NKG2D-Deficient Mice Are Defective in Tumor Surveillance in Models of Spontaneous Malignancy. *Immunity*, *28*(4), 571–580. https://doi.org/10.1016/j.immuni.2008.02.016
Haberthur, K., Brennan, K., Hoglund, V., Balcaitis, S., Chinn, H., Davis, A., … Crane, C. A. (2016). NKG2D ligand expression in pediatric brain tumors. *Cancer Biology and Therapy*, *17*(12), 1253–1265. https://doi.org/10.1080/15384047.2016.1250047
Hallmann, R., Zhang, X., Di Russo, J., Li, L., Song, J., Hannocks, M. J., & Sorokin, L. (2015). The regulation of immune cell trafficking by the extracellular matrix. *Current Opinion in Cell Biology*. https://doi.org/10.1016/j.ceb.2015.06.006
Hambardzumyan, D., Gutmann, D. H., & Kettenmann, H. (2016). The role of microglia and macrophages in glioma maintenance and progression, *19*(1). https://doi.org/10.1038/nn.4185
Hammers, C. M., & Stanley, J. R. (2014). Antibody phage display: Technique and applications. *Journal of Investigative Dermatology*, *134*(2). https://doi.org/10.1038/jid.2013.521
Hanahan, D. (2022). Hallmarks of Cancer: New Dimensions. *Cancer Discovery*, *12*(1), 31–46. https://doi.org/10.1158/2159-8290.CD-21-1059
Hanahan, D., & Weinberg, R. A. (2011). Hallmarks of Cancer: The Next Generation. *Cell*, *144*(5), 646–674. https://doi.org/10.1016/j.cell.2011.02.013
Harrow, S., Papanastassiou, V., Harland, J., Mabbs, R., Petty, R., Fraser, M., … Rampling, R. (2004). HSV1716 injection into the brain adjacent to tumour following surgical resection of high-grade glioma: Safety data and long-term survival. *Gene Therapy*, *11*(22), 1648–1658. https://doi.org/10.1038/sj.gt.3302289
Haspels, H. N., Rahman, M. A., Joseph, J. V., Navarro, A. G., & Chekenya, M. (2018). Glioblastoma stem-like cells are more susceptible than differentiated cells to natural killer cell lysis mediated through killer immunoglobulin-like receptors-human leukocyte antigen ligand mismatch and activation receptor-ligand interactions. *Frontiers in Immunology*, *9*(JUN), 1–17. https://doi.org/10.3389/fimmu.2018.01345
He, B, Chou, J., Brandimarti, R., Mohr, I., Gluzman, Y., & Roizman, B. (1997). Suppression of the phenotype of gamma(1)34.5- herpes simplex virus 1: failure of activated RNA-dependent protein kinase to shut off protein synthesis is associated with a deletion in the domain of the alpha47 gene. *Journal of Virology*, *71*(8), 6049–6054. https://doi.org/10.1128/jvi.71.8.6049-6054.1997
He, Bin, Gross, M., & Roizman, B. (1997). The γ134.5 protein of herpes simplex virus 1 complexes with protein phosphatase 1α to dephosphorylate the α subunit of the eukaryotic translation initiation factor 2 and preclude the shutoff of protein synthesis by double-stranded RNA-activated protein ki. *Proceedings of the National Academy of Sciences of the United States of America*, *94*(3), 843–848. https://doi.org/10.1073/pnas.94.3.843
Hegi, M. E., Diserens, A.-C., Gorlia, T., Hamou, M.-F., de Tribolet, N., Weller, M., … Stupp, R. (2005). MGMT Gene Silencing and Benefit from Temozolomide in Glioblastoma . *New England Journal of Medicine*, *352*(10), 997–1003. https://doi.org/10.1056/nejmoa043331
Heise, C., Sampson-Johannes, A., Williams, A., Mccormick, F., Von Hoff, D. D., & Kirn, D. H. (1997). ONYX-015, an E1B gene-attenuated adenovirus, causes tumor-specific cytolysis and antitumoral efficacy that can be augmented by standard chemotherapeutic agents. *Nature Medicine*, *3*(6), 639–645. https://doi.org/10.1038/nm0697-639
Henke, E., Nandigama, R., & Ergün, S. (2020). Extracellular Matrix in the Tumor Microenvironment and Its Impact on Cancer Therapy. *Frontiers in Molecular Biosciences*, *6*(January), 1–24. https://doi.org/10.3389/fmolb.2019.00160
Hermiston, T. W., & Kuhn, I. (2002). Armed therapeutic viruses: Strategies and challenges to arming oncolytic viruses with therapeutic genes. *Cancer Gene Therapy*, *9*(12), 1022–1035. https://doi.org/10.1038/sj.cgt.7700542
Hilpert, J., Baltz-Ghahremanpour, K., Schmiedel, B. J., Kanz, L., Jung, G., Grosse-Hovest, L., & Salih, H. R. (2011). Fc-Engineered NKG2D-IgG1 Fusion Proteins Target Leukemia Cells for Antibody-Dependent Cellular Cytotoxicity (ADCC) of NK Cells. *Blood*, *118*(21), 1537–1537. https://doi.org/10.1182/blood.v118.21.1537.1537
HLA Nomenclature @ hla.alleles.org. (n.d.). Retrieved November 10, 2020, from http://hla.alleles.org/proteins/classo.html
Holmgaard, R. B., Zamarin, D., Li, Y., Gasmi, B., Munn, D. H., Allison, J. P., … Wolchok, J. D. (2015). Tumor-Expressed IDO Recruits and Activates MDSCs in a Treg-Dependent Manner. *Cell Reports*, *13*(2). https://doi.org/10.1016/j.celrep.2015.08.077
Holthaus, L., Lamp, D., Gavrisan, A., Sharma, V., Ziegler, A. G., Jastroch, M., & Bonifacio, E. (2018).

CD4+ T cell activation, function, and metabolism are inhibited by low concentrations of DMSO. *Journal of Immunological Methods*, *463*(September), 54–60. https://doi.org/10.1016/j.jim.2018.09.004

Hoption Cann, S. A., Van Netten, J. P., & Van Netten, C. (2003). Dr William Coley and tumour regression: A place in history or in the future. *Postgraduate Medical Journal*, *79*(938), 672–680.

Horiguchi, M., Ota, M., & Rifkin, D. B. (2012). Matrix control of transforming growth factor-β function. *Journal of Biochemistry*, *152*(4), 321–329. https://doi.org/10.1093/jb/mvs089

Horng, T., Bezbradica, J. S., & Medzhitov, R. (2007). NKG2D signaling is coupled to the interleukin 15 receptor signaling pathway. *Nature Immunology*, *8*(12), 1345–1352. https://doi.org/10.1038/ni1524

Hornyák, L., Dobos, N., Koncz, G., Karányi, Z., Páll, D., Szabó, Z., … Székvölgyi, L. (2018). The role of indoleamine-2,3-dioxygenase in cancer development, diagnostics, and therapy. *Frontiers in Immunology*. https://doi.org/10.3389/fimmu.2018.00151

Hosomi, S., Grootjans, J., Tschurtschenthaler, M., Krupka, N., Matute, J. D., Flak, M. B., … Blumberg, R. (2017). Intestinal epithelial cell endoplasmic reticulum stress promotes MULT1 up-regulation and NKG2D-mediated inflammation. *Journal of Experimental Medicine*, *214*(10), 2985–2997. https://doi.org/10.1084/jem.20162041

Hsu, M. J., Wu, C. Y., Chiang, H. H., Lai, Y. L., & Hung, S. L. (2010). PI3K/Akt signaling mediated apoptosis blockage and viral gene expression in oral epithelial cells during herpes simplex virus infection. *Virus Research*, *153*(1), 36–43. https://doi.org/10.1016/j.virusres.2010.07.002

Isernhagen, A., Malzahn, D., Bickeböller, H., & Dressel, R. (2016). Impact of the MICA-129Met/val dimorphism on NKG2D-mediated biological functions and disease risks. *Frontiers in Immunology*, *7*(DEC), 1–9. https://doi.org/10.3389/fimmu.2016.00588

Jackson, C., Ruzevick, J., Phallen, J., Belcaid, Z., & Lim, M. (2011). Challenges in immunotherapy presented by the glioblastoma multiforme microenvironment. *Clinical and Developmental Immunology*, *2011*. https://doi.org/10.1155/2011/732413

Jackson, M., Hassiotou, F., & Nowak, A. (2014). Glioblastoma stem-like cells: At the root of tumor recurrence and a therapeutic target. *Carcinogenesis*, *36*(2), 177–185. https://doi.org/10.1093/carcin/bgu243

Jahan, N., Ghouse, S. M., Martuza, R. L., & Rabkin, S. D. (2021). In situ cancer vaccination and immunovirotherapy using oncolytic hsv. *Viruses*, *13*(9), 1–27. https://doi.org/10.3390/v13091740

Jan Chalupny, N., Sutherland, C. L., Lawrence, W. A., Rein-Weston, A., & Cosman, D. (2003). ULBP4 is a novel ligand for human NKG2D. *Biochemical and Biophysical Research Communications*, *305*(1), 129–135. https://doi.org/10.1016/S0006-291X(03)00714-9

Jarnagin, W. R., Zager, J. S., Hezel, M., Stanziale, S. F., Adusumilli, P. S., Gonen, M., … Fong, Y. (2006). Treatment of cholangiocarcinoma with oncolytic herpes simplex virus combined with external beam radiation therapy. *Cancer Gene Therapy*, *13*(3), 326–334. https://doi.org/10.1038/sj.cgt.7700890

Jensen, H., Andresen, L., Nielsen, J., Christensen, J. P., & Skov, S. (2011). Vesicular stomatitis virus infection promotes immune evasion by preventing NKG2D-ligand surface expression. *PLoS ONE*, *6*(8), 1–8. https://doi.org/10.1371/journal.pone.0023023

Jiang, H., Rivera-Molina, Y., Gomez-Manzano, C., Clise-Dwyer, K., Bover, L., Vence, L. M., … Fueyo, J. (2017). Oncolytic adenovirus and tumor-targeting immune modulatory therapy improve autologous cancer vaccination. *Cancer Research*, *77*(14), 3894–3907. https://doi.org/10.1158/0008-5472.CAN-17-0468

Jinushi, M., Takehara, T., Tatsumi, T., Kanto, T., Groh, V., Spies, T., … Hayashi, N. (2003). Expression and role of MICA and MICB in human hepatocellular carcinomas and their regulation by retinoic acid. *International Journal of Cancer*, *104*(3), 354–361. https://doi.org/10.1002/ijc.10966

Johnson, R. A., Wang, X., Ma, X.-L., Huong, S.-M., & Huang, E.-S. (2001). Human Cytomegalovirus Up-Regulates the Phosphatidylinositol 3-Kinase (PI3-K) Pathway: Inhibition of PI3-K Activity Inhibits Viral Replication and Virus-Induced Signaling. *Journal of Virology*, *75*(13), 6022–6032. https://doi.org/10.1128/JVI.75.13.6022-6032.2001

June, C. H., Riddell, S. R., & Schumacher, T. N. (2015). Adoptive cellular therapy: A race to the finish line. *Science Translational Medicine*, *7*(280), 1–9. https://doi.org/10.1126/scitranslmed.aaa3643

Jung, H., Hsiung, B., Pestal, K., Procyk, E., & Raulet, D. H. (2012). RAE-1 ligands for the NKG2D receptor are regulated by E2F transcription factors, which control cell cycle entry. *Journal of*

Experimental Medicine, *209*(13), 2409–2422. https://doi.org/10.1084/jem.20120565

Kambara, H., Okano, H., Chiocca, E. A., & Saeki, Y. (2005). An oncolytic HSV-1 mutant expressing ICP34.5 under control of a nestin promoter increases survival of animals even when symptomatic from a brain tumor. *Cancer Research*, *65*(7), 2832–2839. https://doi.org/10.1158/0008-5472.CAN-04-3227

Kanai, R., Zaupa, C., Sgubin, D., Antoszczyk, S. J., Martuza, R. L., Wakimoto, H., & Rabkin, S. D. (2012). Effect of γ34.5 Deletions on Oncolytic Herpes Simplex Virus Activity in Brain Tumors. *Journal of Virology*, *86*(8), 4420–4431. https://doi.org/10.1128/JVI.00017-12

Kaufman, H. L., Kim, D. W., Deraffele, G., Mitcham, J., Coffin, R. S., & Kim-Schulze, S. (2010). Local and distant immunity induced by intralesional vaccination with an oncolytic herpes virus encoding GM-CSF in patients with stage IIIc and IV melanoma. *Annals of Surgical Oncology*, *17*(3), 718–730. https://doi.org/10.1245/s10434-009-0809-6

Kaufman, H. L., Ruby, C. E., Hughes, T., & Slingluff, C. L. (2014). Current status of granulocyte-macrophage colony-stimulating factor in the immunotherapy of melanoma. *Journal for ImmunoTherapy of Cancer*, *2*(1). https://doi.org/10.1186/2051-1426-2-11

Kaur, B., Antonio Chiocca, E., & P. Cripe, T. (2012). Oncolytic HSV-1 Virotherapy: Clinical Experience and Opportunities for Progress. *Current Pharmaceutical Biotechnology*, *13*(9), 1842–1851. https://doi.org/10.2174/138920112800958814

Kebenko, M., Goebeler, M. E., Wolf, M., Hasenburg, A., Seggewiss-Bernhardt, R., Ritter, B., … Fiedler, W. (2018). A multicenter phase 1 study of solitomab (MT110, AMG 110), a bispecific EpCAM/CD3 T-cell engager (BiTE®) antibody construct, in patients with refractory solid tumors. *OncoImmunology*, *7*(8), 1–11. https://doi.org/10.1080/2162402X.2018.1450710

Kelly, E., & Russell, S. J. (2007). History of oncolytic viruses: Genesis to genetic engineering. *Molecular Therapy*, *15*(4), 651–659. https://doi.org/10.1038/sj.mt.6300108

Kesari, S., Randazzo, B. P., Valyi-Nagy, T., Huang, Q. S., Brown, S. M., MacLean, A. R., … Fraser, N. W. (1995). Therapy of experimental human brain tumors using a neuroattenuated herpes simplex virus mutant. *Laboratory Investigation; a Journal of Technical Methods and Pathology*, *73*(5), 636–648. Retrieved from http://www.ncbi.nlm.nih.gov/pubmed/7474937

Khalique, H., Baugh, R., Dyer, A., Scott, E. M., Frost, S., Larkin, S., … Seymour, L. W. (2021). Oncolytic herpesvirus expressing PD-L1 BiTE for cancer therapy: exploiting tumor immune suppression as an opportunity for targeted immunotherapy. *Journal for ImmunoTherapy of Cancer*, *9*(4), e001292. https://doi.org/10.1136/jitc-2020-001292

Kim, S. H., Wong, R. J., Kooby, D. A., Carew, J. F., Adusumilli, P. S., Patel, S. G., … Fong, Y. (2005). Combination of mutated herpes simplex virus type 1 (G207 virus) with radiation for the treatment of squamous cell carcinoma of the head and neck. *European Journal of Cancer*, *41*(2), 313–322. https://doi.org/10.1016/j.ejca.2004.10.018

Kim, Y., Born, C., Bléry, M., & Steinle, A. (2020). MICAgen Mice Recapitulate the Highly Restricted but Activation-Inducible Expression of the Paradigmatic Human NKG2D Ligand MICA. *Frontiers in Immunology*, *11*. https://doi.org/10.3389/fimmu.2020.00960

Kleijn, A., Kloezeman, J., Treffers-Westerlaken, E., Fulci, G., Leenstra, S., Dirven, C., … Lamfers, M. (2014). The in vivo therapeutic efficacy of the oncolytic adenovirus Delta24-RGD is mediated by tumor-specific immunity. *PLoS ONE*, *9*(5). https://doi.org/10.1371/journal.pone.0097495

Kleijn, A., van den Bossche, W., Haefner, E. S., Belcaid, Z., Burghoorn-Maas, C., Kloezeman, J. J., … Lamfers, M. L. M. (2017). The Sequence of Delta24-RGD and TMZ Administration in Malignant Glioma Affects the Role of CD8+T Cell Anti-tumor Activity. *Molecular Therapy - Oncolytics*, *5*(June), 11–19. https://doi.org/10.1016/j.omto.2017.02.002

Klinger, M., Brandl, C., Zugmaier, G., Hijazi, Y., Bargou, R. C., Topp, M. S., … Kufer, P. (2012). Immunopharmacologic response of patients with B-lineage acute lymphoblastic leukemia to continuous infusion of T cell-engaging CD19/CD3-bispecific BiTE antibody blinatumomab. *Blood*, *119*(26), 6226–6233. https://doi.org/10.1182/blood-2012-01-400515

Kmiecik, J., Poli, A., Brons, N. H. C., Waha, A., Eide, G. E., Enger, P. Ø., … Chekenya, M. (2013). Elevated CD3+ and CD8+ tumor-infiltrating immune cells correlate with prolonged survival in glioblastoma patients despite integrated immunosuppressive mechanisms in the tumor microenvironment and at the systemic level. *Journal of Neuroimmunology*, *264*(1–2), 71–83. https://doi.org/10.1016/j.jneuroim.2013.08.013

Köhler, G., & Milstein, C. (1975). Continuous cultures of fused cells secreting antibody of predefined specificity. *Nature*, *256*(5517). https://doi.org/10.1038/256495a0

Komohara, Y., Ohnishi, K., Kuratsu, J., & Takeya, M. (2008). Possible involvement of the M2 anti-inflammatory macrophage phenotype in growth of human gliomas. *The Journal of Pathology*,

216(1), 15–24. https://doi.org/10.1002/path.2370

Kong, K., Kumar, M., Taruishi, M., & Javier, R. T. (2014). The Human Adenovirus E4-ORF1 Protein Subverts Discs Large 1 to Mediate Membrane Recruitment and Dysregulation of Phosphatidylinositol 3-Kinase. *PLoS Pathogens*, *10*(5), e1004102. https://doi.org/10.1371/journal.ppat.1004102

Krmpotic, A., Hasan, M., Loewendorf, A., Saulig, T., Halenius, A., Lenac, T., … Jonjic, S. (2005). NK cell activation through the NKG2D ligand MULT-1 is selectively prevented by the glycoprotein encoded by mouse cytomegalovirus gene m145. *Journal of Experimental Medicine*, *201*(2), 211–220. https://doi.org/10.1084/jem.20041617

Kuhn, I., Harden, P., Bauzon, M., Chartier, C., Nye, J., Thorne, S., … Hermiston, T. W. (2008). Directed evolution generates a novel oncolytic virus for the treatment of colon cancer. *PLoS ONE*, *3*(6), 1–11. https://doi.org/10.1371/journal.pone.0002409

Labani-Motlagh, A., Ashja-Mahdavi, M., & Loskog, A. (2020). The Tumor Microenvironment: A Milieu Hindering and Obstructing Antitumor Immune Responses. *Frontiers in Immunology*, *11*(May), 1–22. https://doi.org/10.3389/fimmu.2020.00940

Lam, A. R., Le Bert, N., Ho, S. S. W., Shen, Y. J., Tang, M. L. F., Xiong, G. M., … Gasser, S. (2014). RAE1 Ligands for the NKG2D Receptor Are Regulated by STING-Dependent DNA Sensor Pathways in Lymphoma. *Cancer Research*, *74*(8), 2193–2203. https://doi.org/10.1158/0008-5472.CAN-13-1703

Lamb, L. S., Bowersock, J., Dasgupta, A., Gillespie, G. Y., Su, Y., Johnson, A., & Spencer, H. T. (2013). Engineered Drug Resistant γδ T Cells Kill Glioblastoma Cell Lines during a Chemotherapy Challenge: A Strategy for Combining Chemo- and Immunotherapy. *PLoS ONE*, *8*(1), 1–9. https://doi.org/10.1371/journal.pone.0051805

Lamb, L. S., Pereboeva, L., Youngblood, S., Gillespie, G. Y., Nabors, L. B., Markert, J. M., … Spencer, H. T. (2021). A combined treatment regimen of MGMT-modified γδ T cells and temozolomide chemotherapy is effective against primary high grade gliomas. *Scientific Reports*, *11*(1), 1–8. https://doi.org/10.1038/s41598-021-00536-8

Lamfers, M. L. M., Idema, S., Bosscher, L., Heukelom, S., Moeniralm, S., Van Der Meulen-Muileman, I. H., … Dirven, C. M. F. (2007). Differential effects of combined Ad5-Δ24RGD and radiation therapy in in vitro versus in vivo models of malignant glioma. *Clinical Cancer Research*, *13*(24), 7451–7458. https://doi.org/10.1158/1078-0432.CCR-07-1265

Lança, T., Correia, D. V., Moita, C. F., Raquel, H., Neves-Costa, A., Ferreira, C., … Silva-Santos, B. (2010). The MHC class Ib protein ULBP1 is a nonredundant determinant of leukemia/lymphoma susceptibility to γδ T-cell cytotoxicity. *Blood*, *115*(12), 2407–2411. https://doi.org/10.1182/blood-2009-08-237123

Lanier, L. L. (2005). NK CELL RECOGNITION. *Annual Review of Immunology*, *23*(1), 225–274. https://doi.org/10.1146/annurev.immunol.23.021704.115526

Lanier, L. L. (2008). Evolutionary struggles between NK cells and viruses. *Nature Reviews Immunology*, *8*(4), 259–268. https://doi.org/10.1038/nri2276

Lauko, A., Lo, A., Ahluwalia, M. S., & Lathia, J. D. (2021). Cancer cell heterogeneity & plasticity in glioblastoma and brain tumors. *Seminars in Cancer Biology*, (December 2020). https://doi.org/10.1016/j.semcancer.2021.02.014

Lee, J., Kotliarova, S., Kotliarov, Y., Li, A., Su, Q., Donin, N. M., … Fine, H. A. (2006). Tumor stem cells derived from glioblastomas cultured in bFGF and EGF more closely mirror the phenotype and genotype of primary tumors than do serum-cultured cell lines. *Cancer Cell*, *9*(5), 391–403. https://doi.org/10.1016/j.ccr.2006.03.030

Lee, S. W., Woo, J. K., Park, J. A., Yoon, K. C., Kwon, Y. W., & Kim, K. W. (2006). Blood-brain barrier interfaces and brain tumors. *Archives of Pharmacal Research*, *29*(4), 265–275. https://doi.org/10.1007/BF02968569

Lee, S. Y. (2016). Temozolomide resistance in glioblastoma multiforme. *Genes and Diseases*, *3*(3), 198–210. https://doi.org/10.1016/j.gendis.2016.04.007

Lenac, T., Budt, M., Arapovic, J., Hasan, M., Zimmermann, A., Simic, H., … Jonjic, S. (2006). The herpesviral Fc receptor fcr-1 down-regulates the NKG2D ligands MULT-1 and H60. *Journal of Experimental Medicine*, *203*(8), 1843–1850. https://doi.org/10.1084/jem.20060514

Li, H., Lakshmikanth, T., Garofalo, C., Enge, M., Spinnler, C., Anichini, A., … Selivanova, G. (2011). Pharmacological activation of p53 triggers anticancer innate immune response through induction of ULBP2. *Cell Cycle*, *10*(19), 3346–3358. https://doi.org/10.4161/cc.10.19.17630

Li, Y., Patel, S. P., Roszik, J., & Qin, Y. (2018). Hypoxia-driven immunosuppressive metabolites in the tumor microenvironment: New approaches for combinational immunotherapy. *Frontiers in Immunology*. https://doi.org/10.3389/fimmu.2018.01591

Liang, M. (2018). Oncorine, the World First Oncolytic Virus Medicine and its Update in China. *Current Cancer Drug Targets*, *18*(2). https://doi.org/10.2174/1568009618666171129221503

Liebner, S., Dijkhuizen, R. M., Reiss, Y., Plate, K. H., Agalliu, D., & Constantin, G. (2018). Functional morphology of the blood–brain barrier in health and disease. *Acta Neuropathologica*, *135*(3), 311–336. https://doi.org/10.1007/s00401-018-1815-1

Liu, A. Y., Robinson, R. R., Hellström, K. E., Murray, E. D., Chang, C. P., & Hellström, I. (1987). Chimeric mouse-human IgG1 antibody that can mediate lysis of cancer cells. *Proceedings of the National Academy of Sciences of the United States of America*, *84*(10). https://doi.org/10.1073/pnas.84.10.3439

Liu, G., Atteridge, C. L., Wang, X., Lundgren, A. D., & Wu, J. D. (2010). Cutting Edge: The Membrane Type Matrix Metalloproteinase MMP14 Mediates Constitutive Shedding of MHC Class I Chain-Related Molecule A Independent of A Disintegrin and Metalloproteinases. *The Journal of Immunology*, *184*(7), 3346–3350. https://doi.org/10.4049/jimmunol.0903789

Liu, Q., Yin, X., Languino, L. R., & Altieri, D. C. (2018). Evaluation of Drug Combination Effect Using a Bliss Independence Dose–Response Surface Model. *Statistics in Biopharmaceutical Research*, *10*(2), 112–122. https://doi.org/10.1080/19466315.2018.1437071

Lodoen, M. B., Abenes, G., Umamoto, S., Houchins, J. P., Liu, F., & Lanier, L. L. (2004). The Cytomegalovirus m155 Gene Product Subverts Natural Killer Cell Antiviral Protection by Disruption of H60–NKG2D Interactions. *Journal of Experimental Medicine*, *200*(8), 1075–1081. https://doi.org/10.1084/jem.20040583

Lodoen, M. B., & Lanier, L. L. (2005). Viral modulation of NK cell immunity. *Nature Reviews Microbiology*, *3*(1), 59–69. https://doi.org/10.1038/nrmicro1066

Lodoen, M., Ogasawara, K., Hamerman, J. A., Arase, H., Houchins, J. P., Mocarski, E. S., & Lanier, L. L. (2003). NKG2D-mediated Natural Killer Cell Protection Against Cytomegalovirus Is Impaired by Viral gp40 Modulation of Retinoic Acid Early Inducible 1 Gene Molecules. *Journal of Experimental Medicine*, *197*(10), 1245–1253. https://doi.org/10.1084/jem.20021973

Lorger, M. (2012). Tumor microenvironment in the brain. *Cancers*, *4*(1), 218–243. https://doi.org/10.3390/cancers4010218

Louis, D. N., Perry, A., Wesseling, P., Brat, D. J., Cree, I. A., Figarella-Branger, D., … Ellison, D. W. (2021). The 2021 WHO classification of tumors of the central nervous system: A summary. *Neuro-Oncology*, *23*(8), 1231–1251. https://doi.org/10.1093/neuonc/noab106

Lu, R. M., Hwang, Y. C., Liu, I. J., Lee, C. C., Tsai, H. Z., Li, H. J., & Wu, H. C. (2020). Development of therapeutic antibodies for the treatment of diseases. *Journal of Biomedical Science*. https://doi.org/10.1186/s12929-019-0592-z

Lukashev, D., Klebanov, B., Kojima, H., Grinberg, A., Ohta, A., Berenfeld, L., … Sitkovsky, M. (2006). Cutting Edge: Hypoxia-Inducible Factor 1α and Its Activation-Inducible Short Isoform I.1 Negatively Regulate Functions of CD4 + and CD8 + T Lymphocytes . *The Journal of Immunology*, *177*(8), 4962–4965. https://doi.org/10.4049/jimmunol.177.8.4962

Ma, J., Ramachandran, M., Jin, C., Quijano-Rubio, C., Martikainen, M., Yu, D., & Essand, M. (2020). Characterization of virus-mediated immunogenic cancer cell death and the consequences for oncolytic virus-based immunotherapy of cancer. *Cell Death and Disease*, *11*(1). https://doi.org/10.1038/s41419-020-2236-3

Ma, R., Lu, T., Li, Z., Teng, K.-Y., Mansour, A. G., Yu, M., … Yu, J. (2021). An Oncolytic Virus Expressing IL15/IL15Rα Combined with Off-the-Shelf EGFR-CAR NK Cells Targets Glioblastoma. *Cancer Research*, *81*(13), 3635–3648. https://doi.org/10.1158/0008-5472.CAN-21-0035

Ma, Y., Jin, H., Valyi-Nagy, T., Cao, Y., Yan, Z., & He, B. (2012). Inhibition of TANK Binding Kinase 1 by Herpes Simplex Virus 1 Facilitates Productive Infection. *Journal of Virology*, *86*(4), 2188–2196. https://doi.org/10.1128/jvi.05376-11

MacLean, A. R., Ul-Fareed, M., Robertson, L., Harland, J., & Brown, S. M. (1991). Herpes simplex virus type 1 deletion variants 1714 and 1716 pinpont neurovirulence-related sequences in Glasgow strain 17+ between immediate early gene 1 and the “a” sequence. *Journal of General Virology*, *72*(3), 631–639. https://doi.org/10.1099/0022-1317-72-3-631

Mahata, B., Biswas, S., Rayman, P., Chahlavi, A., Ko, J., Bhattacharjee, A., … Biswas, K. (2015). GBM derived gangliosides induce T cell apoptosis through activation of the caspase cascade involving both the extrinsic and the intrinsic pathway. *PLoS ONE*, *10*(7), 1–19. https://doi.org/10.1371/journal.pone.0134425

Mantovani, A., Sica, A., Sozzani, S., Allavena, P., Vecchi, A., & Locati, M. (2004). The chemokine system in diverse forms of macrophage activation and polarization. *Trends in Immunology*, *25*(12), 677–686. https://doi.org/10.1016/j.it.2004.09.015

Mantovani, A., Sozzani, S., Locati, M., Allavena, P., & Sica, A. (2002). *Macrophage polarization: tumor-associated macrophages as a paradigm for polarized M2 mononuclear phagocytes*. *TRENDS in Immunology* (Vol. 23). Retrieved from http://immunology.trends.com1471-4906/02/$-seefrontmatter

Maragkos, G. A., Schüpper, A. J., Lakomkin, N., Sideras, P., Price, G., Baron, R., … Robin, A. M. (2021). Fluorescence-Guided High-Grade Glioma Surgery More Than Four Hours After 5-Aminolevulinic Acid Administration. *Frontiers in Neurology*, *12*(March), 1–7. https://doi.org/10.3389/fneur.2021.644804

Marconi, P., & Manservigi, R. (2014). Herpes Simplex Virus Growth, Preparation, and Assay, *1144*, 19–29. https://doi.org/10.1007/978-1-4939-0428-0_2

Markert, J. M., Liechty, P. G., Wang, W., Gaston, S., Braz, E., Karrasch, M., … Gillespie, G. Y. (2009). Phase Ib Trial of Mutant Herpes Simplex Virus G207 Inoculated Pre-and Post-tumor Resection for Recurrent GBM. *Molecular Therapy*, *17*(1), 199–207. https://doi.org/10.1038/mt.2008.228

Markert, J. M., Razdan, S. N., Kuo, H.-C., Cantor, A., Knoll, A., Karrasch, M., … Gillespie, G. Y. (2014). A Phase 1 Trial of Oncolytic HSV-1, G207, Given in Combination With Radiation for Recurrent GBM Demonstrates Safety and Radiographic Responses. *Molecular Therapy*, *22*(5), 1048–1055. https://doi.org/10.1038/mt.2014.22

Markert, J. M., Yancey Gillespie, G., Weichselbaum, R. R., Roizman, B., & Whitley, R. J. (2000). Genetically engineered HSV in the treatment of glioma: A review. *Reviews in Medical Virology*, *10*(1), 17–30. https://doi.org/10.1002/(SICI)1099-1654(200001/02)10:1<17::AID-RMV258>3.0.CO;2-G

Markert, J., Rabkin, S., Gillespie, G., Todo, T., Hunter, W., Palmer, C., … Martuza, R. (2000). Conditionally replicating herpes simplex virus mutant, G207 for the treatment of malignant glioma: results of a phase I trial. *Gene Therapy*, *7*, 867–874. Retrieved from www.nature.com/gt

Märklin, M., Hagelstein, I., Koerner, S. P., Rothfelder, K., Pfluegler, M. S., Schumacher, A., … Salih, H. R. (2019). Bispecific NKG2D-CD3 and NKG2D-CD16 fusion proteins for induction of NK and T cell reactivity against acute myeloid leukemia. *Journal for ImmunoTherapy of Cancer*, *7*(1). https://doi.org/10.1186/s40425-019-0606-0

Marshall, E. E., Bierle, C. J., Brune, W., & Geballe, A. P. (2009). Essential Role for either TRS1 or IRS1 in Human Cytomegalovirus Replication . *Journal of Virology*, *83*(9), 4112–4120. https://doi.org/10.1128/jvi.02489-08

Martuza, R. L., Malick, A., Markert, J. M., Ruffner, K. L., & Coen, D. M. (1991). Experimental Therapy of Human Glioma by Means of a Genetically Engineered Virus Mutant. *Science*, *252*(5007), 854–856. https://doi.org/10.1126/science.1851332

Matusali, G., Tchidjou, H. K., Pontrelli, G., Bernardi, S., D'Ettorre, G., Vullo, V., … Doria, M. (2013). Soluble ligands for the NKG2D receptor are released during HIV-1 infection and impair NKG2D expression and cytotoxicity of NK cells. *The FASEB Journal*, *27*(6), 2440–2450. https://doi.org/10.1096/fj.12-223057

McFaline-Figueroa, J. R., & Lee, E. Q. (2018). Brain Tumors. *American Journal of Medicine*, *131*(8), 874–882. https://doi.org/10.1016/j.amjmed.2017.12.039

McSharry, B. P., Burgert, H.-G., Owen, D. P., Stanton, R. J., Prod'homme, V., Sester, M., … Wilkinson, G. W. G. (2008). Adenovirus E3/19K Promotes Evasion of NK Cell Recognition by Intracellular Sequestration of the NKG2D Ligands Major Histocompatibility Complex Class I Chain-Related Proteins A and B. *Journal of Virology*, *82*(9), 4585–4594. https://doi.org/10.1128/jvi.02251-07

Metchnikoff, I., & Prize, N. (2015). Mini - review : Macrophage Polarization. *Biorad*, *2*, 1–8. https://doi.org/10.1158/2326-6066.CIR-15-0157

Mezhir, J. J., Advani, S. J., Smith, K. D., Darga, T. E., Poon, A. P. W., Schmidt, H., … Weichselbaum, R. R. (2005). Ionizing radiation activates late herpes simplex virus 1 promoters via the p38 pathway in tumors treated with oncolytic viruses. *Cancer Research*, *65*(20), 9479–9484. https://doi.org/10.1158/0008-5472.CAN-05-1927

Mineta, T., Rabkin, S. D., & Martuza, R. L. (1994). Treatment of Malignant Gliomas Using Ganciclovir-hypersensitive, Ribonucleotide Reductase-deficient Herpes Simplex Viral Mutant. *Cancer Research*, *54*(15), 3963–3966.

Mineta, T., Rabkin, S. D., Yazaki, T., Hunter, W. D., & Martuza, R. L. (1995). Attenuated multi-mutated herpes simplex virus-1 for the treatment of malignant gliomas. *Nature Medicine*, *1*(9), 938–943. https://doi.org/10.1038/nm0995-938

Molinero, L. L., Fuertes, M. B., Rabinovich, G. A., Fainboim, L., & Zwirner, N. W. (2002). Activation-induced expression of MICA on T lymphocytes involves engagement of CD3 and CD28.

Journal of Leukocyte Biology, *71*(5), 791–797. https://doi.org/10.1189/jlb.71.5.791

Morantz, R. A., Wood, G. W., Foster, M., Clark, M., & Gollahon, K. (1979). Macrophages in experimental and human brain tumors. *Journal of Neurosurgery*, *50*(3), 305–311. https://doi.org/10.3171/jns.1979.50.3.0305

Morgan, R. A., Yang, J. C., Kitano, M., Dudley, M. E., Laurencot, C. M., & Rosenberg, S. A. (2010). Case report of a serious adverse event following the administration of t cells transduced with a chimeric antigen receptor recognizing ERBB2. *Molecular Therapy*, *18*(4), 843–851. https://doi.org/10.1038/mt.2010.24

Mukherjee, S., Jensen, H., Stewart, W., Stewart, D., Ray, W. C., Chen, S.-Y., … Das, J. (2017). In silico modeling identifies CD45 as a regulator of IL-2 synergy in the NKG2D-mediated activation of immature human NK cells. *Science Signaling*, *10*(485), eaai9062. https://doi.org/10.1126/scisignal.aai9062

Nachmani, D., Stern-Ginossar, N., Sarid, R., & Mandelboim, O. (2009). Diverse Herpesvirus MicroRNAs Target the Stress-Induced Immune Ligand MICB to Escape Recognition by Natural Killer Cells. *Cell Host & Microbe*, *5*(4), 376–385. https://doi.org/10.1016/j.chom.2009.03.003

Nausch, N., & Cerwenka, A. (2008). NKG2D ligands in tumor immunity. *Oncogene*, *27*(45), 5944–5958. https://doi.org/10.1038/onc.2008.272

Nedvetzki, S., Sowinski, S., Eagle, R. A., Harris, J., Vély, F., Pende, D., … Davis, D. M. (2007). Reciprocal regulation of human natural killer cells and macrophages associated with distinct immune synapses. *Blood*, *109*(9), 3776–3785. https://doi.org/10.1182/blood-2006-10-052977

Neira, J. A., Ung, T. H., Sims, J. S., Malone, H. R., Chow, D. S., Samanamud, J. L., … Bruce, J. N. (2017). Aggressive resection at the infiltrative margins of glioblastoma facilitated by intraoperative fluorescein guidance. *Journal of Neurosurgery*, *127*(1), 111–122. https://doi.org/10.3171/2016.7.JNS16232

Nguyen, H.-M., & Saha, D. (2021). The Current State of Oncolytic Herpes Simplex Virus for Glioblastoma Treatment. *Oncolytic Virotherapy*, *Volume 10*, 1–27. https://doi.org/10.2147/ov.s268426

Nice, T. J., Deng, W., Coscoy, L., & Raulet, D. H. (2010). Stress-Regulated Targeting of the NKG2D Ligand Mult1 by a Membrane-Associated RING-CH Family E3 Ligase. *The Journal of Immunology*, *185*(9), 5369–5376. https://doi.org/10.4049/jimmunol.1000247

Nicoll, M. P., Proença, J. T., & Efstathiou, S. (2012). The molecular basis of herpes simplex virus latency. *FEMS Microbiology Reviews*, *36*(3), 684–705. https://doi.org/10.1111/j.1574-6976.2011.00320.x

Norman, J. M., Mashiba, M., McNamara, L. A., Onafuwa-Nuga, A., Chiari-Fort, E., Shen, W., & Collins, K. L. (2011). The antiviral factor APOBEC3G enhances the recognition of HIV-infected primary T cells by natural killer cells. *Nature Immunology*, *12*(10), 975–983. https://doi.org/10.1038/ni.2087

O'Cathail, S. M., Davis, S., Holmes, J., Brown, R., Fisher, K., Seymour, L., … Hawkins, M. A. (2020). A phase 1 trial of the safety, tolerability and biological effects of intravenous Enadenotucirev, a novel oncolytic virus, in combination with chemoradiotherapy in locally advanced rectal cancer (CEDAR). *Radiation Oncology*, *15*(1), 1–8. https://doi.org/10.1186/s13014-020-01593-5

O'Rourke, D. M., Nasrallah, M. P., Desai, A., Melenhorst, J. J., Mansfield, K., Morrissette, J. J. D., … Maus, M. V. (2017). A single dose of peripherally infused EGFRvIII-directed CAR T cells mediates antigen loss and induces adaptive resistance in patients with recurrent glioblastoma. *Science Translational Medicine*, *9*(399). https://doi.org/10.1126/scitranslmed.aaa0984

Offner, S., Hofmeister, R., Romaniuk, A., Kufer, P., & Baeuerle, P. A. (2006). Induction of regular cytolytic T cell synapses by bispecific single-chain antibody constructs on MHC class I-negative tumor cells. *Molecular Immunology*, *43*(6), 763–771. https://doi.org/10.1016/j.molimm.2005.03.007

Oh, S.-J., Yang, J.-I., Kim, O., Ahn, E.-J., Kang, W. D., Lee, J.-H., … Cho, D. (2017). Human U87 glioblastoma cells with stemness features display enhanced sensitivity to natural killer cell cytotoxicity through altered expression of NKG2D ligand. *Cancer Cell International*, *17*(1), 22. https://doi.org/10.1186/s12935-017-0397-7

Orrego, E., Castaneda, C. A., Castillo, M., Bernabe, L. A., Casavilca, S., Chakravarti, A., … Ojeda, L. (2018). Distribution of tumor-infiltrating immune cells in glioblastoma. *CNS Oncology*, *7*(4), CNS21. https://doi.org/10.2217/cns-2017-0037

Orvedahl, A., Alexander, D., Tallóczy, Z., Sun, Q., Wei, Y., Zhang, W., … Levine, B. (2007). HSV-1 ICP34.5 Confers Neurovirulence by Targeting the Beclin 1 Autophagy Protein. *Cell Host and Microbe*, *1*(1), 23–35. https://doi.org/10.1016/j.chom.2006.12.001

Ostrom, Q. T., Gittleman, H., Fulop, J., Liu, M., Blanda, R., Kromer, C., … Barnholtz-Sloan, J. S.

(2015). CBTRUS statistical Report: primary brain and central nervous system tumors diagnosed in the United States in 2008-2012. *Neuro-Oncology*, *17*, iv1–iv62. https://doi.org/10.1093/neuonc/nov189

Ozcan, M., Janikovits, J., von Knebel Doeberitz, M., & Kloor, M. (2018). Complex pattern of immune evasion in MSI colorectal cancer. *OncoImmunology*, *7*(7). https://doi.org/10.1080/2162402X.2018.1445453

Ozuer, A., Wechuck, J. B., Wendell, S. K., Wolfe, D. P., Goins, W. F., Krisky, D. M., … Glorioso, J. C. (2003). 950. Production of Replication-Defective HSV-1 Viral Vectors and Development of Precise Assay Systems To Analyze the Quality of Clinical-Grade HSV Vectors. *Molecular Therapy*, *7*(5), S365–S366. https://doi.org/10.1016/S1525-0016(16)41392-4

Pan, S., Liu, X., Ma, Y., Cao, Y., & He, B. (2018). Herpes Simplex Virus 1 γ 1 34.5 Protein Inhibits STING Activation That Restricts Viral Replication. *Journal of Virology*, *92*(20). https://doi.org/10.1128/JVI.01015-18

Pansky, A., Hildebrand, P., Fasler-Kan, E., Baselgia, L., Ketterer, S., Beglinger, C., & Heim, M. H. (2000). Defective Jak-STAT signal transduction pathway in melanoma cells resistant to growth inhibition by interferon-α. *International Journal of Cancer*, *85*(5), 720–725. https://doi.org/10.1002/(SICI)1097-0215(20000301)85:5<720::AID-IJC20>3.0.CO;2-O

Papanastassiou, V., Rampling, R., Fraser, M., Petty, R., Hadley, D., Nicoll, J., … Brown, M. (2002). The potential for efficacy of the modified (ICP 34.5−) herpes simplex virus HSV1716 following intratumoural injection into human malignant glioma: a proof of principle study. *Gene Therapy*, *9*(6), 398–406. https://doi.org/10.1038/sj.gt.3301664

Patel, D. M., Foreman, P. M., Nabors, L. B., Riley, K. O., Gillespie, G. Y., & Markert, J. M. (2016). Design of a Phase i Clinical Trial to Evaluate M032, a Genetically Engineered HSV-1 Expressing IL-12, in Patients with Recurrent/Progressive Glioblastoma Multiforme, Anaplastic Astrocytoma, or Gliosarcoma. *Human Gene Therapy Clinical Development*, *27*(2), 69–78. https://doi.org/10.1089/humc.2016.031

Perazzoli, G., Prados, J., Ortiz, R., Caba, O., & Cabeza, L. (2015). Temozolomide Resistance in Glioblastoma Cell Lines : Implication of MGMT , MMR , P- Glycoprotein and CD133 Expression, 1–23. https://doi.org/10.1371/journal.pone.0140131

Pereboeva, L., Harkins, L., Wong, S., & Lamb, L. S. (2015). The safety of allogeneic innate lymphocyte therapy for glioma patients with prior cranial irradiation. *Cancer Immunology, Immunotherapy*, *64*(5), 551–562. https://doi.org/10.1007/s00262-015-1662-z

Perez, C., Gruber, I., & Arber, C. (2020). Off-the-Shelf Allogeneic T Cell Therapies for Cancer: Opportunities and Challenges Using Naturally Occurring “Universal” Donor T Cells. *Frontiers in Immunology*, *11*(November), 1–16. https://doi.org/10.3389/fimmu.2020.583716

Pesonen, S., Diaconu, I., Cerullo, V., Escutenaire, S., Raki, M., Kangasniemi, L., … Hemminki, A. (2012). Integrin targeted oncolytic adenoviruses Ad5-D24-RGD and Ad5-RGD-D24-GMCSF for treatment of patients with advanced chemotherapy refractory solid tumors. *International Journal of Cancer*, *130*(8), 1937–1947. https://doi.org/10.1002/ijc.26216

Peters, C., Paget, M., Tshilenge, K., Saha, D., Antoszczyk, S., Baars, A., … Rabkin, S. D. (2018). Restriction of Replication of Oncolytic Herpes Simplex Virus with a Deletion of γ34.5 in Glioblastoma Stem-Like Cells. *Journal of Virology*, *92*(15), 1–17. https://doi.org/10.1128/JVI.00246-18

Pokrovska, T. D., Jacobus, E. J., Puliyadi, R., Prevo, R., Frost, S., Dyer, A., … Lei-Rossmann, J. (2020). External beam radiation therapy and enadenotucirev: Inhibition of the DDR and mechanisms of radiation-mediated virus increase. *Cancers*, *12*(4), 1–22. https://doi.org/10.3390/cancers12040798

Poon, M. T. C., Bruce, M., Simpson, J. E., Hannan, C. J., & Brennan, P. M. (2021). Temozolomide sensitivity of malignant glioma cell lines – a systematic review assessing consistencies between in vitro studies. *BMC Cancer*, *21*(1), 1–9. https://doi.org/10.1186/s12885-021-08972-5

Poppers, J., Mulvey, M., Khoo, D., & Mohr, I. (2000). Inhibition of PKR Activation by the Proline-Rich RNA Binding Domain of the Herpes Simplex Virus Type 1 Us11 Protein. *Journal of Virology*, *74*(23), 11215–11221. https://doi.org/10.1128/JVI.74.23.11215-11221.2000

Preston, V. G., Palfreyman, J. W., & Dutia, B. M. (1984). Identification of a herpes simplex virus type 1 polypeptide which is a component of the virus-induced ribonucleotide reductase. *The Journal of General Virology*, *65 (Pt 9)*(9), 1457–1466. https://doi.org/10.1099/0022-1317-65-9-1457

Przepiorka, D., Ko, C. W., Deisseroth, A., Yancey, C. L., Candau-Chacon, R., Chiu, H. J., … Pazdur, R. (2015). FDA approval: Blinatumomab. *Clinical Cancer Research*, *21*(18), 4035–4039. https://doi.org/10.1158/1078-0432.CCR-15-0612

Qin, S., Xu, L., Yi, M., Yu, S., Wu, K., & Luo, S. (2019). Novel immune checkpoint targets: Moving beyond PD-1 and CTLA-4. *Molecular Cancer*, *18*(1). https://doi.org/10.1186/s12943-019-1091-2

Qiu, Z. K., Shen, D., Chen, Y. S., Yang, Q. Y., Guo, C. C., Feng, B. H., & Chen, Z. P. (2014). Enhanced MGMT expression contributes to temozolomide resistance in glioma stem-like cells. *Chinese Journal of Cancer*, *33*(2), 115–122. https://doi.org/10.5732/cjc.012.10236

Raab, S., Steinbacher, J., Schmiedel, B. J., Kousis, P. C., Steinle, A., Jung, G., … Salih, H. R. (2014). Fc-Optimized NKG2D–Fc Constructs Induce NK Cell Antibody-Dependent Cellular Cytotoxicity against Breast Cancer Cells Independently of HER2/neu Expression Status. *The Journal of Immunology*, *193*(8), 4261–4272. https://doi.org/10.4049/jimmunol.1400872

Rampling, R., Cruickshank, G., Papanastassiou, V., Nicoll, J., Hadley, D., Brennan, D., … Brown, M. (2000). Toxicity evaluation of replication-competent herpes simplex virus (ICP 34.5 null mutant 1716) in patients with recurrent malignant glioma. *Gene Therapy*, *7*(10), 859–866. https://doi.org/10.1038/sj.gt.3301184

Raulet, D. H. (2003). Roles of the NKG2D immunoreceptor and its ligands. *Nature Reviews Immunology*, *3*(10), 781–790. https://doi.org/10.1038/nri1199

Raulet, D. H., Gasser, S., Gowen, B. G., Deng, W., & Jung, H. (2013). Regulation of Ligands for the NKG2D Activating Receptor. *Annual Review of Immunology*, *31*(1), 413–441. https://doi.org/10.1146/annurev-immunol-032712-095951

Rivera-Molina, Y., Jiang, H., Fueyo, J., Nguyen, T., Shin, D. H., Youssef, G., … Gomez-Manzano, C. (2019). GITRL-armed Delta-24-RGD oncolytic adenovirus prolongs survival and induces anti-glioma immune memory. *Neuro-Oncology Advances*, *1*(1), 1–11. https://doi.org/10.1093/noajnl/vdz009

Rodriguez, P. C., Zea, A. H., Culotta, K. S., Zabaleta, J., & Ochoa Augusto C Ochoa, J. B. (2002). Regulation of T cell receptor CD3ζ chain expression by L-arginine. *Journal of Biological Chemistry*, *277*(24), 21123–21129. article. https://doi.org/10.1074/jbc.M110675200

Rohaan, M. W., Wilgenhof, S., & Haanen, J. B. A. G. (2019). Adoptive cellular therapies: the current landscape. *Virchows Archiv*, *474*(4), 449–461. https://doi.org/10.1007/s00428-018-2484-0

Rosso, L., Brock, C. S., Gallo, J. M., Saleem, A., Price, P. M., Turkheimer, F. E., & Aboagye, E. O. (2009). A New Model for Prediction of Drug Distribution in Tumor and Normal Tissues: Pharmacokinetics of Temozolomide in Glioma Patients. *Cancer Research*, *69*(1), 120–127. https://doi.org/10.1158/0008-5472.CAN-08-2356

Rozanov, D. V., Savinov, A. Y., Golubkov, V. S., Rozanova, O. L., Postnova, T. I., Sergienko, E. A., … Strongin, A. Y. (2009). Engineering a leucine zipper-TRAIL homotrimer with improved cytotoxicity in tumor cells. *Molecular Cancer Therapeutics*, *8*(6), 1515–1525. https://doi.org/10.1158/1535-7163.MCT-09-0202

Russell, S. J., & Peng, K. W. (2007). Viruses as anticancer drugs. *Trends in Pharmacological Sciences*, *28*(7), 326–333. https://doi.org/10.1016/j.tips.2007.05.005

Saha, D., Martuza, R. L., & Rabkin, S. D. (2017). Macrophage Polarization Contributes to Glioblastoma Eradication by Combination Immunovirotherapy and Immune Checkpoint Blockade. *Cancer Cell*, *32*(2), 253-267.e5. https://doi.org/10.1016/j.ccell.2017.07.006

Saha, D., Rabkin, S. D., & Martuza, R. L. (2020). Temozolomide antagonizes oncolytic immunovirotherapy in glioblastoma. *Journal for ImmunoTherapy of Cancer*, *8*(1), e000345. https://doi.org/10.1136/jitc-2019-000345

Salih, H. R., Antropius, H., Gieseke, F., Lutz, S. Z., Kanz, L., Rammensee, H.-G., & Steinle, A. (2003). Functional expression and release of ligands for the activating immunoreceptor NKG2D in leukemia. *Blood*, *102*(4), 1389–1396. https://doi.org/10.1182/blood-2003-01-0019

Samson, A., Scott, K. J., Taggart, D., West, E. J., Wilson, E., Nuovo, G. J., … Melcher, A. A. (2018). Intravenous Delivery of Oncolytic Reovirus to Brain Tumor Patients Immunologically Primes for Subsequent Checkpoint Blockade. *Science Translational Medicine*, *7577*(January), eaam7577. https://doi.org/10.1126/scitranslmed.aam7577

Saxena, M., van der Burg, S. H., Melief, C. J. M., & Bhardwaj, N. (2021). Therapeutic cancer vaccines. *Nature Reviews Cancer*, *21*(6), 360–378. https://doi.org/10.1038/s41568-021-00346-0

Schellens, I. M. M., Hoof, I., Meiring, H. D., Spijkers, S. N. M., Poelen, M. C. M., Van Gaans-Van Den Brink, J. A. M., … Kesmir, C. (2015). Comprehensive analysis of the naturally processed peptide repertoire: Differences between HLA-A and B in the Immunopeptidome. *PLoS ONE*, *10*(9), 1–18. https://doi.org/10.1371/journal.pone.0136417

Schepis, D., D'Amato, M., Studahl, M., Bergström, T., Kärre, K., & Berg, L. (2009). Herpes simplex virus infection downmodulates NKG2D ligand expression. *Scandinavian Journal of*

Immunology, *69*(5), 429–436. https://doi.org/10.1111/j.1365-3083.2009.02241.x

Schmiedel, D., Tai, J., Levi-Schaffer, F., Dovrat, S., & Mandelboim, O. (2016). Human Herpesvirus 6B Downregulates Expression of Activating Ligands during Lytic Infection To Escape Elimination by Natural Killer Cells. *Journal of Virology*, *90*(21), 9608–9617. https://doi.org/10.1128/jvi.01164-16

Schneider, C. L., & Hudson, A. W. (2011). The human herpesvirus-7 (HHV-7) U21 immunoevasin subverts NK-mediated cytoxicity through modulation of MICA and MICB. *PLoS Pathogens*, *7*(11). https://doi.org/10.1371/journal.ppat.1002362

Schoenfeld, A. J., & Hellmann, M. D. (2020). Acquired Resistance to Immune Checkpoint Inhibitors. *Cancer Cell*, *37*(4), 443–455. https://doi.org/10.1016/j.ccell.2020.03.017

Schrambach, S., Ardizzone, M., Leymarie, V., Sibilia, J., & Bahram, S. (2007). In Vivo Expression Pattern of MICA and MICB and Its Relevance to Auto-Immunity and Cancer. *PLoS ONE*, *2*(6), e518. https://doi.org/10.1371/journal.pone.0000518

Scott, E. M., Frost, S., Khalique, H., Freedman, J. D., Seymour, L. W., & Lei-Rossmann, J. (2020). Use of Liquid Patient Ascites Fluids as a Preclinical Model for Oncolytic Virus Activity. In *Methods in Molecular Biology* (Vol. 2058, pp. 261–270). article, New York, NY: Springer New York. https://doi.org/10.1007/978-1-4939-9794-7_17

Scott, E. M., Jacobus, E. J., Lyons, B., Frost, S., Freedman, J. D., Dyer, A., … Duffy, M. R. (2019). Bi- And tri-valent T cell engagers deplete tumour-associated macrophages in cancer patient samples. *Journal for ImmunoTherapy of Cancer*, *7*(1), 1–18. https://doi.org/10.1186/s40425-019-0807-6

Seidel, E., Le, V. T. K., Bar-On, Y., Tsukerman, P., Enk, J., Yamin, R., … Mandelboim, O. (2015). Dynamic Co-evolution of Host and Pathogen: HCMV Downregulates the Prevalent Allele MICA*008 to Escape Elimination by NK Cells. *Cell Reports*, *10*(6), 968–982. https://doi.org/10.1016/j.celrep.2015.01.029

Sène, D., Levasseur, F., Abel, M., Lambert, M., Camous, X., Hernandez, C., … Caillat-Zucman, S. (2010). Hepatitis C Virus (HCV) Evades NKG2D-Dependent NK Cell Responses through NS5A-Mediated Imbalance of Inflammatory Cytokines. *PLoS Pathogens*, *6*(11), e1001184. https://doi.org/10.1371/journal.ppat.1001184

Seymour, L. W., & Fisher, K. D. (2016, February 16). Oncolytic viruses: finally delivering. *Br J Cancer*. Cancer Research UK. Retrieved from http://dx.doi.org/10.1038/bjc.2015.481

Shankaran, V., Ikeda, H., Bruce, A. T., White, J. M., Swanson, P. E., Old, L. J., & Shreiber, R. D. (2001). IFNgamma and lympohcytes prevent primary tomour development and shape tomour immunogenicity. *Nature*, *410*(6832), 1107–1111.

Shiraishi, K., Mimura, K., Kua, L.-F., Koh, V., Siang, L. K., Nakajima, S., … Kono, K. (2016). Inhibition of MMP activity can restore NKG2D ligand expression in gastric cancer, leading to improved NK cell susceptibility. *Journal of Gastroenterology*, *51*(12), 1101–1111. https://doi.org/10.1007/s00535-016-1197-x

Shirata, N., Kudoh, A., Daikoku, T., Tatsumi, Y., Fujita, M., Kiyono, T., … Tsurumi, T. (2005). Activation of Ataxia Telangiectasia-mutated DNA Damage Checkpoint Signal Transduction Elicited by Herpes Simplex Virus Infection. *Journal of Biological Chemistry*, *280*(34), 30336–30341. https://doi.org/10.1074/jbc.M500976200

Si, Y., Melkonian, A. L., Curry, K. C., Xu, Y., Tidwell, M., Liu, M., … Liu, X. (Margaret). (2021). Monoclonal antibody-based cancer therapies. *Chinese Journal of Chemical Engineering*, *30*, 301–307. https://doi.org/10.1016/j.cjche.2020.11.009

Silbergeld, D. L., Rostomily, R. C., & Alvord, E. C. (1991). The cause of death in patients with glioblastoma is multifactorial: - Clinical factors and autopsy findings in 117 cases of supratentorial glioblastoma in adults. *Journal of Neuro-Oncology*, *10*(2), 179–185. https://doi.org/10.1007/BF00146880

Singh, S. K., Hawkins, C., Clarke, I. D., Squire, J. A., Bayani, J., Hide, T., … Dirks, P. B. (2004). Identification of human brain tumour initiating cells. *Nature*, *432*(7015), 396–401. https://doi.org/10.1038/nature03128

Smith, K. D., Mezhir, J. J., Bickenbach, K., Veerapong, J., Charron, J., Posner, M. C., … Weichselbaum, R. R. (2006). Activated MEK Suppresses Activation of PKR and Enables Efficient Replication and In Vivo Oncolysis by Δγ 1 34.5 Mutants of Herpes Simplex Virus 1 . *Journal of Virology*, *80*(3), 1110–1120. https://doi.org/10.1128/jvi.80.3.1110-1120.2006

Smyth, M. J., Swann, J., Cretney, E., Zerafa, N., Yokoyama, W. M., & Hayakawa, Y. (2005). NKG2D function protects the host from tumor initiation. *Journal of Experimental Medicine*, *202*(5), 583–588. https://doi.org/10.1084/jem.20050994

Sondak, V. K., Smalley, K. S. M., Kudchadkar, R., Grippon, S., & Kirkpatrick, P. (2011). Ipilimumab.

Nature Reviews Drug Discovery, *10*(6), 411–412. https://doi.org/10.1038/nrd3463

Sørensen, B. S., & Horsman, M. R. (2020). Tumor Hypoxia: Impact on Radiation Therapy and Molecular Pathways. *Frontiers in Oncology*. https://doi.org/10.3389/fonc.2020.00562

Soriani, A., Iannitto, M. L., Ricci, B., Fionda, C., Malgarini, G., Morrone, S., … Santoni, A. (2014). Reactive Oxygen Species– and DNA Damage Response–Dependent NK Cell Activating Ligand Upregulation Occurs at Transcriptional Levels and Requires the Transcriptional Factor E2F1. *The Journal of Immunology*, *193*(2), 950–960. https://doi.org/10.4049/jimmunol.1400271

Spear, P., Barber, A., Rynda-Apple, A., & Sentman, C. L. (2013). NKG2D CAR T-cell therapy inhibits the growth of NKG2D ligand heterogeneous tumors. *Immunology & Cell Biology*, *91*(6), 435–440. https://doi.org/10.1038/icb.2013.17

Staba, M. J., Wickham, T. J., Kovesdi, I., & Hallahan, D. E. (2000). Modifications of the fiber in adenovirus vectors increase tropism for malignant glioma models. *Cancer Gene Therapy*, *7*(1), 13–19. https://doi.org/10.1038/sj.cgt.7700104

Stanziale, S. F., Petrowsky, H., Joe, J. K., Roberts, G. D., Zager, J. S., Gusani, N. J., … Fong, Y. (2002). Ionizing radiation potentiates the antitumor efficacy of oncolytic herpes simplex virus G207 by upregulating ribonucleotide reductase. *Surgery*, *132*(2), 353–359. https://doi.org/10.1067/msy.2002.125715

Stavrakaki, E., Dirven, C. M. F., & Lamfers, M. L. M. (2021). Personalizing oncolytic virotherapy for glioblastoma: In search of biomarkers for response. *Cancers*, *13*(4), 1–22. https://doi.org/10.3390/cancers13040614

Stern-Ginossar, N., Elefant, N., Zimmermann, A., Wolf, D. G., Saleh, N., Biton, M., … Mandelboim, O. (2007). Host Immune System Gene Targeting by a Viral miRNA. *Science*, *317*(5836), 376–381. https://doi.org/10.1126/science.1140956

Stern-Ginossar, Noam, Gur, C., Biton, M., Horwitz, E., Elboim, M., Stanietsky, N., … Mandelboim, O. (2008). Human microRNAs regulate stress-induced immune responses mediated by the receptor NKG2D. *Nature Immunology*, *9*(9), 1065–1073. https://doi.org/10.1038/ni.1642

Stork, R., Campigna, E., Robert, B., Müller, D., & Kontermann, R. E. (2009). Biodistribution of a bispecific single-chain diabody and its half-life extended derivatives. *Journal of Biological Chemistry*, *284*(38), 25612–25619. https://doi.org/10.1074/jbc.M109.027078

Stupp, R., Mason, W. P., van den Bent, M. J., Weller, M., Fisher, B., Taphoorn, M. J. B., … Mirimanoff, R. O. (2005). Radiotherapy plus Concomitant and Adjuvant Temozolomide for Glioblastoma. *New England Journal of Medicine*, *352*(10), 987–996. https://doi.org/10.1056/NEJMoa043330

Sundar, R., Cho, B. C., Brahmer, J. R., & Soo, R. A. (2015). Nivolumab in NSCLC: Latest evidence and clinical potential. *Therapeutic Advances in Medical Oncology*. https://doi.org/10.1177/1758834014567470

Sze, P., & Herman, R. C. (1992). The herpes simplex virus type 1 ICP6 gene is regulated by a “leaky” early promoter. *Virus Research*, *26*(2), 141–152. https://doi.org/10.1016/0168-1702(92)90153-Z

Szefel, J., Danielak, A., & Kruszewski, W. J. (2019). Metabolic pathways of L-arginine and therapeutic consequences in tumors. *Advances in Medical Sciences*. article, Netherlands: Elsevier B.V. https://doi.org/10.1016/j.advms.2018.08.018

Taguchi, S., Fukuhara, H., & Todo, T. (2019). Oncolytic virus therapy in Japan: Progress in clinical trials and future perspectives. *Japanese Journal of Clinical Oncology*, *49*(3), 201–209. https://doi.org/10.1093/jjco/hyy170

Takano, S., Yamashita, T., & Ohneda, O. (2010). Molecular therapeutic targets for glioma angiogenesis. *Journal of Oncology*, *2010*(Figure 4). https://doi.org/10.1155/2010/351908

Tamura, K., Wakimoto, H., Agarwal, A. S., Rabkin, S. D., Bhere, D., Martuza, R. L., … Shah, K. (2013). Multimechanistic tumor targeted oncolytic virus overcomes resistance in brain tumors. *Molecular Therapy*, *21*(1), 68–77. https://doi.org/10.1038/mt.2012.175

Tanaka, A., & Sakaguchi, S. (2017). Regulatory T cells in cancer immunotherapy. *Cell Research*. https://doi.org/10.1038/cr.2016.151

Teachey, D. T., Rheingold, S. R., Maude, S. L., Zugmaier, G., Barrett, D. M., Seif, A. E., … Grupp, S. A. (2013). Cytokine release syndrome after blinatumomab treatment related to abnormal macrophage activation and ameliorated with cytokine-directed therapy. *Blood*, *121*(26), 5154–5157. https://doi.org/10.1182/blood-2013-02-485623

Teng, M. W. L., Swann, J. B., Koebel, C. M., Schreiber, R. D., & Smyth, M. J. (2008). Immune-mediated dormancy: an equilibrium with cancer. *Journal of Leukocyte Biology*, *84*(4), 988–993. https://doi.org/10.1189/jlb.1107774

Terada, K., Wakimoto, H., Tyminski, E., Chiocca, E. A., & Saeki, Y. (2006). Development of a rapid method to generate multiple oncolytic HSV vectors and their in vivo evaluation using syngeneic mouse tumor models. *Gene Therapy*, *13*(8), 705–714. https://doi.org/10.1038/sj.gt.3302717

Textor, S., Fiegler, N., Arnold, A., Porgador, A., Hofmann, T. G., & Cerwenka, A. (2011). Human NK Cells Are Alerted to Induction of p53 in Cancer Cells by Upregulation of the NKG2D Ligands ULBP1 and ULBP2. *Cancer Research*, *71*(18), 5998–6009. https://doi.org/10.1158/0008-5472.CAN-10-3211

Thomas, M., Boname, J. M., Field, S., Nejentsev, S., Salio, M., Cerundolo, V., … Lehner, P. J. (2008). Down-regulation of NKG2D and NKp80 ligands by Kaposi's sarcoma-associated herpesvirus K5 protects against NK cell cytotoxicity. *Proceedings of the National Academy of Sciences*, *105*(5), 1656–1661. https://doi.org/10.1073/pnas.0707883105

Thomas, S., Kuncheria, L., Roulstone, V., Kyula, J. N., Mansfield, D., Bommareddy, P. K., … Coffin, R. S. (2019). Development of a new fusion-enhanced oncolytic immunotherapy platform based on herpes simplex virus type 1. *Journal for ImmunoTherapy of Cancer*, *7*(1), 1–17. https://doi.org/10.1186/s40425-019-0682-1

Thurber, G. M., Zajic, S. C., & Wittrup, K. D. (2007). Theoretic criteria for antibody penetration into solid tumors and micrometastases. *Journal of Nuclear Medicine*, *48*(6), 995–999. https://doi.org/10.2967/jnumed.106.037069

Todo, T., Martuza, R. L., Rabkin, S. D., & Johnson, P. A. (2001). Oncolytic herpes simplex virus vector with enhanced MHC class I presentation and tumor cell killing. *Proceedings of the National Academy of Sciences of the United States of America*, *98*(11), 6396–6401. https://doi.org/10.1073/pnas.101136398

Tokuyama, M., Lorin, C., Delebecque, F., Jung, H., Raulet, D. H., & Coscoy, L. (2011). Expression of the RAE-1 Family of Stimulatory NK-Cell Ligands Requires Activation of the PI3K Pathway during Viral Infection and Transformation. *PLoS Pathogens*, *7*(9), e1002265. https://doi.org/10.1371/journal.ppat.1002265

Tumangelova-Yuzeir, K., Naydenov, E., Ivanova-Todorova, E., Krasimirova, E., Vasilev, G., Nachev, S., & Kyurkchiev, D. (2019). Mesenchymal stem cells derived and cultured from glioblastoma multiforme increase tregs, downregulate th17, and induce the tolerogenic phenotype of monocyte-derived cells. *Stem Cells International*, *2019*. https://doi.org/10.1155/2019/6904638

Umemura, N., Saio, M., Suwa, T., Kitoh, Y., Bai, J., Nonaka, K., … Takami, T. (2008). Tumor-infiltrating myeloid-derived suppressor cells are pleiotropic-inflamed monocytes/macrophages that bear M1- and M2-type characteristics. *Journal of Leukocyte Biology*, *83*(5), 1136–1144. https://doi.org/10.1189/jlb.0907611

Unni, A. M., Bondar, T., & Medzhitov, R. (2008). Intrinsic sensor of oncogenic transformation induces a signal for innate immunosurveillance. *Proceedings of the National Academy of Sciences*, *105*(5), 1686–1691. https://doi.org/10.1073/pnas.0701675105

Valés-Gómez, M., Browne, H., & Reyburn, H. T. (2003). Expression of the UL16 glycoprotein of Human Cytomegalovirus protects the virus-infected cell from attack by natural killer cells. *BMC Immunology*, *4*, 4. https://doi.org/10.1186/1471-2172-4-4

Valés-Gómez, M., Chisholm, S. E., Cassady-Cain, R. L., Roda-Navarro, P., & Reyburn, H. T. (2008). Selective induction of expression of a ligand for the NKG2D receptor by proteasome inhibitors. *Cancer Research*, *68*(5), 1546–1554. https://doi.org/10.1158/0008-5472.CAN-07-2973

Van Den Bossche, W. B. L., Kleijn, A., Teunissen, C. E., Voerman, J. S. A., Teodosio, C., Noske, D. P., … Lamfers, M. L. M. (2018). Oncolytic virotherapy in glioblastoma patients induces a tumor macrophage phenotypic shift leading to an altered glioblastoma microenvironment. *Neuro-Oncology*, *20*(11), 1494–1504. https://doi.org/10.1093/neuonc/noy082

Van Der Bruggen, P., Traversari, C., Chomez, P., Lurquin, C., De Plaen, E., Van Den Eynde, B., … Boon, T. (1991). A gene encoding an antigen recognized by cytolytic T lymphocytes on a human melanoma. *Science*, *254*(5038). https://doi.org/10.1126/science.1840703

van Putten, E. H. P., Kleijn, A., van Beusechem, V. W., Noske, D., Lamers, C. H. J., de Goede, A. L., … Dirven, C. M. F. (2022). Convection enhanced delivery of the oncolytic adenovirus Delta24-RGD in recurrent GBM patients; a phase I clinical trial including correlative studies. *Clinical Cancer Research : An Official Journal of the American Association for Cancer Research*, 1–14. https://doi.org/10.1158/1078-0432.CCR-21-3324

Vantourout, P., Willcox, C., Turner, A., Swanson, C. M., Haque, Y., Sobolev, O., … Hayday, A. (2014). Immunological Visibility: Posttranscriptional Regulation of Human NKG2D Ligands by the EGF Receptor Pathway. *Science Translational Medicine*, *6*(231), 231ra49-231ra49. https://doi.org/10.1126/scitranslmed.3007579

Venkataraman, G. M., Suciu, D., Groh, V., Boss, J. M., & Spies, T. (2007). Promoter Region

Architecture and Transcriptional Regulation of the Genes for the MHC Class I-Related Chain A and B Ligands of NKG2D. *The Journal of Immunology*, *178*(2), 961–969. https://doi.org/10.4049/jimmunol.178.2.961

Verpooten, D., Ma, Y., Hou, S., Yan, Z., & He, B. (2009). Control of TANK-binding Kinase 1-mediated Signaling by the γ134.5 Protein of Herpes Simplex Virus 1. *Journal of Biological Chemistry*, *284*(2), 1097–1105. https://doi.org/10.1074/jbc.M805905200

Vetter, C. S., Groh, V., Straten, P. thor, Spies, T., Bröcker, E.-B., & Becker, J. C. (2002). Expression of Stress-induced MHC Class I Related Chain Molecules on Human Melanoma. *Journal of Investigative Dermatology*, *118*(4), 600–605. https://doi.org/10.1046/j.1523-1747.2002.01700.x

Vigano, S., Alatzoglou, D., Irving, M., Ménétrier-Caux, C., Caux, C., Romero, P., & Coukos, G. (2019). Targeting Adenosine in Cancer Immunotherapy to Enhance T-Cell Function. *Frontiers in Immunology*, *10*, 925–925. article. https://doi.org/10.3389/fimmu.2019.00925

Von Strandmann, E. P., Hansen, H. P., Reiners, K. S., Schnell, R., Borchmann, P., Merkert, S., … Engert, A. (2006). A novel bispecific protein (ULBP2-BB4) targeting the NKG2D receptor on natural killer (NK) cells and CD138 activates NK cells and has potent antitumor activity against human multiple myeloma in vitro and in vivo. *Blood*, *107*(5), 1955–1962. https://doi.org/10.1182/blood-2005-05-2177

Wakimoto, H., Kesari, S., Farrell, C. J., Curry, W. T., Zaupa, C., Aghi, M., … Rabkin, S. D. (2009). Human glioblastoma-derived cancer stem cells: Establishment of invasive glioma models and treatment with oncolytic herpes simplex virus vectors. *Cancer Research*, *69*(8), 3472–3481. https://doi.org/10.1158/0008-5472.CAN-08-3886

Waldhauer, I., Goehlsdorf, D., Gieseke, F., Weinschenk, T., Wittenbrink, M., Ludwig, A., … Steinle, A. (2008). Tumor-associated MICA is shed by ADAM proteases. *Cancer Research*, *68*(15), 6368–6376. https://doi.org/10.1158/0008-5472.CAN-07-6768

Wan, P. K. T., Ryan, A. J., & Seymour, L. W. (2021). Beyond cancer cells: Targeting the tumor microenvironment with gene therapy and armed oncolytic virus. *Molecular Therapy*, *29*(5), 1668–1682. https://doi.org/10.1016/j.ymthe.2021.04.015

Wang, H., Zhou, H., Xu, J., Lu, Y., Ji, X., Yao, Y., … Wan, J. (2021). Different T-cell subsets in glioblastoma multiforme and targeted immunotherapy. *Cancer Letters*, *496*, 134–143. https://doi.org/10.1016/j.canlet.2020.09.028

Wang, J., Shen, F., Yao, Y., Wang, L. L., Zhu, Y., & Hu, J. (2020). Adoptive Cell Therapy: A Novel and Potential Immunotherapy for Glioblastoma. *Frontiers in Oncology*. https://doi.org/10.3389/fonc.2020.00059

Warburg, O., Wind, F., & Negelein, E. (1924). Über den Stoffwechsel der Tumoren (Original German article). *Biochem. Z.*, *152*.

Waters, A. M., Johnston, J. M., Reddy, A. T., Fiveash, J., Madan-Swain, A., Kachurak, K., … Friedman, G. K. (2017). Rationale and Design of a Phase 1 Clinical Trial to Evaluate HSV G207 Alone or with a Single Radiation Dose in Children with Progressive or Recurrent Malignant Supratentorial Brain Tumors. *Human Gene Therapy. Clinical Development*, *28*(1), 7–16. https://doi.org/10.1089/humc.2017.002

Watson, N. F. S., Spendlove, I., Madjd, Z., McGilvray, R., Green, A. R., Ellis, I. O., … Durrant, L. G. (2006). Expression of the stress-related MHC class I chain-related protein MICA is an indicator of good prognosis in colorectal cancer patients. *International Journal of Cancer*, *118*(6), 1445–1452. https://doi.org/10.1002/ijc.21510

Wei, S. C., Duffy, C. R., & Allison, J. P. (2018). Fundamental mechanisms of immune checkpoint blockade therapy. *Cancer Discovery*, *8*(9), 1069–1086. https://doi.org/10.1158/2159-8290.CD-18-0367

Weiss, T., Schneider, H., Silginer, M., Steinle, A., Pruschy, M., Polic, B., … Roth, P. (2018). NKG2D-Dependent antitumor effects of chemotherapy and radiotherapy against glioblastoma. *Clinical Cancer Research*, *24*(4), 882–895. https://doi.org/10.1158/1078-0432.CCR-17-1766

Weiss, T., Weller, M., Guckenberger, M., Sentman, C. L., & Roth, P. (2018). NKG2D-based CAR T cells and radiotherapy exert synergistic efficacy in glioblastoma. *Cancer Research*, *78*(4), 1031–1043. https://doi.org/10.1158/0008-5472.CAN-17-1788

Welte, S. A., Sinzger, C., Lutz, S. Z., Singh-Jasuja, H., Sampaio, K. L., Eknigk, U., … Steinle, A. (2003). Selective intracellular retention of virally induced NKG2D ligands by the human cytomegalovirus UL16 glycoprotein. *European Journal of Immunology*, *33*(1), 194–203. https://doi.org/10.1002/immu.200390022

Wen, C., He, X., Ma, H., Hou, N., Wei, C., Song, T., … Zhong, H. (2008). Hepatitis C Virus Infection Downregulates the Ligands of the Activating Receptor NKG2D. *Cellular & Molecular*

Immunology, *5*(6), 475–478. https://doi.org/10.1038/cmi.2008.60

Whisenhunt, T. R., Rajneesh, K. F., Hackney, J. R., & Markert, J. M. (2015). Extended disease-free interval of 6 years in a recurrent glioblastoma multiforme patient treated with G207 oncolytic viral therapy. *Oncolytic Virotherapy*, *4*, 33–38. https://doi.org/10.2147/OV.S62461

Wick, W., Platten, M., & Weller, M. (2001). Glioma cell invasion: regulation of metalloproteinase activity by TGF-beta. *Journal of Neuro-Oncology*, *53*(2), 177–185. https://doi.org/10.1023/a:1012209518843

Williams, B. R. (1999). PKR; a sentinel kinase for cellular stress. *Oncogene*, *18*, 6112.

Wirsching, H. G., Zhang, H., Szulzewsky, F., Arora, S., Grandi, P., Cimino, P. J., … Holland, E. C. (2019). Arming oHSV with ULBP3 drives abscopal immunity in lymphocyte-depleted glioblastoma. *JCI Insight*, *4*(13), 1–13. https://doi.org/10.1172/jci.insight.128217

Wischhusen, J., Friese, M. A., Mittelbronn, M., Meyermann, R., & Weller, M. (2005). HLA-E protects glioma cells from NKG2D-mediated immune responses in vitro: Implications for immune escape in vivo. *Journal of Neuropathology and Experimental Neurology*, *64*(6), 523–528. https://doi.org/10.1093/jnen/64.6.523

Wolf, E., Hofmeister, R., Kufer, P., Schlereth, B., & Baeuerle, P. A. (2005). BiTEs: Bispecific antibody constructs with unique anti-tumor activity. *Drug Discovery Today*. https://doi.org/10.1016/S1359-6446(05)03554-3

Woroniecka, K. I., Rhodin, K. E., Chongsathidkiet, P., Keith, K. A., & Fecci, P. E. (2018). T-Cell dysfunction in glioblastoma: Applying a new framework. *Clinical Cancer Research*, *24*(16), 3792–3802. https://doi.org/10.1158/1078-0432.CCR-18-0047

Wu, J., Chalupny, N. J., Manley, T. J., Riddell, S. R., Cosman, D., & Spies, T. (2003). Intracellular Retention of the MHC Class I-Related Chain B Ligand of NKG2D by the Human Cytomegalovirus UL16 Glycoprotein. *The Journal of Immunology*, *170*(8), 4196–4200. https://doi.org/10.4049/jimmunol.170.8.4196

Xu, B., Tian, L., Chen, J., Wang, J., Ma, R., Dong, W., … Yu, J. (2021). An oncolytic virus expressing a full-length antibody enhances antitumor innate immune response to glioblastoma. *Nature Communications*, *12*(1). https://doi.org/10.1038/s41467-021-26003-6

Xu, F., Sternberg, M. R., Kottiri, B. J., McQuillan, G. M., Lee, F. K., Nahmias, A. J., … Markowitz, L. E. (2006). Trends in herpes simplex virus type 1 and type 2 seroprevalence in the United States. *Journal of the American Medical Association*, *296*(8), 964–973. https://doi.org/10.1001/jama.296.8.964

Yamamoto, K. (2001). Oxidative stress increases MICA and MICB gene expression in the human colon carcinoma cell line (CaCo-2). *Biochimica et Biophysica Acta (BBA) - General Subjects*, *1526*(1), 10–12. https://doi.org/10.1016/S0304-4165(01)00099-X

Yang, D., Sun, B., Dai, H., Li, W., Shi, L., Zhang, P., … Zhao, X. (2019). T cells expressing NKG2D chimeric antigen receptors efficiently eliminate glioblastoma and cancer stem cells. *Journal for ImmunoTherapy of Cancer*, *7*(1), 1–13. https://doi.org/10.1186/s40425-019-0642-9

Yang, W., Li, Y., Gao, R., Xiu, Z., & Sun, T. (2020). MHC class I dysfunction of glioma stem cells escapes from CTL-mediated immune response via activation of Wnt/β-catenin signaling pathway. *Oncogene*, *39*(5), 1098–1111. https://doi.org/10.1038/s41388-019-1045-6

Yao, X., Labelle, M., Lamb, C. R., Dugan, J. M., Williamson, C. A., Spencer, D. R., … Wittrup, K. D. (2013). Determination of 35 cell surface antigen levels in malignant pleural effusions identifies CD24 as a marker of disseminated tumor cells. *International Journal of Cancer*, *133*(12), 2925–2933. https://doi.org/10.1002/ijc.28312

Ylösmäki, E., & Cerullo, V. (2020). Design and application of oncolytic viruses for cancer immunotherapy. *Current Opinion in Biotechnology*, *65*(Ici), 25–36. https://doi.org/10.1016/j.copbio.2019.11.016

Yu, F., Hong, B., & Song, X.-T. (2017). A T-cell engager-armed oncolytic vaccinia virus to target the tumor stroma. *Cancer Translational Medicine*, *3*(4), 122. https://doi.org/10.4103/ctm.ctm_13_17

Yu, F., Wang, X., Guo, Z. S., Bartlett, D. L., Gottschalk, S. M., & Song, X. T. (2014). T-cell engager-armed oncolytic vaccinia virus significantly enhances antitumor therapy. *Molecular Therapy*, *22*(1), 102–111. https://doi.org/10.1038/mt.2013.240

Zachos, G., Clements, B., & Conner, J. (1999). Herpes simplex virus type I infection stimulates p38/c-Jun N-terminal mitogen-activated protein kinase pathways and activates transcription factor AP-1. *Journal of Biological Chemistry*, *274*(8), 5097–5103. https://doi.org/10.1074/jbc.274.8.5097

Zhang, K. X., Matsui, Y., Hadaschik, B. A., Lee, C., Jia, W., Bell, J. C., … Rennie, P. S. (2010). Down-regulation of type I interferon receptor sensitizes bladder cancer cells to vesicular

stomatitis virus-induced cell death. *International Journal of Cancer*. https://doi.org/10.1002/ijc.25088

Zhang, T., & Sentman, C. L. (2011). Cancer Immunotherapy Using a Bispecific NK Receptor Fusion Protein that Engages both T Cells and Tumor Cells. *Cancer Research*, *71*(6), 2066–2076. https://doi.org/10.1158/0008-5472.CAN-10-3200

Zhang, X., Rao, A., Sette, P., Deibert, C., Pomerantz, A., Kim, W. J., … Amankulor, N. (2016). IDH mutant gliomas escape natural killer cell immune surveillance by downregulation of NKG2D ligand expression. *Neuro-Oncology*, *18*(10), 1402–1412. https://doi.org/10.1093/neuonc/now061

Zingoni, A., Molfetta, R., Fionda, C., Soriani, A., Paolini, R., Cippitelli, M., … Santoni, A. (2018). NKG2D and Its Ligands: "One for All, All for One." *Frontiers in Immunology*, *9*(MAR). https://doi.org/10.3389/fimmu.2018.00476

Zou, Y., Bresnahan, W., Taylor, R. T., & Stastny, P. (2005). Effect of Human Cytomegalovirus on Expression of MHC Class I-Related Chains A. *The Journal of Immunology*, *174*(5), 3098–3104. https://doi.org/10.4049/jimmunol.174.5.3098

7 Appendices

7.1.1 Representative flow cytometry histograms for MICA/B and NKG2DL staining

As described in section 3.3.1, DLD-1 colorectal carcinoma cells, U87 and A172 GBM cell lines were stained for surface MICA/B and total NKG2DLs using a commercially available antibody and rhNKG2D-Fc-Bio-Strep-PE, respectively. The representative histograms following staining each of the cells is shown in Figure 7.1, including relevant staining controls.

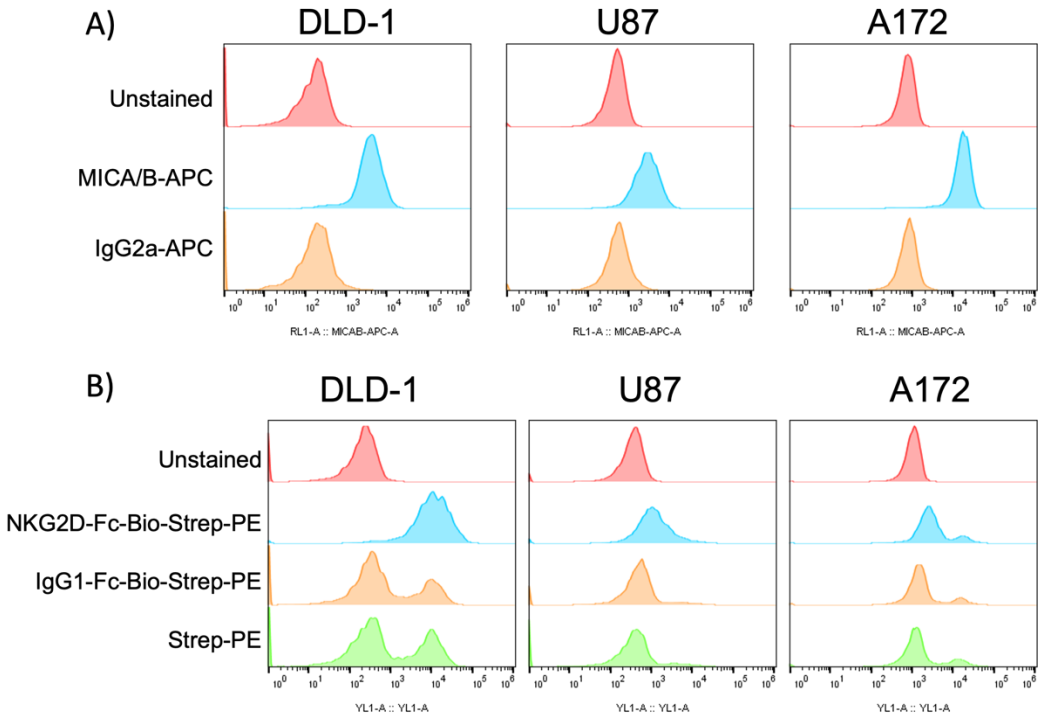

Figure 7.1 Representative flow cytometry histograms of cell lines stained for MICA/B and total NKG2DLs
(**A**) Cancer cell lines DLD-1 (colorectal carcinoma), U87 (GBM) and A172 (GBM) cells were stained for flow cytometric analysis with either anti-MICA/B-APC or IgG2a-APC isotype or left unstained. Percentage of cells positive for MICA/B or Isotype. (**B**) DLD-1, U87 and A172 cells were also stained for total surface NKG2DLs using biotinylated recombinant human NKG2D-Fc and Streptavidin-PE secondary (NKG2D-Fc-Bio-Strep-PE), biotinylated human IgG1 isotype (IgG1), or Streptavidin-PE secondary only (Strep-PE). Percentage of cells positive for NKG2D-Fc, IgG1 and Strep-PE compared to unstained. Histograms represent the number of single cells and their fluorescence intensity as determined by flow cytometry.

7.1.2 Optimisation of TMZ and radiation pre-treatment dosages

After observing the effects of TMZ (Figure 4.3) or radiation (Figure 4.4) monotherapy on increasing NKG2DL expression on U87 and A172 cells, we next sought to recreate concomitant TMZ and radiotherapy in this cell line model. The goal was to find an optimal dosage of TMZ and radiation that balanced increased NKG2DL expression with minimal cytotoxicity. Once identified, this optimal dosage would then be used for future experiments combining TMZ and radiation as pre-treatments before using the NKG2D BiTE (and eventually, oHSV-1 expressing the NKG2D BiTE).

U87 and A172 cells were treated 50 μM and 100 μM TMZ, 2 Gy and 5 Gy radiation and a combination before being assessed for total NKG2DL expression by flow cytometry 72 hours later (Figure 7.2A and B, respectively).

NKG2DLs expression significantly increased on U87 cells (Figure 7.2A) in response to 50 μM and 100 μM TMZ alone. Radiation treatment alone did increase expression slightly; however, this was not statistically significant. Radiation in combination with TMZ did induce a significant increase in NKG2DL expression on U87 cells.

The relative NKG2DL expression on A172 cells (Figure 7.2B) showed a similar pattern, with significant increases in response to TMZ alone. Additionally, 2 Gy radiation also induces a significant increase. However, the other treatment conditions did induce slight increases in expression, but they did not reach statistical significance.

The observations from Figure 7.2 suggest that TMZ consistently induces a statistically significant increase in surface NKG2DLs, while radiation alone trends towards increasing expression but not as much as TMZ. Nevertheless, a combination of 2 Gy with TMZ induced an additive increase in NKG2DL expression compared to either monotherapy. Therefore, the dosages selected for further experiments were 100 μM TMZ and 2 Gy radiation.

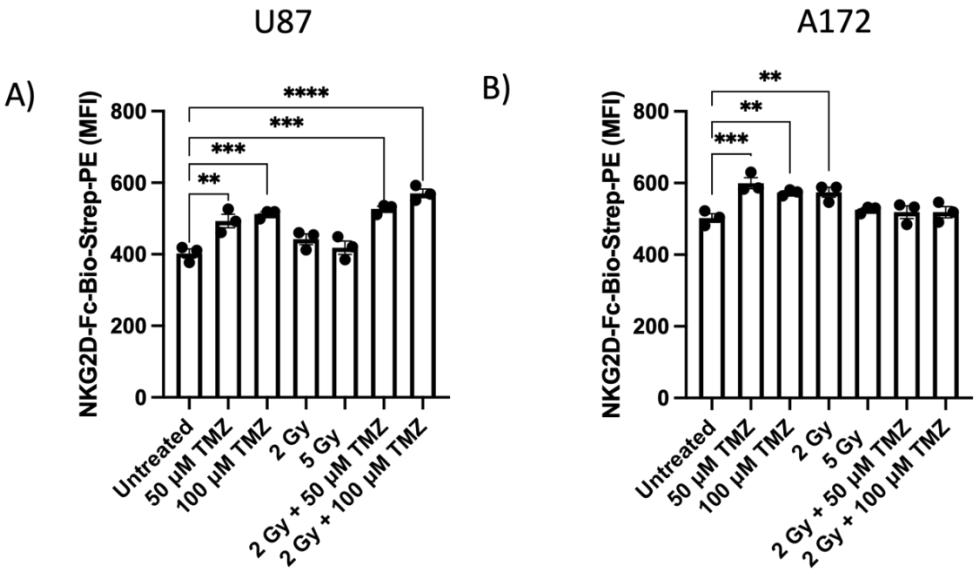

Figure 7.2 Effects of TMZ and radiation combinations on NKG2DL expression on GBM cell lines

(**A**) U87 and (**B**) A172 cells were seeded in individual T25 flasks in 10% DMEM and treated with either 50 μM or 100 μM TMZ, 2 Gy or 5 Gy radiation, or a combination of 2 Gy + 50 μM TMZ or 2 Gy + 100 μM TMZ. 72 hours after treatment, cells were harvested with non-enzymatic cell dissociation buffer and stained with biotinylated recombinant human NKG2D-Fc and Streptavidin-PE secondary (NKG2D-Fc-Bio-Strep-PE) for flow cytometric analysis. Data represents the mean fluorescence intensity (MFI) of triplicate repeats ± S.D. Statistical significance was assessed by one-way ANOVA followed by Bonferroni post hoc analysis. Significance was assessed versus untreated cells (ns $p>0.05$, *$p\leq0.05$, **$p\leq0.01$, ***$p\leq0.001$ and ****$p\leq0.0001$).

U87 and A172 cells were pre-treated with the same treatment dosages as determined in Figure 7.2, (100 μM TMZ, 2 Gy radiation, and 2 Gy + 100 μM TMZ) 72 hours before being co-cultured with T cells and treated with NKG2D BiTE. Cells were co-cultured for a further 72 hours before assessing expression of T cell CD25 and CD69 expression and target cell viability by flow cytometry. Additionally, after the initial pre-treatment (when cells were dissociated for seeding), cells were stained for surface MICA/B expression by flow cytometry to confirm the increased expression after pre-treatment.

The relative surface MICA/B expression following pre-treatment on U87 and A172 cells is shown in Figure 7.3A and B, respectively. These data confirm the previous observations, that 100 μM TMZ and 2 Gy + 100 μM significantly increased surface MICA/B expression in both cell lines. In U87 cells, 2 Gy alone did not induce a significant increase compared to no pre-treatment, but it did in A172 cells.

Nevertheless, these pre-treatments generally increased surface MICA/B expression on both cell lines.

T cell activation in co-cultures treated with NKG2D BiTE, Control BiTE or no BiTE was then analysed. The percentage of $CD25^+$ T cells in co-culture with U87 and A172 cells is shown in Figure 7.3C and D, respectively, and percentage of $CD69^+$ T cells in Figure 7.3E and F, respectively.

$CD8^+$ T cells express the NKG2D receptor, and so have the potential to respond to an increase in NKG2DL ligands. However, pre-treatment of U87 cells had no effect on T cell activation in the absence of BiTE for both cell lines (Figure 7.3C-F), suggesting that increased surface NKG2DL expression in response to the various pre-treatments did not sensitise target cells to T cells without BiTE. Additionally, this T cell activity remained at this baseline for U87 cells when treated with the Control BiTE (Figure 7.3C and E), suggesting that the pre-treatments did not interfere with the non-specific activity of the Control BiTE in these co-cultures. However, pre-treated A172 cells did show a slight but significant increase in T cell activation in co-cultures treated with Control BiTE (Figure 7.3D and F). This may suggest that pre-treatment of A172 cells with TMZ and radiation increases the non-specific binding of the Control BiTE to these cells resulting in this increase in non-specific BiTE activity.

The NKG2D BiTE activated T cells in co-cultures with both U87 (Figure 7.3C and E) and A172 cells (Figure 7.3D and F). However, pre-treatment did not increase T cell activation with either cell line. In co-cultures with U87 cells, the percentage of CD25+ cells slightly decreased with pre-treatments compared to no pre-treatment. (Figure 7.3C) A similar decrease was observed in pre-treated A172 cells (Figure 7.3D), with significant decreases after TMZ pre-treatment and 2 Gy + TMZ compared to no pre-treatment. Pre-treated U87 cells (Figure 7.3E) demonstrated significant decreases in the percentage of CD69+ T cells in response to all pre-treatments. Additionally, A172 cells (Figure 7.3F) showed significant decreases after pre-treatment with TMZ and 2 Gy + TMZ compared to no pre-treatment, but 2 Gy did slightly increase. Together these data indicate that pre-treatment with 100 μM TMZ and 2 Gy radiation alone or in combination resulted in a decrease in T cell activity with the NKG2D BiTE compared to no pre-treatment, despite the increase in surface NKG2DLs.

The overall goal of combining conventional GBM therapy of radiation and TMZ with the NKG2D BiTE immunotherapy is to kill GBM cells. Therefore, the percentage of live U87 and A172 cells was measured by flow cytometry (Figure 7.3G and H, respectively). The viabilities of both GBM cell lines were tested in monocultures (without T cells) to assess the cytotoxic effects of TMZ and radiation pre-treatment alone, and in co-cultures (with T cells) to observe the effects of combination with NKG2D BiTE immunotherapy.

Pre-treatment of U87 cells with TMZ and 2 Gy + TMZ significantly decreased viability in monoculture with no BiTE compared to no pre-treatment (Figure 7.3G), but DMSO, 2 Gy and 2 Gy + DMSO had no effect. This effect was replicated in co-cultures in the absence of BiTE and in the presence of Control BiTE. These findings suggest that TMZ and 2 Gy + TMZ cause a significant decrease in the viability of U87 cells, but that 2 Gy radiation alone does not have any noticeable effect.

For A172 cells (Figure 7.3H), pre-treatments had a larger effect on viability in the absence of NKG2D BiTE. A172 cells in monoculture and no BiTE showed significant sensitivity to the pre-treatments. This trend was again demonstrated in co-cultures with no BiTE and co-cultures with Control BiTE. This reflects the data observed in Figure 4.3 and Figure 4.4, that A172 cells are highly sensitive to TMZ and radiation.

NKG2D BiTE treatment of U87 + T cell co-cultures reduced U87 cell viability dramatically (Figure 7.3G). Compared to co-cultures with no pre-treatment and no BiTE (91%) or Control BiTE (93%), the cytotoxic activity of the NKG2D BiTE with no pre-treatment can be seen (54%). The viability of U87 cells decreased significantly further when U87 cells were pre-treated with TMZ (29%) or 2 Gy + TMZ (25%). This shows that the combination of 100 μM TMZ or 2 Gy + 100 μM TMZ with NKG2D BiTE significantly reduces the viability of U87 cells compared to either conventional or immunotherapy therapy on its own.

A172 cells were also highly sensitive to NKG2D BiTE (Figure 7.3H). Without pre-treatment, A172 viability dropped to 24% in co-cultures treated with NKG2D BiTE, compared to 88% with no BiTE or 87% with Control BiTE. Unlike U87 cells in Figure 7.3G, the viability of A172 cells in co-cultures treated with NKG2D BiTE did not change in response to the various pre-treatments, except for a slight but

significant decrease in viability after 2 Gy + TMZ pre-treatment (19%). These findings suggest that A172 cells are highly sensitive to the conventional therapy of TMZ and 2 Gy, as well as NKG2D BiTE immunotherapy. The viability of A172 cells did not change when pre-treated and given NKG2D BiTE compared to no pre-treatment suggests that the NKG2D BiTE may already be working at maximum activity. This may indicate that the T cell-mediated killing is saturated when A172 cells are the target cells, such that increases in NKG2DL expression and additional contributions towards cytotoxicity from TMZ or radiation are masked by the high activity of the NKG2D BiTE.

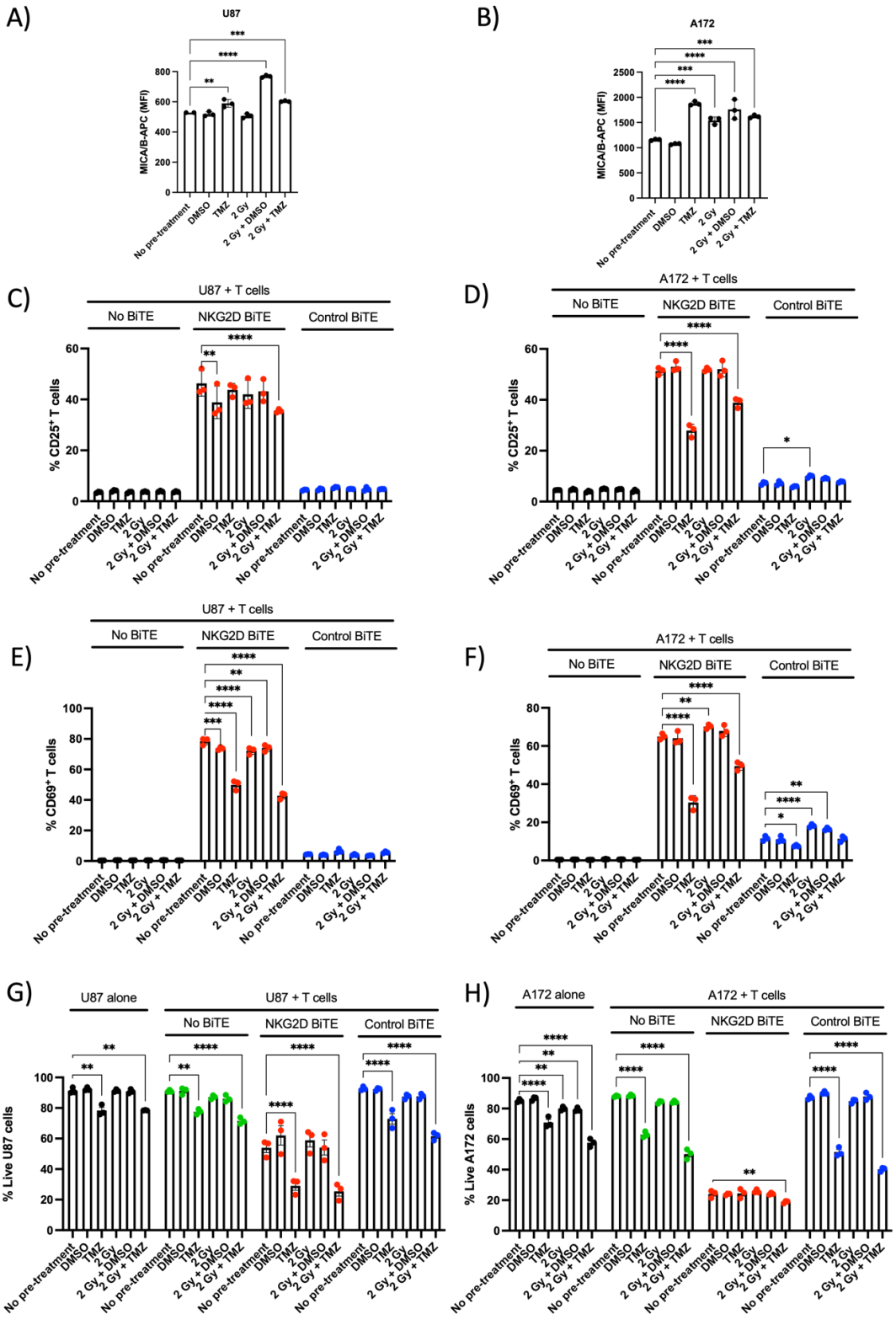

Figure 7.3 Initial investigation into the effects of pre-treatment with 100 μM TMZ and 2 Gy on NKG2D BiTE activity

U87 (left) and A172 (right) cells were treated with a single dose of 100 μM temozolomide (TMZ) or equivalent vehicle control (DMSO), or a single dose of 2 Gray (Gy) radiation either alone (2 Gy) or in combination with 100 μM TMZ (2 Gy + TMZ) or vehicle control (2 Gy + DMSO) or left untreated (no pre-treatment). (**A**) 48 hours after pre-treatment, U87 and (**B**) A172 cells were

harvested with non-enzymatic dissociation buffer and stained for surface MICA/B-APC for flow cytometric analysis. Data represents the mean fluorescence intensity (MFI) of triplicate repeats ± S.D. Additionally, 72 hours after the initial pre-treatment, cells were seeded in co-cultures with PBMC-derived T cells at an E: T ratio 5:1 and treated with 1 nM NKG2D BiTE, 1 nM Control BiTE or left untreated. After a further 72 hours of co-culture, all cells were harvested and stained for flow cytometric analysis. (**C**) T cells in co-cultures with U87 and (**D**) A172 cells were stained for activation marker CD25, or CD69 (**E** and **F** for U87 and A172, respectively). Data represents the mean percentage of $CD25^+$ or $CD69^+$ T cells of triplicate repeats ± S.D in co-cultures with U87 or A172 cells treated with 1 nM NKG2D BiTE (red), 1 nM Control BiTE (blue) or left untreated (black). (G) U87 and (H) A172 cells were stained with a viability dye for flow cytometric analysis. Data represents the percentage of viable U87 or A172 cells of triplicate repeats ± S.D from monocultures (black), untreated co-cultures (green), and co-cultures treated with 1 nM NKG2D BiTE (red) or Control BiTE (blue). Statistical significance was assessed by two-way ANOVA followed by Bonferroni post hoc analysis. Significance was assessed versus no pre-treatment within the relevant group (ns $p>0.05$, *$p\leq0.05$, **$p\leq0.01$, ***$p\leq0.001$ and ****$p\leq0.0001$).

Based on the findings in Figure 7.3H, it seems that A172 cells are too sensitive to the NKG2D BiTE for any subtle changes in viability to be detectable after pre-treatment with TMZ and radiation. This finding is in concordance with the data in Figure 3.5G, in which A172 cell viability is more greatly reduced when treated with 1 nM NKG2D BiTE after 72 hours than U87 cells. Furthermore, A172 cells were highly sensitive to TMZ and radiation in the absence of NKG2D BiTE, resulting in fewer viable cells left in the well before the T cells and NKG2D BiTE were added and therefore fewer target cells for the BiTE and T cells to engage with. This may subsequently result in an apparent decrease in T cell activation despite an overall increase in NKG2DL expression on each live cell. Therefore, U87 cells were selected for further experiments to assess the relationship between pre-treatment and NKG2D BiTE activity.

While U87 cells did show a significant decrease in viability in co-cultures with NKG2D BiTE after pre-treatment compared to no pre-treatment (Figure 7.3H), the expression of T cell activation markers CD25 and CD69 decreased in response to pre-treatment (Figure 7.3C and E, respectively). The decrease in T cell activation may be due to a similar reason as discussed above for A172 cells; that the pre-treatments resulted in a decrease in the number of viable target cells remaining in the well, despite an overall increase in NKG2DL expression (Figure 7.3A). The decrease in the number of target cells then presents fewer target cells to T cells and NKG2D BiTE, translating into a decrease in the T cell activity, but still resulting in a large decrease in U87 cell viability (Figure 7.3G). Additionally, the 100 μM TMZ seemed to be having a greater effect on the U87 viability than 2 Gy radiation alone.

Therefore, for future experiments, the concentration of TMZ used for pre-treatment was reduced from 100 μM to 50 μM, but the radiation was kept at 2 Gy.

7.1.3 Viral quality control assessment, titration, and replicative ability

The quantification of total viral particles was determined by PicoGreen assay (Materials and Methods section 2.9.3), whereby the concentration of viral genomes (dsDNA) was measured against a standard curve of dsDNA. Infectious virus particles were quantified by plaque agar assay in Vero cells (Materials and Methods section 2.9.4).

The values of virus titre as measured by PicoGreen assay (vp/mL), infectious viral particles as measured by plaque assay (PFU/mL) and the ratio of virus particles: infectious virus particles (vp: PFU) are listed in a table in Figure 7.4A. The vp/mL and PFU/mL for all three viruses (G207, G207-NKG2DBiTE and G207-ControlBiTE) were all within a similar range of each other suggesting each viral stock was approximately comparable in its viral concentration.

Traditionally, plaques can then be measured by counting viral plaques formed in the cell monolayer by crystal violet (1%, v/v) staining of the plate. However, this technique is limited as it relies on the ability of the user to detect and visibly see the plaques, hence smaller plaques may be missed, and hence give an underestimate of the final PFU/mL. Since the G207 viral backbone contains eGFP, the visualisation of viral plaques using a fluorescent microscope could be much more sensitive than simply using the naked eye and crystal violet. Therefore, plaques were counted after 4-5 days across the dilutions and replicates using fluorescence microscopy.

The insertion of transgenes into viral vectors may result in alterations in the ability of the virus to replicate its genome and complete its normal life cycle. For instance, insertion of a large transgene may increase the viral genome size to the degree that means that viral replication takes longer than the empty parental virus. Alternatively, integration of the transgene into the genome may occur in a region that affects the function of other viral genes that may be important for infection, replication, or packaging. However, this outcome is unlikely due to the site-specific nature of the recombination sites used to insert the BiTE transgenes, and the

recombination to remove the viral genome from the BAC plasmid. Finally, the highly driven transcription of the transgene by the CMV promoter and subsequent translation of these non-viral proteins may affect transcription, translation or function of the normal viral genes and gene products. Therefore, it is important to demonstrate incorporating the NKG2D and Control BiTEs into the G207 virus has not significantly altered the activity of the virus to replicate and infect compared to the parental G207.

To measure the effects of the transgene insertion, the G207-NKG2D and G207-ControlBiTE viruses were infected at a range of MOIs in the highly permissive Vero cells and the viability of the Vero cells was assessed 72 hours later. This experiment was conducted in the absence of T cells to observe the effects of the viral infection and lysis specifically and not be confounded by the additional cytotoxicity induced by the NKG2D BiTE and T cells (Figure 7.4B). For this experiment, Vero cells were infected with parental G207, G207-NKG2DBiTE or G207-ControlBiTE across a range of MOIs. Relative Vero cell viability was assessed by MTS viability assay (Materials and Methods section 2.4.9) 72 hours later compared to uninfected controls (Figure 7.4B). All viruses showed little cytotoxicity between MOIs 0.0001 and 0.01. The relative viability at MOI 0.1 then dropped significantly to around 0.5 for all three viruses and then further still at MOI 1 to around 0.25. There was no significant difference in the relative viabilities between the G207 parental virus, the G207-NKG2DBiTE, or the G207-ControlBiTE virus, indicating that the insertion of the NKG2D or Control BiTE had not affected the activity of the G207 virus itself and that infectivity, replication and oncolytic activity were retained.

A)

	Virus titre (vp/mL)	Infectious particles (PFU/mL)	vp:PFU ratio
G207	2.01×10^{10}	1.25×10^{8}	168.00
G207-NKG2D BiTE	4.27×10^{10}	9.66×10^{7}	441.63
G207-Control BiTE	1.12×10^{10}	8.43×10^{7}	132.75

B)

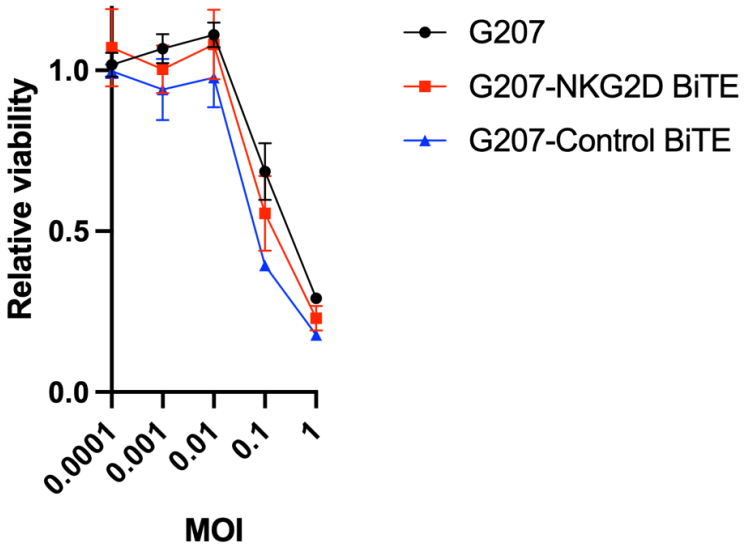

Figure 7.4 G207 and BiTE-armed G207 viral titres and replicative ability.
(A) Table showing the quantitative assessments of G207, G207-NKG2DBiTE and G207-ControlBiTE viruses. Virus titre of virus particles (vp)/mL was measured by PicoGreen assay. Infectious viral particles of plaque forming units (PFU)/mL was measured by plaque agar assay. Ratio of virus particles: infectious viral particles (vp:PFU) was calculated by dividing the relative numbers. (B) Assessment of viral replicative activity. Vero cells were infected with G207 (black), G207-NKG2DBiTE (red) or G207-ControlBiTE (blue) at MOI 0.0001, 0.001, 0.01, 0.1 and 1 for 72 hours before viability was measured by MTS assay (Promega). Relative viability is assessed compared to uninfected cells. Data represents mean relative viability of triplicate repeats ± S.D.

7.1.4 Assessment of shedding of NKG2DLs from GBM cells

The loss of surface expression of NKG2DLs is a strategy often employed by both cancer cells and viruses to achieve immune evasion from the innate immune response (Baugh et al., 2020). While some viruses such as CMV commonly downregulate surface ligands by retaining these ligands intracellularly, many cancers often lose surface expression by shedding the NKG2DLs from their surface. Additionally, soluble NKG2DLs (sNKG2DLs) shed from the cancer cells may act as decoy receptors for the NKG2D BiTE, thus diminishing the effective concentration

of the BiTE. We therefore sought to assess whether U87 cells produced a detectable level of sNKG2DLs. Furthermore, to investigate the mechanism behind the downregulation of NKG2DLs, particularly MICA/B, from the surface of GBM cell lines infected with G207 (Figure 4.1), the concentration of sNKG2DLs in cell culture supernatants from uninfected and G207-infected U87 cells was measured by competitive ELISA (Materials and Methods section 2.9.8). Cells were also infected with G207-NKG2DBiTE and G207-ControlBiTE, to determine if any NKG2D BiTE produced by the cells infected with G207-NKG2DBiTE virus was able to bind and sequester sNKG2DLs in the media and prevent binding to the ELISA plate (Figure 7.5).

The supernatant from uninfected U87 cells contained 0.76 ng/mL sNKG2DLs as a baseline. This increased slightly to 0.92, 0.89 and 0.83 ng/mL for U87 cells infected with G207, G207-NKG2DBiTE and G207-ControlBiTE respectively. The uninfected supernatants treated with 1 nM NKG2D BiTE slightly decreased compared to untreated and uninfected cells and contained 0.65 ng/mL sNKG2DLs. However, none of these results reached statistical significance by one way ANOVA.

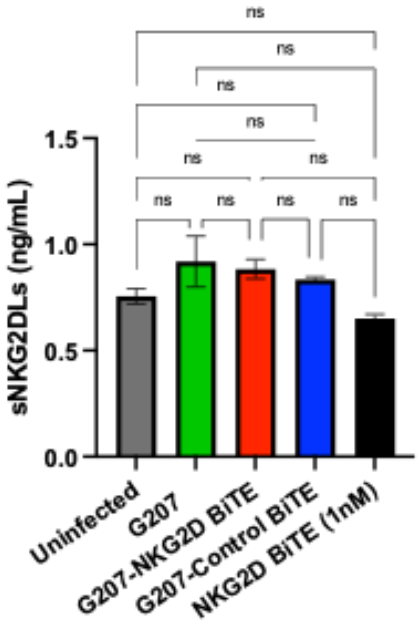

Figure 7.5 Measurement of sNKG2DLs produced from U87 cells infected with G207 viruses

U87 cells were infected with empty parental G207 (green), G207-NKG2DBiTE (red) or G207-ControlBiTE (blue) or were left uninfected (grey) or treated with 1 nM NKG2D BiTE (black) for 72 hours before supernatants were harvested. The concentration of soluble NKG2DLs (sNKG2DLs) present in the culture supernatants was assessed using a competitive ELISA kit (MyBioSource #MBS744276) according to the manufacturer's instructions. Experiment was carried out in duplicate. Data represents mean concentration of sNKG2DLs (ng/mL) of

duplicate repeats ± S.D. Statistical significance was assessed by one-way ANOVA. (ns p>0.05, *p≤0.05, **p≤0.01, ***p≤0.001 and ****p≤0.0001).

These data are challenging to interpret, as the U87 cells appear to shed a relatively low level of NKG2DLs at baseline, and so subtle changes in this in response to the G207 viruses may be hard to detect. However, although none of these reached statistical significance, the data did trend towards a slight increase in sNKG2DLs in the infected supernatants compared to the uninfected untreated cells, indicating there may be a small amount of shedding of NKG2DLs from the surface of these infected cells in response to the G207 virus. Furthermore, a slight decrease in the sNKG2DLs in supernatants treated with 1 nM NKG2D BiTE may indicate that the NKG2D BiTE is interacting with the sNKG2DLs in the media, and thus preventing them from binding to the capture antibodies in the ELISA. While this is a topic for further investigation in future, it may suggest that the G207 virus may cause a decrease in surface NKG2DLs by actively shedding the ligands. However, these findings are limited by the U87 cells used in this assay.

7.1.5 Pre-treatment of TMZ and radiation enhances G207-NKG2DBiTE virus activity

For simplicity, the graphs in Figure 5.5 and Figure 5.6 show the viability and cytotoxicity of U87 cells in co-cultures only. For additional controls, the experiment was also performed in monocultures. The full data is shown in Figure 7.6.

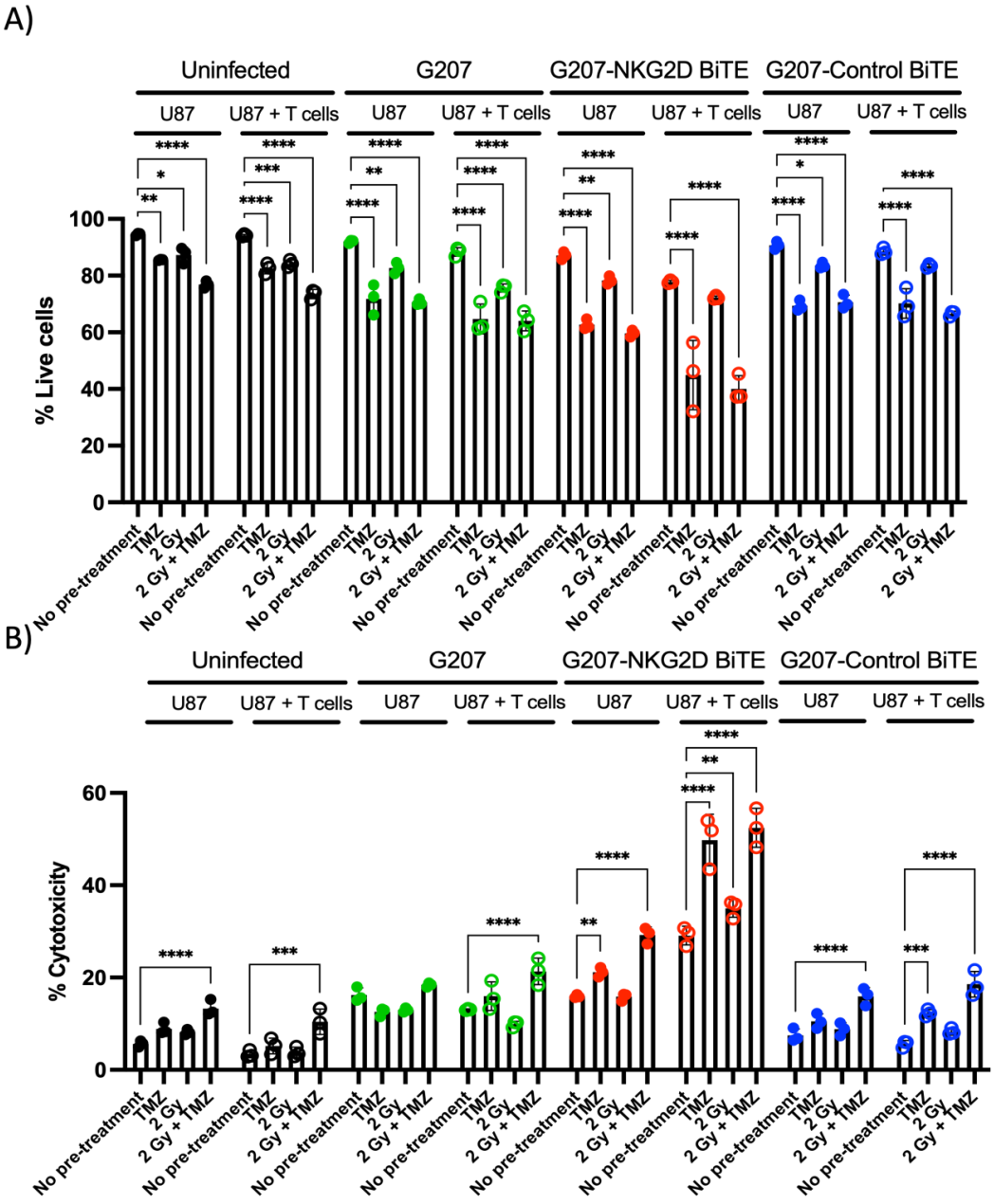

Figure 7.6 Conventional GBM therapy pre-treatment synergises with G207-NKG2DBiTE virus to kill U87 cells

(**A**) U87 cells were pre-treated with 50 μM temozolomide (TMZ), a single dose of 2 Gray (Gy) radiation alone (2 Gy) or in combination with 50 μM TMZ (2 Gy + TMZ) or left untreated (no pre-treatment). 72 hours after pre-treatment, U87 cells were infected with parental G207 (green), G207-NKG2DBiTE (red) or G207-ControlBiTE (blue) at a multiplicity of infection (MOI) of 0.1 or left uninfected (black). 4 hours after infection, PBMC-derived T cells were added at an E: T ratio 5:1 (right, hollow dots) or left as monocultures (left, filled dots). After culturing for 72 hours, cells were harvested, stained and percentage of live U87 cells was assessed using a flow cytometric viability dye, or (**B**) cytotoxicity was measured by lactate dehydrogenase (LDH) release. Data represents mean percentage of live U87 cells from triplicate repeats ± S.D. Statistical significance was assessed by two-way ANOVA followed by Bonferroni post hoc analysis. Significance was assessed versus no pre-treatment within the relevant group (ns $p>0.05$, *$p\leq0.05$, **$p\leq0.01$, ***$p\leq0.001$ and ****$p\leq0.0001$).

7.2 Supplementary information and tables

7.2.1 Recipe table

Table 7.1 Recipes for buffers, solutions and media used for multiple applications

Buffer	Application	Recipe
Neurobasal media (NBM)	GSC culture	500 mL Neurobasal medium (#21103-049, Gibco); 10 mL 50x B27 Plus supplement (#A3582801, Thermo Fisher Scientific); 20 ng/ mL final concentration recombinant human EGF basic (#AF-100-15, Peprotech); 20 ng/mL final concentration recombinant human FGF basic (#100-18B, Peprotech), 2 mM final concentration GlutaMAX-I (#35050061, Gibco); Pen/strep.
MACS buffer	Flow cytometry	2.5 g bovine serum albumin (BSA; #A3059, Sigma Aldrich), 5 mL 0.2 M EDTA in 500 mL sterile DPBS
TE buffer	Picogreen assay	5 mL 1 M Tris-HCl, pH 8; 1 mL 0.5 M EDTA, pH 8; add H_2O up to 500 mL
TAE buffer (50x)	Agarose gel electrophoresis	242 g Tris (#107089976001, Roche). 100 mL 0.5 ETDA, 57.1 mL acetic acid (#A6283, Sigma Aldrich) in 1 L H_2O
SDS running buffer (10x)	SDS-PAGE gel electrophoresis	19.8 g Tris, 86.4 g glycine, 6 g SDS (#L3771, Sigma Aldrich), H_2O up to 1 L
PBST buffer	Western blotting	1 mL Tween® 20 (#P1379, Sigma Aldrich) in 1 L PBS
2x DMEM	Plaque assay	2x DMEM powder (#52100-039, Gibco) in 500 mL H_2O supplemented with 12.5 mL 1 M HEPES, and 1.85 g $NaHCO_3$ (#102475W, BDH laboratory supplies), sterilised
1.4% low melting point agarose	Plaque assay	1.4 g low melting point agarose (#16520050, Invitrogen) in 100 mL H_2O
Agarose-DMEM 2% FCS, 1x P/S, 10 mM HEPES	Plaque assay	A 1: 1 mix of 2x DMEM and 1.4% agarose, with 2% FCS
Solutions for oHSV-1 density gradient ultracentrifugation		
Solution B	Ingredient for Solution D	2.8 mL 5 M NaCl; 6 mL HEPES 1M, pH 7.3 (#J484, VWR Life Science); 1.2 mL 0.5 M EDTA, pH 8.0; add H_2O to a final volume of 100 mL and sterile filter. Store at 4 ^oC.
Solution C	Ingredient for solution E	2.8 mL 5 M NaCl; 1 mL 1 M HEPES, pH 7.3; 200 μL 0.5 M EDTA, pH 8.0; add H_2O to a final volume and sterilise. Store at 4 ^oC.
Solution D	Initial layering solution	5 volumes of OptiPrep (#M1248, Biovision) and 1 volume of solution B
Solution E	Mix with HSV-1 for layering on top of solution D	8.5 mL solution C and 1.5 mL HSV-1 resuspended in DPBS
Solution F	Top up solution	1.27 mL solution C and 1 mL solution D

7.2.2 DNA and protein sequences

NKG2D BiTE (Sig-NKG2D-GS-αCD3-GS-NKG2D-10xHis) – DNA sequence (1704 bp)

ATGGGATGGAGCTGCATCATCCTATTCCTCGTGGCGACGGCCACTGGAGTGCATAGCGAACT
GGTGTTCCTAAACTCATTATTCAACCAAGAAGTTCAAATTCCCTTGACCGAAAGTTACTGTGGC
CCATGTCCTAAAAACTGGATATGTTACAAAAATAACTGCTACCAATTTTTTGATGAGAGTAAAA
ACTGGTATGAGAGCCAGGCTTCTTGTATGTCTCAAAATGCCAGCCTTCTGAAAGTATACAGCA
AAGAGGACCAGGATTTACTTAAACTGGTGAAGTCATATCATTGGATGGGACTAGTACACATTC
CAACAAATGGATCTTGGCAGTGGGAAGATGGCTCCATTCTCTCACCCAACCTACTAACAATAA
TTGAAATGCAGAAGGGAGACTGTGCACTCTATGCCTCGAGCTTTAAAGGCTATATAGAAAACT
GTTCAACTCCAAATACATACATCTGCATGCAAAGGACTGTGTCCTCCGGCGGCGGTGGAAGC
GATGTGCAACTCGTGCAGTCCGGTGCGGAAGTGAAAAAGCCGGGCGCGAGCGTCAAAGTGT
CATGCAAGGCGTCAGGATATACGTTTACTAGATACACTATGCACTGGGTGCGCCAGGCACCT
GGTCAGGGCCTTGAATGGATCGGCTACATCAATCCGTCGAGAGGCTACACTAATTACGCGGA
CTCAGTCAAAGGGCGCTTCACGATTACGACCGACAAGTCCACCTCGACTGCATACATGGAAC
TGTCCTCGCTGAGAAGCGAGGACACCGCTACTTACTACTGCGCTAGATACTACGATGATCACT
ACTGCCTCGATTACTGGGGCCAGGGAACCACTGTCACGGTGTCATCGGGAGAGGGCACCTC
AACCGGATCAGGGGGATCGGGAGGCTCGGGCGGCGCAGACGACATCGTCCTGACCCAGTC
GCCCGCCACCTTGTCGCTGTCCCCAGGAGAAAGAGCGACCCTGTCATGCCGGGCGTCGCAA
AGCGTGAGCTATATGAATTGGTATCAGCAGAAGCCAGGAAAGGCGCCGAAGAGATGGATCTA
CGACACCTCCAAGGTCGCTTCAGGTGTCCCGGCTAGATTCTCAGGATCGGGATCAGGAACGG
ACTACTCCCTGACCATCAATTCACTGGAAGCAGAAGATGCGGCCACCTACTACTGTCAGCAGT
GGTCCTCCAACCCGCTGACTTTCGGAGGCGGAACTAAGGTCGAGATCAAGTCCAGCGGCGG
AGGCGGTTCCTTTCTGAATAGCCTGTTTAACCAGGAGGTGCAGATCCCTCTAACTGAGTCGTA
TTGCGGACCTTGCCCCAAGAATTGGATCTGCTATAAGAACAATTGTTATCAGTTCTTCGACGA
AAGCAAGAATTGGTACGAATCACAAGCCAGCTGCATGAGCCAGAACGCCTCTCTGCTCAAGG
TGTATTCTAAGGAAGATCAAGATCTGCTGAAGCTCGTTAAAAGCTACCACTGGATGGGCTTGG
TGCATATCCCCACCAACGGCAGCTGGCAATGGGAGGACGGAAGCATATTGAGCCCAAATCTG
CTGACAATCATCGAGATGCAGAAAGGCGATTGCGCTCTGTACGCTAGCTCGTTCAAGGGATA
CATCGAGAATTGCAGCACCCCCAACACCTATATTTGTATGCAGCGCACCGTACATCACCATCA
CCATCACCACCATCACCATTAG

Control BiTE (Sig-NKG2Db5-GS-αCD3-GS-NKG2Db5-10xHis) – DNA sequence (1704 bp) – mutations in bold lower case

ATGGGATGGAGCTGCATCATCCTATTCCTCGTGGCGACGGCCACTGGAGTGCATAGCGAACT
GGTGTTCCTAAACTCATTATTCAACCAAGAAGTTCAAATTCCCTTGACCGAAAGTTACTGTGGC
CCATGTCCTAAAAACTGGATATGTTACAAAAATAACTGCTACCAATTTTTTGATGAGAGTAAAA
ACTGGTATGAGAGCCAGGCTTCTTGTATGTCTCAAAATGCCAGCCTTCTGAAAGTATACAGCA
AAGAGGACCAGGATTTACTTAAACTGGTGAAGTCATATCATTGGATGGGACTAGTACACATTC
CAACAAATGGATCTTGGCAGTGGGAAGATGGCTCCATTCTCTCACCCAACCTACTAACA**cgcgg**
cggcaaacgcAAGGGAGACTGTGCACTCTATGCCTCGAGCTTTAAAGGCTATATAGAAAACTGTT
CAACTCCAAATACATACATCTGCATGCAAAGGACTGTGTCCTCCGGCGGCGGTGGAAGCGAT
GTGCAACTCGTGCAGTCCGGTGCGGAAGTGAAAAAGCCGGGCGCGAGCGTCAAAGTGTCAT
GCAAGGCGTCAGGATATACGTTTACTAGATACACTATGCACTGGGTGCGCCAGGCACCTGGT
CAGGGCCTTGAATGGATCGGCTACATCAATCCGTCGAGAGGCTACACTAATTACGCGGACTC
AGTCAAAGGGCGCTTCACGATTACGACCGACAAGTCCACCTCGACTGCATACATGGAACTGT
CCTCGCTGAGAAGCGAGGACACCGCTACTTACTACTGCGCTAGATACTACGATGATCACTACT
GCCTCGATTACTGGGGCCAGGGAACCACTGTCACGGTGTCATCGGGAGAGGGCACCTCAAC
CGGATCAGGGGGATCGGGAGGCTCGGGCGGCGCAGACGACATCGTCCTGACCCAGTCGCC
CGCCACCTTGTCGCTGTCCCCAGGAGAAAGAGCGACCCTGTCATGCCGGGCGTCGCAAAGC
GTGAGCTATATGAATTGGTATCAGCAGAAGCCAGGAAAGGCGCCGAAGAGATGGATCTACGA

CACCTCCAAGGTCGCTTCAGGTGTCCCGGCTAGATTCTCAGGATCGGGATCAGGAACGGACT
ACTCCCTGACCATCAATTCACTGGAAGCAGAAGATGCGGCCACCTACTACTGTCAGCAGTGG
TCCTCCAACCCGCTGACTTTCGGAGGCGGAACTAAGGTCGAGATCAAGTCCAGCGGCGGAG
GCGGTTCCTTTCTGAATAGCCTGTTTAACCAGGAGGTGCAGATCCCTCTAACTGAGTCGTATT
GCGGACCTTGCCCCAAGAATTGGATCTGCTATAAGAACAATTGTTATCAGTTCTTCGACGAAA
GCAAGAATTGGTACGAATCACAAGCCAGCTGCATGAGCCAGAACGCCTCTCTGCTCAAGGTG
TATTCTAAGGAAGATCAAGATCTGCTGAAGCTCGTTAAAAGCTACCACTGGATGGGCTTGGTG
CATATCCCCACCAACGGCAGCTGGCAATGGGAGGACGGAAGCATATTGAGCCCAAATCTGCT
GACA**agaggaggaaagagaaaa**GGCGATTGCGCTCTGTACGCTAGCTCGTTCAAGGGATACATCG
AGAATTGCAGCACCCCCAACACCTATATTTGTATGCAGCGCACCGTACATCACCATCACCATC
ACCACCATCACCATTAG

Human NKG2D ectodomain (amino acids 78-216) – protein

FLNSLFNQEVQIPLTESYCGPCPKNWICYKNNCYQFFDESKNWYESQASCMSQNASLLKVYSKE
DQDLLKLVKSYHWMGLVHIPTNGSWQWEDGSILSPNLLTIIEMQKGDCALYASSFKGYIENCSTPN
TYICMQRTV

Mutant NKG2D ectodomain (amino acids 78-216) – protein (mutation in bold)

FLNSLFNQEVQIPLTESYCGPCPKNWICYKNNCYQFFDESKNWYESQASCMSQNASLLKVYSKE
DQDLLKLVKSYHWMGLVHIPTNGSWQWEDGSILSPNLLT**RGGKR**KGDCALYASSFKGYIENCST
PNTYICMQRTV

GS linker

SSGGGGS

Signal peptide

MGWSCIILFLVATATGVHSELV

αCD3 scFv

DVQLVQSGAEVKKPGASVKVSCKASGYTFTRYTMHWVRQAPGQGLEWIGYINPSRGYTNYADS
VKGRFTITTDKSTSTAYMELSSLRSEDTATYYCARYYDDHYCLDYWGQGTTVTVSSGEGTSTGS
GGSGGSGGADDIVLTQSPATLSLSPGERATLSCRASQSVSYMNWYQQKPGKAPKRWIYDTSKVA
SGVPARFSGSGSGTDYSLTINSLEAEDAATYYCQQWSSNPLTFGGGTKVEIK

10x His

HHHHHHHHHH*

pTransfer plasmid – DNA

ggccgcaatcgggcaaatcgctgaatattccttttgtctccgaccatcaggcacctgagtcgctgtctttttcgtgacattcagttcgctgcgctc
acggctctggcagtgaatgggggtaaatggcactacaggcgccttttatggattcatgcaaggaaactcaaaataatacaagaaaagcc
cgtcacgggcttctcagggcgttttatggcgggtctgctatgtggtgctatctgactttttgctgttcagcagttcctgccctctgattttccagtctg
accacttcggattatcccgtgacaggtcattcagactggctaatgcacccagtaaggcagcggtatcatcaacggggtctgacgctcagtg
gaacgaaaactcacgttaagggattttggtcatgagattatcaaaaaggatcttcacctagatccttttaaattaaaaatgaagttttaaatca
atctaaagtatatatgagtaaacttggtctgacagttaccaatgcttaatcagtgaggcacctatctcagcgatctgtctatttcgttcatccata
gttgcctgactccccgtcgtgtagataactacgatacgggagggcttaccatctggccccagtgctgcaatgataccgcgagacccacgct
caccggctccagatttatcagcaataaaccagccagccggaagggccgagcgcagaagtggtcctgcaactttatccgcctccatccag

tctattaattgttgccgggaagctagagtaagtagttcgccagttaatagtttgcgcaacgttgttgccattgctacaggcatcgtggtgtcacg
ctcgtcgtttggtatggcttcattcagctccggttcccaacgatcaaggcgagttacatgatcccccatgttgtgcaaaaaagcggttagctcc
ttcggtcctccgatcgttgtcagaagtaagttggccgcagtgttatcactcatggttatggcagcactgcataattctcttactgtcatgccatcc
gtaagatgcttttctgtgactggtgagtactcaaccaagtcattctgagaatagtgtatgcggcgaccgagttgctcttgcccggcgtcaatac
gggataataccgcgccacatagcagaactttaaaagtgctcatcattggaaaacgttcttcggggcgaaaactctcaaggatcttaccgct
gttgagatccagttcgatgtaacccactcgtgcacccaactgatcttcagcatcttttactttcaccagcgtttctgggtgagcaaaaacagga
aggcaaaatgccgcaaaaaagggaataagggcgacacggaaatgttgaatactcatactcttccttttcaatattattgaagcatttatca
gggttattgtctcatgagcggatacatatttgaatgtatttagaaaaataaacaaatagggggttccgcgcacatttccccgaaaagtgccactt
gcatcgatgaattgatccgaagttcctattctctagaaagtataggaacttcgaattgtcgacaagcttgatctggcttatcgaaattaatacga
ctcactatagggagaccggaattcgagctcggtacccgggggatccggaacccttaatataacttcgtataatgtatgctatacgaagttatt
aggtccctcgacctgcaggcatggctaattctgtcagccgttaagtgttcctgtgtcactgaaaattgctttgagaggctctaagggcttctcag
tgcgttacatccctggcttgttgtccacaaccgttaaaccttaaaagctttaaaagccttatatattcttttttttcttataaaacttaaaaccttaga
ggctatttaagttgctgatttatattaattttattgttcaaacatgagagcttagtacgtgaaacatgagagcttagtacgttagccatgagagctt
agtacgttagccatgagggtttagttcgttaaacatgagagcttagtacgttaaacatgagagcttagtacgtgaaacatgagagcttagtac
gtactatcaacaggttgaactgcggatcttgcggcc

7.2.3 Plasmid maps

pTransfer

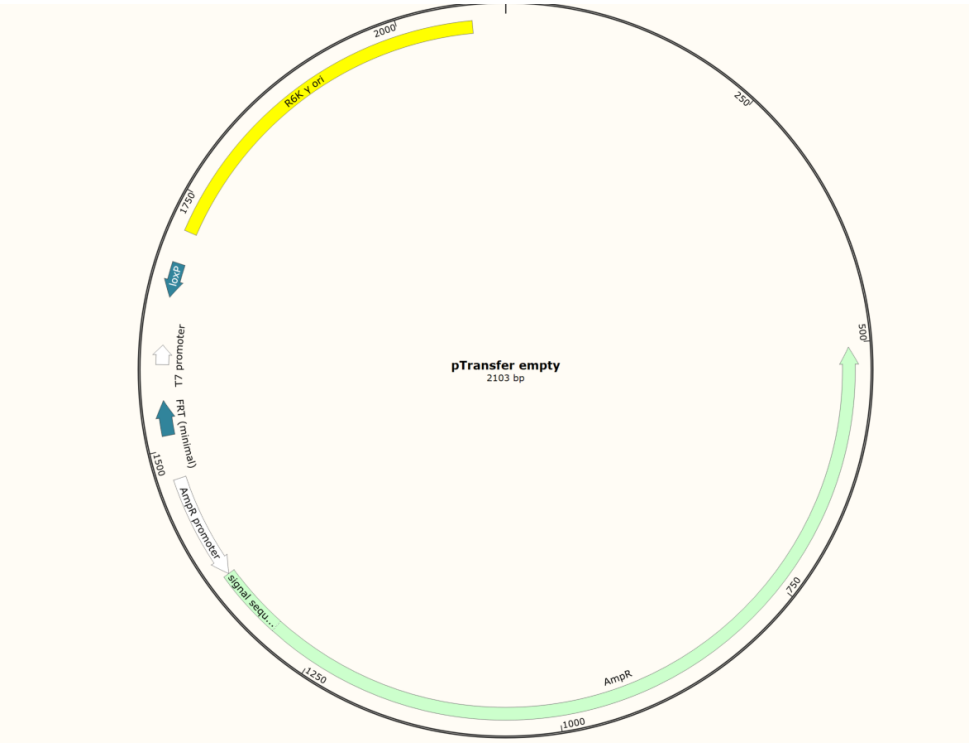

pTransfer -NKG2D BiTE

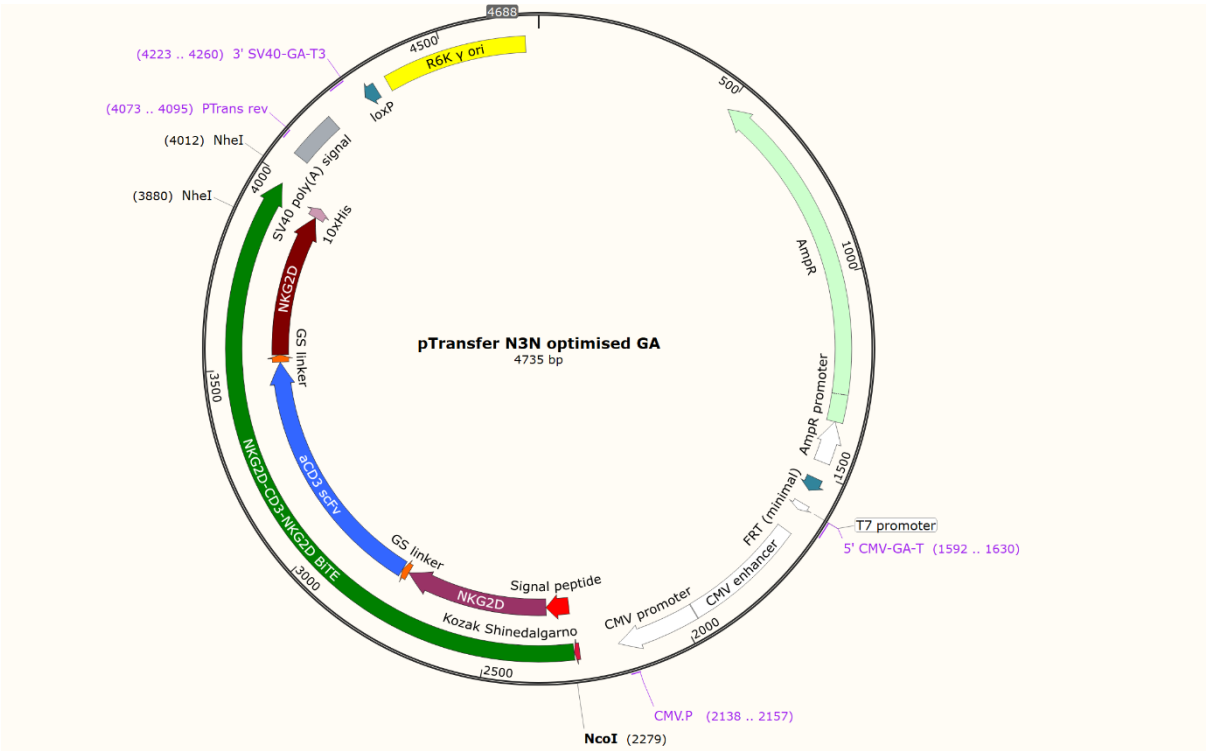

pTransfer-Control BiTE

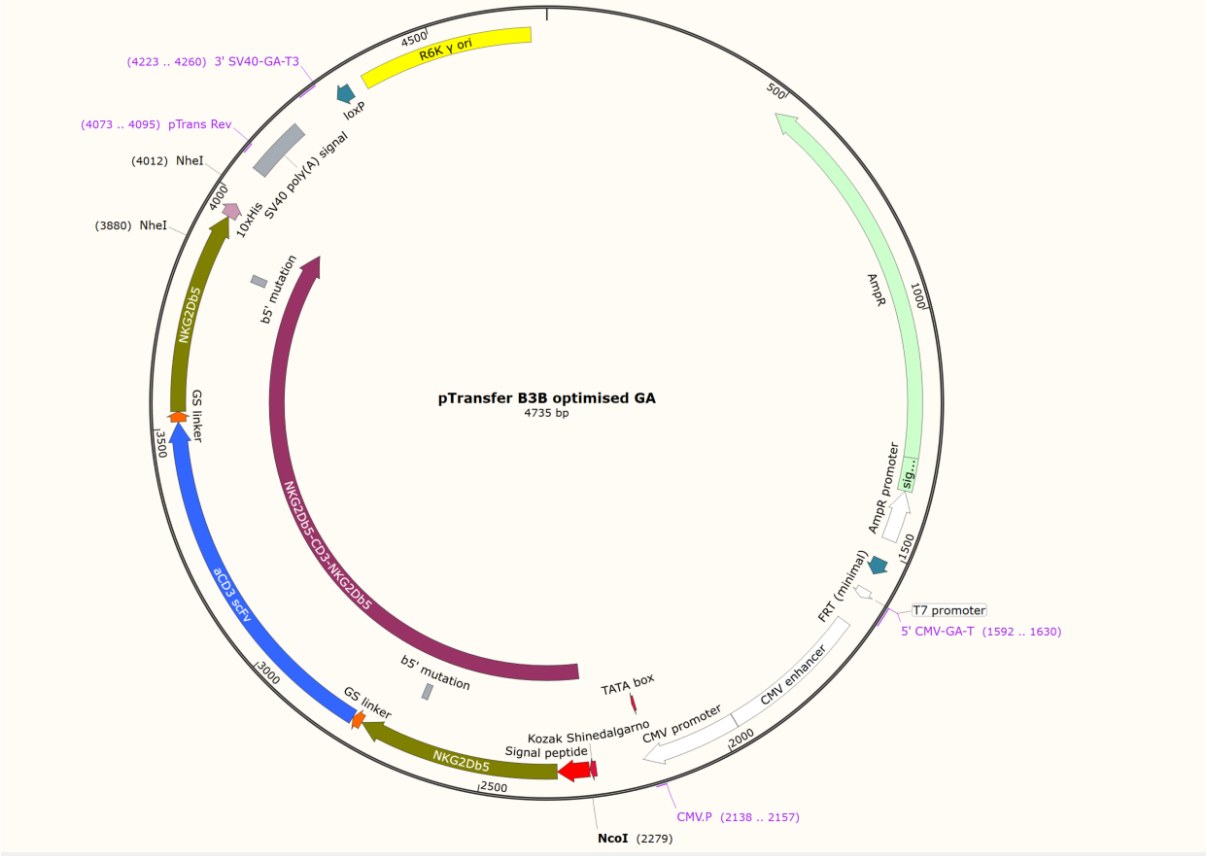

7.2.4 Oligonucleotides used for PCR and Sanger sequencing

Table 7.2 Oligonucleotides used for PCR and Sanger sequences

Primer	Target	Sequence	Tm (°C)
5'-CMV.P	CMV promoter of pTransfer	TGTACGGTGGGAGGTCTATA	56
3'-pTransRev	Downstream of construct in pTransfer	AGTTGTGGTTTGTCCAAACTCAT	60
5'-CMV-GA-T	Gibson assembly upstream of CMV-NKG2D	TCACTATAGGGAGACCGGCTAGTAATCAATTACGGGGTC	70
3'-SV40-GA-T3	Gibson assembly downstream of SV40 polyA	CGGGTACCGAGCTCGTTAAAAAACCTCCCACACCTCCC	74
5'-UL42	Forward primer for HSV-1 UL42 gene	GCCAGCGAGACGCTGAT	59
3'-UL42	Reverse primer for HSV-1 UL42 gene	ACGCAGGTACTCGTGGTGA	61